Wearable Textile-Based Contact Sensing for Functional Fit Assessment

A Dissertation
SUBMITTED TO THE FACULTY OF THE GRADUATE SCHOOL
OF THE UNIVERSITY OF MINNESOTA
BY

Crystal Marie Compton

IN PARTIAL FULFILLMENT OF THE REQUIREMENTS
FOR THE DEGREE OF
DOCTOR OF PHILOSOPHY

Dr. Lucy E. Dunne
Dr. Brad Holschuh
Dr. Elizabeth Bye
Dr. Pete Marchetto

August 2021

Acknowledgments

I am extremely grateful for all of the support I have received throughout my dissertation and PhD. I would first like to thank my advisor, Dr. Lucy Dunne, who has provided invaluable expertise and guidance over the many years I have been incredibly fortunate to work with. During my time with her, I have been able to learn and grow so much as a researcher, designer, engineer, and human being and I am forever grateful for the experience. I would like to thank my committee members Dr. Brad Holschuh, Dr. Elizabeth Bye, and Dr. Pete Marchetto for all of the helpful feedback, questions, and encouragement. I am also very grateful for the support, mentorship, and advice from Dr. Abbie Clarke-Sather.

I have had the opportunity to work with the Anthropometry and Biomechanics Facility (ABF) at NASA Johnson Space Center (JSC) throughout this dissertation and have received exceptional mentorship from Dr. Sudhakar Rajulu, Dr. Han Kim, Linh Vu, Yaritza Hernandez, and Elizabeth Benson. The support I received has helped tremendously to make this research possible.

I would also like to thank my friends and family. I have had the opportunity to travel and meet individuals across planet Earth through various academic conferences and internships, and have made long-lasting friendships that mean the world to me. I feel so fortunate to have been part of the Wearable Technology Lab (WTL) during my academic studies where I have been able to work with so many amazing individuals – thank you

for being such an incredible form of support, advice, and friendship. Thank you to my dad for your lighthearted nature and great jokes, my mom for being so kind and supportive, and my brother.

This work was supported by the University of Minnesota Wearable Technology Lab, College of Design, NASA, and the Minnesota Space Grant Consortium (MnSGC).

Dedication

To Mom and Dad for the continuous support, encouragement, and love throughout my life.

Abstract

Fit of a wearable system influences many human factors, including comfort, performance, and risk of injury. Sensors can provide objective and quantitative measures of mechanical interactions between the body and the wearable system for functional fit assessment. However, accurate on-body sensing is a challenge due to contaminating variables that can affect accuracy, including forces introduced by garment/body interactions such as stretching and folding. Contact sensing is a simpler sensing approach that is less susceptible to on-body contaminating variables. However, there is currently no gold-standard reference measure for on-body contact measurement. Here, multiple imperfect sources of information are compared and their respective limitations contrasted.

This research focuses on evaluating methods to quantify functional fit of a wearable system by measuring contact between the body and a spacesuit component mockup during controlled robotic manikin testing through a wearable contact and force sensing e-textile garment. This study compared two sensor-based fit quantification methods (contact and force sensors) with a non-wearable reference (optical Motion Capture (MoCap)). Garment-integrated sensors were characterized in a bench test apparatus (Instron) under controlled loading conditions. The translation of these methods to the wearable environment was investigated using a robotic manikin that performs repeatable dynamic movements for a controlled on-body sensing scenario. Two different manikin conditions were evaluated to simulate effects of anthropometric differences.

Under controlled conditions, contact sensors showed some hysteresis and generally exhibited higher closing forces compared to opening forces. Using the threshold calibration model, contact sensors accurately measured contacts above about 0.5 N, but

recorded intermittent false negative contacts between approximately 0-0.5 N. Force sensors reliably measured contacts above 0.15 N and comparatively recorded a smaller range of false negatives between 0-0.15 N, but a much larger proportion of false positives. However, under on-body conditions, the contact-threshold calibration did not accurately translate for force sensors. There were no strong similarities found between contact sensor, force sensor, and MoCap marker data. Force sensors were difficult to calibrate and sensitive to factors like donning forces, movement, and wrinkling. Contact sensors were influenced by fewer and more resolvable contaminating variables, and were found to be better suited for on-body applications.

Contents

List of Tables

List of Figures

List of Acronyms

NASA	National Aeronautics and Space Administration
JSC	Johnson Space Center
ABF	Anthropometry and Biomechanics Facility
WTL	Wearable Technology Laboratory
IVA	Intravehicular activity
EVA	Extravehicular activity
IEVA	Intra/extravehicular activity
xEMU	Exploration Extravehicular Mobility Unit
LTA	Lower Torso Assembly
WBH	Waist Brief Hip
RQ	Research question
HUT	Hard Upper Torso
RTW	Ready-to-wear
3D	Three-dimensional
ROM	Range of motion
NBL	Neutral Buoyancy Laboratory
MoCap	Motion Capture
IMU	Inertial measurement unit
ISS	International Space Station
FSR	Force sensitive resistor
LDPM	Laser Doppler Perfusion Monitor
FOP	Flight Opportunities Program

LCG	Liquid Cooling Garment
LCVG	Liquid Cooling and Ventilation Garment
OL	Open loop
SD	Standard deviation
kPa	Kilopascal
Ag	Silver
Sn	Tin
Ni	Nickel
Cu	Copper
DC	Direct current
AWG	American Wire Gauge
LoNE	Lines of non-extension
CAD	Computer-aided design
cs	Contact sensor
fs	Force sensor
ABS	Acrylonitrile Butadiene Styrene
V	Volt
V_{out}	Output voltage
V_{in}	Input voltage
SLA	Stereolithography
in	Inches
cm	Centimeters
mm	Millimeters
sec	Seconds
min	Minutes
N	Newton
DAQ	Data acquisition
Hz	Hertz
L	Left
R	Right
B	Brief

NB	No brief
c	Contact
nc	No contact

Chapter 1

1 Introduction

Spacesuits are worn by astronauts for protection against the harsh environment and dangers of space to keep them safe and alive during various aspects of human space flight. There are three main types of spacesuits that the National Aeronautics and Space Administration (NASA) uses: intravehicular activity (IVA), extravehicular activity (EVA), and intra-extravehicular activity (IEVA) suits [1]. IVA suits are worn while a crewmember is within a pressurized spacecraft for protection in case of a loss of pressure. These suits generally are less bulky, lighter weight, and composed of a greater amount of softer materials in comparison to EVA suits. EVA suits are worn while a crewmember is outside of a spacecraft during Extravehicular Activity (EVA) (also referred to as a spacewalk). Extra protection is needed since EVA suits act as a miniature spacecraft for a human to work in. IEVA suits are a combination of both launch and entry or IVA and EVA suits, designed to reduce volume and weight. This research focuses on the NASA EVA suits and will be the focus going forward.

Over many years and different spaceflight programs, there have been newly developed versions of the spacesuit. The most current suit in development is the Exploration Extravehicular Mobility Unit (xEMU) (Figure 1.1). The xEMU is being developed for NASA's Artemis program to return humans to the Moon for lunar surface exploration. A key advancement with the xEMU suit is on increasing wearer mobility for improved

ability to perform surface exploration tasks. Additionally, another key focus with the xEMU is to accommodate sizing of smaller (female) body types, which previously has not been developed. NASA spacesuits are composed of interchangeable components fabricated in different sizes to accommodate different body shapes and sizes. These components are a combination of both hard and soft goods.

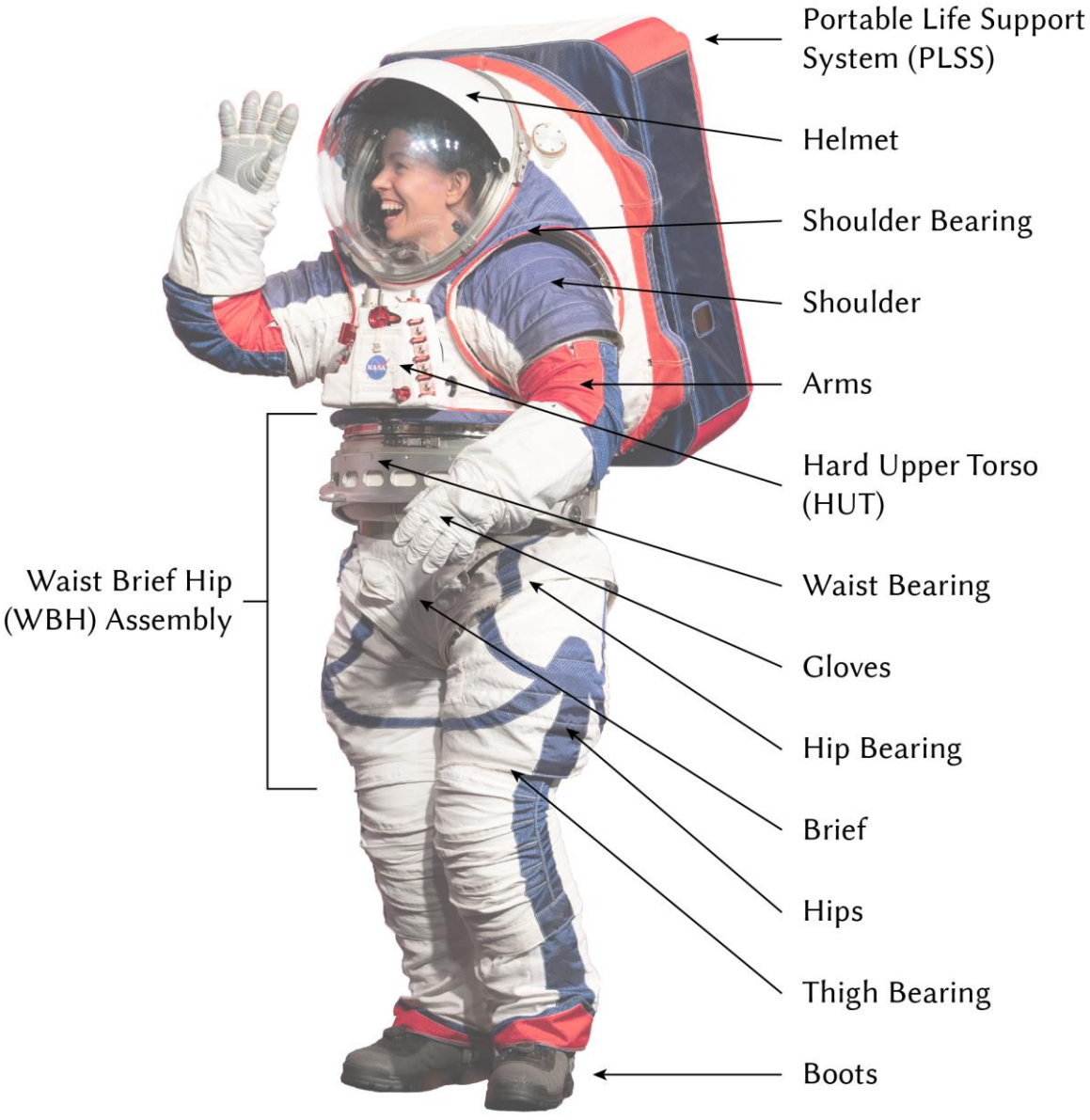

Figure 1.1: xEMU spacesuit components (image adapted from NASA).

Contact, force, or pressure sensing can provide objective, quantitative information that can be used to better understand human-wearable system interactions. Understanding these interactions can help inform the relationship between the body and a wearable system, which can be used as a method to evaluate functional fit for improved system performance, comfort, and sizing and fit. This dissertation addresses the research gap between textile sensor development and garment integration, influences of on-body sensing, and contact sensing performance by developing an e-textile wearable sensing garment that allows comparison of textile-based contact and force sensors to assess contact patterns between the body and a wearable system with different manikin size and shape conditions.

1.1 Motivation and Problem Statement

Spacesuit fit is known to influence many factors such as crewmember comfort, performance, range of motion, and risk of injury [2] [3]. There is a need to understand how suit fit affects these different human parameters [4] in order to improve suit fit [5].

Human bodies vary greatly in shape and size, which can make both achieving and maintaining optimal suit fit a continuous challenge for the diverse range of body shapes present within the astronaut corps. Additionally, the body experiences changes during microgravity that can cause changes in how the suit fits an individual. Indexing – which is the positioning and movement of an object relative to another – of the human inside of the spacesuit is influenced by suit fit and thus how the body interacts with the suit.

Understanding body-suit interaction is an important first step in understanding the degree to which current suit designs accommodate a given crewmember's anthropometry and biomechanics, and this understanding can help inform and improve suit sizing and fit and reduce potential injuries. Existing methods such as using optical motion capture to understand contact that occurs between the body and a wearable system do not work effectively for all body sensing scenarios, due to the line-of-sight requirement for both surfaces and the non-repeatable movements humans make (which

would not allow an effective 2-part data collection approach for comparison). Textile-based wearable force and contact sensors are appealing technologies that have many wearability advantages that can help quantify human-suit interactions but have not been extensively used due to inherent challenges common to textile-based sensing such as sensor durability and repeatability.

Optimal sensor integration can be a challenge for on-body and garment integrated sensing. The sensor system should be durable enough for the testing environment, sensors should remain securely attached (need to have a secure integration method), not impact the body's ability to move, low profile/not create bulk (wires mostly), conform to the body, manage multiple sensor leads. Since there is currently a lack of a gold-standard reference measure to measure contact on the body, it can be challenging to validate. Comparing multiple imperfect sources of information is an alternative approach in the absence of a validated reference measure.

This research focuses on quantifying the human-spacesuit interactions by measuring contact that occurs between the body and the lower torso assembly (LTA) brief spacesuit component during repeated, controlled robotic manikin testing through a wearable contact and force sensing e-textile garment to improve understanding of suit fit.

1.2 Research Objectives

The objective of this research is to develop and evaluate the performance of textile-based, wearable contact and force sensing technologies that can be used to quantitatively measure body-wearable system interactions. An e-textile sensing garment is developed specifically for the wearable sensing scenario, and integrated sensors are characterized in a bench test apparatus to assess sensor responses under controlled loading conditions. Subsequently, the garment is used with a lower body spacesuit component mockup (LTA brief) (Figure 1.2 and Figure 1.3) for evaluation of body-spacesuit interactions. A robotic manikin that performs repeatable dynamic movements is used in a controlled on-body sensing scenario for sensor validation. The manikin's body is treated symmetrically about

the midline for sensor type comparison, and contact and force sensors are placed on corresponding manikin sides (right and left) in the lower body pelvis/buttock area. Through controlled dynamic manikin testing, location and duration of contact between the manikin and the brief is evaluated. Differences in contact/force profiles for two different manikin body shapes/sizes are also evaluated. These findings can be used to understand textile sensor performance, evaluate contact patterns on a body surface during movement and between sizes, and understand on-body sensing challenges.

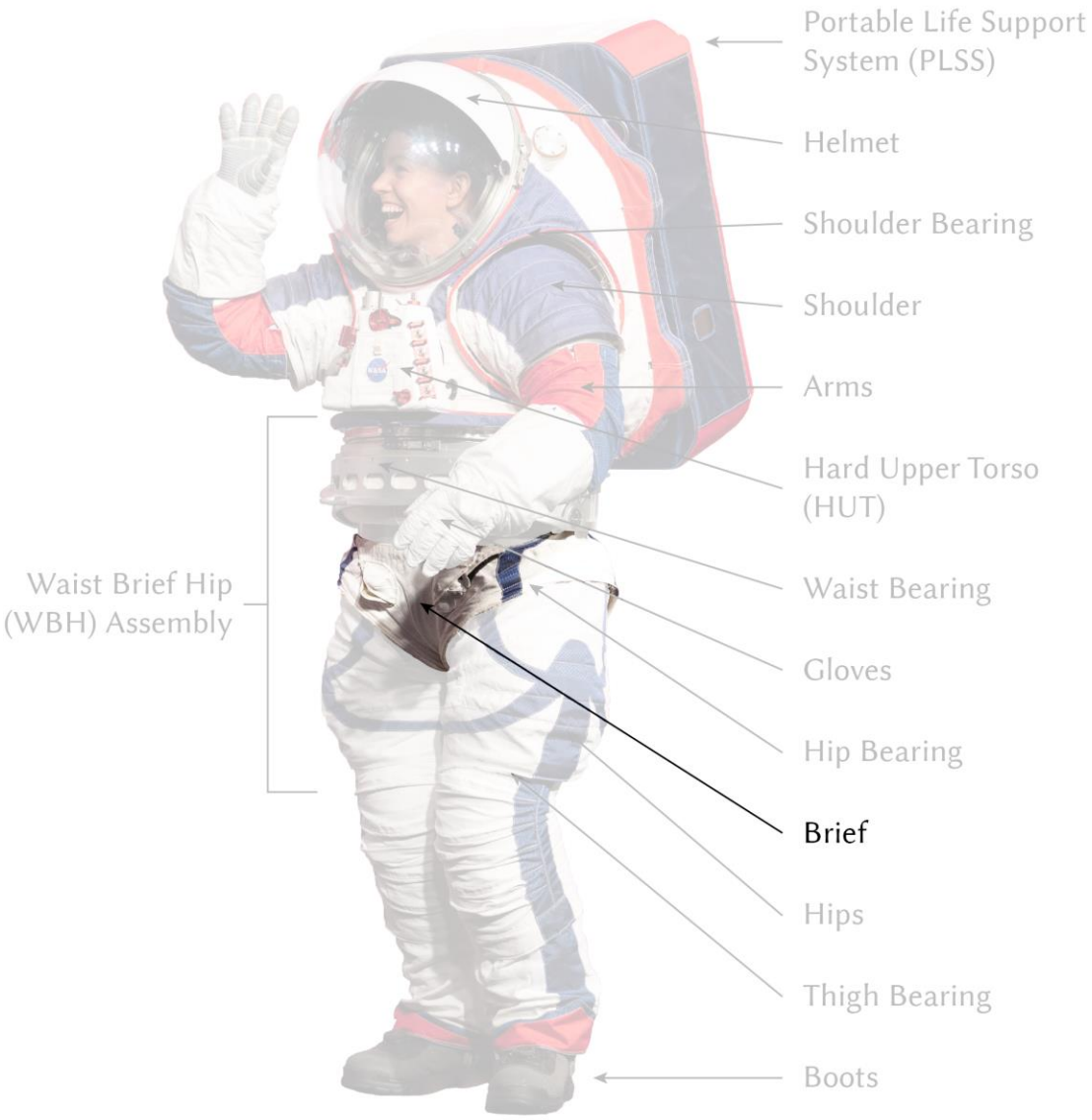

Figure 1.2. xEMU spacesuit components with the brief component highlighted (image adapted from NASA).

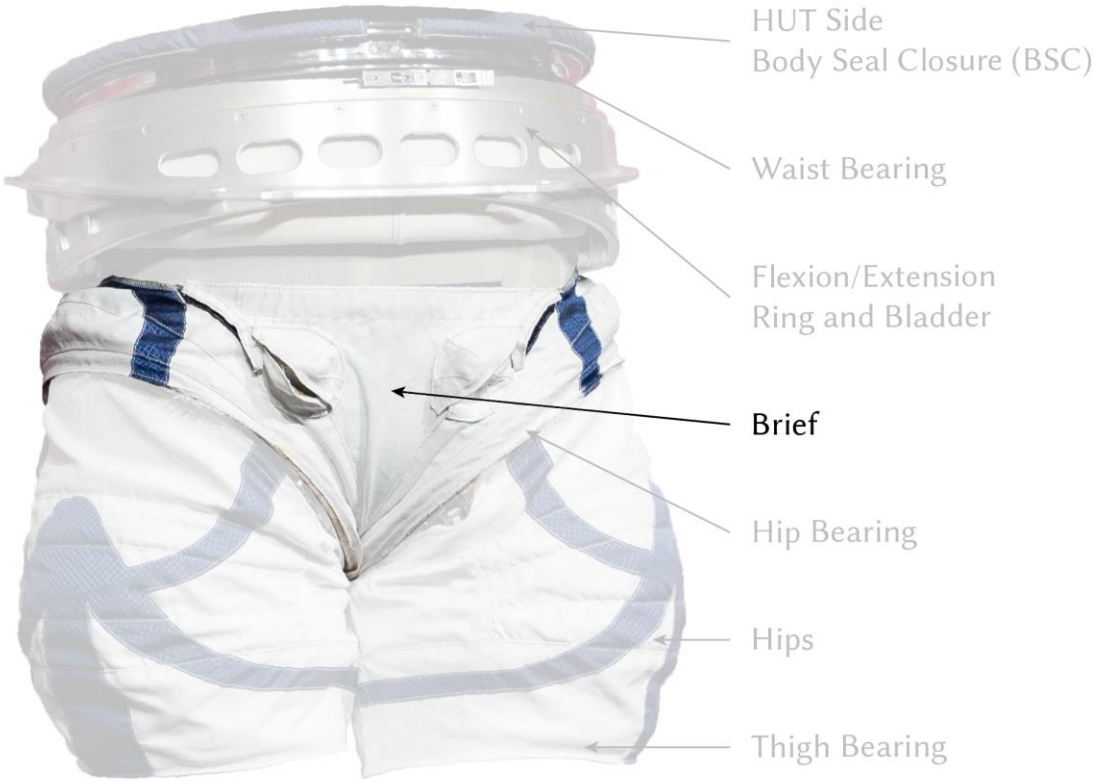

Figure 1.3: xEMU spacesuit Waist Brief Hip (WBH) assembly with the brief component highlighted (image adapted from NASA).

1.3 Research Questions

Listed below are research questions (RQ) used to guide this dissertation.

RQ1) How accurately do the textile-based wearable contact and force sensors used in this study measure contact in a controlled applied force testing environment?

RQ2) How accurately do the sensors used in this study measure contact in an e-textile garment for on-body sensing?

RQ3) How does duration and location of body/suit contact vary during movement?

RQ4) How does duration and location of body-spacesuit (LTA brief component) contact differ for different body shapes and sizes?

1.4 Outline

The following structure for this dissertation includes background information on spacesuits and fit assessment methods (Chapter 2 Background), the design and development of an e-textile sensing garment and brief spacesuit component (Chapter 3 Sensor and E-Textile Sensing Garment Development), description of the test methods and analysis used for Instron and manikin testing (Chapter 4 Methods), results and discussion from Instron (Chapter 5 Instron Test Results and Discussion) and manikin (Chapter 6 Manikin Test Results and Discussion) testing are presented, followed by conclusions and future work (Chapter 7 Conclusion). The appendix includes all test results for individual sensors (Appendix A. Plots).

Chapter 2

2 Background

The human body is a complex system and is the foundation of wearable product development [6] [7]. Bodies vary greatly in size and shape which introduces challenges in the development of a sizing system and can limit the ability to achieve optimal fit for a given population. Since there are many negative consequences of poor or suboptimal suit fit, fit testing should be performed, and objective testing can inform the design of suits [2]. Understanding the body-spacesuit relationship is imperative for successful spacesuit development and analysis of fit.

Approaches to understanding the body-suit relationship and fit range in complexity, price, required equipment, and the type of data they afford. For example, photography or video recording is relatively less expensive and requires less equipment to track human body movement compared to a Motion Capture System setup. However, data must be extracted manually from photography or video records, and therefore is typically much more limited in scope and quantity than the data that can be collected automatically by a motion capture system. Additionally, the specific types of body-suit relationship data obtained by these approaches vary and may not be suitable for the intended application – not all approaches afford force or contact measurement and instead may only track movement, which can give some indication of body-suit relationship but measuring individual discrete contact locations on the body is not possible. These methods also

range in the type of data obtained. Both subjective and objective data approaches have been used, each with inherent advantages and limitations.

The following subsections review topics relevant to understanding the body-spacesuit relationship.

2.1 Spacesuit

A spacesuit is used to protect a human while in the harsh space environment. It serves as a miniature, body-sized spacecraft containing many different elements for an astronaut to safely carry out essential tasks outside of the main spacecraft. There are three main functions that a spacesuit must fulfill for successful missions: 1) system to support life, 2) protection from hazardous environment, and 3) allow sufficient mobility and sensory stimuli [8].

The spacesuit is a modular system made up of different components. In this study, focus is placed on the xEMU since this is the current suit in development. Figure 1.1 illustrates different suit components of the xEMU suit. Generally speaking, these suit components consist of the: helmet; hard upper torso (HUT); arm assemblies; gloves; waist, hip; and thigh bearings; brief; legs; and boots. Many of these components are produced in different sizes, and have some built-in adjustability features, to afford multiple variations of suit fit in order to accommodate the large variation in body shapes and sizes of the astronaut population. The spacesuit is composed of both soft- and hard-goods components. The soft goods suit components (such as the arms and legs) are fabricated out of materials that have some sort of compliance (textiles and films). These materials have some flexibility and are easily deformed. The hard goods suit components (such as the HUT, LTA brief, and scye bearings) are rigid and non-flexible. These components do not have any compliance. Materials used for suit components have an influence on suit fit and material properties also may change while wearing the suit, such as during pressurization. This will be discussed further in the following Subsection 2.1.1 Spacesuit Fit. One of the main improvements of the xEMU suit being developed for future space

exploration is increasing user mobility, especially with the lower torso. This is achieved by using advanced materials and joint bearings enabling bending and rotation at the hips, as well as bending at the knees.

It has previously been reported that injuries that occur in the groin area while wearing the spacesuit are a result of contact due to fit [9]. The LTA brief has been selected as an initial suit component to use for testing as the LTA is currently in an active development and testing phase for the next generation xEMU spacesuit. Additionally, as planetary exploration becomes increasingly important it is necessary to understand implications of lower-body suit fit. The Waist Brief Hip (WBH) assembly is part of the LTA. Figure 1.2 illustrates the brief component highlighted relative to the entire suit system, and Figure 1.3 shows a more detailed view of the brief relative to other components within the WBH assembly. Understanding body-suit interactions can help inform optimal suit fit and decrease potential injuries while working and performing tasks in a spacesuit.

2.1.1 Spacesuit Fit

Proper spacesuit fit is recognized among the spacesuit community to be an extremely important aspect to reduce negative effects – such as discomfort, increased energy expenditure, reduced mobility, and risk of injury – while working in the spacesuit environment [4] [10] [2] [3]. Achieving optimal suit fit is a continuous challenge given the development (sizing limitations) and design constraints (system requirements) of a spacesuit. This challenge is further exacerbated by the need to fit an immensely diverse population in size and shape – often aiming to fit a population of males and females that falls within the 1^{st} to 99^{th} percentile. Spacesuit development, though different from ready-to-wear (RTW) garments, is similar in that when developing different component sizes, a balance between the number of sizes and cost will need to be considered. Restrictions such as cost will influence the number of suit sizes that can be developed for flight [2]. Although modular suit components of different sizes make this challenge considerably more achievable, challenges can still exist with suit fit. It is important to understand both

the objective and subjective aspects of how the suit fits a human for optimal suit performance and safety.

Spacesuits are thoughtfully designed and engineered wearable systems that provide necessary protection for the human inside effectively. However, with this level of protection, a human inherently needs to expend more energy to complete required tasks compared to being unsuited. Aspects such as rigidity, bulk, and pressurization – many necessities of keeping a human safe in the harsh environment of space – can contribute to a decreased ability to move freely and with minimal effort. An increase in exertion and fatigue is common as suit pressure increases [1]. Astronauts go through rigorous physicals, trainings, and exercise to ensure they are prepared for the physical exertion required to work and carry out tasks while wearing a spacesuit. However, suboptimal suit fit can results in an unnecessary increase in energy exertion compared to proper suit fit [2]. Obtaining a better understanding of the body-spacesuit relationship can help inform how well the suit is fitting the intended target population.

Adjustability of suits to correct minor fit issues or changes that occur while wearing the suit is important to maintain optimal suit fit. Suit fit can change due to things like pressurization, dynamic movement, and elongation of the body while in microgravity.

Spacesuits are pressurized to 4.3 psi [1]. Since the soft good suit components have some amount of compliance, when the spacesuit is pressurized, it affects these components making them more rigid and stiff emphasizing the importance of optimal suit fit [11]. This pressurization essentially changes the form/fit of the spacesuit and how it moves with the body. If the suit is fitted in a certain static posture, there can be certain areas of suboptimal fit while performing dynamic movements, due to indexing differences of the body-suit when the body is in different positions/orientations. It is important to consider not only the static but also the dynamic fit of the spacesuit. Additionally, elongation of the spine is a common occurrence while working in space. If a suit is fitted prior to this elongation, fit issues may arise after elongation. This emphasizes the importance of allowing some adjustability of suit fit to accommodate these changes that may occur while wearing the spacesuit.

2.2 Non-Sensor Fit Assessment Methods

Analyzing fit is a multifaceted task that involves both objective and subjective aspects. Fit can be described in various ways, both objectively and subjectively; however, traditionally fit is broadly defined as the relationship between the garment (or wearable system) and the human body [12] [13] [14] [15] [16] [17]. This body-garment relationship is evaluated based on how well it fulfills set garment requirements [18].

Sizing systems developed for apparel manufacturers are often informed by anthropometric surveys/databases [19] [20]. These sizing systems are developed specifically for each manufacturer, sometimes adopting aspects of previously developed sizing systems. Anthropometry is the study of human body measurements to analyze and understand shape variations [21], and is essential for the design of any product a human interacts with (including body-worn systems) [22] [23]. To create a sizing system, a population is divided into different sizes based on key body dimensions with the goal to accommodate as much of the population with the smallest number of sizes. For a sizing system to be effective, variations in body dimensions need to be understood to develop two-dimensional patterns into three-dimensional garments/products [24]. Similarly, in the development of spacesuit sizing, NASA also considers anthropometric databases as a starting point and body dimensions to inform suit sizing development [2].

The fit of a RTW garment is traditionally assessed based on five different elements: 1) ease, 2) line, 3) grain, 4) balance, and 5) set [13]. A panel of fit experts examine the fit of a prototype garment on a fit model during a fit session. During the fit session necessary changes that need to be made to align with the intended garment design fit are noted and altered for the next prototype. This process is repeated until the desired fit is achieved or deemed acceptable. Achieving optimal fit is a continuous challenge not only for the apparel industry, but also extends to more complex wearable systems such as spacesuits. Functional garments and wearable systems (e.g., spacesuits) are designed to meet user specific requirements and typically emphasize function or performance over aesthetics

[25] [26] [27]. Spacesuits are a pertinent example of functional clothing with specific user requirements that protect and keep a human alive in the harsh space environment. These requirements – such as a pressurized environment, temperature regulation, and oxygen supply to name a few – must be met for a spacesuit to perform effectively. With functional garments, this method of evaluating fit is not always appropriate or an effective way to evaluate fit. Therefore, additional measures or approaches should be taken to evaluate the fit of these types of garments. Functional clothing is often evaluated using more objective or quantitative approaches with technologies such as three-dimensional body scanning, motion capture systems, or sensors compared to RTW clothing.

Spacesuits previously were custom tailored and sized to an individual during the Mercury, Gemini, and Apollo Programs. Later, a modular sizing approach was taken for the Shuttle Program to improve manufacturing, reduce cost, and afford easier maintenance and resizing. These modular suit components were originally aimed to fit an incredibly diverse anthropometric population ranging from the 5th percentile female to 95th percentile male [28]. However, sizing of the HUT, which is a main suit component, especially for the upper body – and is located near what has been the primary source of body movements required while working in a spacesuit, such as rotational shoulder movement – was reduced to a smaller number of larger sizes (medium, large, and extra-large) based on crewmember population projects, limiting the inclusion of smaller individuals. Limitations in sizes produced for suit components other than the HUT also exist but some components have adjustability features (primarily with soft goods suit components) to increase fit accommodations. Spacesuit fit is evaluated during both suit development and when a crewmember is fitted to wear a suit. Once a suit is developed it commonly is assessed through subjective fit checks. During these fit checks the suit it donned and an expert evaluates the suit fit using a checklist or by asking questions during a series of functional movement/tasks.

The following sections discuss various approaches/methods that can be used to evaluate the body-wearable system relationship to assess functional fit.

2.2.1 Three-Dimensional (3D) Scanning and Modeling

Three-dimensional (3D) scanning digitally captures the surface volume of an object or body. This technology can be used for spacesuit fit assessment by capturing the body form and spacesuit for fit indexing evaluation of different body positions and suit sizes. There are different types of body scanning systems that exist but most scanning technologies use a form of light (e.g., laser, structured light) to capture the surface of an object. The data collected from a scan is a point cloud of X, Y, and Z coordinates that makeup the form. Infinite measurements and data types, including both traditional linear measurements and body shape/angles, can be extracted from three-dimensional body scans [29].

Body scanning is a technology that has been widely used in the apparel industry and can be a very useful approach to understand an individual's anthropometrics (body dimensions and shape, as well as distribution of volume), as well as develop, evaluate, and improve garment or product fit [30] [31] [32] [33] [34]. This technology can be used early on in the apparel design process for accurate pattern development to support optimal garment fit. It can also be used later on during the garment/product development prototyping phase to identify fit issues. Scanning can be used not only to obtain a body shape but also the accompanying apparel form, structure, or drape worn on the body. Scanning both ("clothed" and "unclothed") can be particularly useful for examining the relationship between the two (body and garment).

Three-dimensional body scans can be taken of many individuals in various static positions. This is advantageous as it affords virtual body-wearable system evaluations to take place while a human is not present, saving time and interaction. Scanning is a relatively quick process which usually only takes approximately 10-15 seconds to scan the entire body. There are pre-existing databases of body scans that can be used; however, thorough evaluations for more functional wearable systems often require specific positions (functional poses) that may not exist in the collection of three-dimensional body scans. Even if a position needed is just slightly different from a scan, an entirely new scan would be necessary. To obtain this, the same exact person would need to physically go

into the laboratory to be scanned in the desired position. This raises many potential issues such as participant availability, compensation, and time that has passed since the original scan. It is possible that the participant may not have time to be scanned again or may have moved away from the location of scanning. If a decent amount of time has passed since the original scans there is great potential that for body shape and size change – either smaller or larger, or shifting of volume to different areas of the body (as the human body shape naturally changes with age). Capturing a human's position can introduce error if multiple scans are required for comparison as it is difficult to achieve the exact same position, even if extra precaution is used. Three-dimensional body scanning systems typically are limited to only be able to capture the body statically. Recent advancements in three-dimensional scanning technology have made capturing dynamic movement available (3dMD) [35]; however, this equipment is very costly, requires a large working space, and can be challenging to parse the large amount of data collected into meaningful and interpretable results. It also can be difficult to accurately assess the distance between the body and a worn system (such as a spacesuit) unless two separate trials (suited and unsuited) take place – again there is likely human error present here though with variation in exact body movement/position between clothed and unclothed scans. Lastly, it has been found that issues exist with the consistency in measuring techniques between scanners [29]. This issue particularly relates to how each scanner collects certain body measurements, as there currently is not a standardized method across scanning systems.

Body scanning has been used previously for human-spacesuit evaluation and digital modeling [3] [36] [37] [38] [39]. Similar to the analysis of body-apparel products, a three-dimensional scanned human body or generated model can be evaluated with a digital CAD spacesuit. This approach can be used to quantify suit fit through clearance and overlap distance measurements/comparisons to predict sizing of an individual [39]. It is a useful approach to quickly simulate human-spacesuit interactions to verify suit fit early in the design process and to understand how small changes in suit design may impact performance [36]. Using a single three-dimensional body scan, multiple boundary manikins can be developed to create digital body models that represent extremes in

anthropometry of the intended target population. Computer simulated modelling also enables manipulation of different body positions so that a scanned individual does not need to come back into be scanned again to obtain a different pose. However, these models are statistically generated body forms and are not entirely "human-like" (e.g., lack of skin and muscle deformations and bony protuberances that occur during different movements). Additionally, if there are errors or issues with the original three-dimensional body scan this can be translated to the generated models, so having an accurate initial three-dimensional body scan is important. On the spacesuit side, multiple suit models can also be developed virtually to evaluate fit and range of motion without the need to physically prototype and develop an entirely new suit.

These digital/virtual approaches can be a very useful approach to gain a quick initial understanding of how different body shapes and sizes may interact with spacesuit components, and allow rapid prototyping and evaluation; however, dynamic evaluation is limited and human scans and generated body models, as mentioned previously, do not hold the same life-like properties as a real human (e.g., skin/tissue/muscle deformation and bony areas), which is ultimately important for a complete understanding of accurate body-spacesuit assessment. This method also does not allow sensing of forces between the body and spacesuit.

2.2.2 Photography and Video Recording

Photography/photogrammetry and video recording are similar approaches that can be used to capture visual representations/images both statically (photo) and dynamically (video). Both of these approaches can be used to track the human body (or other visual element) and its position in space over time. These tools can provide visual references of certain body locations or movements to quantitatively measure and inform things such as range of motion (ROM) [40] [41] [42] [43] and gait [44]. They can also be used in the development of apparel as a non-invasive approach to collect measurements and inform garment pattern development [45].

Spacesuit evaluation studies (published and unpublished) have previously used both photography and video recording to evaluate prototype suit performance capabilities, including ROM [43]. To assess spacesuit mobility using this approach, square grid boards have been used to track body angles during suited and unsuited conditions. Images are overlaid and angles are measured using a protractor. Results provided quantification of total joint ranges and percent differences between suited and unsuited conditions. However, with this method the analysis should be performed by an individual who is familiar with the suit mechanics, understanding neutral suit positions, rotational joint centers, and centerlines of joint segments.

Comparatively, these approaches are lower cost, more widely available technologies, and typically do not require as much time or equipment to employ than other approaches (such as motion capture system). However, they can be limited in accuracy and ability to capture multiple planes in one frame, which can be especially limiting for movements involving high multi-rotational joints. Additionally, it is not possible to capture areas that are not "visible" or difficult to see, such as inside of the spacesuit (distance between the body and the suit), as this method relies on capturing *visual* information.

2.2.3 Suit Symptoms and Injuries

Marks or contusions/bruises on the body, fingernail delamination, and musculoskeletal injuries can be visual or physical indications of where body-spacesuit interactions have occurred. They are a real representation of where on the body contact with the suit was made. There have been efforts to characterize these symptoms of working in a spacesuit previously [46] [9] [47].

Williams [46] sought to identify risk-factors that contribute to shoulder injury (Figure 2.1) during EVA training in the Neutral Buoyancy Laboratory (NBL) to ultimately provide suggestions to mitigate or eliminate injury related risks. Shoulder injuries were classified into two categories: minor (minimal medical treatment) and major (medical treatment or surgery). *Minor* injury sources include suboptimal suit fit, lack of padding, frequent

trainings, and working while in inverted body positions. *Major* injury sources include repetitive motion, heavy tools, overhead tasks, frequent trainings, working while in inverted body positions, and limitations to normal shoulder mobility. Many detailed recommendations were outlined, with key recommendations including redesign of EMU shoulder joint, reduction of high-risk activities, improvement of physical conditioning, and optimization of suit fit. It is clear from this report that suit fit has important implications on performance and risk of injury.

Figure 2.1: Shoulder irritation after NBL training: anterior (left), superior (middle), posterior and back (right) (image from [46]).

Related to Williams, Strauss [9] [47] sought to quantify signs, symptoms, and injuries from EVA trainings in the NBL for the entire suit system during an observational study. It was found that body areas that experienced the most significant, frequent, and continuous issues were located on the hands (Figure 2.2), shoulders, and feet. Recommendations were outlined, and among these recommendations included training on achieving optimum suit fit adjustments and future suit designs should consider findings from the study.

Figure 2.2: Fingernail delamination (image from [9]).

These suit symptoms are typically a result of what has happened previously in the suit and are not necessarily real-time indications – symptoms are typically recorded after NBL training is complete. Real-time indications could provide more information about what part of a movement being performed caused the symptom to help mitigate some of the negative effects of NBL trainings. With this method only "contact" that is at or above a certain force threshold (likely one that will induce some amount of pain or at minimum discomfort) will be apparent – smaller forces of contact will likely not make visual or physical indications and thus would be an unsuitable method to obtain information about lower force contact. Furthermore, obtaining useful data using this approach likely requires a wearer to experience discomfort and/or pain, and therefore is not an ideal approach to understand body-suit interactions.

2.2.4 Subjective Feedback

Subjective feedback for spacesuit assessments is a qualitative approach that can be used to better understand how a person feels while wearing a suit. This approach is also a means to supplement/support objective, quantitative data. Subjective data can provide valuable insights into what may be happening on the inside of the spacesuit to the wearer. This approach is useful for spacesuit assessments and is often used during fit checks to inform user preference of suit fit. Objective and quantitative measures of spacesuit fit are

a useful approach to initially fit an individual to a suit size; however, similarly with apparel, fit has a subjective component and therefore subjective evaluation can be a useful tool to fine tune fit to match the preference of each individual.

Subjective feedback can also be used to understand human-spacesuit interaction and has been used previously [48] [49]. Although these studies used a pressure sensing system to quantify body-suit interactions of the shoulder/arm during functional tasks, subjective feedback was also collected. Participants were asked to assess areas of pressure discomfort. However, it was found that accurate identification of contact points through subjective feedback is challenging as subjects did not identify contact points that were found with the quantitative data from the sensing system.

Subjective feedback can be collected during different times of an experiment or assessment but for best results should be asked/collected as soon as possible to ensure participant can retain accurate information to the best of their ability. Since humans can have difficulties accurately defining locations on the body of a particular stimulus, this subjective (qualitative) data can potentially be useful to supplement objective (quantitative) data. However, as mentioned humans are not always able to provide subjective feedback accurate to what is objectively happening and should not be the sole method of data collection for most applications.

2.2.5 Motion Capture (MoCap) System

Motion Capture (MoCap) systems are widely used in many different fields such as medical, animation, video games, filmmaking, functional clothing design, and biomechanics. This technology digitally captures and records body movement and provides three-dimensional, dynamic body data. For functional fit analysis, body movement is typically described by range of motion, which is calculated based on the angle between different body segments. For spacesuit applications, MoCap systems can record both body and spacesuit movement. These systems are produced in both optical and non-optical forms and are discussed further below.

Optical MoCap systems such as Vicon [50] use cameras and reflective markers to track movement through different positions in space (Figure 2.3). These systems are known to provide high accuracy when implemented and used correctly. Cameras are used to track reflective markers placed on specific areas of the body. Typically, bony body landmarks are used to place markers in a consistent and defined location across different bodies. However, placement error exists even when using bony landmarks and can affect intended data collection and accurate comparison between bodies. Multiple cameras are necessary to effectively capture each marker. Typically, three cameras need to be able to see a single marker in order to capture it. This can create challenges and issues when capturing areas of the body that may be difficult to see or when complex body movements are used. Occlusion of markers is one of the main issues of optical MoCap systems and can make accurate body motion tracking challenging. Optical systems also are typically limited to in-lab use only. These systems cannot be used out "in the wild" or in a large undefined space due to limitations of the working camera environment, which is necessary to track markers.

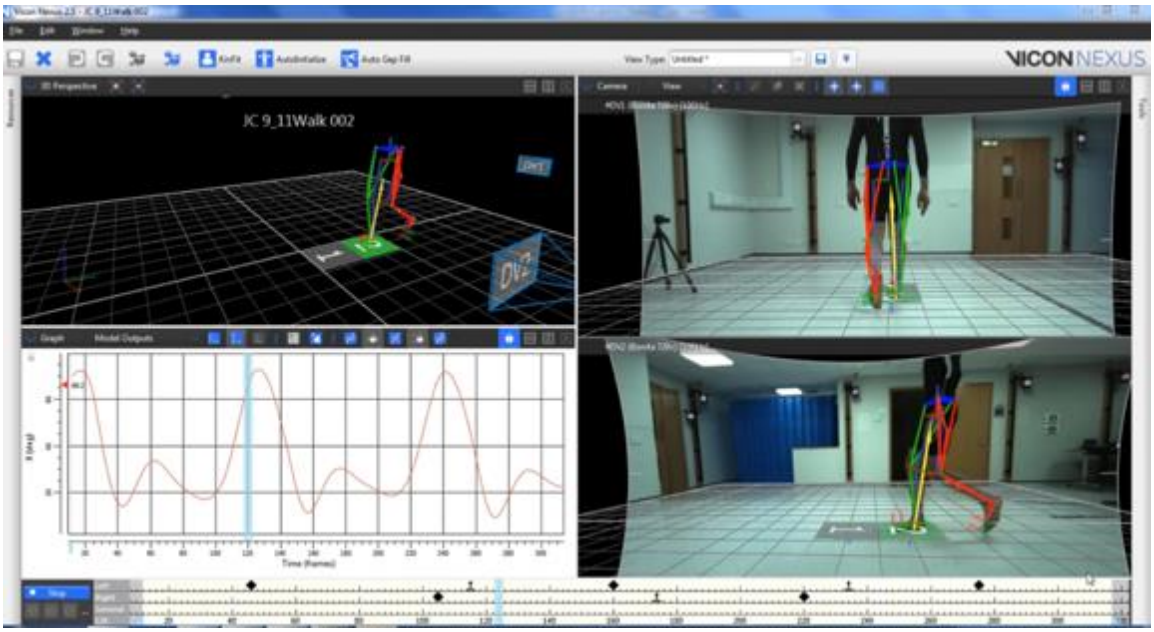

Figure 2.3: Vicon Optical Motion Capture System (image from [50]).

Non-optical MoCap systems such as Xsens [51] use inertial sensors worn on the body to continuously capture body movement (Figure 2.4). These sensors use a combination of gyroscopes, magnetometers, and accelerometers to capture both linear and rotational movements. Unlike optical systems, non-optical systems do not require external cameras and markers to be in continuous view of each other, and thus occlusion is not an issue. Instead, body movement data is collected through the body-worn sensors alone. This also allows data collection to essentially occur in any location and is not limited to in-lab experimentation. These body-worn sensors are typically integrated into a form-fit body suit that an individual wears during evaluation/testing. This approach can be useful for tracking *body* movement, but since it often requires a user to wear an additional garment or wearable band, it may not be the best approach to measure *garment* movement. Additionally, heavy sensors, as well as the fit of a garment, can change the way a garment moves with the body. This can introduce errors as the body may be moving in a different way than the inertial sensing garment moves with the body.

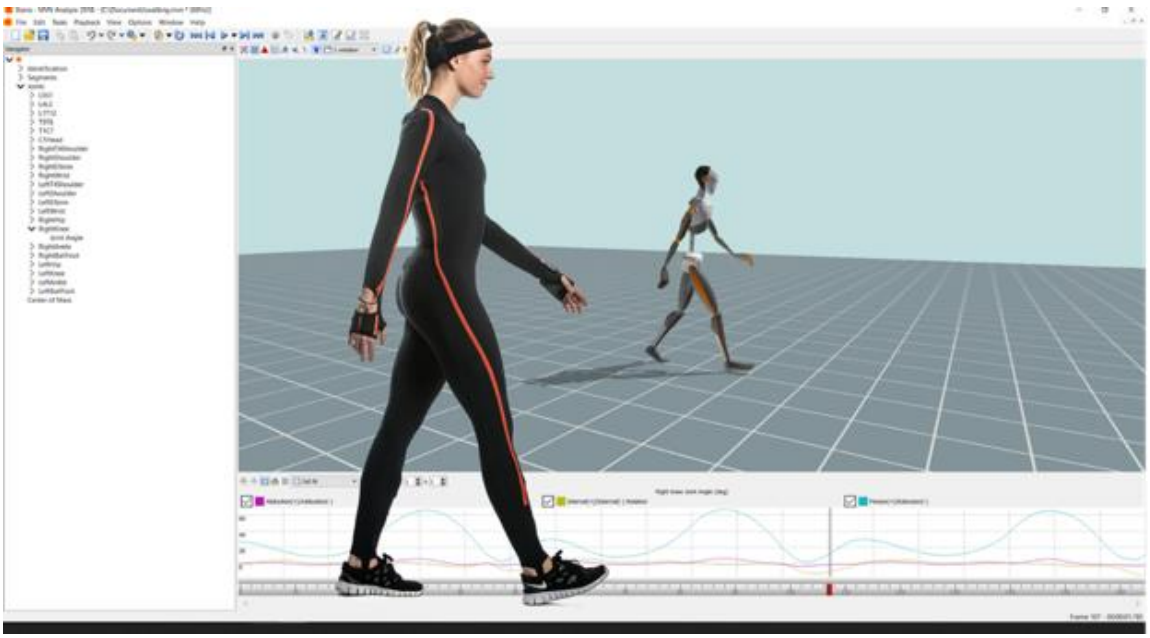

Figure 2.4: Xsens non-optical Motion Capture System (image from [51]).

MoCap has been used previously in the spacesuit community to evaluate human-spacesuit mobility, ROM and reach envelope [52] [53] [54] [55] [56] [57]. Reach envelopes are a basic measure to assess human mobility and important ergonomic considerations for spacesuit design and human-machine interfaces [52]. The reach envelope of a spacesuit is influenced by differences in human anthropometry and the strength of the wearer [52]. It is important to note that the differences in anthropometry can contribute to different suit fit. Therefore, differences in suit fit (and design) will likely have an impact on reach envelope. Abercromby [52] and Kobrick [57] have used MoCap data to capture ROM of an individual in suited and unsuited conditions to evaluate the reach envelopes.

Abercromby [52] evaluated the reach envelope of the Mark III spacesuit to better understand suit and rover interfaces to accommodate crewmembers. As expected, it was found that the suited condition restricted reach capabilities. Comparing suited and unsuited conditions, the medio-lateral reach was not significantly affected but the antero-posterior and vertical reach was significantly affected. This quantified volume reach data provides important information that can be used to inform the design process of vehicle development.

Kobrick [57] noted important factors to consider when using MoCap to capture ROM data across participants. It is important to ensure that specifics in the protocol in exactly how participants perform movements should be clearly detailed and communicated for consistency in testing across participants. For example, the difference between ending arm reach at the participant's maximum amount versus the when the arms are extended straight out can lead to inconsistencies. Clear communication and explicit protocols on detailing experiment movement can increase consistency in movements performed between participants.

Motion data can be captured in various ways and it can be unclear if data between different method sources can be analyzed/evaluated together. Aitchison [53] compared the feasibility of analyzing two-dimensional photogrammetry and three-dimensional

MoCap data that NASA has previously collected. The total ROM for different joint motions were compared between data types. It was found that although the comparisons were considered to be statistically significant, it is not recommended to be used practically as the methods in which the data is captured is quite different. For example, two-dimensional photogrammetry cannot accurately capture three-dimensional movement, which is important for joint angles that have a high multi-rotational nature like the shoulders and hips. That said, it is not recommended to use previously captured three-dimensional MoCap data if only a two-dimensional photogrammetry equipment is an available current resource for evaluation. The data in comparison should match the equipment that is currently available for evaluation.

As discussed, MoCap systems have many important advantages that permit tracking of three-dimensional movement that can be used to inform the development and design of systems (both wearable and non-wearable). For body-garment evaluations (using an optical system since non-optical systems are not suitable for this type of assessment, as previously discussed), two separate data captures – 1) markers on the body, and 2) markers on the garment – need to be taken since the garment would occlude body markers from cameras. Since human movement is variable, a manikin-based approach is required for accurate comparison.

There are limitations with each MoCap system that should be considered if using, including marker occlusion for optical systems and accuracy of data for inertial systems. They also are a time- and equipment-intensive approach, limiting their feasibly and use for movement assessments.

2.3 Wearable Sensor-Based Fit Assessment

Wearable sensors are electronic measurement devices that interface with the human body to provide quantitative information on different body characteristics. They are useful in many domains such as medical, fitness, gaming, robotics, defense, product development, and aerospace. A variety of sensor types exist, ranging from force/pressure/contact sensors, temperature sensors, optical sensors, accelerometers, gyroscopes, magnetometers, heart rate sensors, and pedometers.

Generally, wearable sensors can be defined as sensors that are integrated with a wearable object (e.g., clothing or accessory) or mounted directly onto the body surface (e.g., skin). In either case, they are sensors that are used on the *body*. Wearable sensors range in size and material composition. They can be used to obtain objective, quantitative data for body-related assessments. Recent development and advancements specifically in wearable sensors have increasingly focused on shifting from film-based (hard) sensors to more textile-based (soft) sensors. These sensors are fabricated using similar materials (textiles) as clothing, which offers great advantages in terms of both wearability and integration into clothing. The difference in these textiles compared to traditional textiles is that they are conductive – often by means of coating or plating the fabric or yarns with a conductive element – which allows the flow of electricity and enables sensing capabilities. Textile sensors can be integrated directly into a garment, which allows them to be very close to the body, and they are often conformable to the human body, flexible, and low-profile.

Wearable sensors can be used to obtain objective, quantitative data for body-spacesuit evaluations. There have been different approaches that have utilized this technology, particularly with force/pressure sensing and kinematic sensing. The following sections discuss wearable sensors capable of understanding body-wearable system interactions with a specific focus on spacesuit applications, followed by an overview of some of my previous contributions for wearable sensing.

2.3.1 Inertial Measurement Unit Sensors

An inertial measurement unit (IMU) sensor is a technology that affords tracking of human motion and has been widely used in many domains, including assessment of human-spacesuit interaction. For example, IMUs have been previously used to inform various aspects of body-suit kinematics by measuring joint angles [58] [48] [10] [54] and cadence [59]. IMU sensors can be used to characterize the kinematics of both the human body and spacesuit at the same time.

For example, Bertrand [58] placed IMU sensors in corresponding locations on both the body and the suit to enable elbow and shoulder joint angles to be measured during a set of upper-body movements (Figure 2.5). Results show differences in the kinematics of the body and the spacesuit while the suit was pressurized.

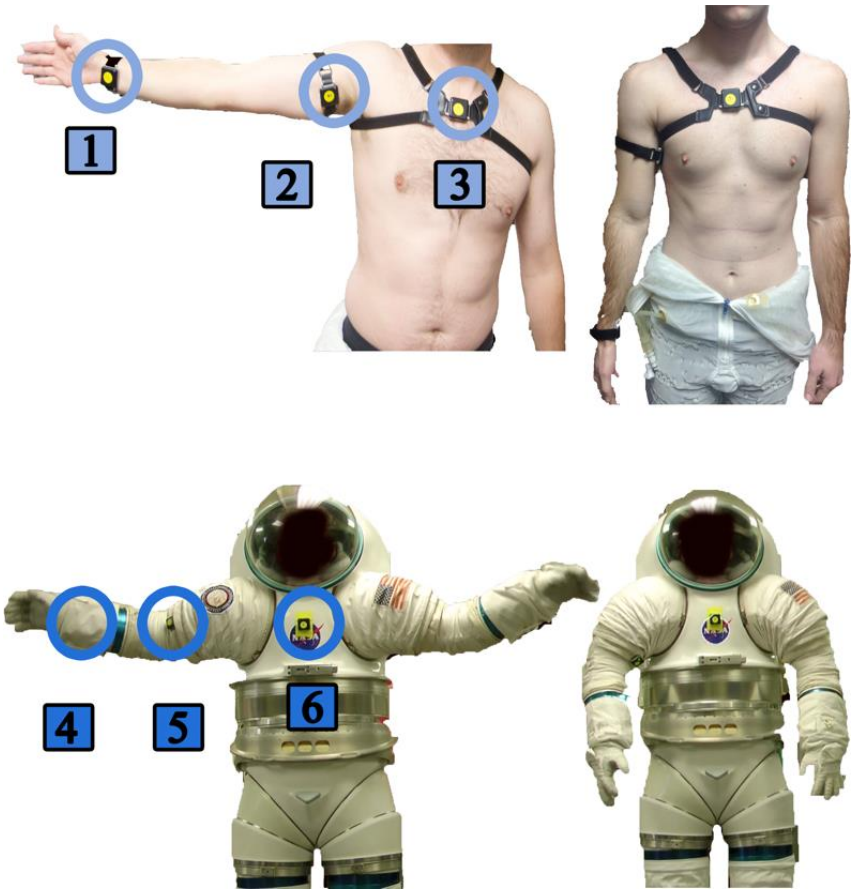

Figure 2.5: Corresponding IMU sensors place on the body and the spacesuit (image from [58]).

Similar to previous wearable sensing with pressures/forces, these efforts have also primarily focused on the evaluation of upper-body movements, since that has traditionally been the body region that requires the most amount of movement to carry out essential tasks. These types of wearable sensors are useful for measurement body and suit movement; however, they are not able to measure force (or contact) of specific isolated points between two surfaces (body and suit).

2.3.2 Strain Sensors

Textile-based strain sensors (StretchSense [60]) have been used to evaluate lumbar motion and angles inside of a spacesuit and predict torso shape [61] [62] [63] (Figure 2.6). Microgravity can have various negative effects on a human, one of which being a decondition effect on the spine. This spinal effect can increase risk of injuries and complications. These flexible strain sensors can be used to obtain information on the lumbar kinematics inside of the spacesuit, based on skin deformation patterns, to inform preventative measure decisions and improve spacesuit design. StretchSense sensors have positive aspects, such as being low profile and flexible, which allows them to be adhered directly to the body or integrated into clothing. This study focused on the validity of sensing lumbar kinematics using wearable sensors and results showed them to be useable with reasonable accuracy and may be used to measure biomechanical movement inside of the spacesuit, which can be influenced by suit fit.

Figure 2.6: Textile-based strain sensors (StretchSense™) (left), diagram of sensor placement on back (middle), static postures (right) (image from [63]).

2.3.3 Force and Pressure Sensors

Force and pressure sensors have been used previously to understand specifics of body-suit interactions [48] [10] [49] [64] [65]. The upper body has been the main source of movement required while performing EVA as it has primarily involved microgravity tasks, such using hands and arms to perform service tasks outside of the International Space Station (ISS). However, as planetary and terrain exploration become increasingly more dominant with the Artemis program, adequate lower body suit mobility is imperative, since the legs and feet will be used more. As such, most of these studies focus on specific upper-body areas that have previously been of high interest. In previous research, the hands and shoulders were identified as the highest reported areas for crewmembers to experience symptoms and injuries [9]. The following studies evaluated areas that are commonly reported for discomfort and injuries.

Anderson [48] [10] and Hilbert [49] focused on sensing the shoulder/arm area (Figure 2.7) while wearing the HUT. A system of both high- and low-pressure sensors were used to sense body-suit pressures in different shoulder and arm locations during a set of tasks focusing on upper-body movements. A high-pressure sensor mat (Novel) was used to detect pressures between the shoulder and the HUT. Low-pressure sensors (Polipo) were developed for this study to measure pressures between the body's arm and the soft goods

arm suit component. These developed sensors are made using a polymer with a microfluidic channel that contained conductive metal. Sensors were mounted to a garment using hook-and-loop fasteners (Velcro), which can be advantageous for quick arrangement of new sensor placement on the body. However, it may not be the most robust method for garment-sensor attachment. Identifying potential hazards of the sensing system to test subjects was among the important lessons learned, which was considered to be acceptable. This research enabled sensors to be evaluated in the suit environment. It was found that sensor durability in the suit environment was a limitation and that future work could benefit from improving the sensor-wiring system and sensor material. Specifically, improving sensor wiring to be able to withstand friction and repeated bending is advantageous. Additionally, it was noted that advancements in smaller and stretchable sensors may have advantages for suit testing.

Figure 2.7: High- and low-pressure sensor systems diagram (left), low-pressure sensor system implemented into garment (right) (image from [48]).

Amick [64] and McFarland [65] focused on evaluation of the hands within the suit gloves (Figure 2.8). Amick [64] used multiple sensor types (force sensitive resistor (FSR), strain gauge, thermocouple, humidity sensor, and Laser Doppler Perfusion Monitor (LDPM)) in a sensor glove to measure both physical and environmental variables during functional tasks. FSRs were used to measure finger contact forces and strain gauges were placed on the fingernails to measure cumulative strain. One of the functional tasks involved subjects to press a button by pushing on a force plate. For FSR results it was found that

measured forces were lower than the observed force plate reaction forces, which could be due to a variety of different factors such as calibration method, tissue deformation, FSR sensor deformation, and force transfer from pressurized (stiff) glove. FSRs were calibrated on a flat surface (manufacturer's specifications); however, hand/finger geometry is complex and these film-based sensors need to conform around the complex curvatures of the fingers. It is possible that sensor deformation (from fitting sensor to the finger curvature as well as tissue deformation during functional tasks) may have altered FSR data. To investigate these potential sensor effects, a plastic puck the size of the sensing area was placed under the FSR to provide a hard sensing surface (similar to the recommended ideal sensing environment). Preliminary results from this indicate that FSR and force plate forces have consistent force values.

McFarland [65] also used a sensor glove with various types of sensors (FSRs, strain gauges, thermocouples, relative-humidity sensors) to quantify and understand physical parameters on the hand. The aim of this study was to evaluate the feasibility of using small sensors to track various physical parameters such as forces on the fingers, skin temperature, humidity, and fingernail strain in a pressurized glove during NBL training. It was found that force data collected during this experiment was higher than previously reported glovebox test data. For some tasks, such as grabbing and opening a tool bag handle, an excess of force that should be required to perform the task was measured. This is hypothesized to be a result of the pressurization and resulting tactile loss in that environment, which can lead to overcompensation. Other key lessons learned from this study that could benefit future studies include better strain relief for sensor-lead connections and improved wire management. These are common challenges associated with wearable sensing and could be improved with textile-based sensors, where the sensor lead can be directly integrated with the sensor through stitching, as well as the sensing garment itself. Additionally, sensor leads can be directly integrated into the garment through stitching of conductive thread, reducing entanglement of multiple detached wires on the body that that have the potential to introduce negative sensing effects.

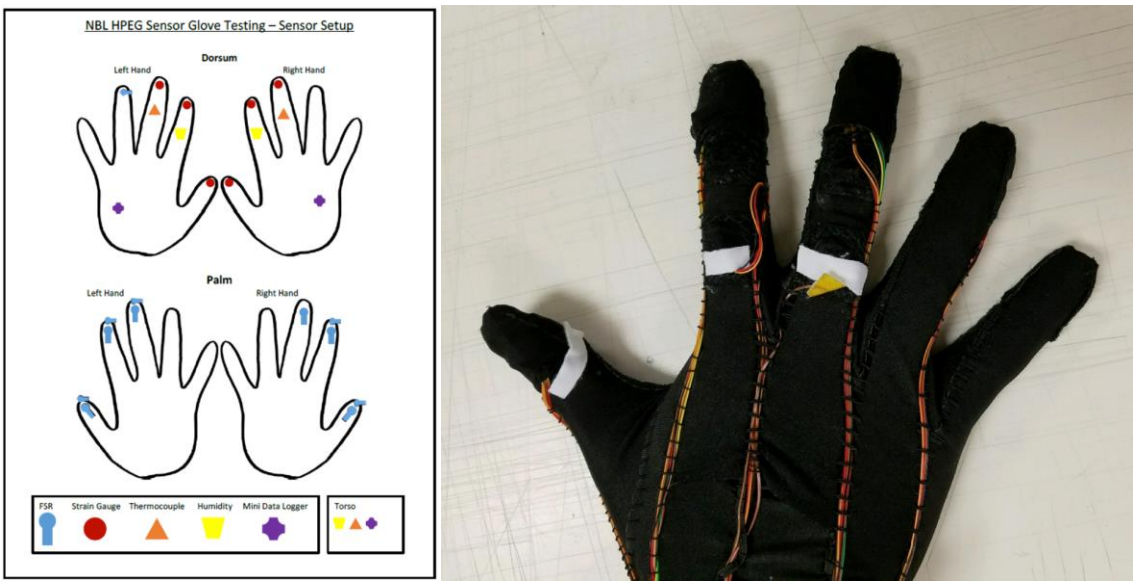

Figure 2.8: Sensor glove setup (image from [65]).

Since most studies using wearable sensors to quantify human-suit interactions to date have focused primarily on upper-body locations, current knowledge is limited to only those areas. As tasks shift from mostly upper-body movements to include more lower-body movements for planetary exploration, there is an important need to understand and quantify how the suit fits on a body during various dynamic movements for optimal performance and crewmember safety. Further, it is important to understand the effects that different body shapes and sizes have on suit fit to reduce risk of injury and optimize wearing comfort.

Some of these studies have performed testing in both pressurized and unpressurized conditions, as this is an important parameter that can change suit fit. For example, in a study on angular ROM and reach envelope for human-suit evaluation by Kobrick [57], it was noted that shoulder degradation occurred between unpressurized and pressurized conditions in the Flight Opportunities Program (FOP) IVA spacesuit that was tested. During this evaluation it was found that the arm was pushed forward from the natural shoulder rotational point and the shoulder of the spacesuit was higher in the pressurized condition compared to the unpressurized condition. Additionally, an expected occurrence was a decrease in angle size with suit pressurization. Testing in a pressurized environment is especially important for evaluating soft good components of the spacesuit

as pressurization changes the rigidity and form of these soft suit components. Testing in a pressurized environment for hard good suit components, while still important, is less crucial while measuring body-spacesuit interaction since the hard good material does not change stiffness or shape with pressurization. Testing in an unpressurized condition is a useful and feasible first step especially for testing isolated hard good components, such as the HUT or the LTA brief, that experience fewer mechanical changes when pressurized. Ultimately, it is important eventually to test the entire spacesuit system to fully understand how different components interact with each other and influence overall suit fit, and to test in a pressurized condition since that is the environment tasks will be performed in.

Many sensors used in previous studies have been commercially available off-the-shelf sensors. These sensors are typically composed of film-based materials and are normally not textile-based materials made from actual fibers. Though films can be considered a type of nonwoven fabric, for this on-body sensing research, a focus will be placed on textiles made from fibers since these are the types of textiles commonly used to fabricate clothing and worn on the body. For wearable sensing scenarios, using a material that mimics clothing that is traditionally worn on the body is important for both wearability and sensor interactions with the body. It is ideal to have a sensor that is comfortable to wear on the body and next to the skin, conforms to the body's complex curvatures, and is flexible to move with the body during body movement. While commercially available, non-textile-based sensors have advantages and typically perform adequately when used in their intended sensing environments – a hard flat surface – using these sensors on the body – a soft non-uniform surface – can potentially introduce challenges, particularly in terms of wearability and sensor integration robustness. These issues often stem from the disparity between hard and soft materials, which can lead to connection issues [66] [67]. This disparity can lead to unusable/faulty sensors that become damaged prior to and during testing [10] – valuable lessons learned that can inform future testing. Textile-based sensors with conductive thread leads are an alternative approach to traditional film-based sensors with wire leads that can offer potential advantages by eliminating this

inherent issue of hard-to-soft connections with wearable sensing, which may improve sensor-lead connection durability and robustness.

On-body and garment-integrated force and pressure sensing can introduce new contaminating variables that can affect accurate sensing. Force sensors can be susceptible to responding to both textile/garment and body movement and deformations, as well as externally applied forces. For pressure sensing, the area of applied force needs to be known, which (depending on the sensor size) can be difficult to quantify or assume, especially for contact areas that are occluded. Additionally, force and pressure sensor calibration to account for variability in geometry of the body's surface and differences in tissue compliance as well as sensor characteristics like drift can influence sensor responses. Typically, these sensor types also require two leads per sensor, which can take up more space on a garment and add up quickly in higher- resolution sensing contexts. Although force and pressure sensing can provide richer information by measuring a range of forces/pressures, it may come at a cost of reduced accuracy.

Contact sensing is a simpler sensing method, using a binary approach, that is less susceptible to the above mentioned challenges of force and pressure sensing. Although it does not provide information that is as rich as force and pressure sensing, different contact forces can be measured by calibrating the sensor response using different manufacturing approaches. Due to the reduction in contaminating variables, contact sensing may be more accurate in quantifying contact between a garment and a body. Further, depending on the configuration of the contact sensing system, contact sensor electrodes may only require one lead per contact electrode, which can reduce the amount of wires needing to be managed overall.

2.4 Prior Work

I have made prior contributions to wearable, textile-based force/contact sensing and body-wearable system interaction. The next subsections will summarize previous related research I have done that precedes this study.

2.4.1 Human-Garment Contact Sensing

Some of my first body-garment contact sensing research focused on developing a wearable sensor system to measure the contact between the body's skin and a garment [68] [69].

This system was based on a switch-like mechanism to detect contact between a grid-electrode patch on the inside of a garment and the body skin surface (acting as the other electrode). In this investigation three main variables were evaluated for their influence on the measurement of body-garment contact: 1) conductive patch materials, 2) applied force, and 3) patch sizes were tested within the body/garment interface. Conductive patch material results showed that 7 out of the 8 tested materials (with the exception of 1 material, which contained the sparsest surface area of conductive material) facilitated a voltage response in the presence of body contact that could be viable for detecting contact between the body and a garment. However, preliminary tests revealed that materials with lower resistivity and more rigid structure facilitated a smoother signal with less noise, which correlated more closely with the input signal. Applied force results showed that the amount of force between the sensor and the body affects the response of the system. However, this force testing was done with a set of weights placed on the sensing system (static force testing), and would benefit from more rigorous force testing by applying controlled dynamic forces to measure with sensor resistance. All patch sizes with the exception of the smallest size tested (0.3175 cm) were effective in measuring body-garment contact.

The smallest conductive patch diameter effective for body-garment testing was preferred, to minimize the effect of the senor implemented into the body-garment system. A 0.635

cm diameter conductive hook fastener sensor was subsequently used, based on bench testing, to implement this method in a pilot evaluation of Liquid Cooling Garment (LCG) fit.

The Liquid Cooling Garment (LCG) / Liquid Cooling and Ventilation Garment (LCVG) is one of the first layers of the spacesuit, closest to the human body, which relies on contact with the body to achieve thermoregulation (Figure 2.9). The conductive patch electrode method was used to evaluate areas of contact and non-contact of the LCG in the body's right-torso region. A modular textile-based contact sensing grid was developed, which was implemented on the inside of the LCG for dynamic body contact-sensing.

Figure 2.9: LCG pulling away from and coming out of contact with the body near the torso while wearer is slightly bending down.

A grid of six analog sensors (maximum amount for microcontroller used) was integrated into the right torso region of the LCG for testing (Figure 2.10). Eight functional tasks/movements were performed to test body-garment contact. Average contact of sensors for each movement/trial is illustrated and results show distinct differences in body contact for each sensor during each movement (Figure 2.11).

Figure 2.10: Grid of contact electrode sensors implemented on inside of LCG for body-garment testing.

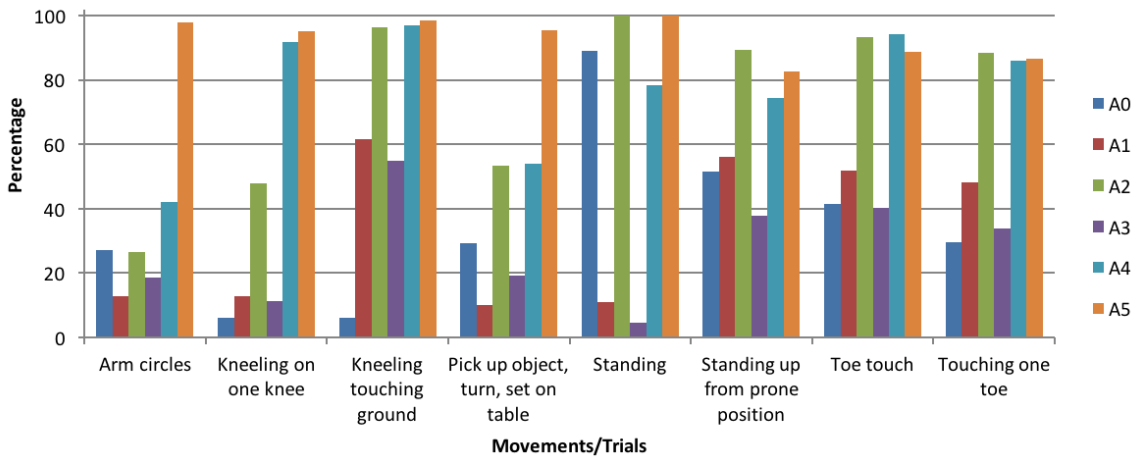

Figure 2.11: Percentage of contact for each movement/trial form dynamic body-LCG testing.

With this approach the contact sensing method was not validated with another method to ensure physical contact was actually occurring during electrical contact. This current study aims to validate this method by using additional approaches to measure contact to verify the electrical contact system. Force testing also was done using a set of hand weights, which has limitations as a complete range of forces is not tested. Future Instron testing could improve the quality of data obtained for force testing. This approach also used the body's skin and rough conductive patches on the inside of a garment (LCG) touching the skin to measure contact. This sensing scenario is not always feasible or ideal, as the conductive hook patches can cause redness and irritation against the skin, and it adds more bulk and rigidity compared to traditional textiles that are lower profile. Though the smallest conductive patch feasible for sensing body-garment contact was used so that it would minimize impact of integration on the garment, it would be advantageous to explore this approach using a more traditional, flexible textile that is common to everyday clothing to minimize bulk and rigidity in the wearable sensing system. Lastly, it is not always possible or appropriate to rely on contact with the skin for sensing. It is important to investigate the feasibility of this contact sensing approach between two layers of a wearable system.

The work described here extends this concept of textile-based contact sensing. More comfortable, smooth, and lower-profile sensors are developed, sensors are evaluated using a more controlled dynamic method of force testing (Instron), a wearable sensing garment is developed specific to the sensing context (facilitating easy donning/doffing of sensors and body contact sensing without requiring bare skin), and contact sensors are compared with other methods to measure contact (force sensors and MoCap).

2.4.2 Manikin-Garment Contact Sensing

Expanding on the previously described contact sensing work, this method was further developed in collaboration with colleagues to focus on a manikin-based approach of measuring contact between the body (manikin) and a garment using a similar method [70]. In this approach a contact sensing manikin (Figure 2.12 and Figure 2.13) was developed in order to determine specific locations of contact on the body (manikin) surface, which previously was not possible. Though manikins are more limited in anthropometric variability compared to humans, they are an alternative to human-based testing offering advantages in precision for controlled experimentation. Two different prototype garments were developed and used to evaluate garment fit (body-garment contact) during repeated donning/doffing.

Figure 2.12: Contact sensing augmented manikin (front and back).

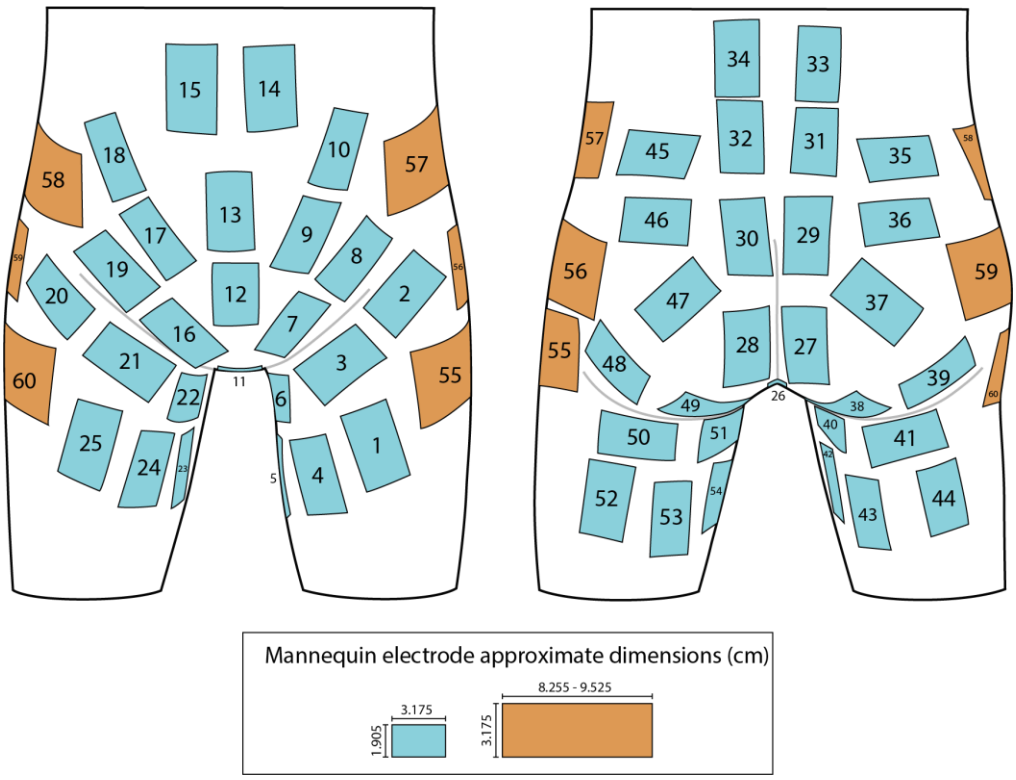

Figure 2.13: Contact sensing augmented manikin electrode placement, dimensions, and numbers.

To facilitate electrical contact sensing, conductivity must be applied to both the body (human or manikin) and the garment to allow an electrical connection to be made. For higher-resolution sensing, isolated electrical contacts are needed on one or both surfaces. Therefore, various materials and approaches were investigated for their utility in electrical contact sensing, both for manikin-integrated electrodes and for garment-integrated electrodes. To characterize the electrical connection of each material, flat prototypes were initially developed to evaluate the feasibility, and preliminary bench testing was performed to evaluate electrical contact parameters. Subsequently, the most promising conductive materials were implemented as electrodes in a developed garment and manikin, which was evaluated in a pilot test of body-garment contact using two different garment forms. Due to hardware limitations, isolated electrodes could be tested only on one of the two surfaces, therefore the multiplexing approach was not evaluated. Since isolated garment-side electrodes were developed in the previous study, this study focused on developing isolated body-side electrodes for testing with a monolithic garment-side electrode. Two prototype garments with different fit properties and electrode materials were developed and tested in conjunction with a silicone-based manikin augmented with an embedded electrode array.

2.4.2.1 Garment-Electrode Bench Testing

In this study, two alternative methods for creating garment-side electrodes were investigated by fabricating a garment out of an entirely conductive textile and by applying conductive ink to a non-conductive textile surface. The first approach affords testing of garment patterns – for example, that would subsequently be made from different fabrics. The other approach affords testing of ready-made garments but doesn't require the attachment of an additional textile layer.

Similar to the manikin-side electrode, initial bench tests were performed with eight garment electrode materials to evaluate their feasibility for use in this contact sensing system. Materials that facilitated low-resistance electrode connections, good repeatability, and were sensitive to low contact pressures were subsequently used to make two prototype garments for manikin.

During tabletop testing not all garment electrodes were able to make electrical contact with the carbon fiber electrode. Results from the materials that were able to make contact are plotted in Figure 2.14 and listed in Table 2.1 for each pressure condition. Resistance values for the textile electrode (Material 8) are considerably smaller than other materials tested and visually are more difficult to see in the plot image. More resistance reflects a weaker electrical connection and no connection (open loop referred to as 'OL') is indicated with infinite resistance.

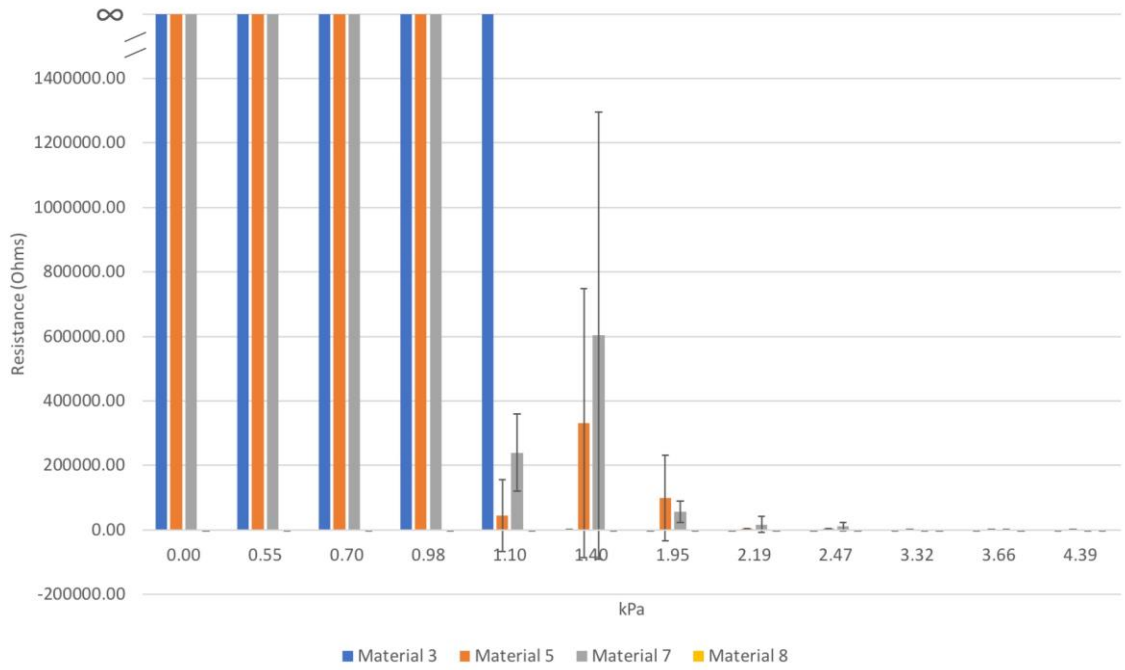

Figure 2.14: Average and standard deviation measured resistance under each pressure condition of garment electrode 3, 5, 7, and 8.

Table 2.1: Garment electrode 3, 5, 7, and 8 average resistance in ohms and standard deviation (SD) for each pressure condition (kPa).

Pressure Applied to Material (kPa)	Material 3		Material 5		Material 7		Material 8	
	Average (Ohms)	SD	Average (Ohms)	SD	Average (Ohms)	SD	Average (Ohms)	SD
4.39	3.88E+01	5.31E+00	1.63E+03	8.72E+01	1.93E+02	1.86E+01	2.77E+01	2.88E+00
3.66	8.34E+01	6.63E+01	2.57E+03	1.56E+02	7.54E+02	8.37E+02	2.91E+01	5.67E+00
3.32	2.88E+01	3.20E+00	2.28E+03	1.56E+02	3.13E+02	1.50E+02	2.52E+01	3.55E+00
2.47	5.38E+01	1.92E+01	3.09E+03	3.66E+02	1.04E+04	1.28E+04	2.86E+01	1.97E+00
2.19	5.95E+01	8.87E+00	3.46E+03	8.43E+02	1.62E+04	2.50E+04	3.04E+01	3.93E+00
1.95	2.64E+02	1.87E+02	9.85E+04	1.33E+05	5.60E+04	3.25E+04	3.29E+01	1.32E+00
1.40	4.41E+02	2.95E+02	3.32E+05	4.17E+05	6.03E+05	6.93E+05	3.71E+01	4.56E+00
1.10	OL	OL	4.43E+04	1.11E+05	2.40E+05	1.21E+05	5.04E+01	4.61E+00
0.98	OL	OL	OL	OL	OL	OL	4.27E+01	4.50E+00
0.70	OL	OL	OL	OL	OL	OL	3.85E+01	7.68E+00
0.55	OL	OL	OL	OL	OL	OL	4.62E+01	6.93E+00
0.00	OL	OL	OL	OL	OL	OL	4.02E+01	4.30E+00

2.4.2.2 Prototype Garment Conditions

The developed contact-sensing manikin was tested in a proof-of-concept evaluation to explore the feasibility of manikin-based contact sensing using two different garment-side electrode paradigms (style/fit and sensing material) (Table 2.2). Since no accessible reference measure existed for body-garment contact, two contrasting garment forms (one with close-fit, "second-skin" contact (Figure 2.15) and one with loose-fit contact and elasticized waist/leg openings (Figure 2.16)) were used in combination with visual analysis of body/garment contact during the evaluation period.

Table 2.2: Prototype garment conditions.

Sensing Material	**Garment Style/Fit**
Fully-conductive	Form-fit
Selectively-conductive	Loose-fit

Figure 2.15: Form-fit contact sensing garment (front and back) on augmented manikin.

Figure 2.16: Loose-fit contact sensing garment (front and back) on augmented manikin.

For each garment condition, the garment-side electrode was monolithic, while the manikin-side electrodes were electrically isolated and individually addressable (Figure 2.17).

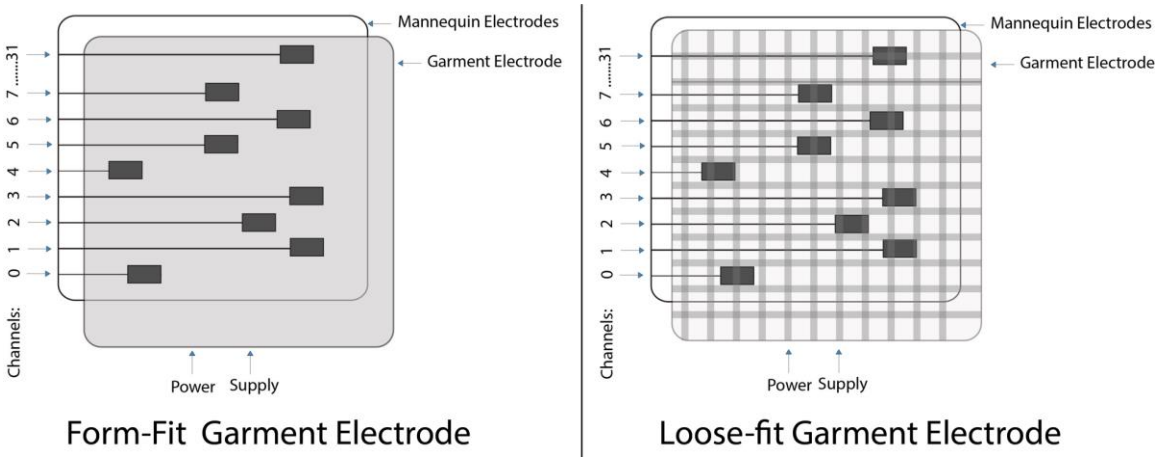

Figure 2.17: Contact-sensing schematic of isolated body (manikin)-side electrodes with monolithic garment-side electrodes: form-fit garment (left), loose-fit garment (right).

The fully conductive, form-fit garment was made entirely of a conductive fabric (Less EMF), so that if a manikin electrode comes in contact with any area of the garment, contact would be made. The selectively conductive, loose-fit garment was created by painting a grid-shaped electrode using conductive ink on the textile, as well as in elasticized garment opening areas (waist and leg openings). The form-fit garment was expected to make contact with the manikin over the entire coverage area. While the loose-fit garment was expected to make contact with the manikin around elasticized garment openings (waist and legs) and intermittently contact in remaining garment locations.

Results from the manikin and prototype garment testing (Figure 2.18 and Figure 2.19) generally supported expected areas where contact and noncontact would likely occur for each garment fit, except for concave shapes on the manikin surface and faulty sensors.

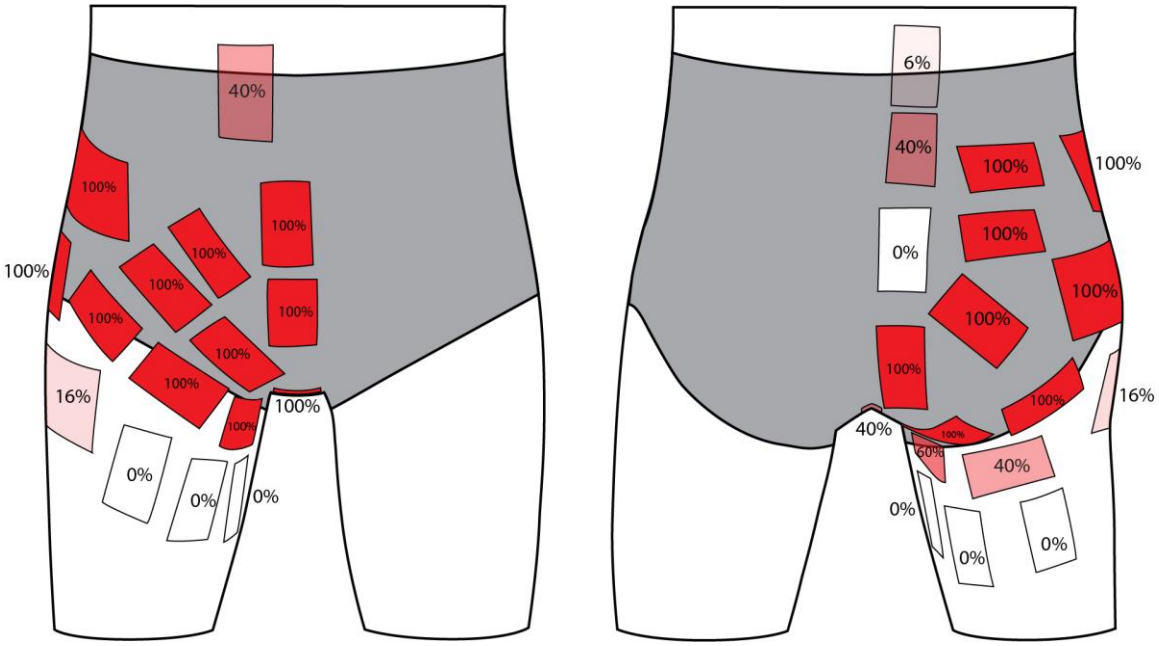

Figure 2.18: Form-fit garment percentage of contact (front and back).

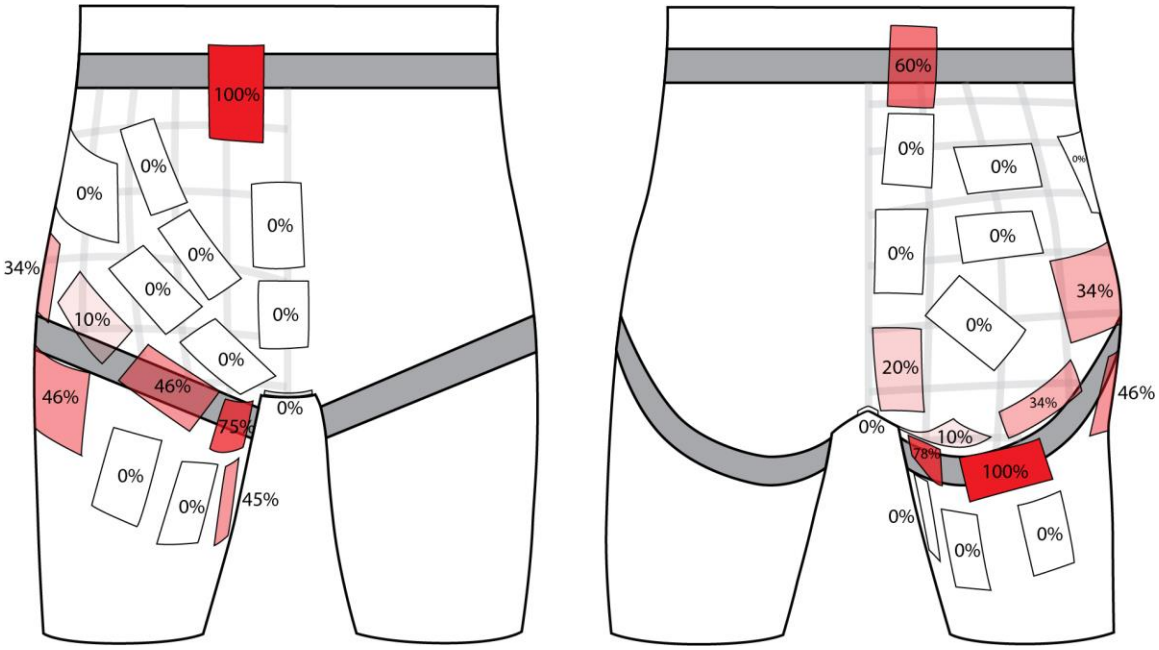

Figure 2.19: Loose-fit garment percentage of contact (front and back).

Knit and non-woven textile structures had different effects on contact sensing. The conductive knit textile electrode had significantly lower resistance than the ink electrode, which alters the voltage level in the contact state. Its conductivity is much more uniform across the surface than the applied ink electrode. During garment development, the non-woven loose-fit garment (ink electrode) was not reliably able to make contact with the manikin electrodes in all garment locations, due to poor saturation of the ink application. The conductive ink was iteratively re-applied to better saturate weak or broken connections on the garment surface. However, the ink electrode was non-uniform in conductivity and tended to be brittle. The roller-ball process of application may also have affected the quality of the applied electrode, and the ability to fully saturate the textile.

It was found that contact sensing is feasible using this electrical method to evaluate the relationship of a body form (manikin) to a garment. Location of garment-to-manikin contact can be identified by the individually addressable manikin electrode locations with both an entirely conductive garment electrode and a non-conductive garment with surface-applied electrodes. However, a key limitation of this evaluation is again the lack of a reliable reference measure. Here, visual analysis was used to confirm that areas in physical contact showed electrical contact, but this is not a robust method of comparison. A more precise reference measure would be needed to fully validate the accuracy and repeatability of the augmented manikin and garment electrodes. Additionally, only static garment fit (contact) was measured during repeated donning/doffing. Dynamic fit was not evaluated with the initial prototype manikin developed here, but as the manikin was fabricated with a flexible silicone base it is feasible that it could be animated with a robotic armature. Future work would benefit from developing a method that would evaluate both static and dynamic fit with an augmented manikin to enable contact-based fit evaluation while the body is in motion.

2.4.3 Textile-Based Force Sensing

Related collaborative textile-based force and pressure sensing work has been explored [71]. In this study, an e-textile force sensing array was developed for on-body sensing. The sensor used to create this array is similar to the sensor developed in this dissertation work, and is composed of three main textile layers: 1) middle piezoresistive fabric sensing layer (Eeonyx/EeonTex Conductive Fabric [72]), 2) conductive fabric lead/electrode layer (with fusible interfacing fabric for stabilization) (Less EMF Stretch Conductive Fabric [73]), and 3) a stabilizing/protective layer (Fusible Featherweight Interfacing [74]) (Figure 2.20). The prior study investigated the challenges of textile-based sensing arrays through the assessment of two force-sensing array architectures: 1) isolated-cell and 2) connected-cell. Sensing arrays enable more information compared to individual, discrete sensors and could be used to sense human-spacesuit interaction for larger body areas. In this study, calibration and applicator testing illuminated challenges such as crosstalk and mechanical deformation of the sensing array, which resulted in inconsistent sensor responses and shorting of electrical sensor leads. These challenges can have a negative effect on the repeatability and accuracy of the sensor response.

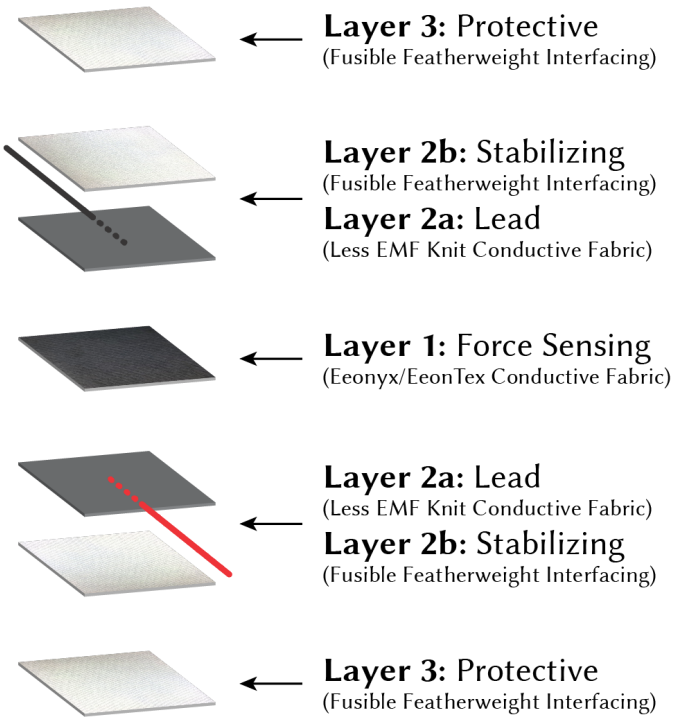

Figure 2.20: Exploded view of force sensor layers.

An isolated-cell (Figure 2.21) approach can help with unwanted mechanical deformation sensing effects but this approach requires two lead per sensor, resulting in numerous leads that can complicate wearability and on-body sensing, especially with a limited array surface area.

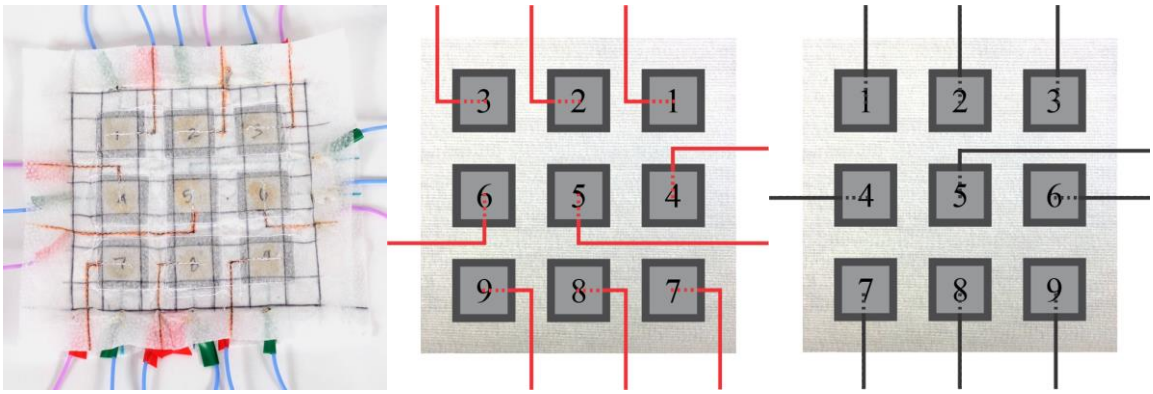

Figure 2.21: Isolated-cell array fabricated and illustration of top- and bottom-layer (inside view) schematic.

With a connected cell array (Figure 2.22), a multiplexing approach can be implemented, which greatly reduces the number of leads required for sensing. For example, this sensing array still contained nine individual cells; however, compared to the isolated-cell approach, leads were reduced by more than half (from 18 to 6 leads). The number of leads is able to be reduced using this approach since 3 cells are connected with one lead (Layer 2 in Figure 2.20), resulting in only 3 columns and 3 rows necessary for all 9 cells.

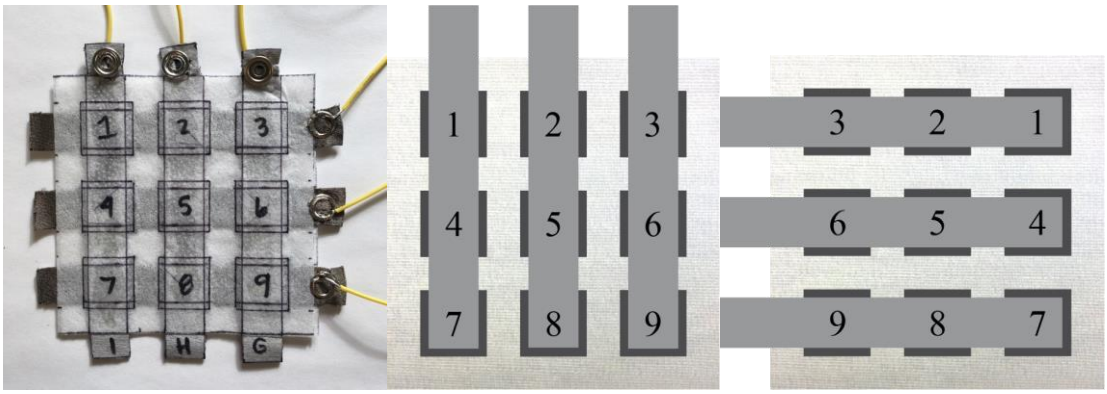

Figure 2.22: Connected-cell array fabricated and illustration of top- and bottom-layer (inside view) schematic.

Since a multiplexing approach with these textile-based sensors can lead to challenges discussed above, an array approach will not be used for this dissertation study and individual sensors will be used instead.

My previous work focused on characterizing force and pressure sensitivity of e-textile sensors as linear (analog) sensors, to measure a range of forces and pressures. However, this dissertation illuminates challenges for accurate analog sensing precisely on the body. For this dissertation study, both contact and force sensors are used. Contact sensors function using a binary, switch-like approach, measuring no contact or contact, rather than an analog approach that can measure a range of contact forces. Although (as illustrated in my previous work) force sensors are capable of a more detailed analog measurement of the amount of force, here they are used as a type of contact sensor (binary) by setting a simple contact-threshold, indicating clear periods of no contact and contact. The reasoning behind this approach is that using a simple binary threshold to detect contact may reduce the impact of the on-body and in-garment issues that degrade the accuracy of analog sensing.

Chapter 3

3 Sensor and E-Textile Sensing Garment Development

This chapter covers the design and development of the e-textile wearable sensing garment (Section 3.1 E-Textile Wearable Sensing Garment Development), as well as the brief suit component (Section 3.2 Lower Torso Assembly (LTA) Brief Development) that are used for testing. The e-textile wearable sensing garment section includes exploratory work done for both the design and development of the garment and sensor, as well as the integration for leads and sensors and lead management. The brief section includes the design and development of the brief using a 3D computer-aided design (CAD) software and 3D scanner, as well as the suit-side electrode.

3.1 E-Textile Wearable Sensing Garment Development

An e-textile wearable sensor garment was custom designed and developed to be used to evaluate contact patterns between an LTA brief spacesuit component mockup and a robotic manikin. The design and development of this e-textile wearable sensor garment includes two main parts, organized into the following subsections: 1) garment design and

development (Section 3.1.1 Garment Development), and sensor design and development (Section 3.1.2 Sensor Development).

3.1.1 Garment Development

This subsection describes the design specifications, features, process, and exploratory work involved in the design and development of the base garment used for sensor integration. Sensor design and development is described in the following subsection.

Since the goal of this study is to understand contact that occurs on the body, the garment needs to have a form-fit style and essentially mimic or act like a second skin on the body. The body area of focus for this study as an initial proof of concept/method is on the lower-body, in the pelvis and buttock region. Sensors which are described in the next subsection are integrated in the garment and concentrated around this body area. A lower-body legging garment was custom designed, patterned, and fabricated as a base layer for sensor integration to be used during testing. Since the garment utilizes a form-fit style, the textile used needed to have sufficient stretch to afford body movement and not restrict the manikin's movement. The textile used also needs to exhibit qualities of good elastic recovery to allow the textile to return to its original/natural, unstretched state after being deformed or stretched on the body. If a textile that has poor elastic recover were to be used, it may not maintain the intended size and shape of the developed garment and the textile/garment could get stretched out and remain in that state. This would generate a looser fit and could introduce variables like garment drift, which can lead to inaccurate data collection. Bunching or folding can also happen with a looser fit garment, also leading to potential sensing inaccuracies.

Knit textiles can achieve stretch through both the looping of the knit structure and through the fiber composition using an elastomeric fiber, such as spandex. When designing garments with stretch or knit fabrics, the specific textile properties must be known prior to patternmaking, as it informs the patternmaking process. Form-fit garments require at least 75% stretch, and textiles that fall in that category must also have

mechanical stretch properties enabled through the use of an elastomeric fiber (not just from the knit structure alone) [75]. A 4-way stretch single knit polyester/spandex blend textile (stretch in both the lengthwise (vertical) and crosswise (horizontal) directions) within the 'very stretchy' category (minimum 75% stretch in both textile directions) [75] was selected for use as the garment base material.

Non-form-fitting garments (often these types of garments may use non-stretch fabrics, but not always) use positive ease, which is an increase in pattern dimension relative to the dimensions of the body. Positive garment ease at minimum includes *wearing ease*, which allow things like donning/doffing of the garment and/or comfortable wear but may also include *style* ease, which is additional ease used to achieve a particular garment design. In contrast, form-fit garments with stretch/knit fabrics require use of negative ease, which is a reduction in pattern dimensions relative to the dimension of the body, allowing the textile to conform to the body surface. The properties of a specific stretch or knit textile, such as the stretch percentage, inform how much negative ease is required.

Previous work I have done with garment-integrated sensing for dynamic body movement has shown that garment anchoring is important to prevent garment drift and shifting and promote on-body sensing accuracy [76]. The developed garment here includes design features of garment anchoring at the two locations (garment openings – waist and ankle) where the garment is not naturally anchored. A silicone-backed elastic waistband on the inside of the garment around the waist/torso and stirrups at the hem of the legging around the ankles anchor the garment to these segments (Figure 3.1). A crotch gusset was included in the garment design to preserve mobility while wearing the garment.

Figure 3.1: Silicone-backed elastic waistband being fabricated and ankle stirrups to promote garment anchoring.

A traditional patternmaking and fit process (relying on expert judgement) was used to develop the base garment. Multiple base patterns were developed first to achieve the final legging pattern used for the base garment. The final legging pattern eliminates the side seam to minimize the number of seams on the garment – to reduce the potential for restricting body movement and to create a lower profile with less bulk from seams for sensor integration. Once the legging pattern was developed it was graded to accommodate the stretch of the base textile. Multiple fit prototypes were evaluated and necessary pattern adjustments were made during the fit process. A combination of virtual 3D and physical fit evaluations were used. A soft goods CAD modeling software (Optitex) was used to digitally model the garment on a human avatar to obtain an initial understanding of the garment fit and to inform alterations to the pattern as shown in Figure 3.2-Figure 3.4. Once fit was achieved virtually, physical prototypes were created and used for physical fit evaluations. The physical prototype and fit evaluations informed any necessary alterations which were made to the pattern. The final garment was constructed using extensible stitches (serge, coverstitch) to prevent restriction of body movement.

Figure 3.2: Virtual fit of the draft base legging pattern using a 3D soft goods CAD modeling software (Optitex).

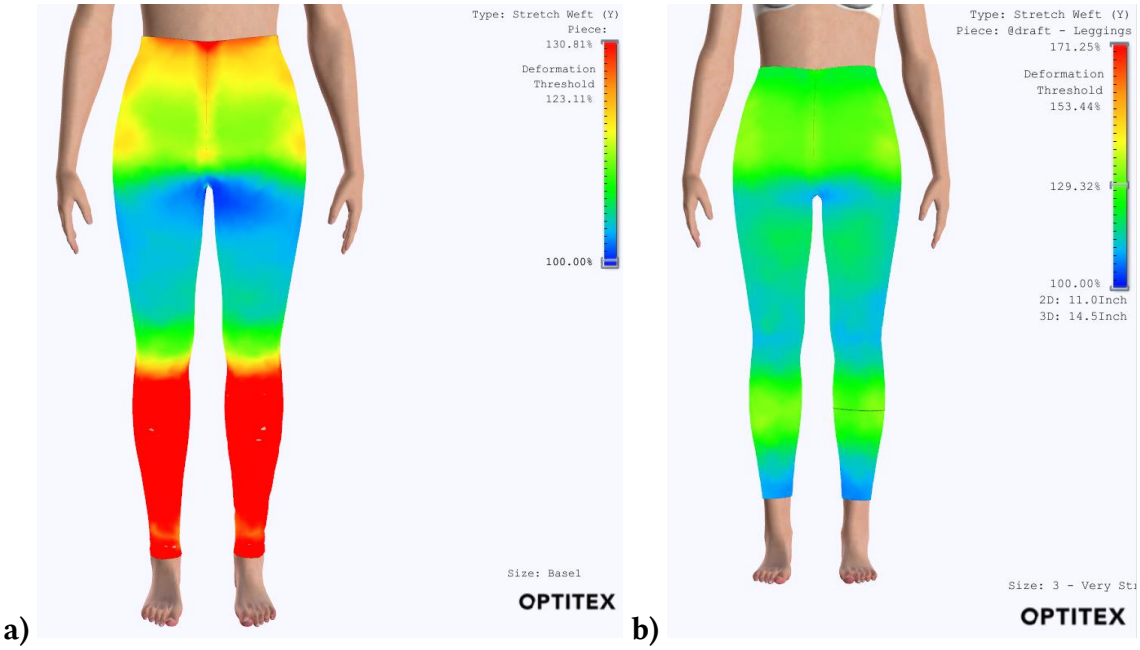

a) b)

Figure 3.3: Virtual fit assessment of the draft base legging pattern showing areas of stress/strain in the course (horizontal) knit textile direction, a) prior to draft pattern alteration, b) after draft pattern alteration.

Figure 3.4: Virtual view and draft pattern for e-textile sensing base garment.

3.1.2 Sensor Development

This subsection describes some of the exploratory work on design, development, and fabrication to inform choices for sensors and integration into the base garment. Two different types of sensors, *contact* and *force* sensors, were developed and used to measure contact/forces on the body. Pilot testing investigated interrelated variables such as: 1) sensor material structure and sensor size, 2) sensor-lead integration, 3) sensor-garment integration, 4) and lead/wire management.

3.1.2.1 Contact and Force Sensors' Principle of Operation

The *contact* sensors developed here are simpler in design and manufacturing compared to the force sensors and consist of a single conductive layer integrated into the sensing garment. The contact sensor has two separate sensing components or contact electrodes. These contact electrodes are typically located on the two surfaces of interest in measuring contact – commonly configured as 1) body-side electrode(s), and 2) wearable system-side electrodes(s) (Figure 3.5). Each contact electrode only requires one lead for an electrical connection.

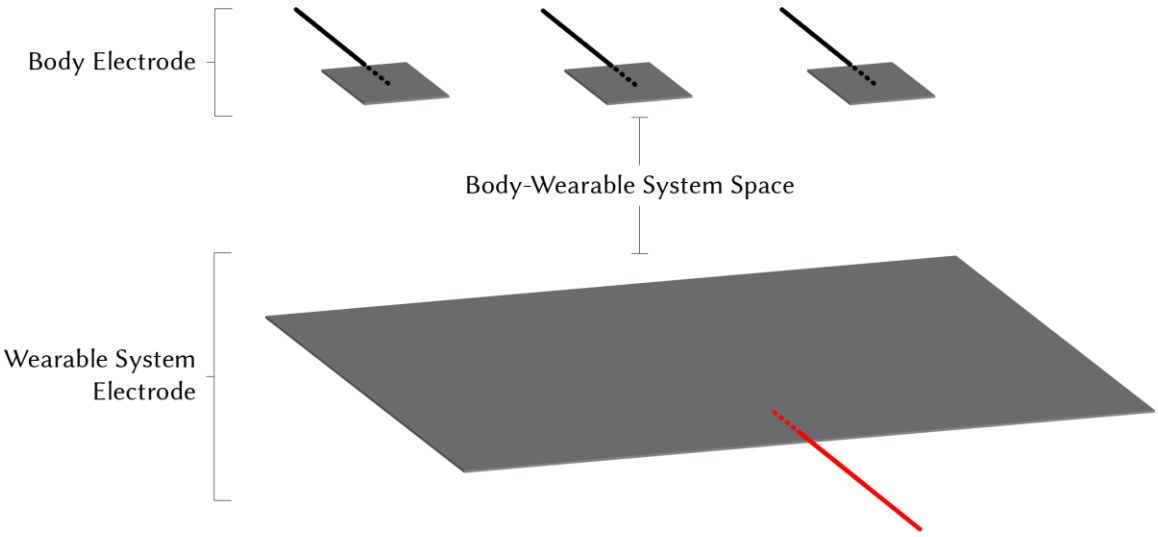

Figure 3.5: Contact sensor layup.

The *force* sensors here are made of a single force-sensitive material component but use a multi-layer system of both conductive and non-conductive textiles (Figure 3.6). The force sensor is made of three main layers/materials: 1) sensing layer, 2) lead layer, and 3) protective layer. The middle sensing layer that enables measuring a range of forces is a piezoresistive material that changes resistance with applied force. The piezoresistive textile used for force sensors in this study is a non-woven 'conductive fabric' (NW170-PI) by EeonTex/Eeonyx [72] (Figure 3.7).

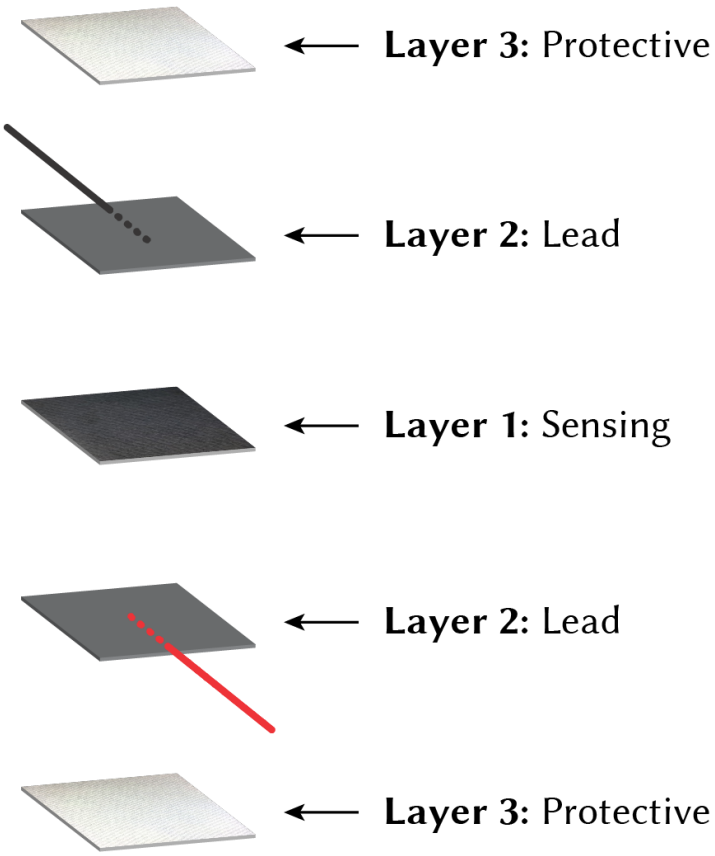

Figure 3.6: Force sensor layup.

Figure 3.7: Piezoresistive force sensing textile (EeonTex/Eeonyx) used for force sensors.

3.1.2.2 Sensor Material Structure and Size

Similar to traditional textiles, conductive textiles can be made with different mechanical structures that affect their mechanical and electrical properties. Parameters like fabric texture, stretch, and thickness can change with different textile structures and can also have an influence on the electrical performance of a textile – for example, altering the resistivity of the textile or the ease of electrical connection.

Many textile electrode materials were evaluated in an exploratory process and materials that were not available in sufficient surface area (at minimum a textile swatch), were discarded from further consideration due to the small surface area that would not enable consistent manufacture of sensors (e.g., textile strips available in a roll). Three main textile electrode materials (including both knit and woven structures) (Figure 3.8) were used to fabricate both contact and force sensors and evaluate their performance using a tensile testing machine (Instron). Conductive textiles tested included: a) 'stretch conductive fabric': 4-way stretch single jersey knit textile with a silver (Ag)-plated Nylon/elastomeric blend and a surface resistivity of < 1 ohm/sq (unstretched) (Less EMF) [73], b) ‘conductive metalized nylon fabric’: ripstop woven textile plated with tin (Sn), nickel (Ni) and silver (Ag) and a surface resistivity of < 0.02 ohm/sq (Shieldex) [77], and c) ‘woven conductive fabric’: plain weave copper (Cu) and nickel (Ni)-plated polyester textile with a surface resistivity of ≤ 0.05 ohm/sq (Shzhou Wanhe Electronic) [78]. The conductive textiles were also tested with a backing of fusible interfacing for stabilization purposes, which was especially helpful for the knit textile as it prevented the textile from curling inward on itself and deforming outside of the original cut and intended measurement area. The knit textile seemed to have better electrical repeatability and easier integration with the sensor structure when fabricated into a sensor and the woven fabrics had a tendency to not respond quite as well. The surface texture of the knit textile compared to the much smoother surface texture of both woven textiles likely facilitated better electrical contact, allowing small fibers from the knit textile to protrude outward on the textile surface and improve the electrical contact. The woven textiles experienced puncturing from a sewing machine needle and created irrecoverable holes in the textile,

and the ripstop textile experienced some discoloration after integration with a stitched uninsulated conductive thread (Figure 3.9).

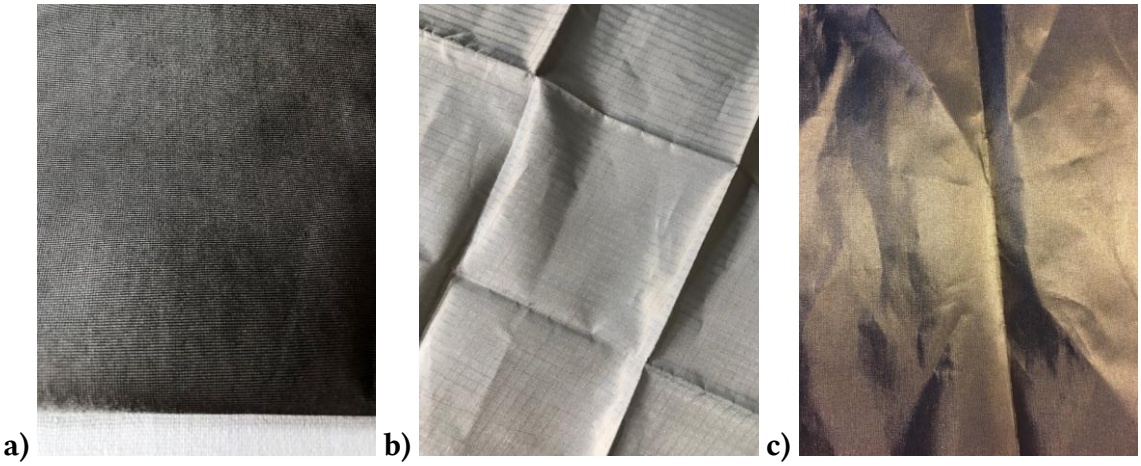

a) b) c)

Figure 3.8: Conductive textile materials evaluated: a) stretch conductive fabric, b) conductive metalized nylon fabric, c) woven conductive fabric.

Figure 3.9: Discoloration on ripstop conductive fabric after stitched uninsulated conductive thread integration.

Contact sensors were made using a single-layer configuration and consisted of a contact electrode(s) on two surfaces (Figure 3.10). The knit conductive fabric (Less EMF) was used due to its ability to create and maintain better electrical contact and was backed with fusible interfacing for stabilization of the knit structure to prevent any potential textile size deformation and curling of edges.

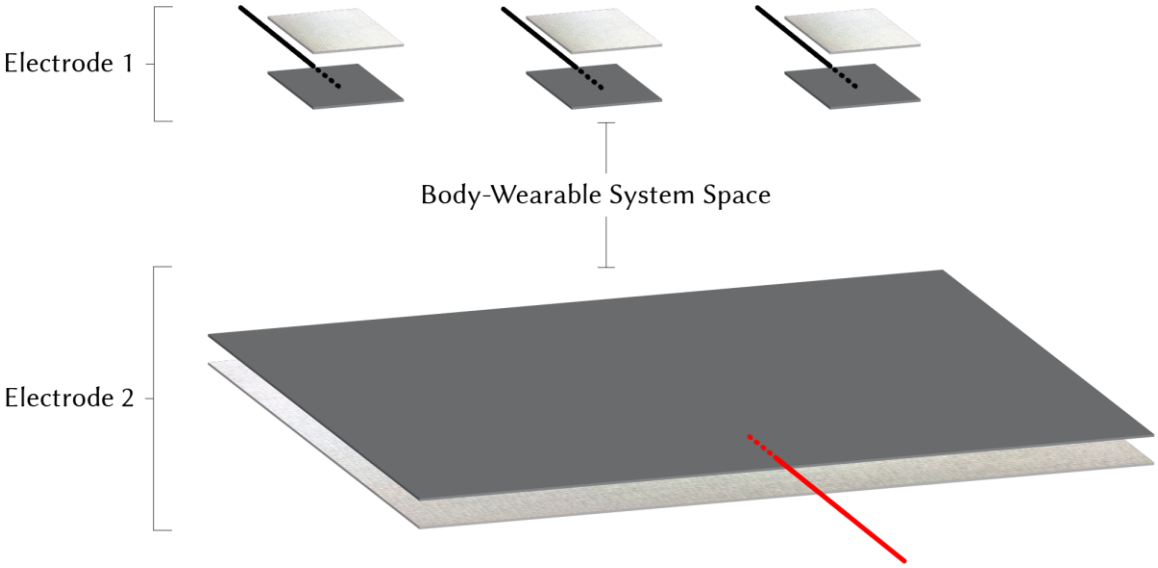

Figure 3.10: Contact sensor exploded view.

For force sensors, different non-conductive textiles were evaluated for the encapsulating layer. This layer acts as a protective layer to electrically isolate the sensor and keep the other layers in place. There were four main materials evaluated, shown in Figure 3.11: a) fusible featherweight interfacing (Pellon) [74], b) woven iron-on mending fabric (Dritz) [79], c), knit iron-on seam tape (Melco) [80], and d) knit mesh textile (source/content unknown). The fusible options were better at keeping all of the sensor layers in place without additional stitching, and the knit iron-on seam tape did an excellent job of securing all sensor layers together and produced a very durable sensor. However, the tightly-affixed layup seemed to induce a strain on the sensor, thereby reducing the sensor response range. The woven iron-on tape also produced similar results of affixing layers together well while also inducing strain on the sensor but was much less flexible than the knit option. The woven and knit textiles are non-fusible options and were initially affixed by stitching around the border. This approach allowed the inner sensor layers to

move around more than the laminated (fusible) versions. Depending on the sensing context (i.e., less dynamic movements) and fabrication of the stitching (stitching very close to the sensing/lead layers), this could be an approach that may work. Another approach investigated was tacking the sensing/lead layers in small locations throughout the layup, but this led to a lot of manufacturing variability between sensors. With this study, more dynamic movement was expected and multiple sensors were being used, making that approach unsuitable. The fusible interfacing, although not as durable as the iron-on tapes, provided a better sensor response (as it did not saturate the sensor), and was used for fabrication.

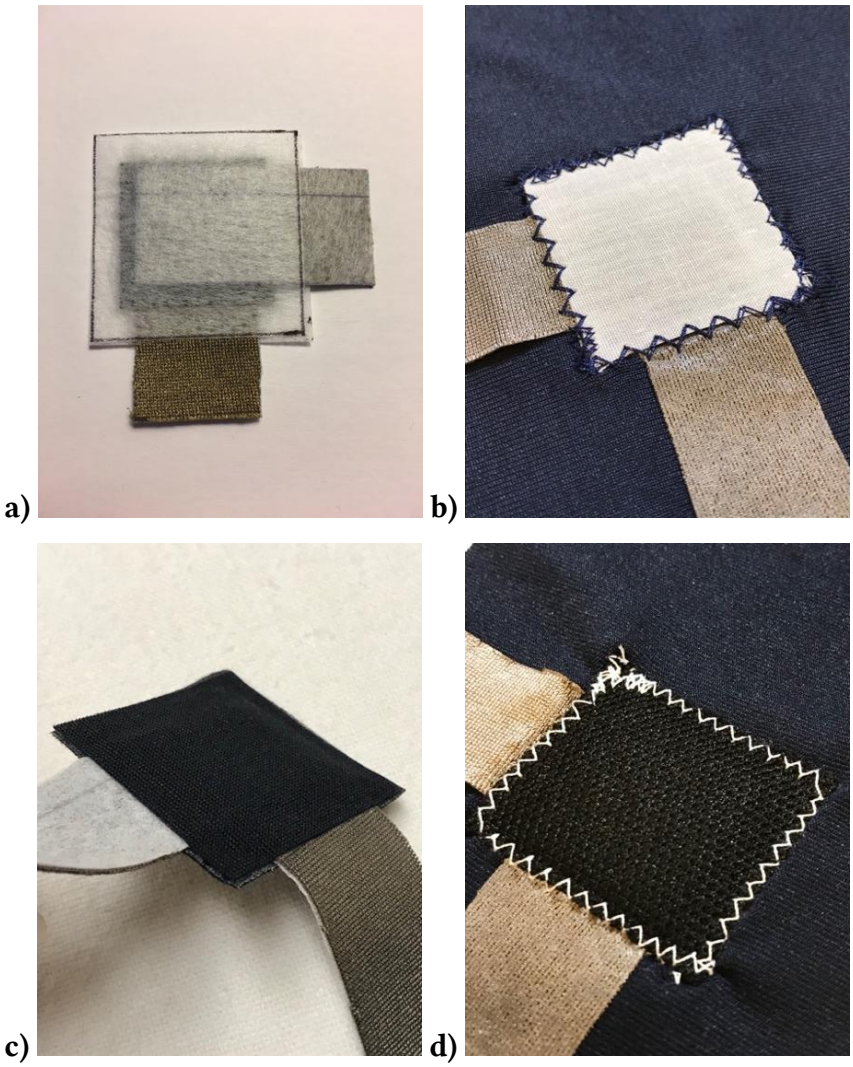

Figure 3.11: Force sensing protective layer approaches: a) fusible interfacing, b) woven iron-on mending fabric, c) knit iron-on seam tape, d) knit mesh textile.

Force sensors were made using a 3-layer configuration (Figure 3.12). *Layer 1* is the middle sensing layer and is made with a piezoresistive fabric (Eeonyx conductive) that changes resistance in response to a change in applied force. *Layer 2* is the lead layer made of the same conductive textile layup that is used for the contact sensor electrodes (knit conductive fabric backed with fusible interfacing). The lead layer must be slightly smaller than the sensing layer and oriented outward in different directions so that leads do not make contact with each other. This makes the actual sensing area of the sensor slightly smaller than the dimensions of the sensing layer itself – the sensing area of the sensor is the dimensions of the overlap of layers 1 (sensing) and 2 (lead). *Layer 3* is the outer protective/encapsulation layer, made of fusible interfacing as it served best to affix sensor layers together without inducing a sensor response. This layer needs to be larger than all other layers to encapsulate the entire sensor layup. A smaller border size (0.125 in / 0.3175 cm) was used to minimize the additional surface area while not interfering with the sensor response.

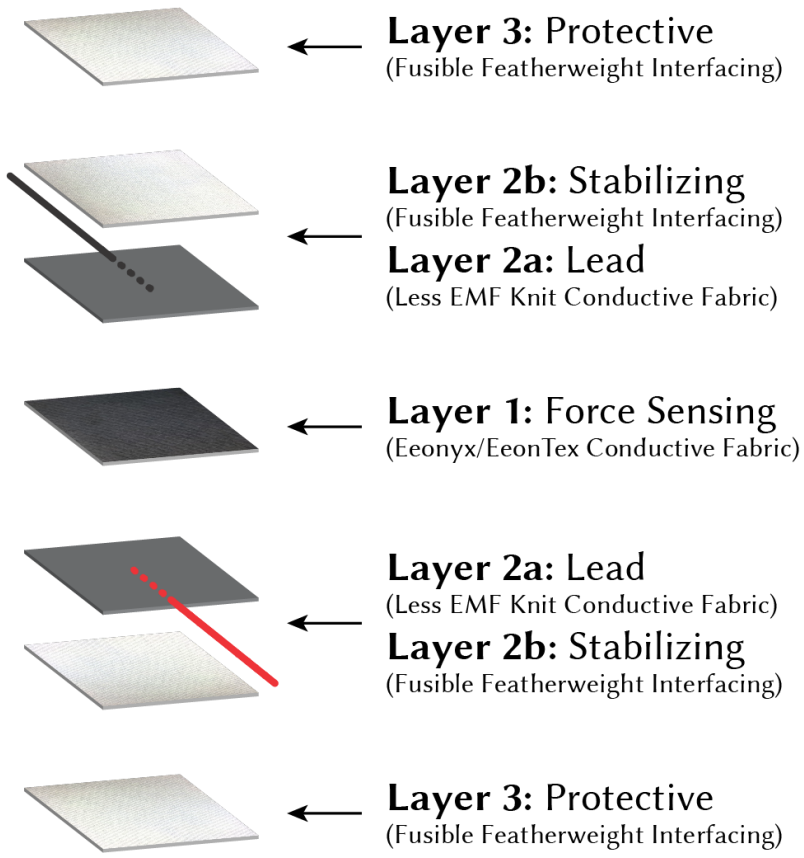

Figure 3.12: Force sensor exploded view.

Both sensor types have a border area that can be used for garment integration. However, this can increase the surface area of the sensor, which can be especially concerning for areas where high sensor resolution is needed. A smaller border size is ideal; however, pilot testing showed that very small border sizes induced force on the sensing layer, and reduced durability of the sensor. The border on the force sensor can be especially important as that is the only place where the protective layers come in contact with each other and fuse together. Two border sizes were fabricated for each sensor type and evaluated: 1) 0.25 in (0.635 cm), and 2) 0.125 in (0.3175 cm) (Figure 3.13). The performance of the two were similar and therefore the smaller border was used for sensor fabrication as it takes up less surface area on the garment.

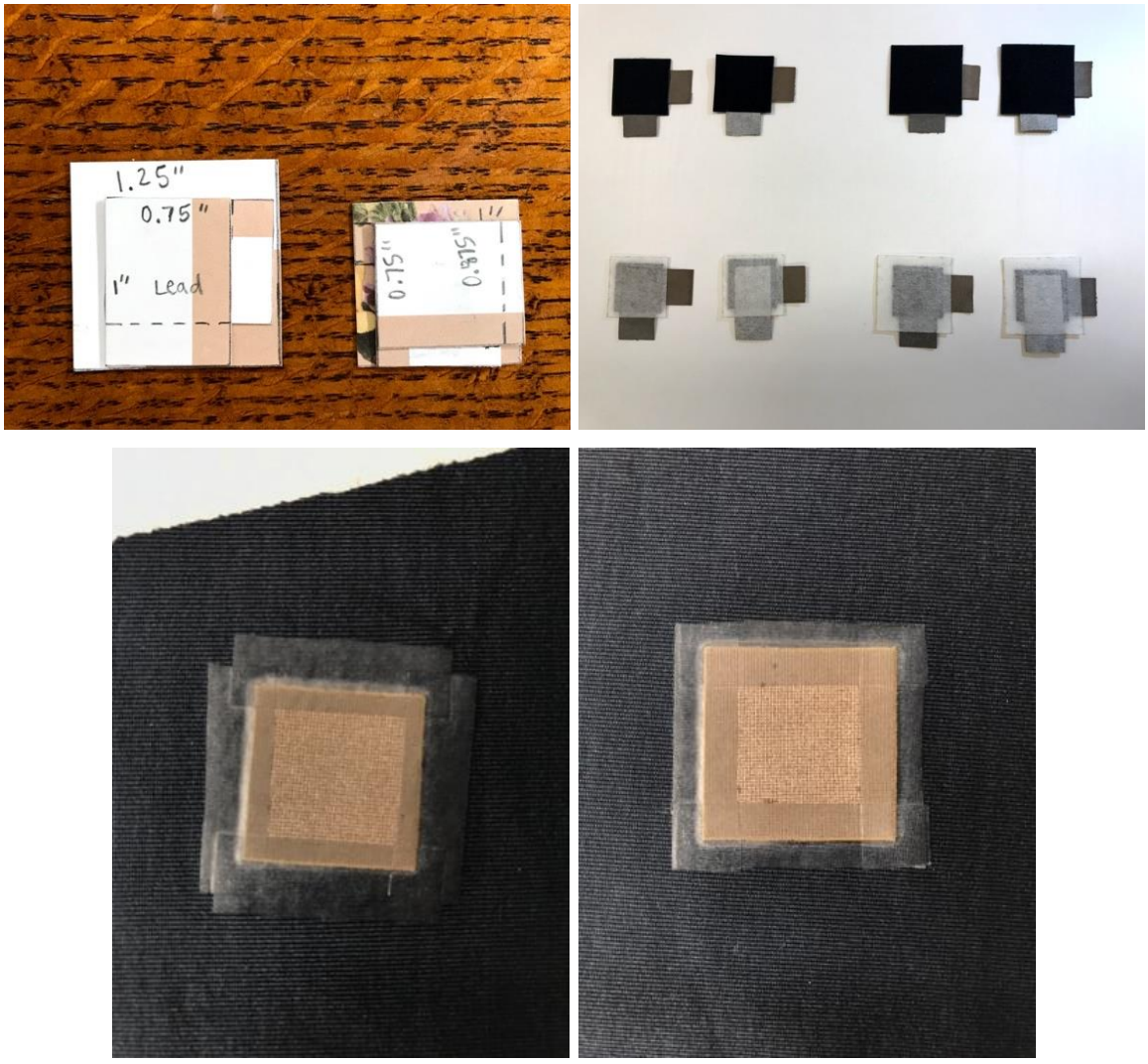

Figure 3.13: Evaluating border size for force and contact sensors.

Different sensing area sizes were also explored. Textile-based sensors are highly customizable – sensors can be made of varying dimensions and shapes. However, tradeoffs exist with sensor size and number of sensors. Larger sensors allow a larger surface area to be measured and require fewer sensors, which results in fewer leads used, but the specific locations of contact within the sensing surface area cannot be determined. In contrast, smaller sensors afford higher resolution or precision for location but have a smaller sensing area and may not cover the surface area needing to be measured. The number of small sensors could be increased to cover a larger sensing area but that would mean more sensors, sensor leads, space for sensor-garment integration, and data processing. These tradeoffs were considered during the design of this garment and a balance between sensor size and number of sensors was used for the intended sensing area. A sensing area of 0.75 in^2 (1.906 cm^2) was selected and allowed a large enough sensing area while still allowing enough available surface area on the garment for things like sensor-garment integration and lead routing. All sensors were hand fabricated, therefore there may be some variation between sensors. However, all sensor materials were laser cut for higher precision. Sensor layer and border positioning was also marked on sensors for more precision and to minimize any potential variation between sensors.

3.1.2.3 Sensor-Lead Integration

One of the main areas where failures can occur in e-textiles is at an interconnect (e.g., solder joint), and the disparity between hard and soft materials can contribute to the likelihood of failure [66]. Creating a soft-to-soft connection may increase the durability of the interconnect and result in less failure. For this study, various conductive lead materials to create soft-to-soft connections were tested and evaluated for use (Figure 3.14): a) non-solderable uninsulated 3-ply silver-coated nylon conductive thread (Shieldex®) [81], b) solderable uninsulated silver-coated conductive thread (Liberator® metal clad fiber) with a Vectran® fiber core (Syscom Advanced Materials) with a direct current (DC) resistance of ~1 ohms Ω/ft (~3.3 ohms Ω/m) [82], c) 'stretch conductive fabric' (Less EMF) [73], d) sewable insulated electrical wire (W. L. Gore & Associates, Inc.) [83], and e) flexible silicone-insulated stranded electrical wire (CBAZY) [84].

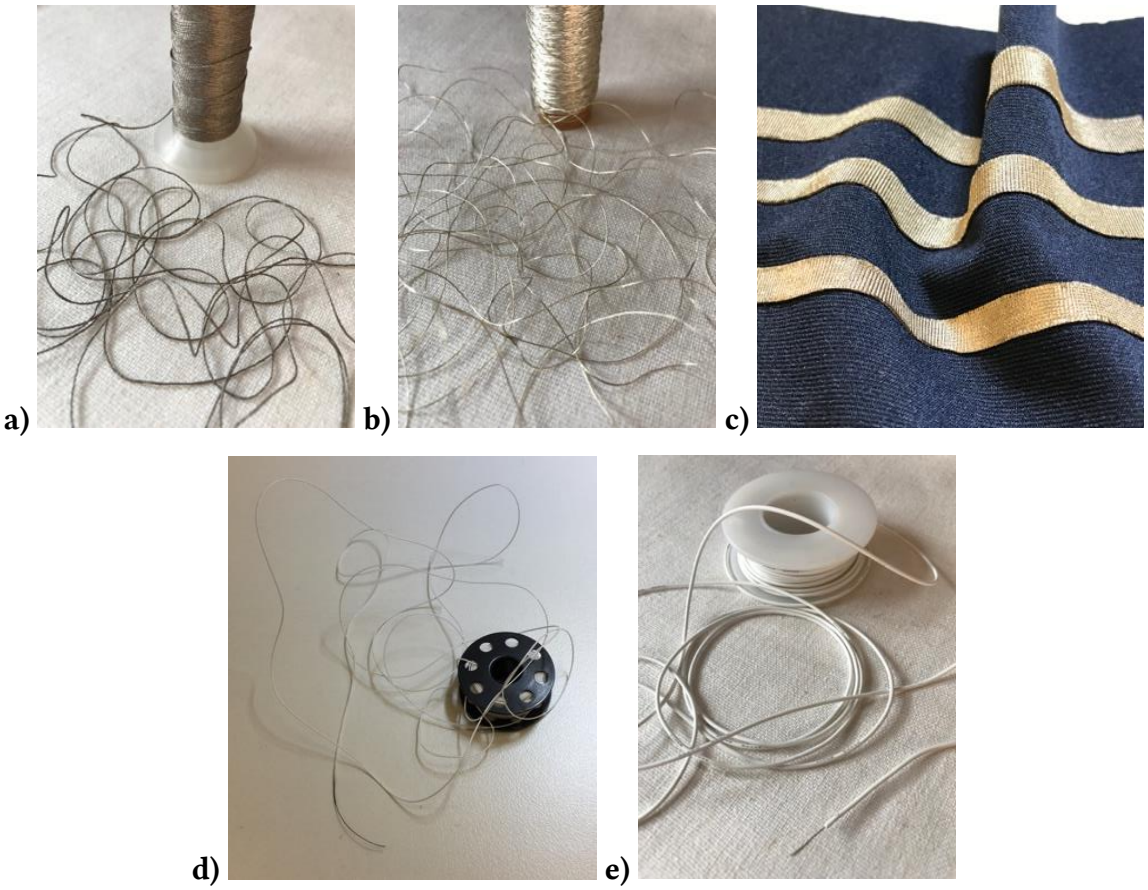

Figure 3.14: Lead materials: a) non-solderable conductive thread, b) solderable conductive thread, c) stretch conductive fabric, d) sewable insulated wire, e) silicone-insulated wire.

Uninsulated conductive thread was stitched using an extensible configuration (zigzag, similar to a serpentine pattern) to not restrict the 4-way stretch textile stretch or body movement and to prevent stitched leads from breaking with textile stretch/elongation (Figure 3.15). The non-solderable uninsulated conductive thread produced the best hand-feel of the garment, and the solderable thread created a slightly stiffer hand-feel as well as a rippling effect in the unstretched textile. Stitchable conductive threads work very well for textile integration and are the best option here with that consideration; however, their inherent uninsulated nature is not conducive for on-body sensing where stitching lead lines can come in contact during fabric deformation or folding. Conductive stitching can be insulated with an additional material (knit iron-on seam tape was tested for insulation), however, this requires an additional manufacturing step, it is limited in

ability to easily form more curvilinear or organic shapes, and it is possible the seam tape may not remain completely adhered with extended use, especially with extreme deformation or heat.

Figure 3.15: Uninsulated stitched conductive thread leads and knit iron-on seam tape insulative approach.

The conductive knit textile also created a great hand-feel when integrated into a garment but similarly makes creating an organic lead path on the garment more difficult, and the wider lead it creates takes up too much surface area for this application.

A very fine insulated stitchable wire prototype from W. L. Gore & Associates, Inc. was also tested. The wire exhibits very low resistance and has a very small gauge, creating an exciting opportunity for e-textile integration, and an electrically stable, low-resistance, and low-profile option. However, a sizeable length of the wire insulation needed to be

removed to accommodate the wire going through the sewing machine components and create both a strong mechanical and electrical connection with the textile sensor by stitching and backstitching with the section of uninsulated wire. Problems initially were experienced with trying to remove the wire insulation, as the best method of insulation removal is with a specialized laser or thermal wire stripper, which were not resources available during prototyping. Since this is a prototype wire, the available length of wire was limited and was likely not going to be enough for use in this garment. Additionally, on a stretch fabric it was difficult to get a true serpentine pattern (zigzag stitch) with the stretch knit fabric that would allow the stitch to remain extensible, as the stiffness of the wire pulls the stitch into a straight line, restricting textile stretch.

Finally, the flexible silicone stranded electrical wire (CBAZY) was evaluated as the silicone insulation creates a very flexible and soft wire and was available in a size 30 American Wire Gauge (AWG) commercially off-the-shelf in abundance (plenty for the entire garment). This wire was used for sensor leads due to its insulated form to prevent any electrical shorting from occurring, soft and flexible material for a low-profile and comfort on the body, material availability for enough to fabricate many sensors with and have long leads for electrical hardware connection during testing.

Although this wire diameter was too large to be threaded through a traditional sewing machine, it was evaluated for textile-integration using a few different approaches (Figure 3.16): a) serpentine pattern formed through an intermittently stitched fabric strip, b) routing the wire through a stitched fabric channel, c) couching over the wire with traditional sewing thread using a sewing machine, d) forming into a zigzag pattern with machine-stitched tacking, e) affixing to the textile with hand-stitched tacking, and f) affixing to the textile with fusible iron-on clear seam tape tacking. The serpentine pattern preserved textile stretch well but took up a much larger surface area on the garment. Routing the wire through a fabric channel took up less space than the serpentine pattern but multiple wires could get bunched together, creating bulk, and with this approach it was more difficult to create a curvilinear shape. Couching the wire created a strong integration but often created a rippling effect on the textile (Figure 3.17). Forming a zigzag

pattern created tension on the fabric. Affixing the wire by tacking with sewing thread in intermittent locations allowed leads to follow a curvilinear shape and allowed leads to expand/contract with textile stretch but was time consuming. This affixing approach was then explored with a clear iron-on seam tape, which had similar qualities but was much less time consuming and was ultimately used as the method for lead routing and lead-garment integration.

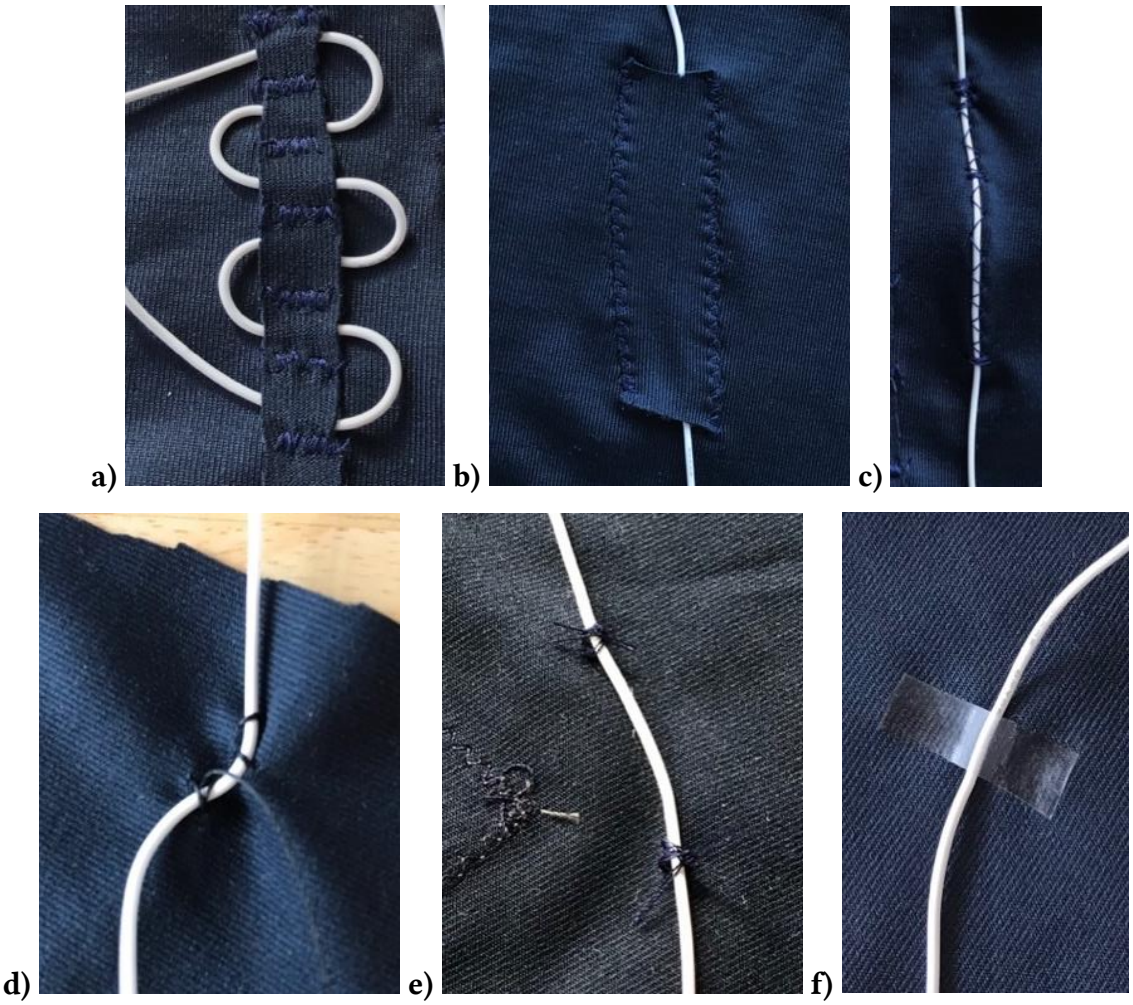

Figure 3.16: Garment-lead integration approaches: a) serpentine pattern, b) fabric channel, c) couching (zigzag stich) over wire, d) tacking in zigzag pattern, e) tacking intermittently with thread, f) tacking intermittently with iron-on seam tape.

Figure 3.17: Fabric rippling from couching wire.

3.1.2.4 Sensor-Garment Integration

Another challenge with e-textiles can be the integration of materials and creating a robust connection that does not decrease wearability. Various approaches were evaluated for sensor-garment integration, such as: 1) adhering the sensor to the garment from the sensor's under-side with a machine sewable fusible web (Pellon) [85], 2) stitching the sensor to the garment surface, and 3) adhering the sensor to the garment along the sensor's borders with a clear polyurethane iron-on seam tape (Bemis, product ST104) [86]. Some characteristics that were important to consider include: durability, surface profile, surface area coverage on the garment, and impact on the performance of the sensor. Using an adhesive on the under-side of the sensor allowed the sensor to be integrated with the garment without requiring any sort of attachment through a border. However, the integration with the garment was not strong enough to keep the entire surface area of the sensor adhered (e.g., corners become unattached) to the garment during deformation and stretching. Stitching the border of the sensors created a strong yet soft mechanical connection with the garment but can create minor variation in the surface profile of the sensor textile in the stitched area. The iron-on seam tape border created a very smooth and uniform connection with the garment and a clean area to electrically insulate the sensor border and maintain a specific sensing area, but, as mentioned previously, adhesives may not be as durable as stitching depending on the sensing context.

A combination of adhering the sensor's underside with a fusible web, stitching, and then adhering iron-on seam tape around the sensor border was used to leverage the durability, uniformity, and insulation advantages of each method. First a fusible web adhesive on the underside of sensors was used to adhere the entire sensor surface area on the garment and to position in place and prevent any areas/pockets of non-integration with the garment textile around the center of sensors. Then the sensor borders were stitched using a sewing machine to form a secure mechanical connection along sensor edges, a likely place where sensors could begin to become detached from the garment with textile deformation (donning/doffing and wearing the garment). Finally, a clear strip of iron-on seam tape was fused around the sensor edges (along the sensor border and slightly extended out onto the garment textile) to create a smooth, low-profile, and uniform sensor integration and transition to the garment textile, as well as sensor border for the sensing area. This clear iron-on seam tape was used to prevent sensor edges and stitched border from catching on anything (including suit textile electrode, which showed intermittent sticking behaviors during Instron testing and is further discussed in Section 5.1.2 Contact Sensor Test Discussion).

3.1.2.5 Lead/Wire Management

Interconnects, wires, and leads can create challenges for wearable applications, as bulk and stiffness can quickly add up, decreasing wearability. Lead and wire management is an important aspect for successful wearable sensing. Leads should not restrict the garment or body movement, should not create pressure points or bulk on the body and should be minimal and low-profile, should be organized/not easily tangled, remain durable enough for the sensing environment, or interfere with the sensor performance. Integrating leads into the garment has advantages for both set-up time and durability of wearable sensing. If leads were to hang free and not be integrated with the garment they could become tangled, create bulk, catch or rub on nearby elements, and interfere with the sensing environment. If leads catch on anything it could create tension and pull on the interconnect, which could potentially break or disrupt the connection with the sensor, or influence sensor responses during data collection.

Routing leads and interconnects along lines of non-extension (LoNE) (Figure 3.18) is a design strategy that can be used for wearable technologies that is based on research from full mobility pressure suits. This research suggests locations on the body where deformation does not occur or is minimal, and therefore are ideal for placement of inflexible elements to preserve mobility and minimize potential restriction. Leads in this study were routed to follow LoNE given the sensor pattern/layout on the garment (Figure 3.19).

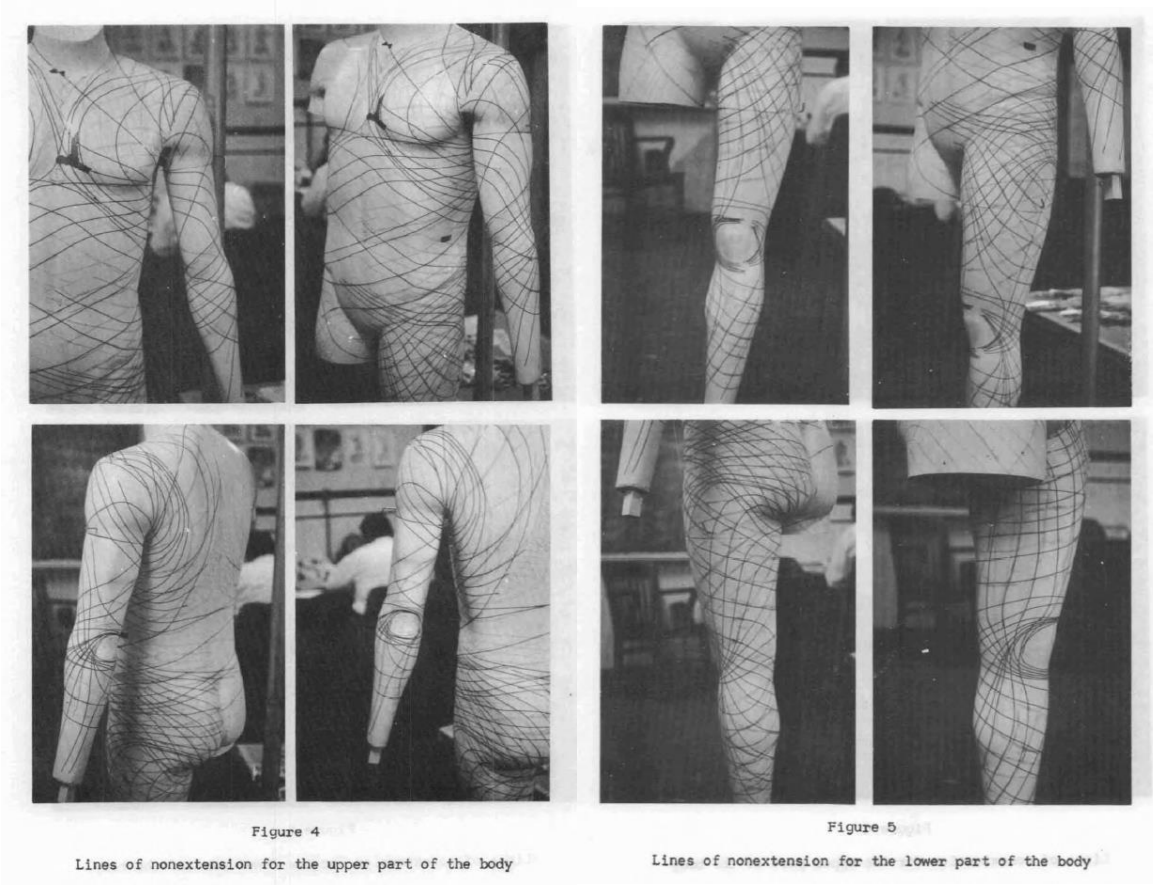

Figure 3.18: Lines of non-extension (upper (left) and lower (right) body).

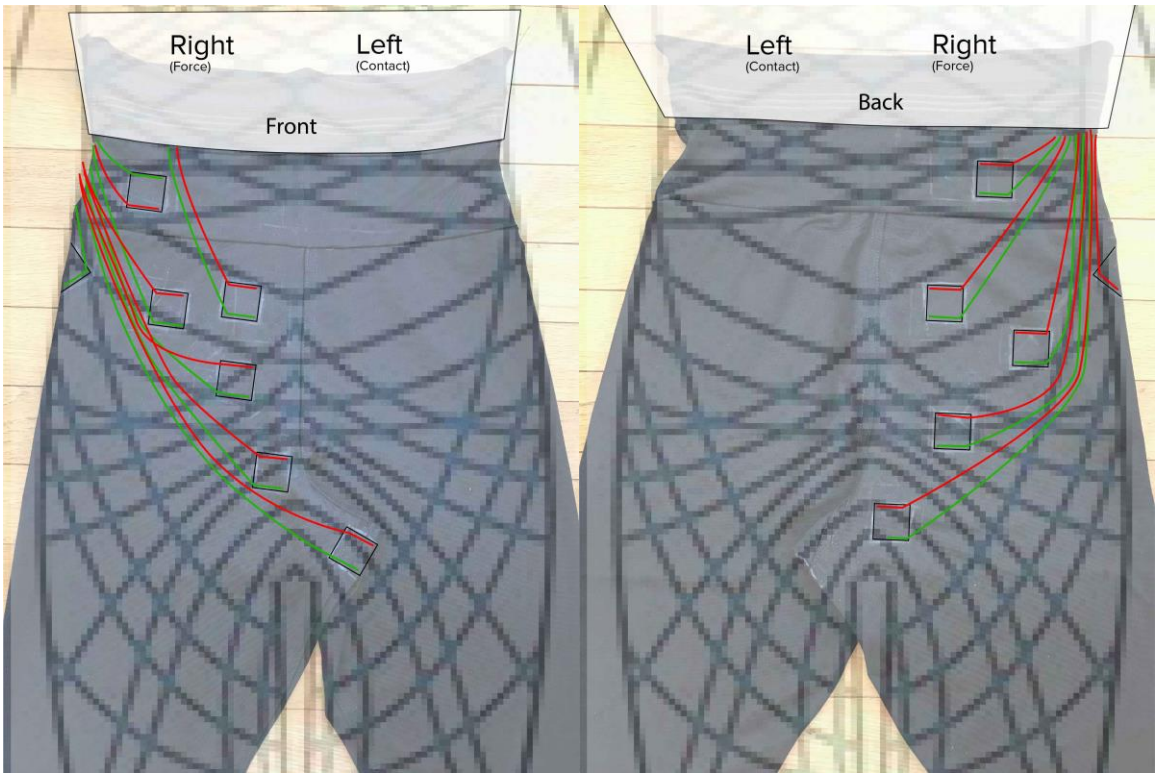

Figure 3.19: Test routing leads to follow LoNE with sensor garment (front (left) and back (right)).

Leads needed to be intermittently secured in locations on the garment to maintain the pattern of LoNE and to not interfere (cross over or under) with sensors. Leads also should not interfere with the testing environment or the body. To minimize any potential interference, electrical leads were brought through the knit textile, to the inside of the garment. This provided a clean outer garment with no leads that could potentially get caught, just sensors. A small patch of iron-on seam tape was used on both sides of the garment where the lead was brought through to restrict the movement of the sensor-lead interconnect and to act as a strain relief. The leads were then routed to follow LoNE on the inside of the garment and tacked in place with strips of clear iron-on seam tape in small areas along the lead line. A similar approach of tacking the wires in place could also be accomplished using thread and stitching but requires more time for fabrication. Tacking leads in small areas to keep them oriented properly can prevent wires from shifting, bunching up, or getting tangled – especially during donning/doffing and while wearing – and creating undesirable bulk or pressure points on the body, or interfering

with sensors. This approach also allows the leads to still extend or contract with garment stretch, as the lead itself can pass through the tacking points, but keeps the leads oriented in the same LoNE configuration. Allowing the leads to expand/contract with garment stretch is helpful for donning/doffing and for fitting bodies of different anthropometry. After all leads were securely routed on the inside of the garment a liner layer was developed and integrated on the inner garment side to completely contain wire leads (Figure 3.20). This creates a completely enclosed system for lead management and minimizes any potential undesirable interference with wires.

Figure 3.20: Inside liner on sensing garment to protect and encapsulate sensor leads (note that waistband is unfinished in this image at this stage – wires in the waistband are covered and protected when the waistband construction steps are complete).

3.1.2.6 Donning Garment Feature

The form-fit garment style along with the design feature to promote garment anchoring (silicone-backed elastic waistband) has both benefits and tradeoffs. It can increase sensing accuracy by decreasing potential garment drift but can make donning the garment more difficult. Increased donning complexity can also be caused from being careful with the garment to avoid potentially breaking anything. To provide an anchor point at which the garment can be pulled up at during donning, donning straps were added to the side of the garment (Figure 3.21). This prevents the need to tug/pull on the actual garment textile area itself where sensors and leads are located. The donning loops are made with a strip of twill tape running down the side of the garment on the inside and is tacked intermittently/periodically with stitching to the garment. Loops are formed at the top of the garment near the waistband as an anchor point to pull up from, to afford easier and more careful donning. The donning straps pull the entire garment up over a body when pulled from the top loops, while minimizing excess strain or deformation on the sensing area.

Figure 3.21: Donning straps along the inside of the base garment sides and loops at the top.

3.1.2.7 Sensor Locations

For this study, multiple sensors are integrated into the developed form-fit body garment in the pelvis and buttock region to measure contact locations on the body. The body is treated symmetrically in the vertical orientation, and contact sensor body-side electrodes are located on the left garment side, and the force sensors are located on the right garment side. Since the contact sensors need an electrode on both surfaces for sensing, a contact electrode needs to also be integrated on the wearable-system or suit (brief)-side. A monolithic suit-side electrode is fabricated on the left brief side to measure contact with the garment integrated contact electrodes on the body-side.

For sensor locations, the body was treated symmetrically and in the vertical orientation along the body's midline. Force sensors were located on the right garment/body side and contact sensors were located on the left garment/body side. Twelve force sensors and twelve contact sensors were integrated on the garment. Locations for force and contact sensors were designed to mirror each other across the body's midline. A goal for sensor placement was to position sensors in areas on the garment/body where both contact and no contact would be experienced. Locations of expected contact were along brief openings (waist and leg) and less contact around the inner/center brief areas. The base sensing garment and brief were donned on the manikin and an outline was drawn in chalk on the base garment to inform placement of sensors along brief openings (waist and legs) (Figure 3.22). Sensors were evenly spaced along the entire leg opening. Sensor placement was designed to cover a variety of locations in which contact and no contact were expected. An illustration of the e-textile garment sensor types and placement with a brief outline overlay in is depicted in Figure 3.23 and the final prototype is shown in Figure 3.24. Sensors are abbreviated in the sensor garment illustration and throughout the text here as contact sensor (cs) and force sensor (fs).

Figure 3.22: Marking brief opening locations on the manikin to inform sensor placement.

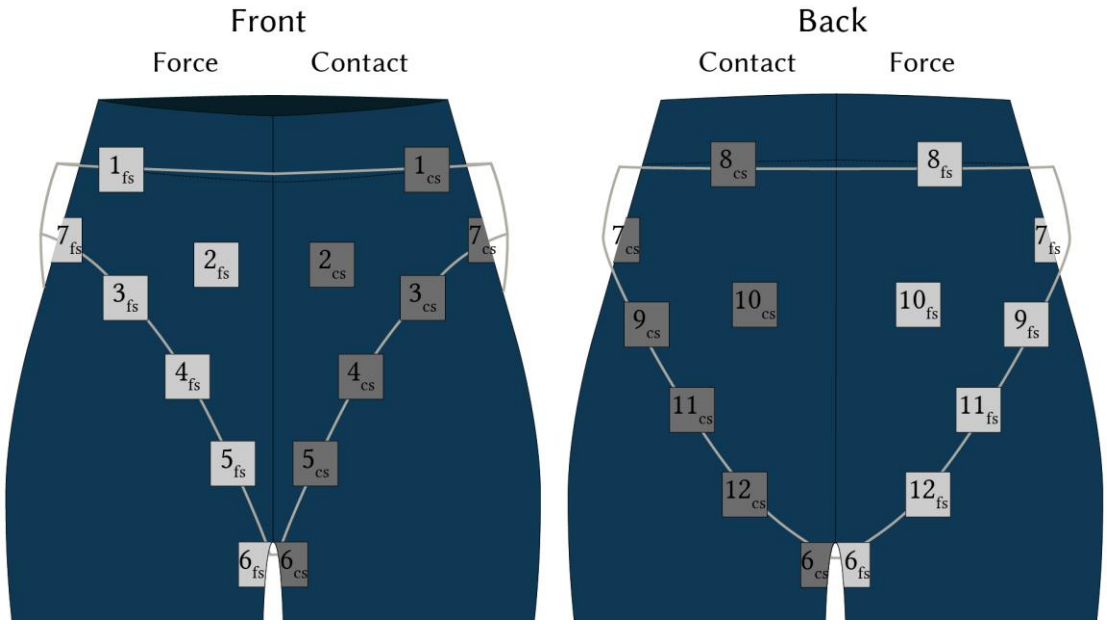

Figure 3.23: E-textile sensing garment illustration showing type (contact sensor (cs) and force sensor (fs)), number, and location on garment.

Figure 3.24: Final e-textile wearable sensing garment prototype (front (left) and back (right)).

During dynamic manikin movement, the brief can move on the manikin's body. Most of this movement is experienced in the front of the body compared to the back. The movement of the brief on the manikin's surface can bring the brief closer to and farther away from the manikin's body – creating instances of contact and no contact between the manikin and the brief. Additionally, part of the brief movement includes the brief shifting over the manikin's body during gait cycles. The manikin has a large range of motion and when the manikin's hips are the most flexed or extended, the upper thigh of the leg that is experiencing flexion can push on the brief, shifting it horizontally (side to side) on the body.

In an ideal scenario with the brief lining up perfectly over all sensors along the outer brief edges (waist and legs). It was hypothesized that the most contact would be experienced along the lower pelvis and butt area and front waist near where the iliac crest on the body is located, since the brief had the closest fit with the manikin, and less

contact in the upper butt/back area, as that location had the largest distance between the manikin and the brief. Sensor locations around the middle of the brief were not expected to make contact as those locations were expected to experience less influences from dynamic movement (e.g., leg pushing up against the brief). It is expected that with a larger body shape (padded manikin), more contact overall – including both *location* as well as *duration* of contact – will occur between the brief and the manikin's surface due a decrease in the distance between the two surfaces.

3.2 Lower Torso Assembly (LTA) Brief Development

An LTA brief mockup spacesuit component was developed and used for manikin testing to understand interactions that occur between a robotic manikin (discussed further in Section 4.2 Manikin Test Method and Data Analysis) and wearable system (brief) during dynamic body movement. This brief mockup is designed to simulate the xEMU LTA brief and used as an initial proof of concept for the sensing garment method.

A 3D computer graphics software (Blender) was used to modify the brief mockup to fit the robotic manikin, and to accommodate testing and 3D printing limitations. The brief was slightly scaled down from its original dimensions to fit the manikin. The brief needed to be scaled down more in the horizontal (side to side) direction to avoid a metal bar located near the right side of the robotic manikin, from which the manikin is suspended. The fit of the brief needed to be small enough that it would fit and make contact with the manikin, and would avoid interfering with the suspension bar, but also large enough to accommodate the manikin's large range of motion and not risk damaging the manikin during testing.

Many virtual fit evaluations and brief alterations using Blender were done prior to 3D printing, to minimize cost and material used. To perform a virtual fit session with the brief and manikin, the manikin needed to be 3D scanned to be evaluated in the virtual environment. The robotic manikin was scanned in 6 different poses to capture the full range of motion experienced during its gait cycle (Figure 3.25). Using these virtual

models, a best-case fit scenario was developed (Figure 3.26). Since the manikin is treated as a hard surface in the virtual fit session, there are locations on the brief where the manikin's body protrudes through the brief. However, in real-life, like humans, the manikin's body (which is covered with self-skinning urethane foam) has some compliance and this fit would likely be appropriate. A mini-scale (10%) 3D print of both the brief and manikin was printed to evaluate brief fit with the manikin (Figure 3.27). The manikin pose that was 3D printed was chosen based on the most extreme example of leg separation during the gait cycle – the point at which fit would be the most difficult. Similar to the virtual environment, the printed manikin does not have any compliance, so this did not directly translate to full-scale fit, but it helped give an indication of fit. The final full-scale (100%) 3D printed brief was then printed using Acrylonitrile Butadiene Styrene (ABS) with a layer height at 0.01 in (0.0254 cm) and double-dense infill (Figure 3.28).

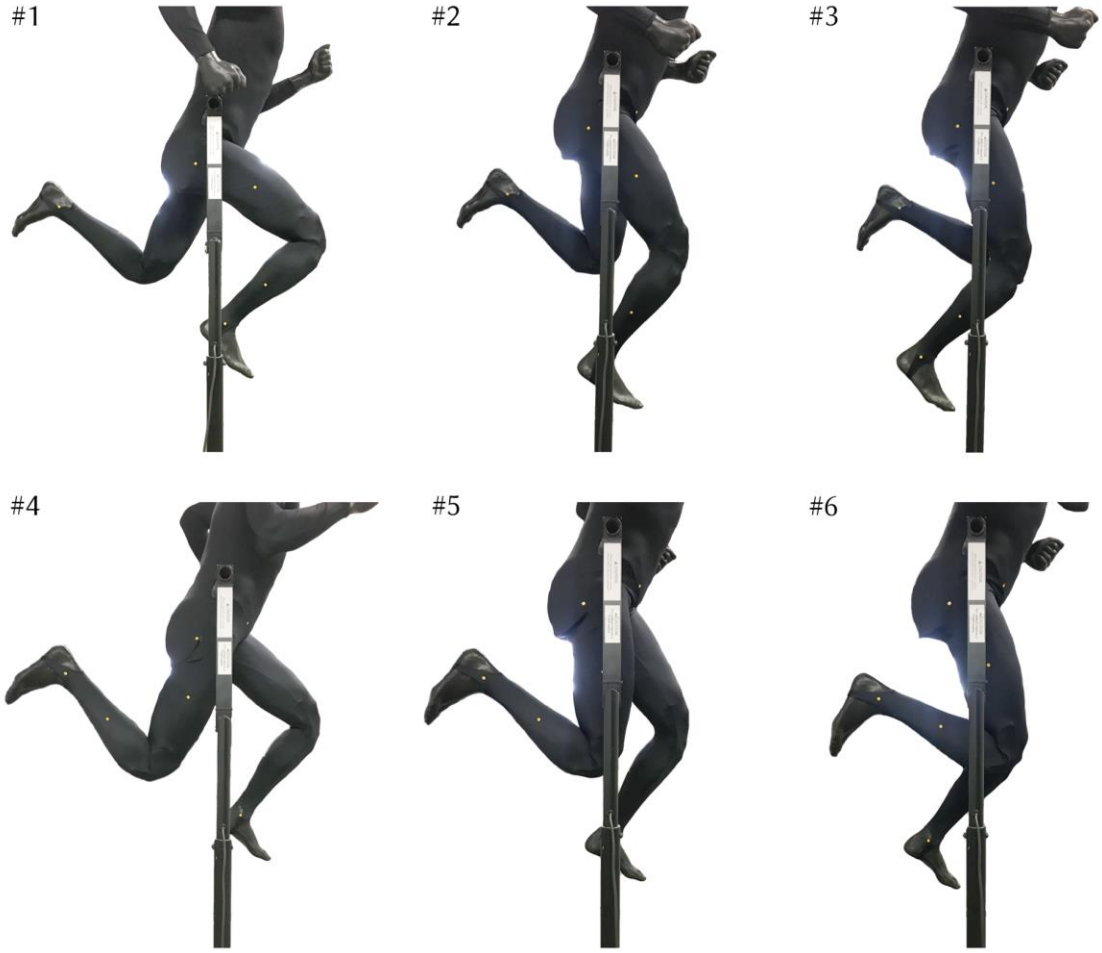

Figure 3.25: Manikin gait poses for 3D scanning.

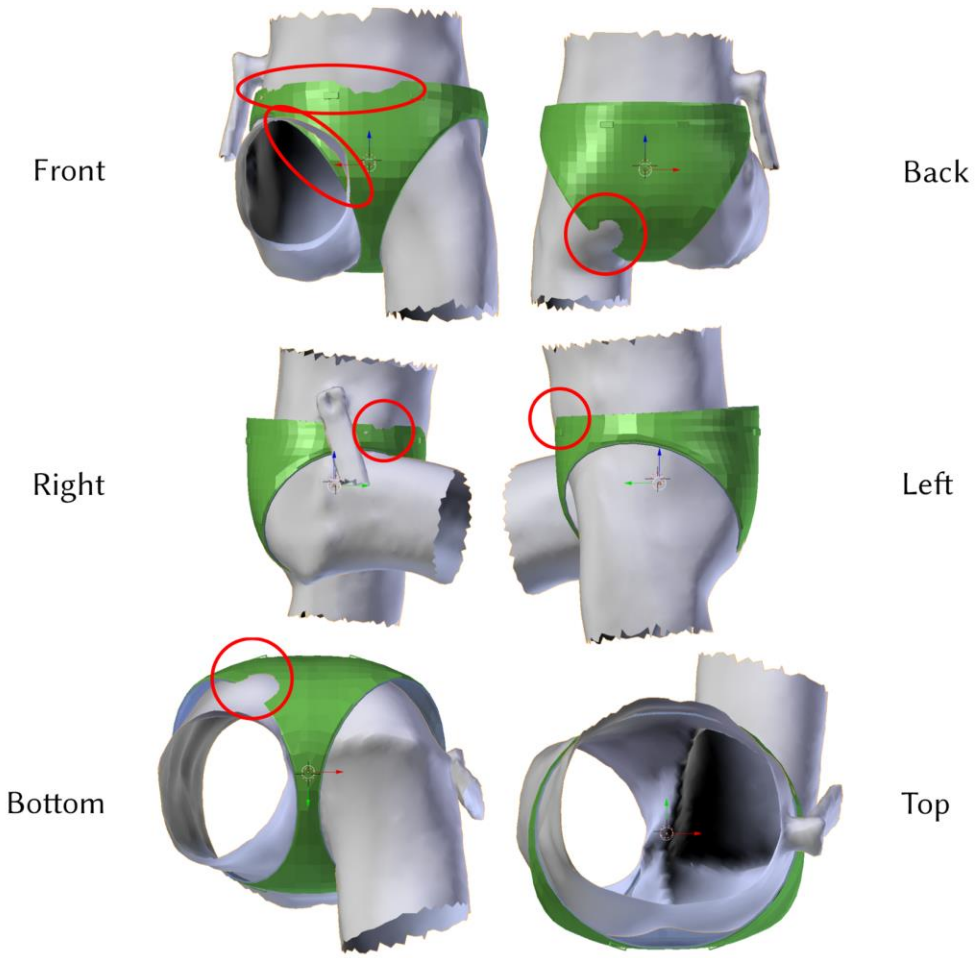

Figure 3.26: Virtual fit evaluation with the brief mockup and robotic manikin.

Figure 3.27: Test fit with mini scale (10%) 3D printed brief and manikin.

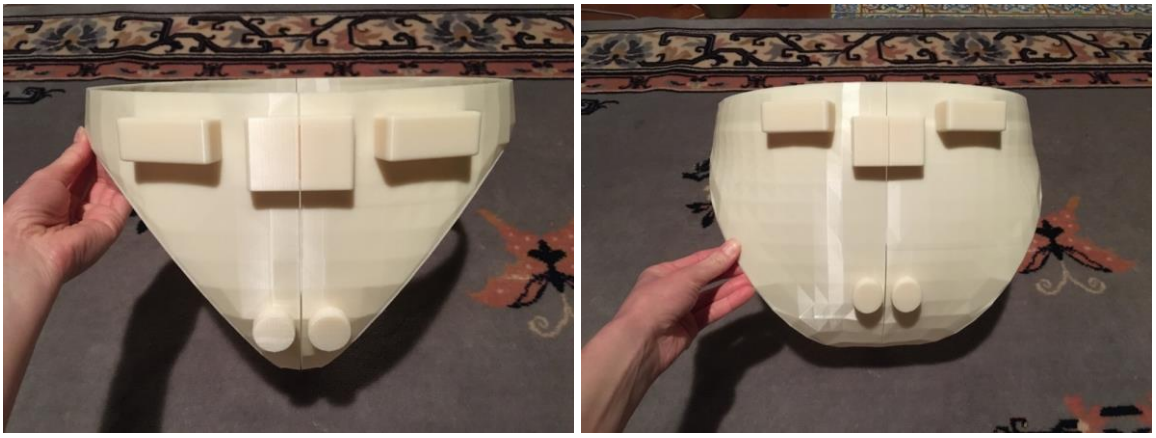

Figure 3.28: Final full scale 3D printed brief (front (left) and back (right)).

The final brief fit had closer contact with the robotic manikin horizontally on the body (sides) and had more spacing front to back (Figure 3.29-Figure 3.31). Due to the positioning of the brief on the manikin the back had much more space than the front. Features were added on the outer shell of the brief for attaching straps to suspend the brief from the manikin for testing (Figure 3.32). The final brief was 3D printed and needed to be split into two components to accommodate the printer bed size. The brief was split vertically down the center, on the body midline. Since dynamic movement of the robotic manikin could shift brief components, other features were added on the outer brief shell to prevent variation in right and left brief component alignment and to keep both components together as one during testing. A rectangular plug and socket was used for brief component alignment, and zip ties were tightened around knobs on left and right brief sides to secure them together.

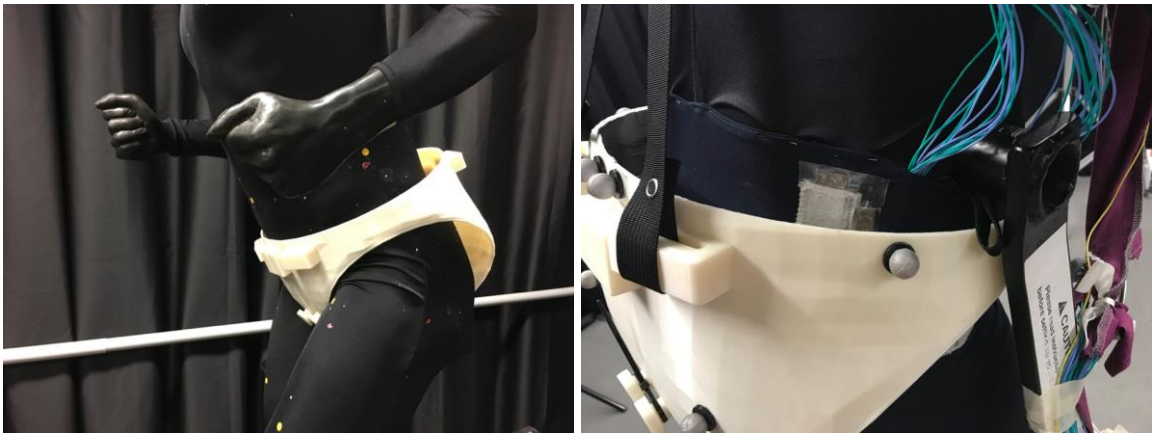

Figure 3.29: Brief fit on robotic manikin showing more distance between manikin and brief in the back compared to the front.

Figure 3.30: Brief fit on robotic manikin making contact with contact sensor #1.

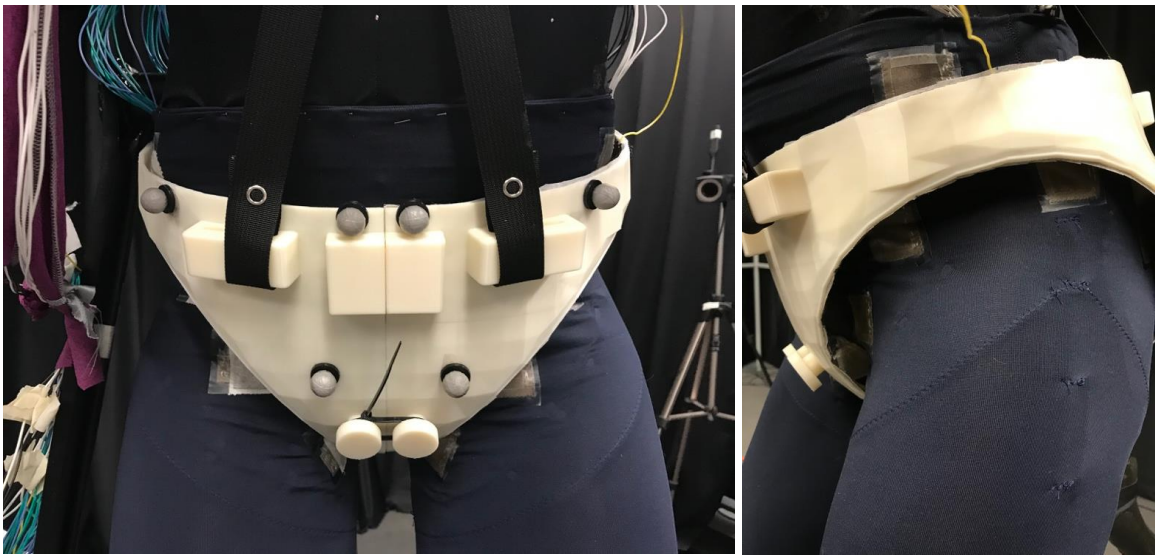

Figure 3.31: Brief fit on robotic manikin showing more distance between manikin and brief towards the top compared to the bottom, near the crotch, of the brief.

Figure 3.32: 3D printed brief additional features: attachment for suspension straps, plug and socket attachment for alignment of left- and right-side, knobs for zip ties to secure left- and right-side 3D printed brief components together during dynamic manikin testing.

To enable contact sensing, the inside of the left side brief component was augmented with a single monolithic conductive textile electrode (Figure 3.33), which was also used for previously described contact sensor Instron testing (prior to brief integration). This electrode is the suit-side electrode that makes contact with the body-side electrodes. The same material, conductive knit textile backed with fusible interfacing was used for this electrode. Similar to the manufacture of individual sensors, backing the electrode with interfacing helped stabilize the fabric, and here prevent wrinkling and curling of the

fabric during brief integration. A single lead using the same soft sensor-lead integration method previously described for body-side electrodes was used here for the suit-side electrode and was positioned to be at the top center of the electrode so that when placed on the manikin it would align with the other garment leads to keep wires co-located for easier management. The electrode was integrated with the brief using a multipurpose spray adhesive (3M™ Super 77™) [87] and carefully positioned to avoid any wrinkling/folding and achieve a uniform surface (Figure 3.34). During the integration, an apparel patternmaking technique of slashing around curvilinear shapes was utilized to create a uniform/smooth surface. Excess fabric was trimmed down to fit to the edges of the brief. The final suit-side electrode is lined on the inside of the left brief component and creates a single, continuous sensor (Figure 3.35).

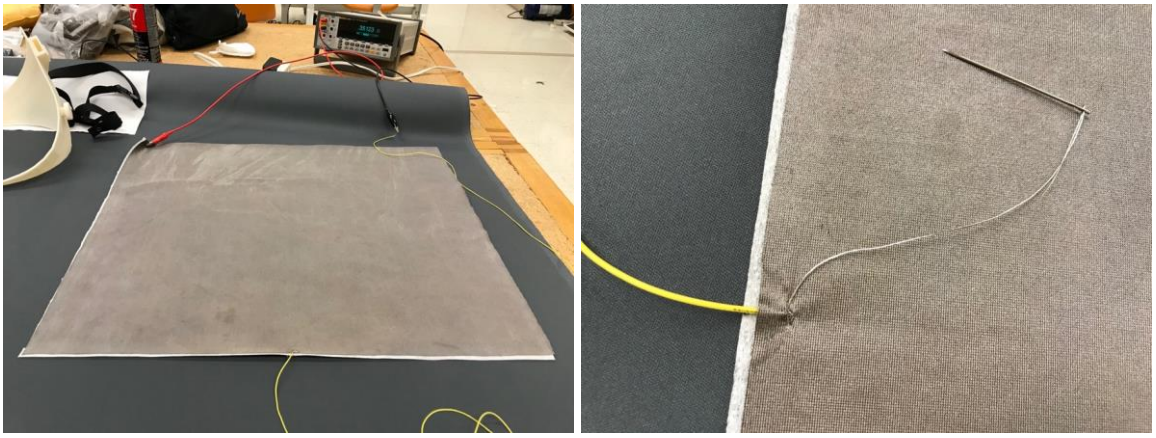

Figure 3.33: Suit contact electrode prior to brief integration (left) and sensor-lead integration (right).

Figure 3.34: Integrating suit contact electrode with the 3D printed brief using a slashed apparel assembly method to create a smooth fit around curved brief leg opening.

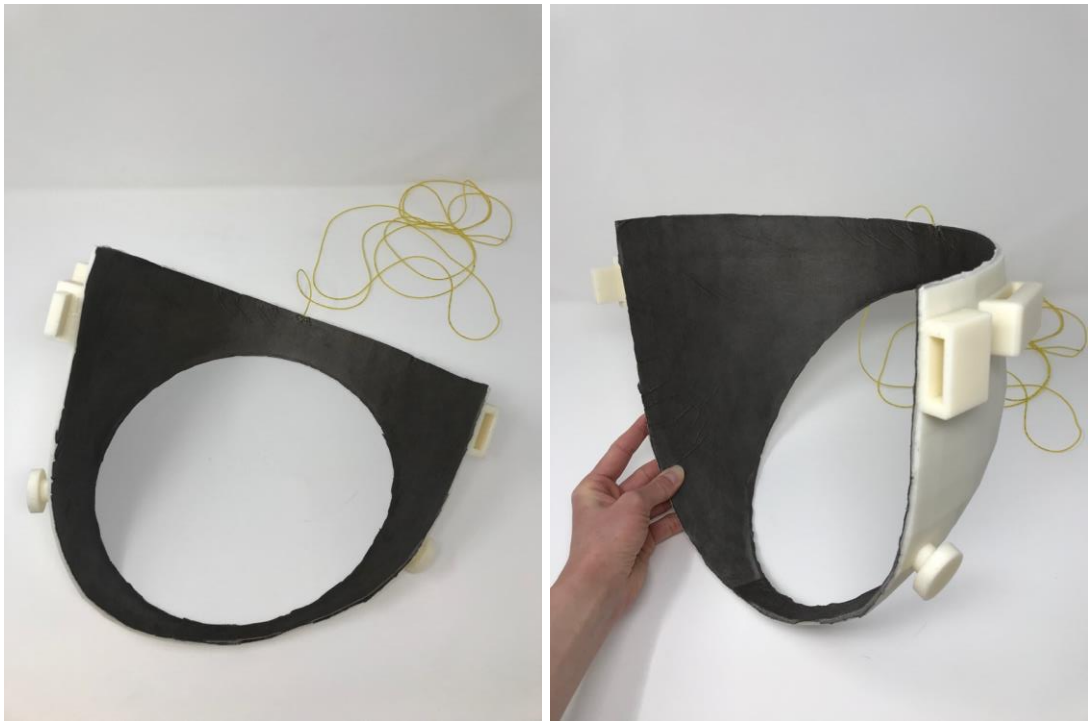

Figure 3.35: Brief suit component after contact electrode integration.

Chapter 4

4 Methods

4.1 Instron Test Method and Data Analysis

This section describes the test method and data analysis for characterizing the performance of sensors using controlled force testing (Instron). Since senor integration into a textile/garment can change the sensor performance, the e-textile wearable sensing garment was completely fabricated with integrated sensors prior to Instron testing.

4.1.1 Instron Test Method

To understand sensor performance a standard mechanical testing machine (Instron, series 3360, model 3365 [88]) was used to perform individual sensor testing for both sensor types (contact and force) in the e-textile wearable sensor garment.

The Instron transducer and a DC power supply (Dr. Meter HY3005F-3) with a voltage divider circuit was used to collect sensor data. Force data was collected from the Instron system load cell. The power supply was powered to 5 Volts (V) for all data collection. With a voltage dividing circuit approach, the output voltage (V_{out}) of the electrical system is a fraction of the input voltage (V_{in}) by applying a voltage source across a series of two resistors (textile sensor and reference resistor) (Figure 4.1). This fraction is measured as output voltage (V_{out}) and varies based on the relative sizes of the two resistors in the

system. As one resistor (the sensor) changes when load is applied, the output voltage will also change. A breadboard was used for the voltage divider circuit and each sensor was connected to the breadboard during testing. The resting resistance of each sensor was measured during the development of the circuit and approximately half of the total resting resistance of each sensor was used for the reference resistor. Analog, time-series data was collected for both sensor types. Although the contact sensor is based on a switch-like principle, an analog data collection approach was used to better understand the force relationship. For both sensor types, one sensor lead was connected to the 5V power supply and the other sensor was tied to the reference resistor and ground. For the contact sensors, since there are two sensing components, the brief contact electrode was wrapped around the top applicator and the e-textile garment contact electrode was located in the bottom platform of the Instron setup, underneath the center of the applicator (Figure 4.2). Since the force sensors only have one sensor component (integrated into the base garment), a sensing component was not needed for the top applicator, and the force sensor was positioned on the bottom platform of the Instron setup, underneath of the center of the applicator (Figure 4.3).

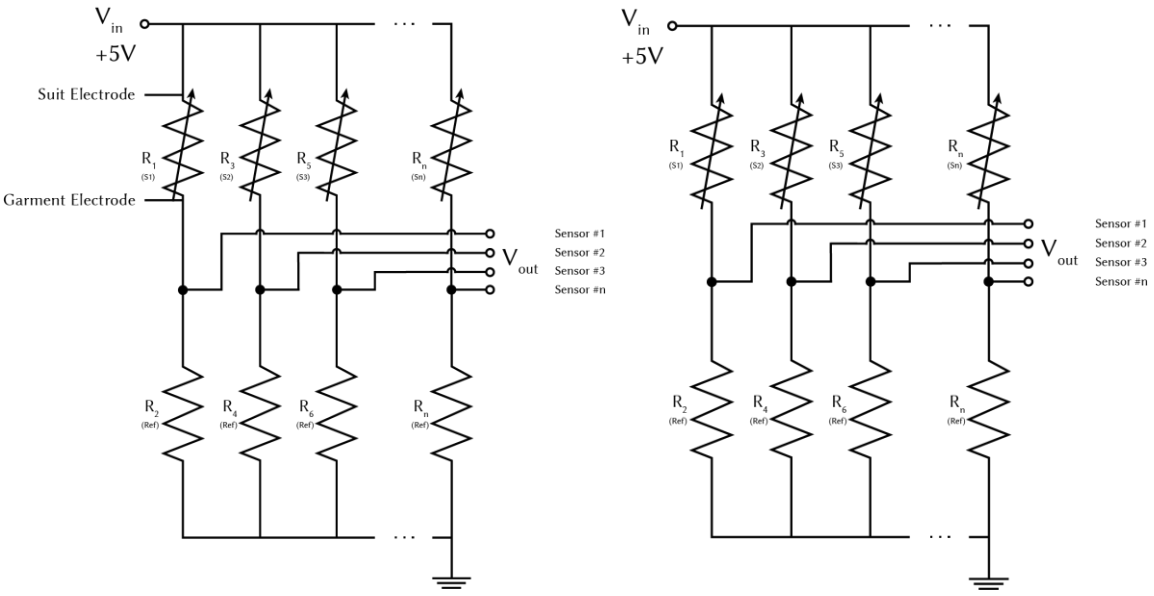

Figure 4.1: Voltage divider circuit used for contact (left) and force (right) sensors during Instron testing.

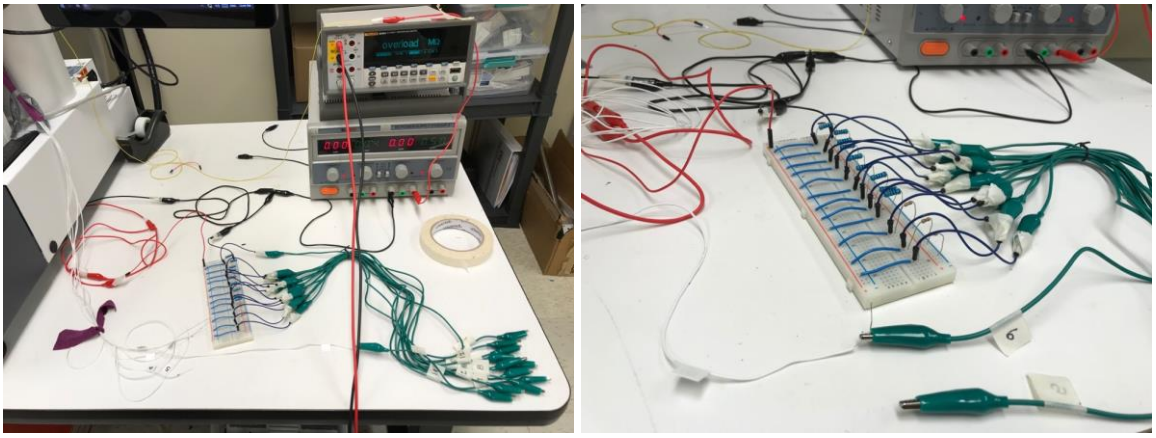

Figure 4.2: Electrical setup for Instron *contact* sensor testing.

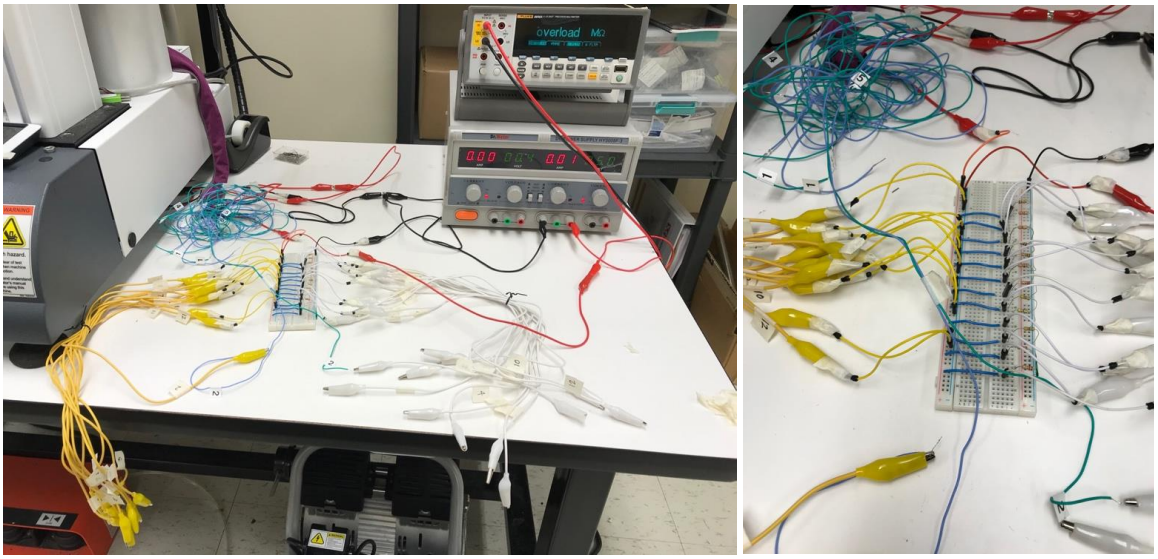

Figure 4.3: Electrical setup for Instron *force* sensor testing.

An Instron compression platen (2501 Series) [89] made of a hard surface (Rockwell HRC 58/60) was used in the bottom of the Instron testing setup. A layer of ballistics gel (0.15 in / 0.38 cm thickness) was added to the bottom platen to simulate the compliance of the body's surface tissue. A 3D printed applicator used to apply force to the sensors was secured in the top Instron grip with pneumatic side action grips for testing. The applicator was printed using Stereolithography (SLA) 3D printing with a clear liquid photopolymer resin material that cures into solid isotropic parts (Form 2 [90]). The top applicator was approximately the same size of the outer sensor dimensions (1.18 in / 3 cm). During testing, the bottom platform remains in place, while the applicator moves up

and down at a controlled, specified rate to apply a predetermined amount of force to the bottom platform (and sensor) (Figure 4.4).

Figure 4.4: Instron testing for contact (left) and force (right) sensors.

Static and cyclic force testing was performed for each sensor type (contact and force). The top applicator was set to a displacement rate of 0.5 millimeters (mm)/second (s) to move up and down and apply a maximum of 1 Newton (N) of force to the sensor. A low force (1 N) was used for testing to simulate contact. For cyclic testing, each sensor was tested for 3 trials using 4 cycles (1-pre cycle, 3-test cycles) per trial. The pre-cycle data was not used for data analysis to accommodate for any potential settling effects in the Instron at the beginning of each trial. Sensors were taken out of the Instron machine and repositioned between trials to capture any position effects of the sensor. For static testing, each sensor was tested for 1 trial, with 60 seconds of no applied force followed by 60 seconds of applied force (1 N).

4.1.2 Instron Test Data Analysis

4.1.2.1 Contact Sensor Contact-Threshold

To accommodate any variation in sensor response (V) between individual sensors, a contact-threshold at which the sensor measures contact was calculated for each individual contact sensor. Treating the contact sensor like a traditional digital switch, 50% of the maximum sensor amplitude from static Instron testing was used to set a threshold for measuring contact. Forces below and above the contact-threshold were measured and plotted to illustrate the range of forces experienced and understand what forces the sensor may not be capturing with this contact-threshold approach.

4.1.2.2 Force Sensor Contact-Threshold

A contact-threshold was also set for each individual force sensor to accommodate variation between individual sensors. The force sensors were treated as an analog signal, measuring a range of forces. To establish a contact-threshold for force sensors, the forces recorded for each unique voltage captured during cyclic Instron testing were identified. Using the unique voltages and corresponding force values, a contact-threshold was set using the first voltage instance above 0 V for which no zero or negative forces were recorded at or above that voltage. The average, standard deviation, minimum, maximum, and range of forces experienced at each unique voltage was also calculated to understand the pattern of forces that may be experienced at each voltage instance.

For manikin testing, it was found that this approach did not provide a useful sensor calibration method for on-body sensing due to variation in sensor responses after being placed on the body (factors like fabric stretching inducing a sensor response, and tension around the manikin inducing load on the sensors), therefore alternative methods were explored for analysis to set a contact-threshold for *on-body* calibration for force sensors. These methods are discussed in Sections 6.1.2.2 Modified Sensor Calibration and Contact-Threshold Debiasing Manikin Sensor Responses and 6.1.2.3 Modified Sensor Calibration and Contact-Threshold Using Marker Contact.

4.2 Manikin Test Method and Data Analysis

A humanoid robotic manikin (Cyberquins, Ltd., UK) that performs a cyclic running sequence was used for controlled sensor testing and validation. The manikin used for testing is not a perfect reflection of a human body in shape or compliance, but it performs precise and repeatable movements for more controlled testing which is advantageous for multiple trials to be compared.

4.2.1 Manikin Test Method

An optical Motion Capture system (Vicon) was used as a reference measure to track *physical* locations of the brief and manikin surfaces for contact assessment. The *physical* contact of the brief and manikin surfaces were compared with *electrical* contact collected from sensors.

For manikin testing, sensors were connected to an integrated MoCap data acquisition (DAQ) system to simultaneously collect MoCap marker data along with electrical sensor data. Both marker and sensor data were collected with a sampling frequency of 100 hertz (Hz) (100 samples per second), well above the frequency of the manikin movement. The voltage divider circuit for the sensors was powered with a DC power supply (Dr. Meter HY3005F-3) and set to 5V for all data collection.

The manikin test method included two different body conditions to assess measurement differences with changes to the underlying body: 1) non-padded, and 2) padded. Padding was added for the padded manikin condition to the butt, hips, and pelvis/crotch area to understand how body size/shape variation influences contact and sensor response. The hip (largest) circumference measurement had a difference of approximately 4 in (10.16 cm) between the non-padded manikin and the padded manikin. Each manikin body condition was tested with 4 different trials: 1) brief, static, 2) brief, dynamic, 3) no brief, static, 4) no brief, dynamic. Table 4.1 lists the manikin conditions tested and trial details. All trials had the e-textile sensing garment donned on the manikin. The two 'brief' trials had the brief donned on the manikin (on top of the e-textile sensing garment) and the

two ‘no brief’ trials were taken without the brief donned on the manikin (only the e-textile sensing garment). The two ‘static’ trials were taken with the manikin in a stationary position of the gait cycle, with thighs in a parallel configuration, and the two ‘dynamic’ trials were captured while the manikin was performing a cyclic running sequence.

Table 4.1: Test conditions.

Manikin Shape	**Manikin Motion**	**Wearable System**
Non-padded	Static	No brief
Padded	Dynamic	Brief

To capture marker data using the MoCap system, 9 cameras were calibrated using the standard calibration procedure and used for data collection. Spherical reflective pearl hard markers (14 mm diameter, threaded on a 17 mm plastic base) were placed in sensor locations, on top of the sensor garment. For contact sensor (cs)6, force sensor (fs)6, and fs7 locations (Figure 3.23), it was not possible to use a marker on the sensor. Fs7 is located on the right side of the manikin’s waist and the metal bar interferes (optically and physically) with this location, and no marker was used. Cs6 and fs6 are located in the crotch area and are spaced too closely to each other for the MoCap system recognize two markers as two individual points. Instead, a single marker to represent both cs6 and fs6 was placed in the center of the crotch. A total of 22 markers were used to track physical locations on the manikin and brief for 24 sensors (Figure 4.5). Eight additional reference markers were placed on the manikin surface to capture any potential manikin bounce and to track position of the gait cycle for subsequent alignment of trial data (Figure 4.6). Markers were located on the manikin’s center front and center back chest to track bounce (a relatively stable location on the manikin that should not be producing dynamic movement). Markers on the manikin’s knee and upper calf were used to track the position of the gait cycle.

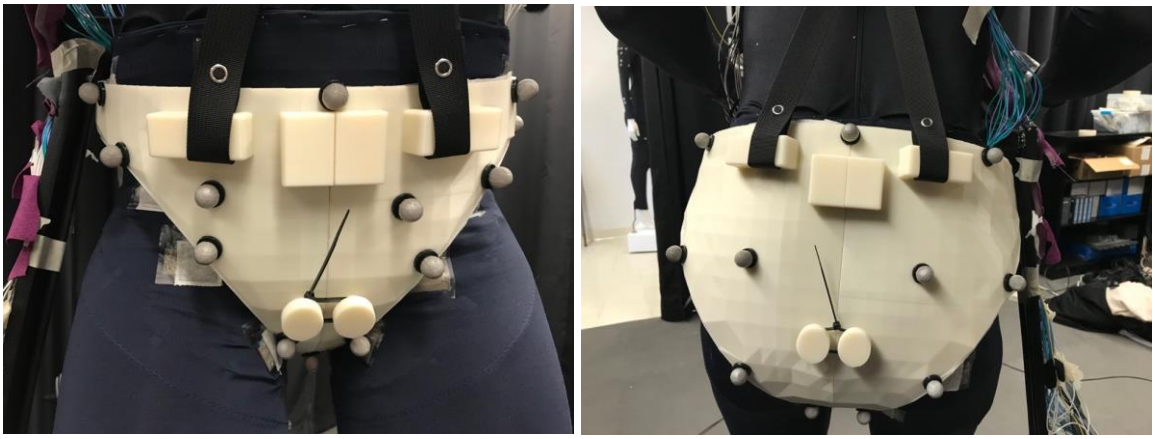

Figure 4.5: MoCap marker locations on the brief (front (left) and back (right)).

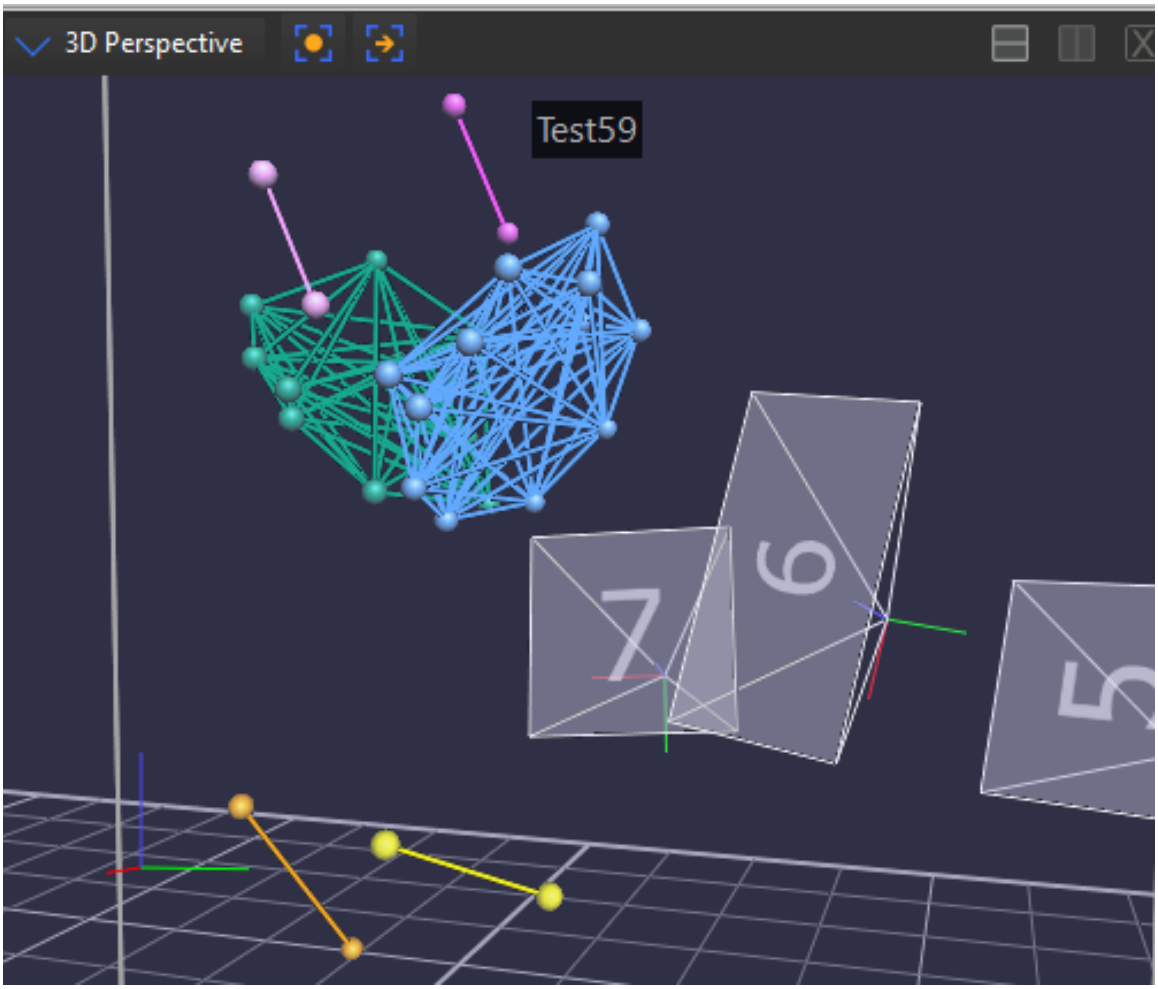

Figure 4.6: MoCap marker locations on the brief left (blue)- and right (green)-side, and manikin's front (light pink) and back (dark pink) torso, right (orange) and left (yellow) knees and calves in the Vicon software system.

4.2.2 Manikin Test Data Analysis

Marker and sensor data were analyzed to determine periods of contact and no contact for both manikin size conditions (non-padded and padded) and compare contact duration and location between the manikin and the brief.

4.2.2.1 Marker Contact Calculation

The MoCap system provides X, Y, Z coordinate data of each marker within the capture environment. To calculate marker contact, marker data from the dynamic *brief* and *no brief* trials were analyzed. Since this method uses a 2-part MoCap data collection, trials needed to be aligned first to achieve the same gait positioning throughout analysis for consistent comparison of trials. Trials were aligned by using the left knee position, which was found to be slightly more stable during movement compared to the right knee. The X coordinate experienced the largest change during gait cycles compared to the Y and Z coordinates and was used for aligning data. The peaks of the X coordinate for the left knee were identified and datasets were trimmed to 10 gait cycles total for analysis. It was found previously that a garment on the manikin settles during the first few gait cycles [91]. To account for any potential settling of the brief or sensor garment, peaks 3-13 were used for analysis. Each gait cycle lasted approximately 5 seconds, with a total of approximately 50 seconds for data analysis.

The X, Y, Z coordinates for each marker pair were used to calculate the Euclidean distance between marker positions in the two trials (brief and no brief) (Equation 1). The thickness of the brief (0.57 in / 1.45 cm) and any marker placement offset between trials was subtracted from the data collected. Markers were placed in the center of sensor locations when possible for all trials. Some markers were not able to be placed directly in the center of the sensor and needed to be offset slightly, due to the sensor center position being occluded from MoCap during manikin movement (e.g., folded within a manikin joint intersection).

$$\sqrt{(x_2 - x_1)^2 + (y_2 - y_1)^2 + (z_2 - z_1)^2} \quad \textbf{(1)}$$

The Euclidean distance between individual marker pairs was used to determine if there was contact or no contact between the brief and the manikin. If the distance between two marker pairs was at or below 0 cm it was measured as marker contact. If the distance was greater than 0 cm it was recorded as no contact.

4.2.2.2 Sensor Contact Calculation

To calculate sensor contact, sensor data from the dynamic *brief* trial only was analyzed to determine when the brief made contact with the manikin. A standard moving average filter in MATLAB was used to filter electromagnetic radiation noise that was observed during testing when connected to the MoCap DAQ system. Instances of sensor contact and no contact were calculated using the previously defined Instron calibration method to set a contact-threshold for sensors (contact sensors: 50% maximum amplitude, force sensors: first voltage instance above 0V with no zero or negative forces observed at or above that value). The contact-threshold for sensors was used to determine periods of contact and no contact. If the sensor response was equal to or above the contact-threshold (V), it was measured as contact. If the sensor response (V) was below the contact-threshold (V) it was measured as no contact.

4.2.2.3 Calculating and Comparing Marker Pair and Sensor Contact

The percentage of contact over the duration of each trial for both markers and sensors was calculated by taking the number of instances of detected contact divided by the total instances of the data analyzed.

Marker pair distance and sensor response data were plotted – to show detailed patterns of contact and no contact over the 10 gait cycles, as well as an overall percentage of contact measured for the entire 10 gait cycle test duration – to visualize and compare *physical* contact captured by the MoCap system and *electrical* contact captured by the sensors. To compare detailed patterns of contact and no contact during the manikin's

gait cycles, marker pair distance and sensor response time-series plots were annotated with periods of contact and no contact for easy visualization. To compare contact detected over the duration of the test, the calculated percentage of contact for marker and sensor data was plotted for comparison.

Chapter 5

5 Instron Test Results and Discussion

This section is a combination of the Instron test results and discussion for contact and force sensors.

5.1 Contact Sensor Test Results and Discussion

Select plots that illustrate contact sensor results from cyclic and static Instron testing are shown in Figure 5.1-Figure 5.10. Figure 5.1 shows the summarized responses of all sensors from cyclic testing. Individual sensor results from both cyclic (Figure 5.2-Figure 5.4) and static (Figure 5.5-Figure 5.7) testing are included to represent the variation in sensor response that can occur between individual sensors, a best (cs6) and worst (cs1) case scenario. These plots also illustrate sensor responses from sensor locations are influenced by garment variables underneath the sensor (cs1, waistband & cs6, crotch seam) and sensors that are located on top of only the base garment textile (cs2). Plots show each sensor response in relation to force, as well as force and sensor response over time. Figure 5.8-Figure 5.10 show forces below and above the established contact-threshold. All results for each individual sensor are included in the Appendix Section A.1.1 Contact Sensors.

5.1.1 Contact Sensor Test Results

Voltage responses to loading forces from *cyclic* Instron testing for contact sensors for 3 trials each are shown in Figure 5.2-Figure 5.4. Trials are indicated with different colored lines (Trial 1: blue, Trial 2: orange, Trial 3: yellow). In the time series plots the applied force (N) has a more translucent opacity than the sensor response (V) which if fully opaque. The individual plots for all sensors are located in the Appendix Section A.1.1.1 Cyclic Testing.

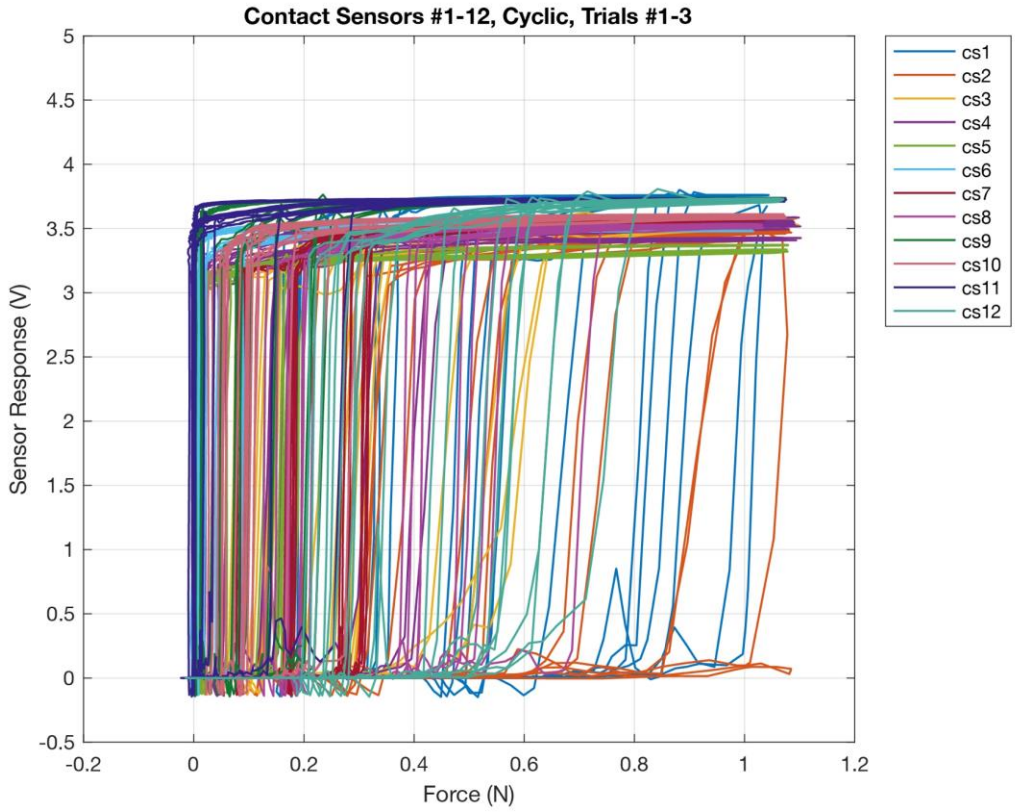

Figure 5.1: Contact sensors #1-12, cyclic testing, force vs. voltage.

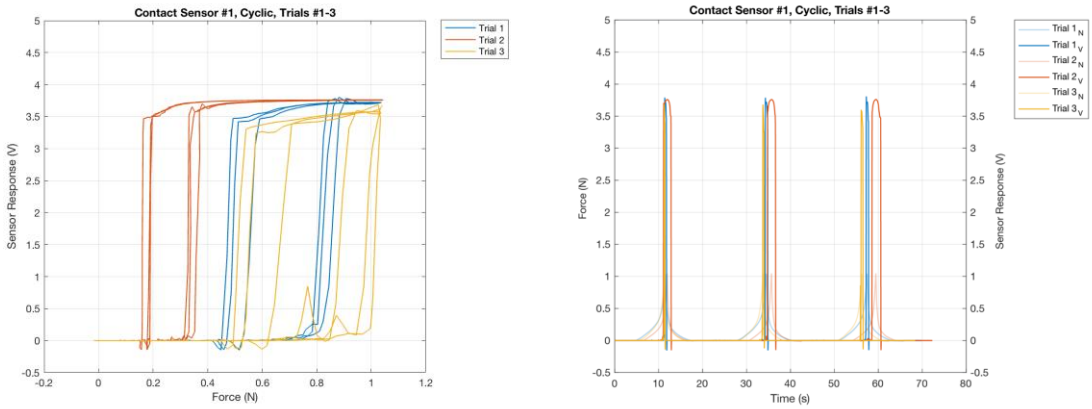

Figure 5.2: Contact sensor #1, cyclic testing, trials #1-3: force vs. voltage (left) and time vs. force and voltage (right).

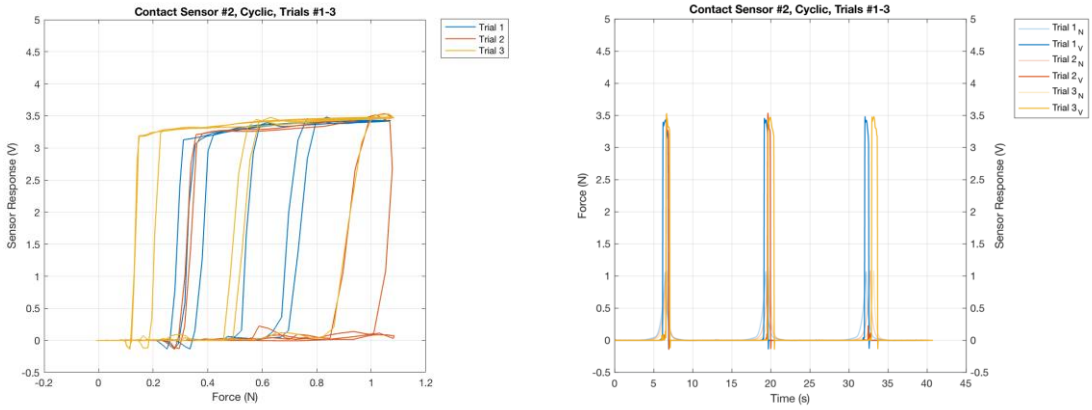

Figure 5.3: Contact sensor #2, cyclic testing, trials #1-3: force vs. voltage (left) and time vs. force and voltage (right).

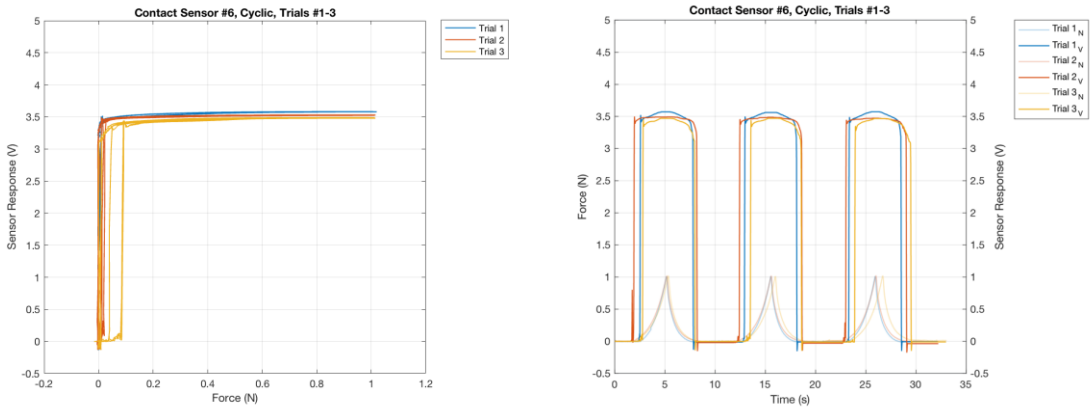

Figure 5.4: Contact sensor #6, cyclic testing, trials #1-3: force vs. voltage (left) and time vs. force and voltage (right).

The *static* Instron test results for the same contact sensors are shown in Figure 5.5-Figure 5.7. For the time series plots (right), the blue line indicates the applied force from the Instron system and the orange line represents the sensor response in Volts. The plots for all sensors can be found in the Appendix Section A.1.1.2 Static Testing.

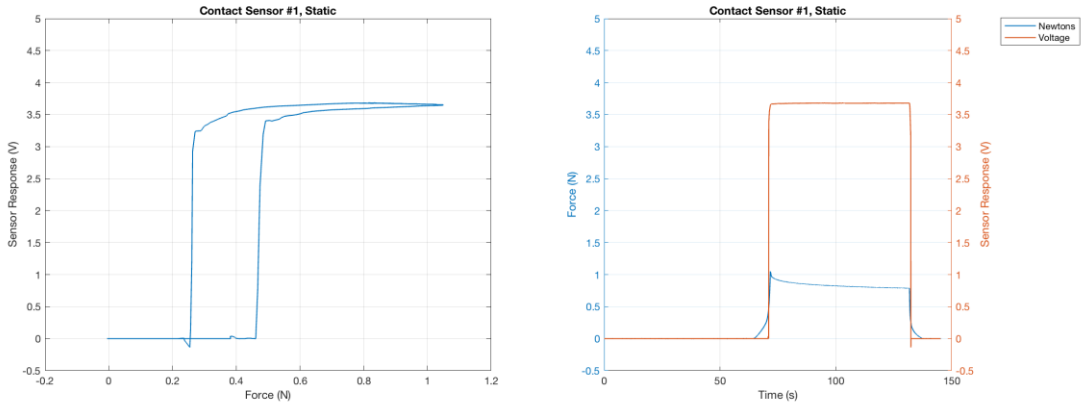

Figure 5.5: Contact sensor #1, static testing a) force vs. voltage, b) time vs. force and voltage.

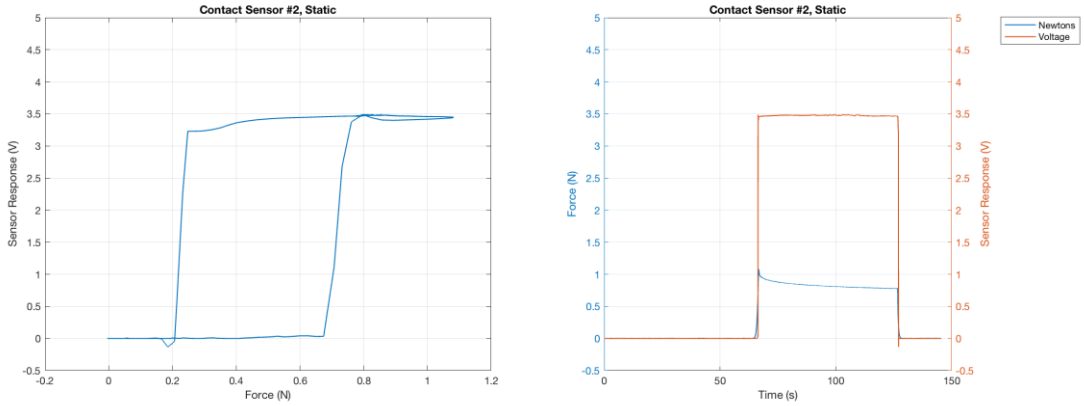

Figure 5.6: Contact sensor #2, static testing a) force vs. voltage, b) time vs. force and voltage.

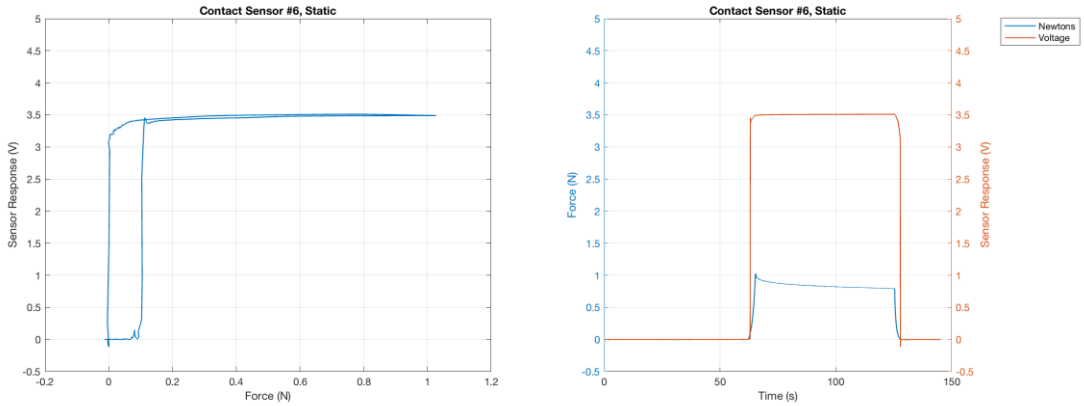

Figure 5.7: Contact sensor #6, static testing a) force vs. voltage, b) time vs. force and voltage.

5.1.2 Contact Sensor Test Discussion

Overall, contact sensors were able to accurately measure contact in a controlled testing environment but some overlap in forces experienced in both below and above the contact-threshold was observed which influenced the accuracy of individual sensors. Sensors make contact at low forces. As expected, there was a very low sensor response with no applied force and the sensor response increased quickly with applied force in a switch-like manner. In the controlled Instron environment, there was some variation observed between trials, where the garment was removed from the testing environment and repositioned, as seen in the differences between trials in the cyclic testing results. This characteristic was not formally evaluated here, but did influence repeatability of the sensor. There was also some hysteresis observed for sensors: in general, the electrical connection was maintained over a larger range of forces during the separation cycle compared to the connection cycle. This may have been due to the fibers of the textile slightly sticking or interlocking with each other when contact was made.

Contact sensors that are located in areas on the garment where there are additional garment variables present underneath the sensor, such as a seam or waistband, can create a protrusion(s) in the profile of the sensor and affect the sensor response. For example, cs6 is located over a seam and makes contact much more quickly and at lower forces compared to cs2 which is not affected by an additional garment variable. It is likely that the crotch seam is deforming cs6 outward and away from the garment, thus making sensor contact occur more quickly and at lower forces and maintaining contact for longer and over more degrees of applied force, compared to other sensors. The longer duration of contact for cs6 is likely affected by the additional textile layers underneath the sensor (due to the protrusion of the 3D crotch seam allowance) compressing and absorbing applied force after contact is made. Another sensor that has an additional garment variable underneath is cs1 which is located over the silicone-backed waistband. This can create irregularities or protrusions on the sensor's profile, but exhibits less influence on sensor response compared to cs6. While there are multiple layers that make up the waistband under cs1, the layers have less of a protrusion and seem to have less of an

effect on deforming the sensor. This shows that particulars of garment construction and geometry can influence sensor responses.

The contact sensors do show some variability between connection and separation force. The connection force for sensors is generally higher than the separation force, where contact seems to be maintained for a longer period of time and over a larger range of applied force. This longer period of contact duration during separation force may be due to the textures of the two contact electrode surfaces holding onto or sticking to each other. The textile fibers may be very slightly interlocking with each other, requiring a slightly longer separation force to break the connection. Essentially, it appears that the contact sensor can stay in contact for slightly longer when the force is unloading.

During static testing, the applied force from Instron was set to 1 N for 60 seconds, but as the plots in Figure 5.5-Figure 5.7 showed, the amount of applied force slightly decreased over the duration. This slight decrease was likely due to the sensor or Instron relaxing while being held at a single displacement. However, the contact sensor responses during static testing remained relatively stable and did not appear to have a substantial issue with drift, which has been common with traditional sensors but can be more common with textile-based sensors. Some drift was observed with the force sensors in this study, as discussed in Section 6.1.2.2 Modified Sensor Calibration and Contact-Threshold Debiasing Manikin Sensor Responses.

5.1.3 Contact Sensor Contact-Threshold

Contact-threshold results based on the previously defined method of calculating 50% of the maximum sensor amplitude from Instron testing for contact sensors are listed in Table 5.1.

Table 5.1: Contact-threshold for contact sensors.

Contact Sensor #	Contact-Threshold (V)
1	1.84
2	1.74
3	1.78
4	1.83
5	1.69
6	1.76
7	1.82
8	1.78
9	1.87
10	1.81
11	1.86
12	1.85
Average	1.80
Standard deviation	0.05

Contact-threshold values are relatively similar for all sensors, with an average contact-threshold of 1.80 V with a standard deviation of 0.05. This contact-threshold is based on a digital switch principle where 50% of the maximum sensor amplitude is used to set a threshold for contact. Depending on the type of contact (lighter versus heavier contact) of interest to capture, a different approach using a similar method of setting the contact-threshold as the force sensors – using an analog response and finding the first non-zero or negative force at or above the sensor response instance – may allow capturing of lighter profiles of contact.

5.1.4 Contact Sensor Forces Below/Above Contact-Threshold

Plots of the forces experienced below and above the contact-threshold from Instron testing (Figure 5.8-Figure 5.10) are shown for the same contact sensors (cs1, cs2, cs6) discussed in the previous sections. The range of force experienced can vary between individual sensors and plots for all sensors can be found in the Appendix Section A.1.1.3 Forces Below and Above the Contact-Threshold.

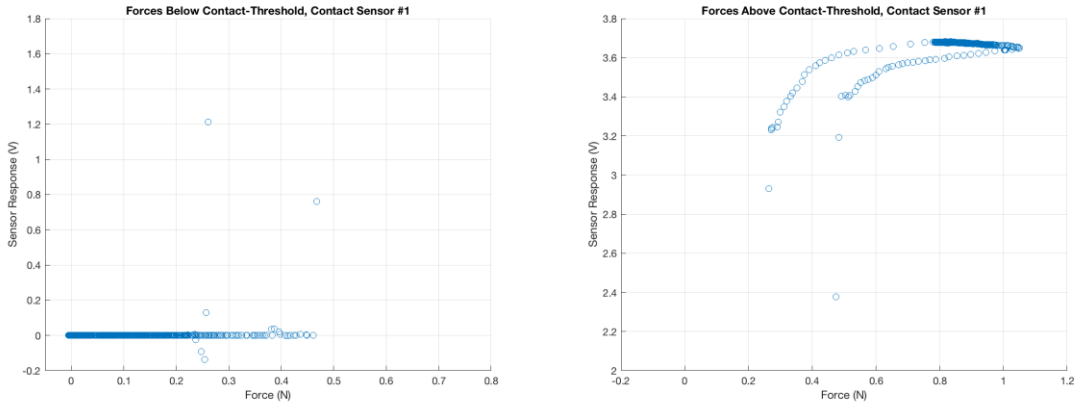

Figure 5.8: Forces below and above the contact-threshold, contact sensor #1.

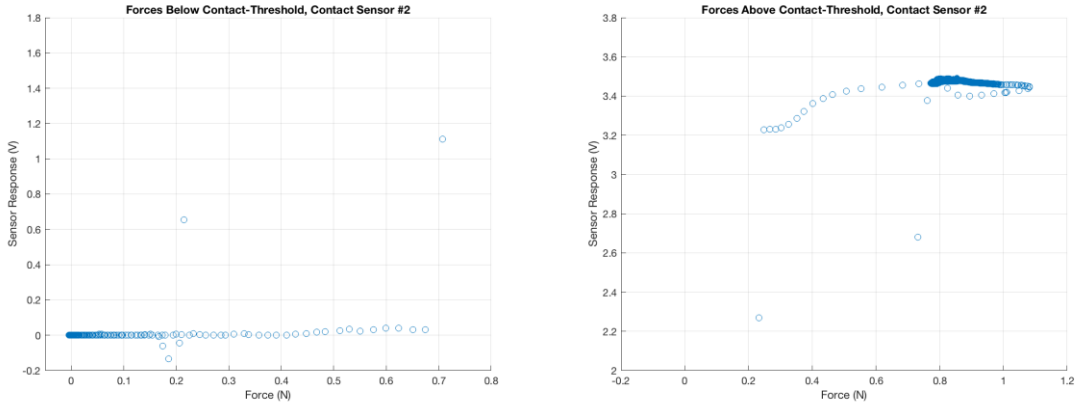

Figure 5.9: Forces below and above the contact-threshold, contact sensor #2.

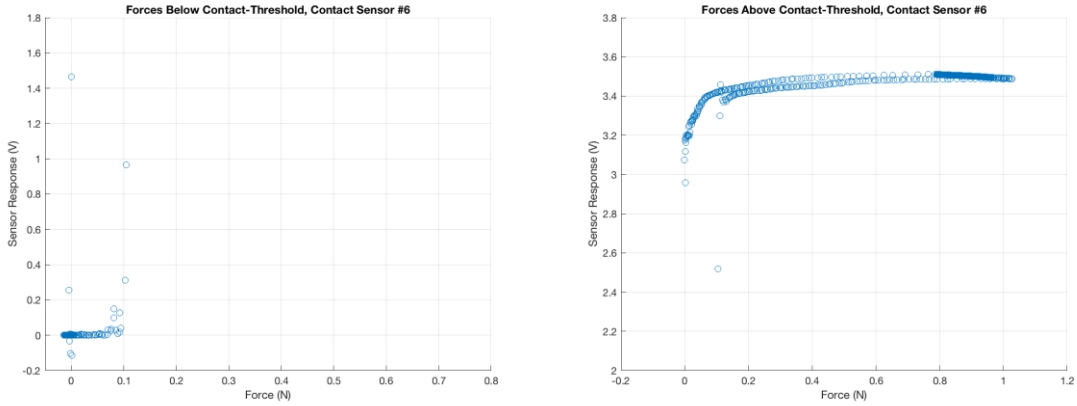

Figure 5.10: Forces below and above the contact-threshold, contact sensor #6.

There were small variations observed in sensor responses, such as a few voltage spikes for the below contact-threshold plots and dips in the above contact-threshold plots. The sampling rate used to collect data from Instron testing was much higher than human movement, which could be contributing to some outliers, as finer-grained data was captured with this higher sampling rate, including sensor noise and the brief analog response in the transition between the binary 'off'' and 'on' sensor states. Using a lower sampling rate would reduce these few outlier instances.

However, more importantly for sensing, there was also some overlap observed in measured forces captured in the below and above the contact-threshold data. Using the threshold calibration model, contact sensors accurately measured contacts above about 0.5 N, but recorded intermittent false negative contacts between approximately 0-0.5 N where there was more overlap in forces between the below and above contact-threshold data. Sensing in this overlap range was less likely to be accurate. However, sensing above the overlap range (approximately 0.5 N) was more reliable as it was only measured as contact (in the above contact-threshold data) and not measured no contact (in the below contact-threshold data). The forces that were more reliable, above the less reliable overlap range, measured at approximately 0.5 N, which is approximately the force applied by half of an apple under the force of gravity (1 N = 1 apple in 1G). Some of the sensors experienced approximately 0.5 N or less of overlap in measured forces between the below and above contact-threshold data. For example, with cs2 (Figure 5.9), the majority of the *below* contact-threshold forces were concentrated between 0-0.2 N. However, less below-threshold forces were found between 0.2 N up to a maximum of 0.7 N. (This sensor experienced the highest forces (around 0.7 N) below the contact-threshold.) For the same sensor, cs2 (Figure 5.9), the forces *above* the contact-threshold were primarily concentrated between 0.8 and 1 N, but less frequent forces were also observed between 0.2-0.8 N. With the both the below and above contact-threshold data for this sensor (cs2), there was an overlap in measured forces from 0.2-0.7 N, meaning that forces within this overlap range could be interpreted either as no contact or contact depending on which voltage was measured. The specific sensing context and contact forces of interest in measuring is important to assess accuracy with an overlap in experienced forces like this.

If the sensing application targets forces that fall within the overlap range, it would make the method less reliable for accurate measurement. However, if the target contact forces are above this overlap range, the contact and no contact judgement of the sensor can provide much more reliable and accurate data.

Most sensors, including cs1 and cs2 (Figure 5.8 and Figure 5.9), experience a larger range of forces *below* the contact-threshold compared to cs6 (Figure 5.10), which has a much narrow range of experienced forces. As mentioned previously, part of cs6 is located over the crotch seam and that part of the sensor can have a slight protrusion above the rest of the sensor and garment. This type of garment variability under a sensor can likely contributes to differences in the sensor response, such as allowing the sensor to make contact more quickly and at lower forces compared to other sensors, including cs1 and cs2. In the below contact-threshold plots there are a few sporadic outliers observed at these lower forces and could likely be due to the sensor response fluctuating at the noise level. There is overlap of observed forces from around 0.25-0.45 N between the below and above contact-threshold data, which can make the sensor less accurate in detecting contact versus no contact within this range.

5.2 Force Sensor Test Results and Discussion

Select plots that illustrate force sensor results from cyclic Instron testing are shown in Figure 5.11-Figure 5.20. Figure 5.11 shows the summarized responses of all force sensors from cyclic testing. Individual sensor results from both cyclic (Figure 5.12-Figure 5.14) and static (Figure 5.15-Figure 5.17) testing are included to represent the variation in sensor response that can occur between force sensors, showing best (fs2) and worst (fs6) case examples as well as sensors that are located around additional garment variables that could influence sensor responses (fs1 and fs6) and a location without any additional garment variables (fs2). Plots show each sensor response in relation to force, as well as force and sensor response over time. Figure 5.18-Figure 5.20 show forces below and above the established contact-threshold. All results for each individual sensor are included in the Appendix Section A.1.2 Force Sensors.

5.2.1 Force Sensor Test Results

Sensor voltage responses under applied force from *cyclic* Instron testing for force sensors during 3 trials are shown in Figure 5.11-Figure 5.14. Figure 5.11 shows sensor responses for all sensors. Figure 5.12-Figure 5.14 show the sensor response for select individual sensors. Trials are indicated with different colored lines. In the time-series plots, the applied force has a more translucent opacity than the sensor response which is fully opaque.

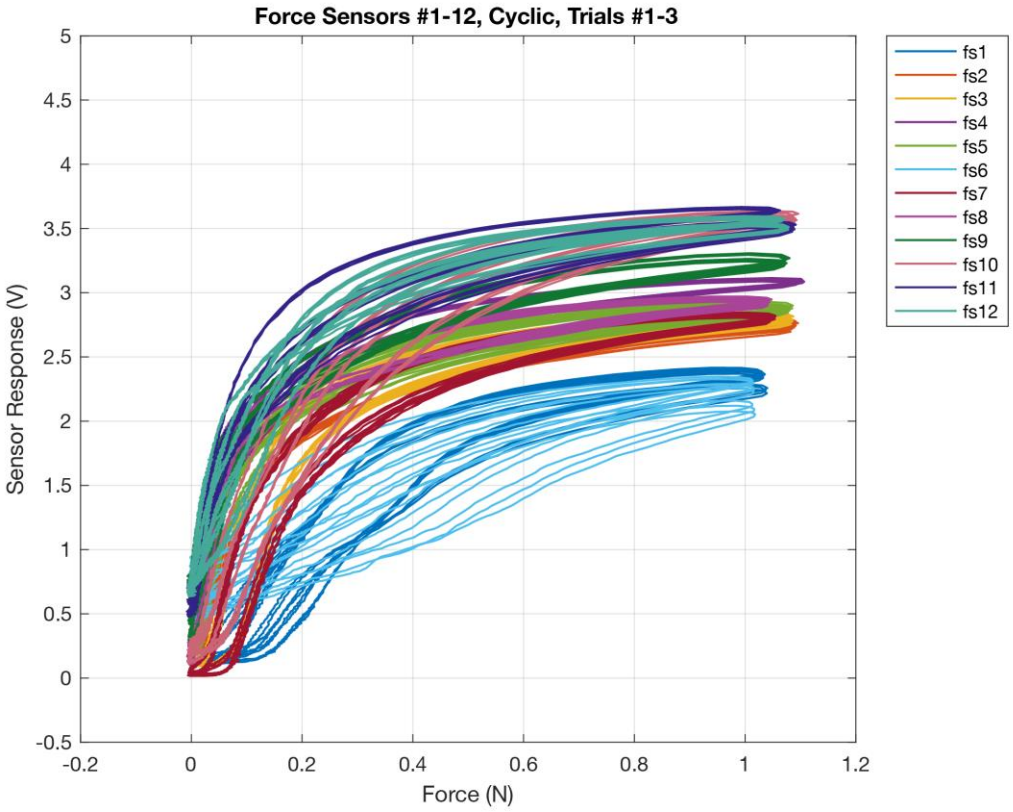

Figure 5.11: Force sensors #1-12, cyclic testing, force vs. voltage.

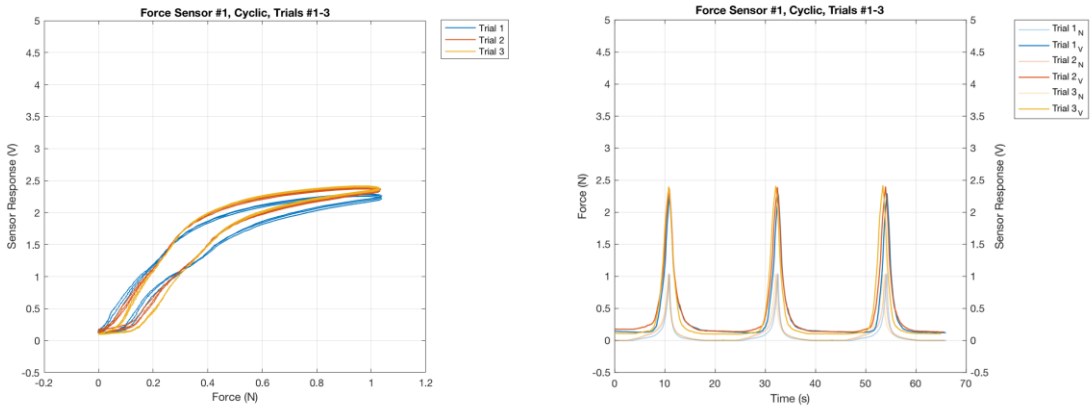

Figure 5.12: Force sensor #1, cyclic testing, trials #1-3: force vs. voltage (left) and time vs. force and voltage (right).

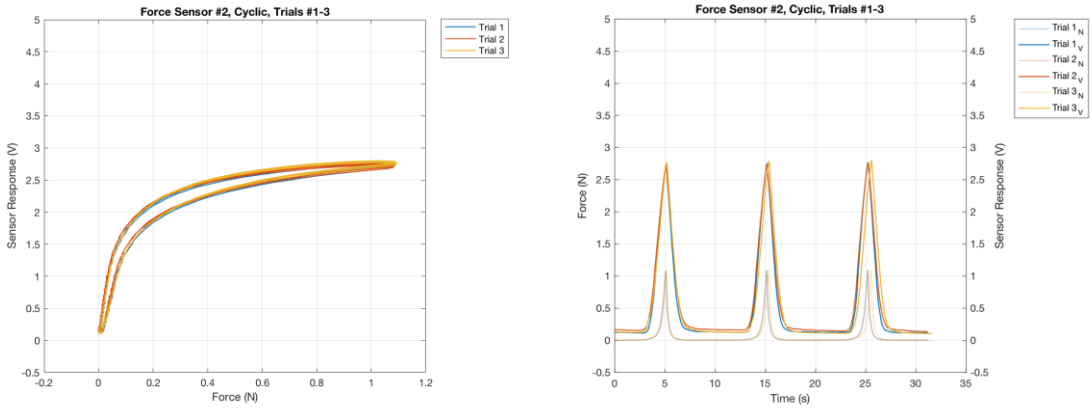

Figure 5.13: Force sensor #2, cyclic testing, trials #1-3: force vs. voltage (left) and time vs. force and voltage (right).

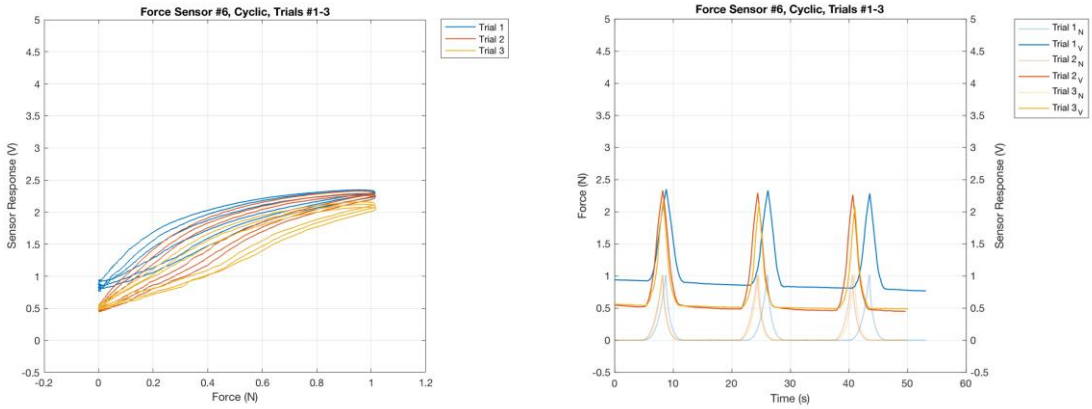

Figure 5.14: Force sensor #6, cyclic testing, trials #1-3: force vs. voltage (left) and time vs. force and voltage (right).

Plots from *static* Instron testing for force sensors during 1 trial of approximately 60 seconds of no applied force, followed by 60 seconds of applied force are shown in Figure 5.15-Figure 5.17.

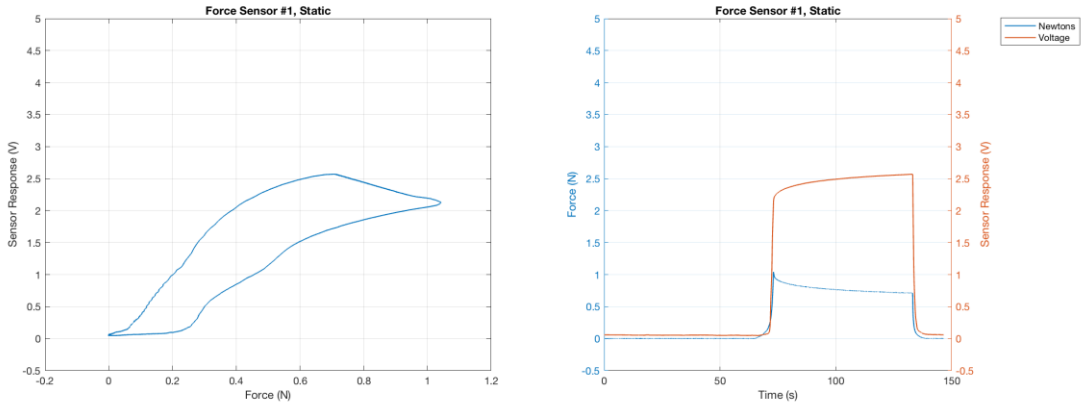

Figure 5.15: Force sensor #1, static testing a) force vs. voltage, b) time vs. force and voltage.

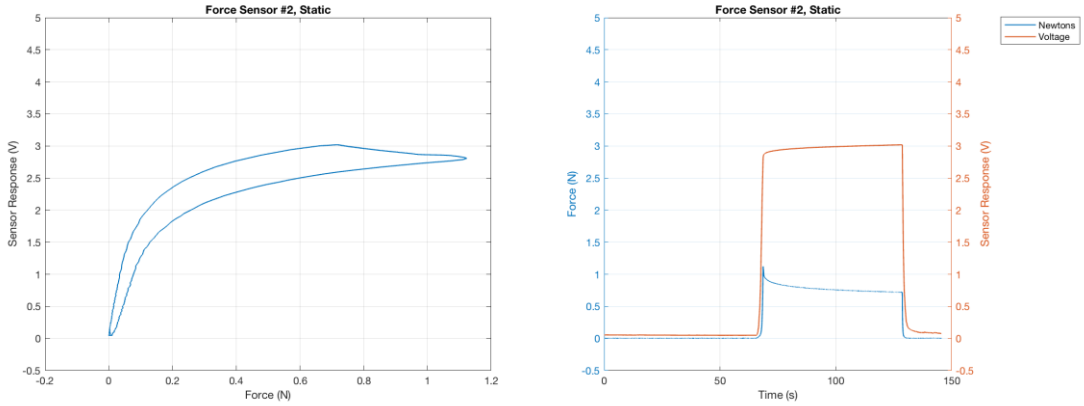

Figure 5.16: Force sensor #2, static testing a) force vs. voltage, b) time vs. force and voltage.

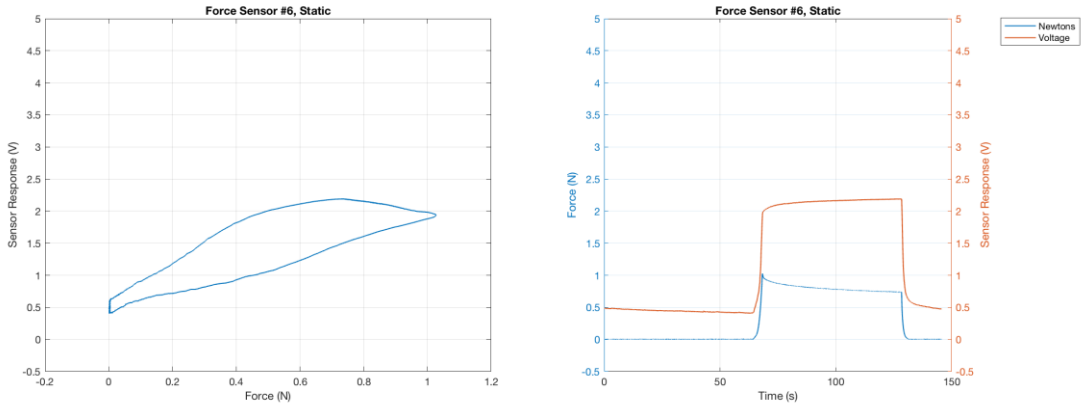

Figure 5.17: Force sensor #6, static testing a) force vs. voltage, b) time vs. force and voltage.

5.2.2 Force Sensor Test Discussion

Similar to the contact sensors, force sensors here also respond to very low forces, which is necessary to measure contact. As expected, force sensors have a more analog response and can measure a range of forces compared to contact sensors, with some force sensors having more of a linear behavior and others having a more logarithmic behavior to applied force. All force sensors exhibit some hysteresis in their responses during loading and unloading cycles, and the static plots show slight drift in sensor responses.

Overall, most of the force sensors are fairly repeatable between repositioning trials, with some (fs6) being less repeatable than others. Fs6 is located along the crotch seam and shows much more variation in the sensor response from Instron testing compared to other force sensors, such as fs2. There is slight variation with fs1, which is also located over a garment area (silicone-backed waistband on the inside), which may have a slight influence on the sensor response. Fs2 is a sensor that is located on an area that does not have any additional garment features that may influence the sensor response and shows high repeatability between cycles and repositioning trials.

Most force sensors have a low sensor response with no applied load, around or slightly above 0 V. However, cs6, which also shows less repeatability compared to other force sensors, has a higher sensor response with no applied load, around 0.5-1 V. It is possible that the seam underneath the senor may be applying a small force that can vary depending on the positioning of the garment, as one trial measures a higher no-load sensor response compared to the two other trials. Cs1 is also located over an additional garment layer (silicone-backed waistband) and shows some variability in repeatability at lower forces but becomes more repeatable at higher forces.

Static Instron testing results for the force sensors exhibit some sensor response drift. Note that the applied force from the Instron system experienced a slight decrease in force over time (likely due to the Instron relaxing while maintaining a fixed position); however, instead of a corresponding decrease in force sensor responses, a slight increase was observed, indicating sensors were prone to drift. Similar to the contact sensors, the force

sensors experienced a fairly quick response with the applied load, but some of the force sensors experienced more linearity at the beginning of the applied load compared to the contact sensors.

5.2.3 Force Sensor Contact-Threshold Results and Discussion

Contact-threshold results for force sensors and corresponding force data from Instron testing are listed in Table 5.2. Note that this is using the initial Instron calibration and an alternative method using on-body calibration is described in Section 6.1.2 Force Sensors.

Table 5.2: Contact-threshold for force sensors (using original Instron calibration).

Force Sensor #	Contact-Threshold (V)	Average Force (N)	Standard Deviation	Minimum Force (N)	Maximum Force (N)
1	0.18	0.05	0.04	0.01	0.14
2	0.22	0.01	0.01	0	0.02
3	0.16	0.02	0.02	0	0.06
4	0.68	0.01	0.01	0	0.02
5	0.39	0.01	0.01	0	0.03
6	0.94	0.07	0.12	0	0.35
7	0.10	0.03	0.02	0	0.05
8	0.48	0	0	0	0
9	0.91	0.02	0	0.02	0.02
10	0.31	0.02	0	0.02	0.02
11	0.77	0.01	0.01	0	0.02
12	0.91	0.03	0.01	0.02	0.03
Average	0.50	0.02	0.02	0.01	0.06
Standard Deviation	0.32	0.02	0.03	0.01	0.10

The contact-threshold established for force sensors is generally low in sensor response (V) and force required to make contact. There is some variability that can be seen between sensors, with an average contact-threshold for all sensors at 0.50 V and a standard deviation of 0.32. It seems that many of the sensors that have a higher contact-threshold are located in more complex garment areas, such as an area where the garment may not lay completely flat (e.g., intersection of two garment pieces, seam). The average force for all force sensors is at 0.02 N, which is a low enough force to be used with the contact sensors, which generally measured contact at about 0.2 N.

5.2.4 Force Sensor Forces Below/Above Contact-Threshold

The plots in Figure 5.18-Figure 5.20 show the forces that were experienced during cyclic Instron testing both below and above the contact-threshold for select sensors. These sensor plots were included to capture the variability between sensors, showing the best (fs2, Figure 5.19) and worst case (fs6, Figure 5.20) examples as well as sensors that were over additional garment layers (fs1 and fs6, Figure 5.18 and Figure 5.20) and sensors that were not located over additional garment layers (fs2, Figure 5.19). All sensors' results are located in the Appendix Section A.1.2.3 Forces Below and Above the Contact-Threshold.

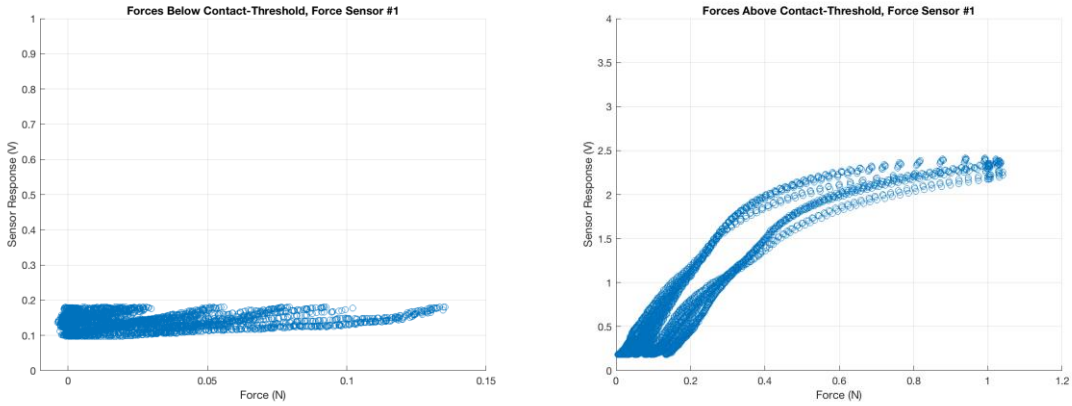

Figure 5.18: Forces below and above the contact-threshold, force sensor #1.

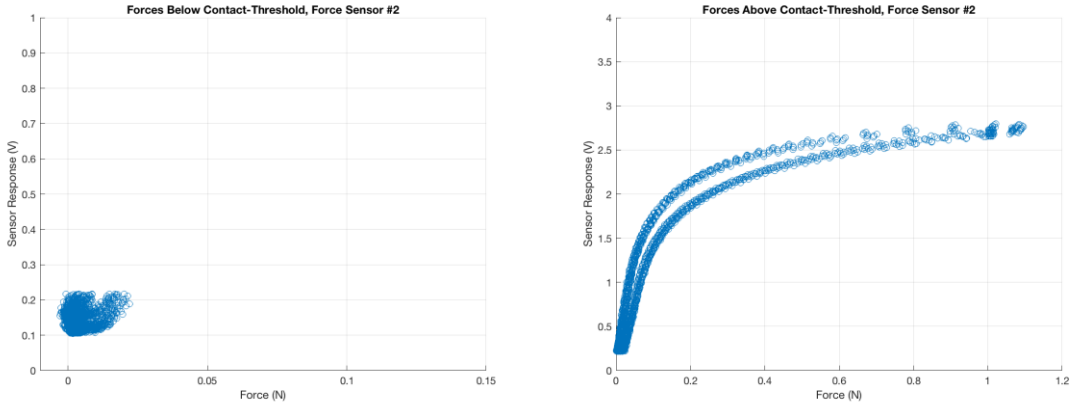

Figure 5.19: Forces below and above the contact-threshold, force sensor #2.

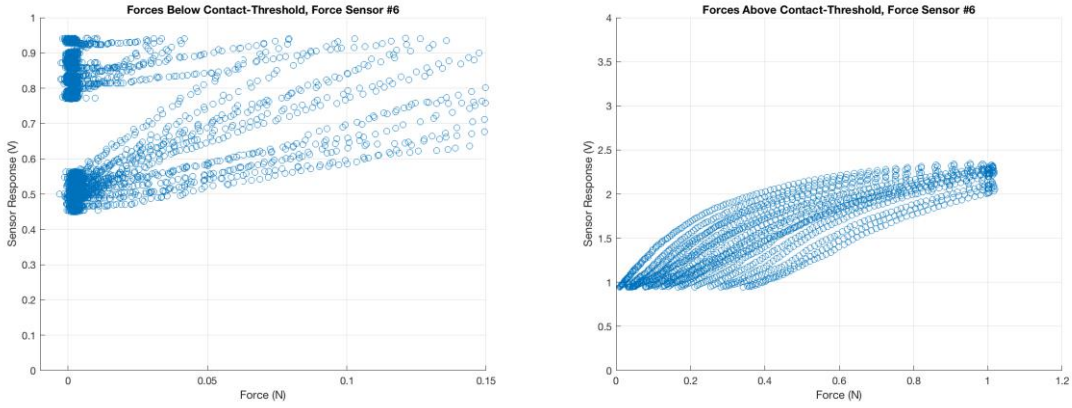

Figure 5.20: Forces below and above the contact-threshold, force sensor #6.

Using the threshold calibration model, force sensors reliably measured contacts above 0.15 N and comparatively recorded a smaller range of false negatives between 0-0.15 N, but a much larger proportion of false positives. Sensing in this overlap region, between 0-0.15 N was less reliable because the sensor could measure either contact or no contact. Sensing above this overlap region (above 0.15 N) was more reliable as the sensor only measured contact.

These figures illustrate some of the variability that can be found between sensors. Fs1 and fs6 are both located over an area on the garment with additional features that can create protrusions (waistband and crotch seam), whereas fs2 is located in a flat, smooth garment area with no additional garment features or textile layers. Fs2 has both a low sensor response and low force measured at the contact threshold. Fs1 and fs6 both require the highest force to reach the contact threshold. This higher force is likely needed due to the additional garment mechanical variables, such as the silicone-backed elastic waistband on the inside under fs1 and the multiple plies of fabric to form the crotch seam for fs6. The response from fs6 is spread out more compared to other sensors and is likely occurring due to the absorption of applied forces by the seam made up of multiple fabric plies underneath. Variability is also observed for the contact sensors that have additional material layers underneath the sensor, creating a protrusion(s) on the sensor's profile, such as cs1 and cs6.

Similar to the contact sensors, it appears that there may be an overlap in experienced forces between the below and above contact-threshold data for force sensors, but it is a much smaller overlap. The maximum force experience by any force sensor below the contact-threshold is below 0.15 N. The forces that are measured as contact for the force sensors are much lower compared to the contact sensors and are sometimes as low as 0 N as contact, which could contribute to the sensor reading too many false positives. The contact sensors experience a greater range of forces below the contact-threshold, but fewer contact sensors measure forces around 0 N as contact.

5.2.5 Comparing Contact and Force Sensors

Overall, both contact and force sensors were responsive to low forces in the controlled Instron testing environment. The accuracy of contact measurement between contact and force sensors varied. The force sensors experienced less overlap in experienced forces between the below and above contact-threshold data from Instron testing, but measured far more 0 N forces as contact than the contact sensors. The contact sensors experienced a larger overlap range between the below and above contact-threshold plots and had less reliable measurements based on this larger overlap range. Based on the data collected from the controlled Instron testing and the threshold-calibration processes used here, the force sensors appeared to be less likely to measure false negative responses compared to the contact sensors, but potentially more likely to measure false positive responses (this has not been quantified here). However, when translated to a body surface, force sensors experienced challenges that further impacted accuracy. This is further discussed in Section 6.1.2 Force Sensors.

The sensor response behavior between sensor types varied as expected, with contact sensors having more of a binary, switch-like behavior and the force sensors having more of an analog, linear or logarithmic behavior. Both sensors were affected by hysteresis, and to some degree showed variability between test cycles and between trials (due to repositioning) as well. The contact sensors showed more variability both between test cycles within a trial and between trials (repositioning), indicating the sensor response can vary with and without repositioning. It is possible that this variation could be caused by the brief analog response in the transition between the binary 'off'' and 'on' sensor states (attach and detach) and slight variations in the textile profile, causing contact to be made in slightly different spots and at different forces. The force sensors experienced less variability between cycles and trials and were less susceptible to effects of repositioning. This may be due to the force sensors only using one sensor component (rather than two components (electrodes) with the contact sensors), creating less friction of forces between two textile surfaces. Particularly for cs6 and fs6, which are sensors located over a garment seam, this contact sensor (cs6) experienced the least amount of variation between cycles and trials, meaning it was less susceptible to repositioning

effects. Whereas for this force sensor (fs6), it experienced the greatest about of variation and was the most susceptible force sensor to repositioning effects. This may indicate that for contact sensors a protrusion can create less variability but for force sensors it can create more variability (perhaps due to changes from the protrusion with the multi-layer sensor system).

Chapter 6

6 Manikin Test Results and Discussion

This section presents the results and discussion from *non-padded* and *padded* manikin testing, as well as a modified approach for force sensor calibration for on-body applications. Results show contact that was measured between the manikin's body and the brief suit component using the three different methods (MoCap marker pairs, force sensors, and contact sensors), but that the accuracy of each method was affected by different influences.

6.1 Non-Padded Manikin Test Results and Discussion

Results and discussion for the *non-padded* manikin conditions for contact and force sensors are covered in this section.

Figure 6.1 and Figure 6.2 showed the movement of the manikin's left (L) and right (R) knee using marker coordinate (X, Y, Z) position during the 'brief' (B) and 'no brief' (NB) dynamic test trials. The left knee X coordinate was used for aligning trials since during initial pilot testing it was found that it can experience the least amount of potential variation during gait cycles.

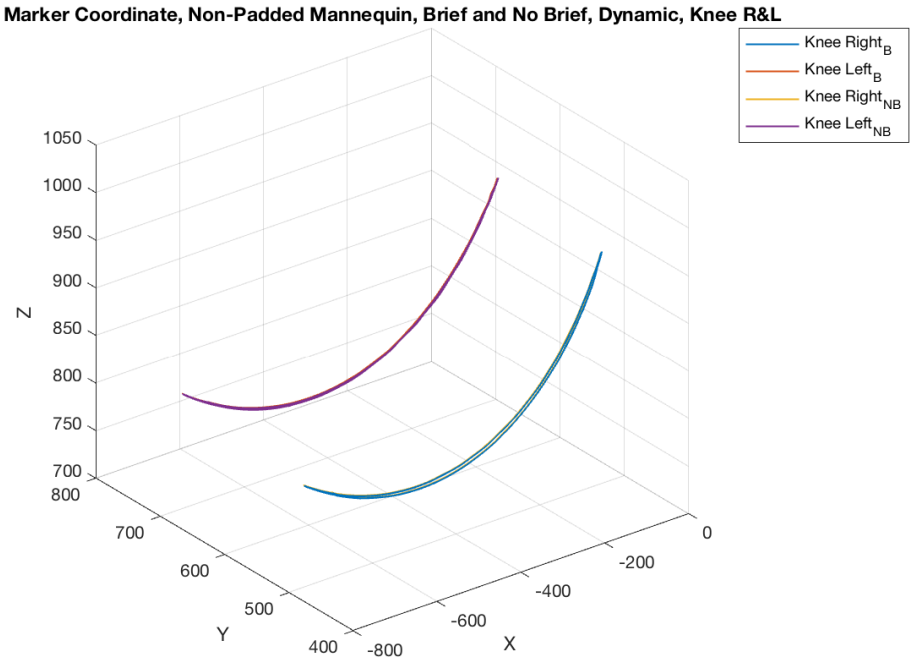

Figure 6.1: Marker coordinate (X, Y, Z) 3D view for manikin's left and right knee between 'brief' and 'no brief' dynamic test trials.

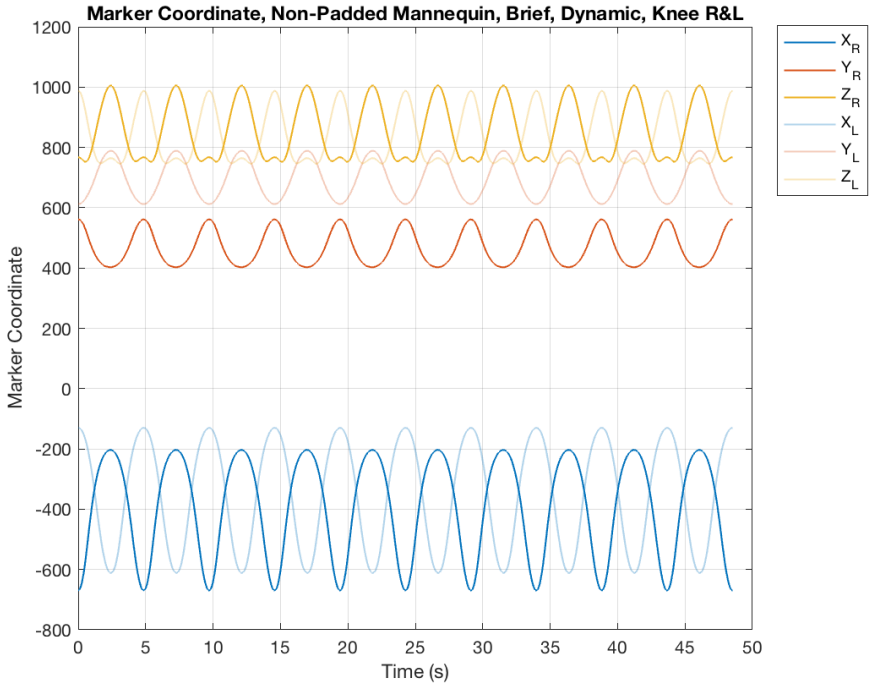

Figure 6.2: Marker coordinate (X, Y, Z) for manikin's left and right knee between 'brief' and 'no brief' dynamic test trials.

6.1.1 Contact Sensors

6.1.1.1 Contact Sensor Test Results

Results for the percentage of contact measured by MoCap markers and contact sensors in each location during the *non-padded* manikin condition test over the entire trial duration is plotted in Figure 6.3.

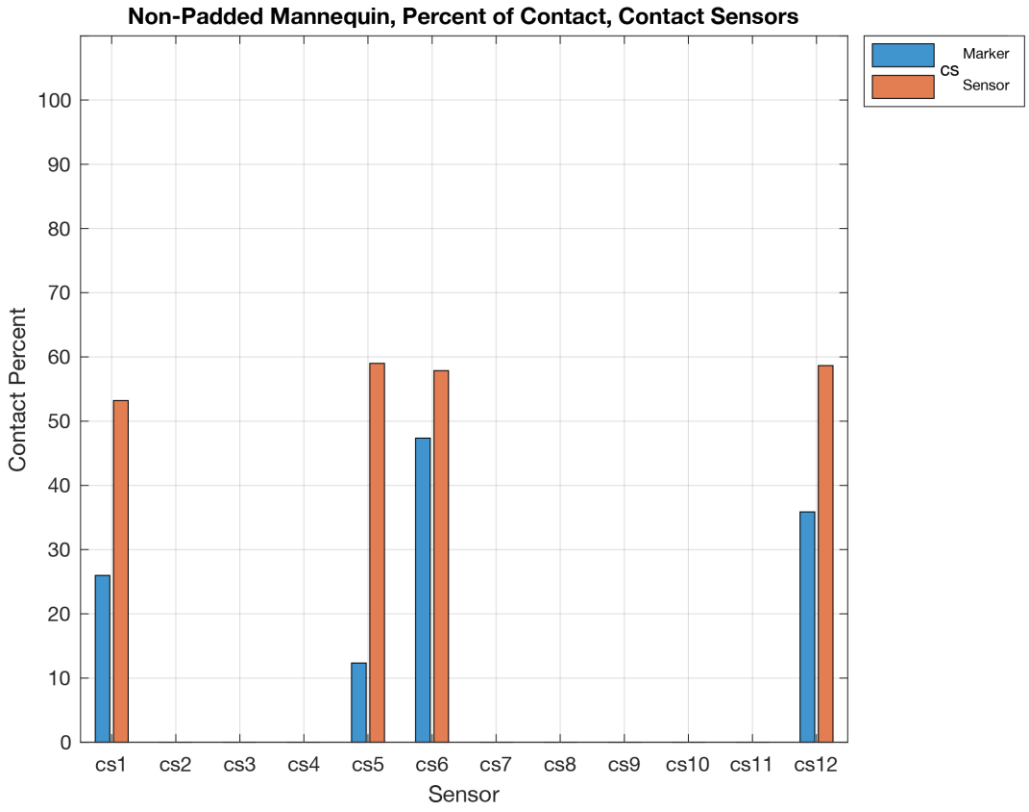

Figure 6.3: Percent of contact for *contact* sensors during the *non-padded* manikin condition.

Selected results showing detailed patterns of contact for marker pairs and contact sensor responses during *non-padded* manikin testing over the entire test duration are in Figure 6.4-Figure 6.7. These figures illustrate select sensor locations (cs9 and cs11) that experience no sensor or marker contact (Figure 6.4 and Figure 6.5) as well as select sensor locations that experience marker and sensor contact (cs5 and cs6) (Figure 6.6 and Figure

6.7). For sensor locations that experience marker and sensor contact, a better (cs5) and worse (cs6) case is shown. Marker pair distance is represented by a blue line and sensor responses are indicated with an orange line. Marker and sensor data are represented with a more translucent line color and a square wave indicating clear periods of contact (c) and no contact (nc) are represented with an opaque line for markers and sensors. Individual results for all sensors can be found in the Appendix Section A.2.1.1 Contact Sensors.

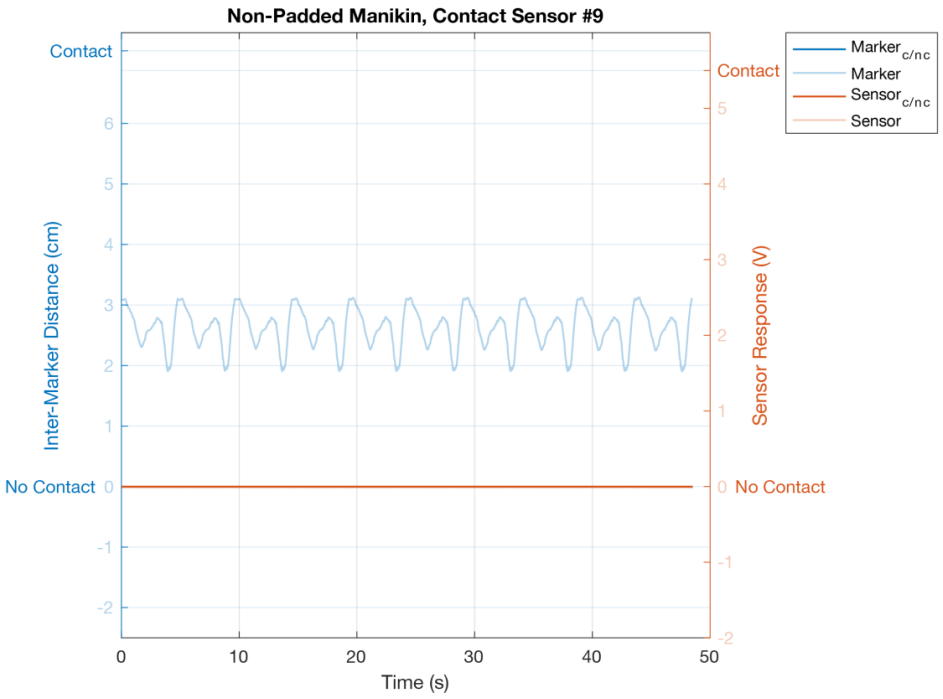

Figure 6.4: Marker pair distance and sensor response for non-padded manikin, contact sensor #9.

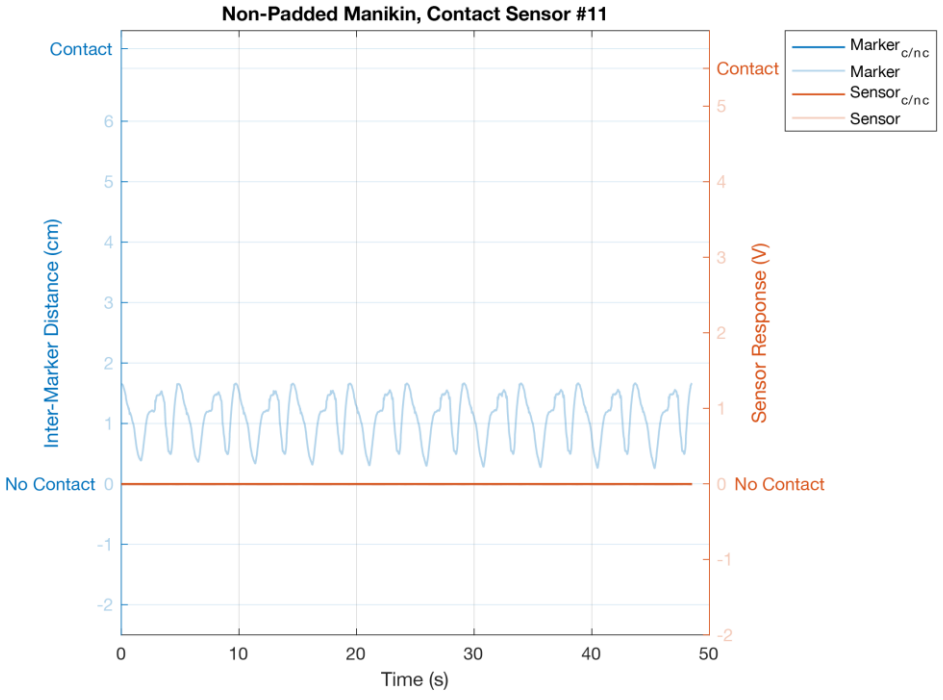

Figure 6.5: Marker pair distance and sensor response for non-padded manikin, contact sensor #11.

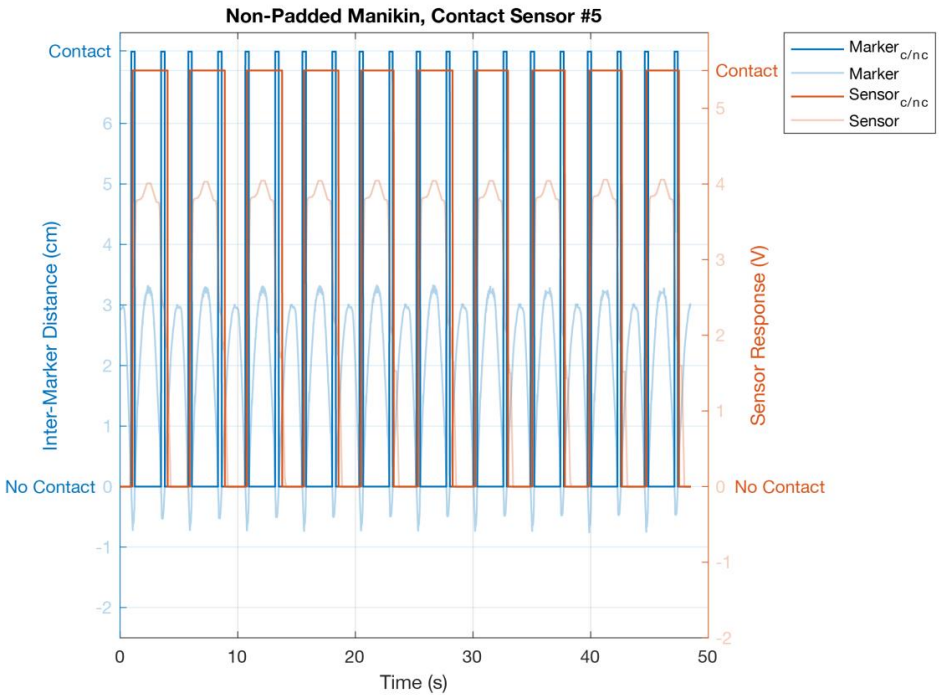

Figure 6.6: Marker pair distance and sensor response for non-padded manikin, contact sensor #5.

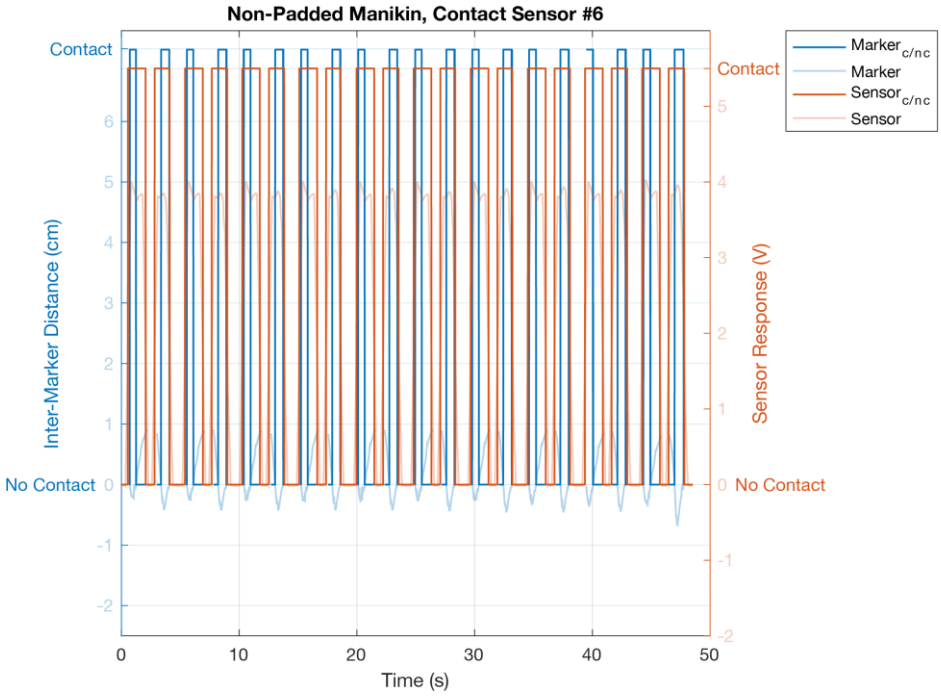

Figure 6.7: Marker pair distance and sensor response for non-padded manikin, contact sensor #6.

6.1.1.2 Contact Sensor Test Discussion

Plots in this section show results for contact sensors from the non-padded manikin condition. From the percentage of contact during the entire duration of the trial overall, there is more sensor contact detected compared to marker contact.

Figure 6.4 and Figure 6.5 show an example of sensors (fs9 and fs11) which do not make any marker or sensor contact. However, it is interesting to note that from the plots it can be seen how the distance between the brief and the manikin becomes smaller, moving from fs9 down to fs11, farther down the backside of the manikin where contact is eventually detected with fs12. It can be seen that fs11 which is above fs12 is almost detecting marker contact, with the brief to manikin distance being approximately 0.5 cm away at some instances. The brief has a much closer fit to the manikin on the backside the farther down the location on the manikin/brief.

In some instances where sensors are detecting contact and markers are not, it appears that movement of the brief over the manikin may be influencing marker contact measurements. Earlier in the gait cycle the manikin and brief markers are making contact, but this distance increases during the trial – perhaps due to the brief shifting. As the surface of the brief is still making contact, the sensor is still able to measure it, but since the marker positions have shifted, they are no longer intersecting during contact. This could be occurring with fs5 and fs6 (Figure 6.6 and Figure 6.7). Fs5 is located around the front pelvis area in an area where marker contact is very difficult to capture. The marker located on the manikin's surface tends to fold into the crease created from dynamic manikin movement, completely occluding the marker. This was also a location where a lot of brief shifting was occurring, likely moving the brief-side marker along the manikin's surface, but not the manikin-side marker. Fs6 was another location where marker contact was difficult to measure, located in the crotch area. Data collected for this marker had missing gaps due to the marker being occluded. This marker was also placed in the center of the crotch area (rather than on the two specific sensor locations), in-between fs6 and cs6, to prevent the MoCap system from merging the two markers together. Cs6 may have experienced marker and sensor contact differences due to

difficulties in capturing marker data in this location, as it was prone to being occluded from MoCap cameras. Because of this occlusion challenge and the marker merging issue if markers are spaced too close together, a marker was unable to be placed on the sensor location directly. The offset distance was later subtracted from the calculated marker position, which decreased the reliability of measured marker contact for the sensor location. For body locations where marker contact is less reliable due to challenges mentioned above, the contact sensors may be a more reliable reference for contact measurement.

Challenges with measuring sensor contact also may be present for sensors in complex body geometry locations, such as cs6. This sensor is located somewhat on a folded area, where the crotch intersects with the upper thigh and leg and experiences a lot of movement. It is possible that the *edge* of the brief (where there is no electrode) may make contact with the upper thigh, preventing the sensor from detecting it as contact. The suit-electrode here is only on the inside of the brief and does not extend to the edges or outside of the brief. In the future, to capture more edge contacts like this, it could be possible to extend the suit-electrode out farther to the edges or outer side of the brief.

6.1.2 Force Sensors

Results for the force sensors using the initial Instron calibration method did not effectively translate for on-body sensing. This section describes why the initial Instron calibration method for force sensors was not appropriate for manikin testing and discusses different approaches – including: 1) debiasing the manikin sensor responses using Instron sensor responses, and 2) using MoCap marker contact to set a contact-threshold – that could be used for more effective on-body force sensor calibration.

6.1.2.1 Original Sensor Calibration and Contact-Threshold Using Instron

It was evident that the original calibration method from Instron testing did not effectively translate for on-body calibration for force sensors. The static sensor responses with no applied force when on the manikin were much higher than static, no load sensor

responses during Instron testing. Therefore, no contact would ever be detected following the Instron force sensor calibration method.

For on-body sensing, it appears that the forces within the garment and between the garment and the body when donned may induce a sensor response. This is partly due to how sensitive the force sensor is, especially in the low-force range. This is necessary for contact sensing and is a limitation for most off-the-shelf sensors but can introduce challenges when placed on the body. Additionally, the difference of how taut or stretched the textile is near the sensor seems to influence the sensor response. During Instron testing the textile is in a relaxed state, but once placed on the manikin the textile is stretched to achieve a form-fit around the body. The stretching of the textile along with the forces from the body surface (from the form-fit style garment) surrounding the sensor can induce a sensor response and therefore change the response without the presence of an external applied force. Further, the ability for the textile to stretch to many different dimensions increases the complexity and adds to the challenge of achieving effective on-body sensing. A modified calibration method for on-body sensing is needed and some approaches for more effective on-body sensing are described in Sections 6.1.2.2 Modified Sensor Calibration and Contact-Threshold Debiasing Manikin Sensor Responses and 6.1.2.3 Modified Sensor Calibration and Contact-Threshold Using Marker Contact.

6.1.2.2 Modified Sensor Calibration and Contact-Threshold Debiasing Manikin Sensor Responses

One alternative method for calibrating and setting a contact-threshold for force sensors could be achieved by debiasing manikin sensor responses using Instron data for a more consistent/equivalent comparison and is discussed here. Sensor responses from Instron testing while the sensor experienced no load/force could be used to debias the manikin sensor responses. This would allow the sensor responses during no experienced external load on the manikin to be shifted down to the range of sensor responses from no applied load during Instron testing. The intent is that sensor responses for no externally applied load in both the Instron and during manikin testing would then be consistent (have the

same responses at no applied load) to allow calibration from Instron data to translate to manikin testing.

This approach was explored; however, it highlighted other challenges for effective on-body force sensing, particularly with difficulty in accurate on-body calibration due to sensor drift. The sensor response voltages at the beginning of Instron testing (un-loaded condition) for each trial were averaged for each sensor. This average from the 3 trials was used as the "un-biased" value reference for manikin sensor responses. The difference (bias) between the Instron un-loaded response and the manikin un-loaded response was removed from the manikin sensor responses to bring those sensor values down to the unloaded sensor responses from Instron for equivalent comparison. However, since the force sensors exhibited drift, the manikin un-loaded response needed to be established from the trial in which it would be applied (the 'brief' condition trial). During that trial there was no period of time where the brief was not donned on the manikin. If contact was being made between the brief and the manikin in any sensor locations at the beginning of the trial (statically, prior to the start of dynamic movement) the brief could be applying force and therefore would not be an unloaded sensor and would be unable to be used with this approach. There was too much drift between the 'no-brief' and 'brief' trial conditions to establish a debiasing value reference from the 'no-brief' condition that could be applied to the 'brief' condition. Theoretically, the force sensors should have a lower sensor response when unloaded, during the 'no brief' manikin test trial, and either an equal or potentially higher sensor response during the 'brief' trial where sensors may be experiencing a load. However, it was found that some sensor responses at the beginning of the 'brief' trial, which occurred first, were lower than the 'no brief' trial, which occurred after the 'brief' trial, indicating sensors were experiencing some drift or fluctuation. Figure 6.8-Figure 6.13 show force sensor responses for a static manikin test trial over a longer duration (~10 minutes) and slight drift or fluctuations can be seen for some force sensors. Fs5 for the non-padded manikin condition (Figure 6.9) and fs1 for the padded manikin condition (Figure 6.12) shows a close-up view of drift over the long duration trial. Fs6 for the non-padded manikin condition (Figure 6.10) and fs2 for the padded manikin condition (Figure 6.13) show some fluctuation and may have been

experiencing a poor connection or separation of sensor layers. Results from the long duration static manikin test trial for all force sensors can be found in the Appendix Section A.2.1.2 Force Sensors (Drift). The drift can be small but can present additional challenges for on-body calibration. Additionally, the linearity of sensors can influence the accuracy of using this debiasing sensor responses on the body approach. Sensors may be more sensitive to applied forces when in a completely unloaded state compared to sensors already experiencing a load from the body. A more complex sensor model could be used for better debiasing and/or calibration in this case.

As mentioned previously, there are many on-body and garment-integrated variables that can affect force sensor responses. The long duration static manikin testing shows that force sensor responses can change over time with drift, but they can also change with differences in surface geometry underneath of a sensor and position on the manikin (causing sensor deformations or folding, which is more likely to occur over a body area that experiences creasing such as the pelvis), as well as how taut the textile surrounding the sensor is. These challenges can cause sensor response variability and difficulty in effectively using this approach for on-body sensor calibration.

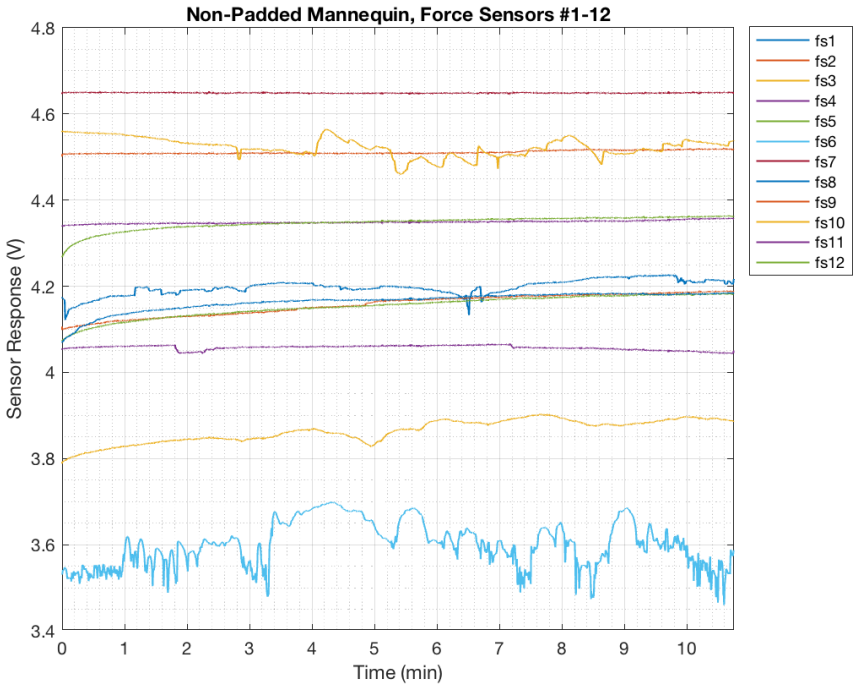

Figure 6.8: Force sensors #1-12 responses for *non-padded* manikin during long duration trial (~10 minutes).

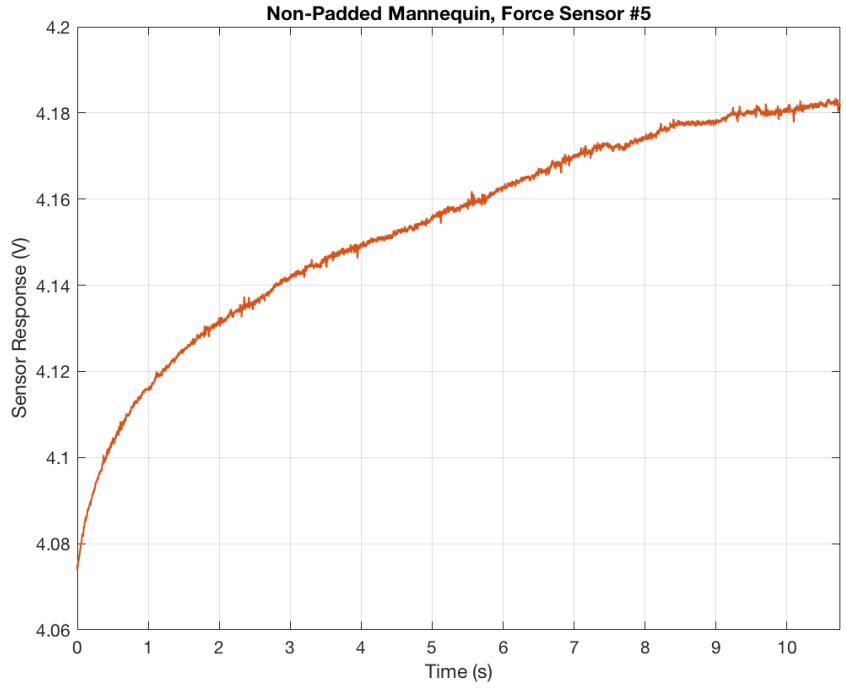

Figure 6.9: Force sensor #5 response for non-padded manikin during long duration trial (~10 minutes).

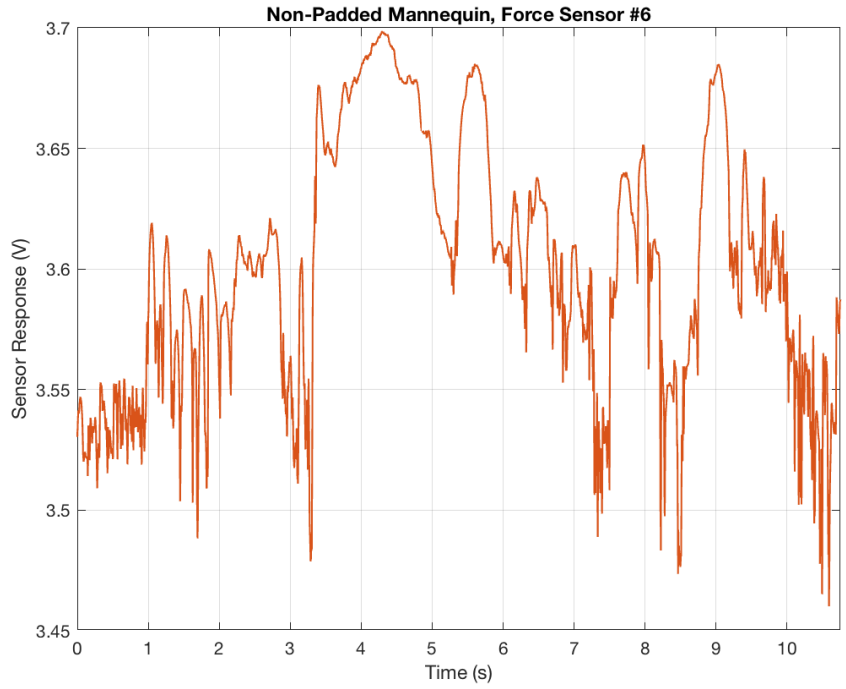

Figure 6.10: Force sensor #6 response for non-padded manikin during long duration trial (~10 minutes).

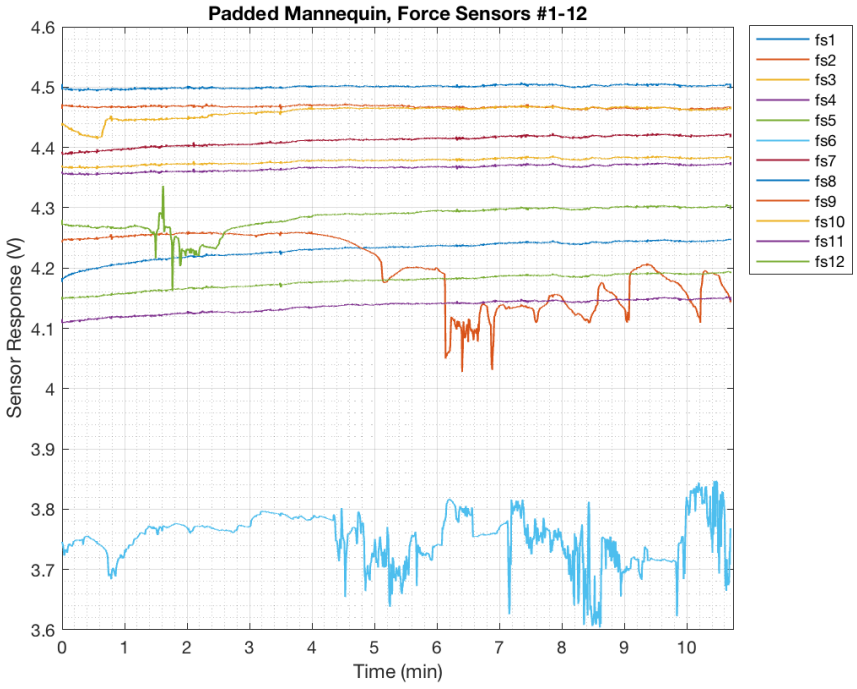

Figure 6.11: Force sensors #1-12 responses for *padded* manikin during long duration trial (~10 minutes).

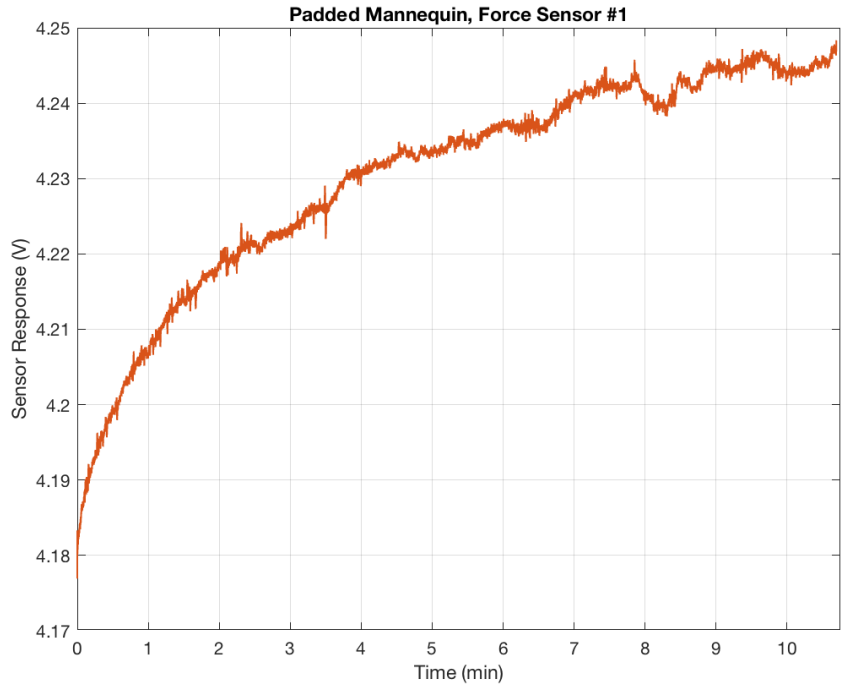

Figure 6.12: Force sensor #1 response for padded manikin during long duration trial (~10 minutes).

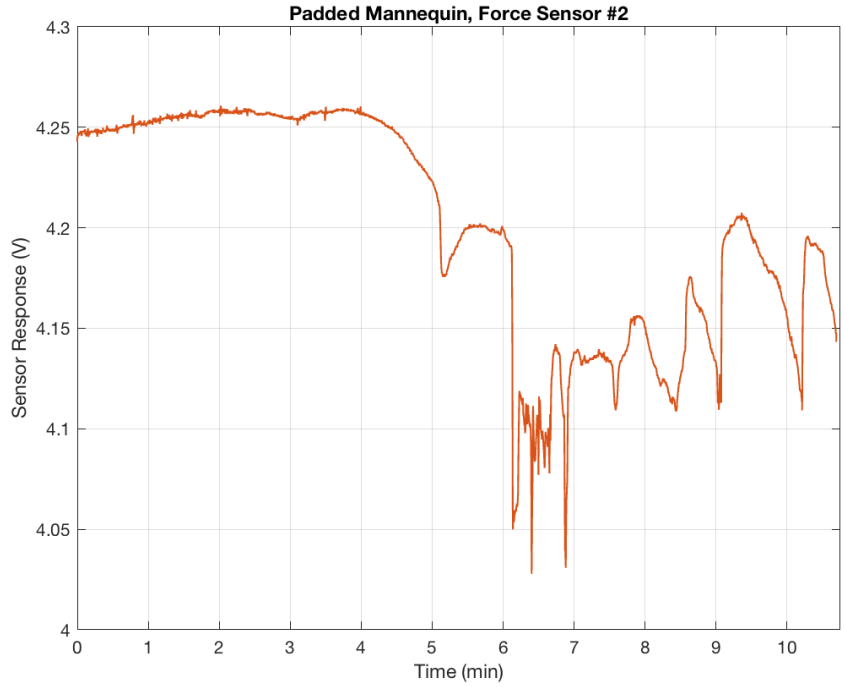

Figure 6.13: Force sensor #2 response for padded manikin during long duration trial (~10 minutes).

6.1.2.3 Modified Sensor Calibration and Contact-Threshold Using Marker Contact

Another alternative method for calibrating a contact-threshold for force sensors using MoCap marker contact is discussed here. Using marker data collected during dynamic manikin testing, a contact-threshold for force sensors could be established using the first instance of marker contact in the MoCap system. Using the marker pair distance data from the dynamic no brief and brief manikin trials, the first instance of marker contact was used to set a contact-threshold for the corresponding force sensor. A contact-threshold was set for sensors that experienced marker contact.

6.1.2.3.1 On-Body Calibration Results

For the non-padded manikin condition four sensors (force sensors 5, 6, 11, and 12) made marker contact in the MoCap data, and a contact-threshold was established.

Results based on the alternative method to establish a contact-threshold for force sensors using the first instance of marker contact are listed in Table 6.1 and used for the following results in this section.

Table 6.1: Non-padded manikin condition contact-threshold for force sensors (using alternative on-body manikin calibration).

Force Sensor #	Contact-Threshold (V)
1	N/A
2	N/A
3	N/A
4	N/A
5	4.20
6	3.66
7	N/A
8	N/A
9	N/A
10	N/A
11	4.47
12	4.38

Results for the percentage of contact for force sensors in the non-padded manikin condition are illustrated in Figure 6.14.

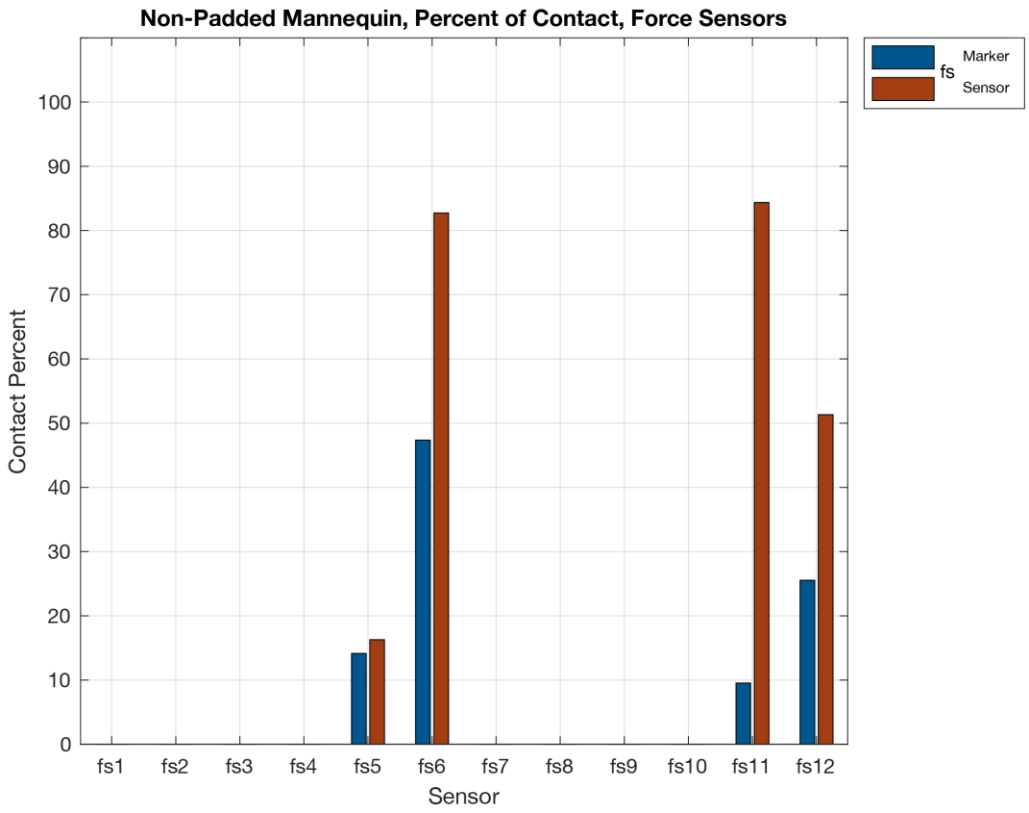

Figure 6.14: Percent of contact for *force* sensors during the *non-padded* manikin condition (for sensors that experienced marker contact).

Select results showing detailed patterns of contact for marker pairs and force sensor responses during non-padded manikin testing over the entire test duration are in Figure 6.15-Figure 6.17. Figure 6.15 shows results from fs1, which does not make marker contact. Figure 6.16 and Figure 6.17 show results for fs5 and fs6, which make marker contact. Individual results for all sensors can be found in the Appendix Section A.2.1.3 Force Sensors.

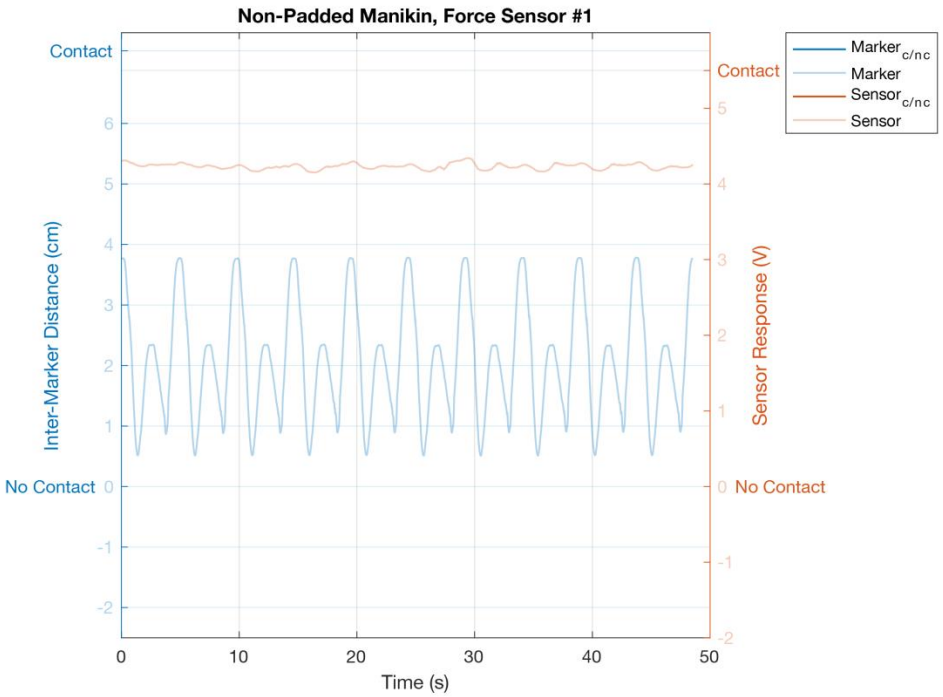

Figure 6.15: Marker pair distance and sensor response for non-padded manikin, force sensor #1.

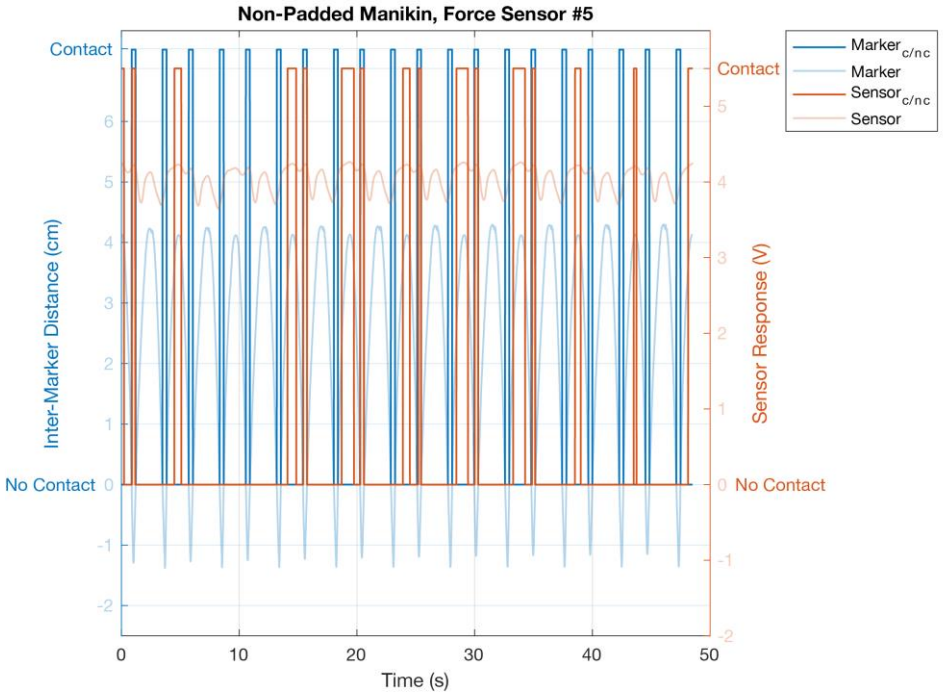

Figure 6.16: Marker pair distance and sensor response for non-padded manikin, force sensor #5.

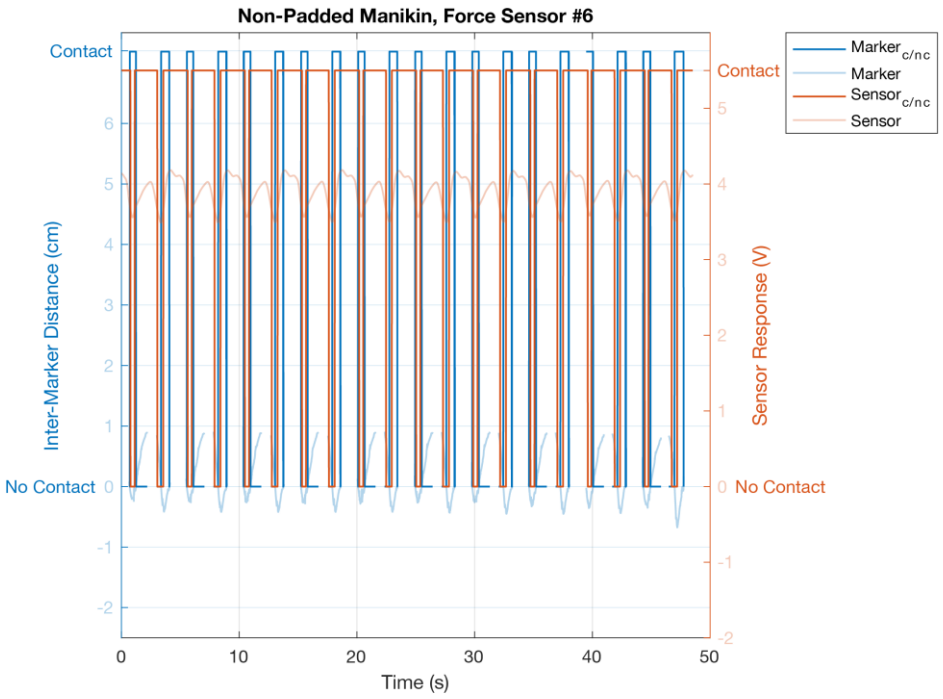

Figure 6.17: Marker pair distance and sensor response for non-padded manikin, force sensor #6.

6.1.2.3.2 On-Body Calibration Discussion

While this alternative approach is one that can be used to set a contact-threshold for on-body sensing it does come with limitations. A contact-threshold can only be established for sensors that experience marker contact and not all sensors locations make marker contact. Additionally, the accuracy of sensor contact here is entirely dependent on the accuracy of detected marker contact, which can be influenced by the variables previously discussed in Section 6.1.1.2 Contact Sensor Test Discussion. The Vicon MoCap system detects markers using a centroid fit based on the gray scale values that are seen by a camera, detecting markers at the center rather than the outer edge of the marker. This could potentially contribute to some small differences in measured marker contact and actual contact using this method.

From the results obtained using this on-body calibration approach, overall, more sensor contact was detected compared to marker contact. This could indicate that marker pairs

may have been affected by variables that impacted the detection of marker contact – such as the of positioning marker pairs in the same exact location between trials (no brief and brief) and the shifting of the brief surface over the manikin's body surface.

Figure 6.15 shows the marker pair distance and sensor response for fs1, which does not detect marker contact. At times the marker pair distance gets close to detecting contact (approximately 1 cm marker separation distance) but does not reach 0 cm or below during the trial using this marker contact-threshold.

Similar to the contact sensors, fs5 and fs6 (Figure 6.16 and Figure 6.17) show variation between marker and sensor contact, with more detected sensor contact compared to marker contact. This is likely due to brief shifting over the body surfacing and maintaining contact with the manikin's body outside of the specific marker pair locations and potentially the offset distance between marker pairs to set the marker contact-threshold.

Because the marker pairs only measure contact when they are in the exact *original location*, measured contact and actual contact may be inconsistent, with more actual contact occurring versus measured contact. The shifting of the brief over the manikin's surface can influence the accuracy of the measured marker contact since it relies on the specific marker pair position and does not account for shifting. In contrast, the sensor locations on the body can measure contact from any part of the brief rather than a single fixed position. However, sensors can become folded into body creases with body movement and become occluded, and can experience a change in position with a change in body shape, which was experienced in this study with the larger body shape (e.g., sensor shifting outside of the brief sensing area). If a sensor is folded into the body it is not exposed and therefore would not be able to detect contact if the brief contacts that sensor location. This issue would likely be present with measuring marker pair contact as well, as the marker can become occluded with folding. With these drawbacks from both measuring marker and sensor contact, the sensors may be more accurate in

measuring contact compared to the marker pairs, in areas where a lot of brief shifting occurs.

For any calibration approach, force sensors can experience a small amount of drift which can change sensor responses and make accurate calibration challenging. This change in sensor response could result in some force sensors experiencing false negative or false positive contact. If the sensor drift is small enough, it is possible that calibration could be performed frequently enough to compensate for this drift.

6.1.3 Comparing Contact and Force Sensing

6.1.3.1 Results

This section presents results and discussion for both contact and force sensors combined for comparison. Results for the percentage of contact measured by MoCap markers and both contact and force sensors in each location during the *non-padded* manikin condition test over the entire trial duration are plotted in Figure 6.18.

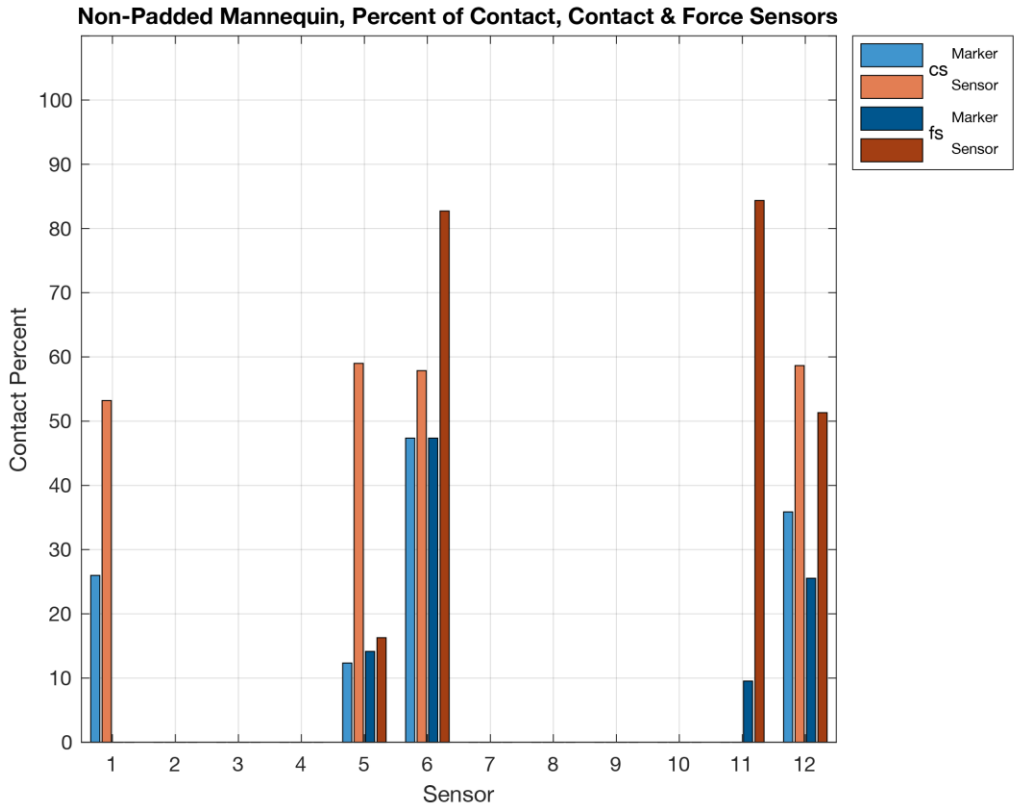

Figure 6.18: Percent of contact for *contact* and *force* sensors during the *non-padded* manikin condition.

6.1.3.2 Discussion

Based on the collected Instron data, the force sensors were expected to be more accurate in measuring contact compared to the contact sensors, due to contact sensors having more overlapping forces experienced below and above the contact-threshold. However,

challenges with on-body calibration made the force sensors less reliable in accurately measuring contact. The accuracy of the measured contact for force sensors calibrated using the method presented here completely relied on the accuracy of the marker pair contact, which as mentioned can have inaccuracies especially due to the offset used. There was overall more contact sensor measured compared to marker pair contact, which was likely due to the brief shifting and breaking marker pair contact but maintaining sensor contact at some point along the brief.

Overall, both marker and sensor contact were measured on the lower areas of the garment around the lower pelvis and near the top waist and the location of the iliac crest which protrudes outward. Less marker and sensor contact were measured towards the top of the garment, for both the front and the back, but especially in the back where there was a lot more space comparatively between the manikin and the brief, and in garment areas towards the center of the brief (not along the edges). Comparing contact sensors and force sensors from the non-padded manikin test condition, it was seen that corresponding marker pairs and sensors did not always make consistent contact. Marker pairs between the left and right body sides generally had consistent measured contact, but a few had more inconsistency (e.g., cs1 and fs1). The percent of marker pair contact between the left (cs) and right (fs) manikin sides for cs1 and fs1 was approximately 25% and was the highest of any sensor location. This large difference was likely due to the manikin's suspension bar which was located on the right side of the manikin near fs1 and could slightly alter the symmetrical orientation of the garment on the manikin. Between contact and force sensors, the sensor locations that made the most similar contact measurement were cs12 and fs12. This was likely because they were located in a more consistent location for contact to occur, on the back of the manikin where there was less distance between the manikin and the brief and less brief shifting. The positioning of the brief and garment was not be perfectly symmetrical on the manikin, which also contributed to differences. Lastly, the method used here for on-body force sensor calibration used marker pair contact to set a contact-threshold for sensors and therefore relies on the accuracy of the marker contact measurement, which was likely to

be affected by variables such as the offset distance and positing of marker pairs between trials affecting complete accuracy.

6.2 Padded Manikin Test Results and Discussion

Results and discussion for the *padded* manikin conditions for contact and force sensors are covered in this section. The manikin has a similar knee movement pattern as the non-padded condition (Figure 6.1 and Figure 6.2).

6.2.1 Contact Sensors

6.2.1.1 Results

Results for the percentage of contact for markers and contact sensors during the *padded* manikin condition test over the entire trial duration are plotted in Figure 6.19. Results for both manikin conditions (*non-padded* and *padded*) are plotted in Figure 6.20.

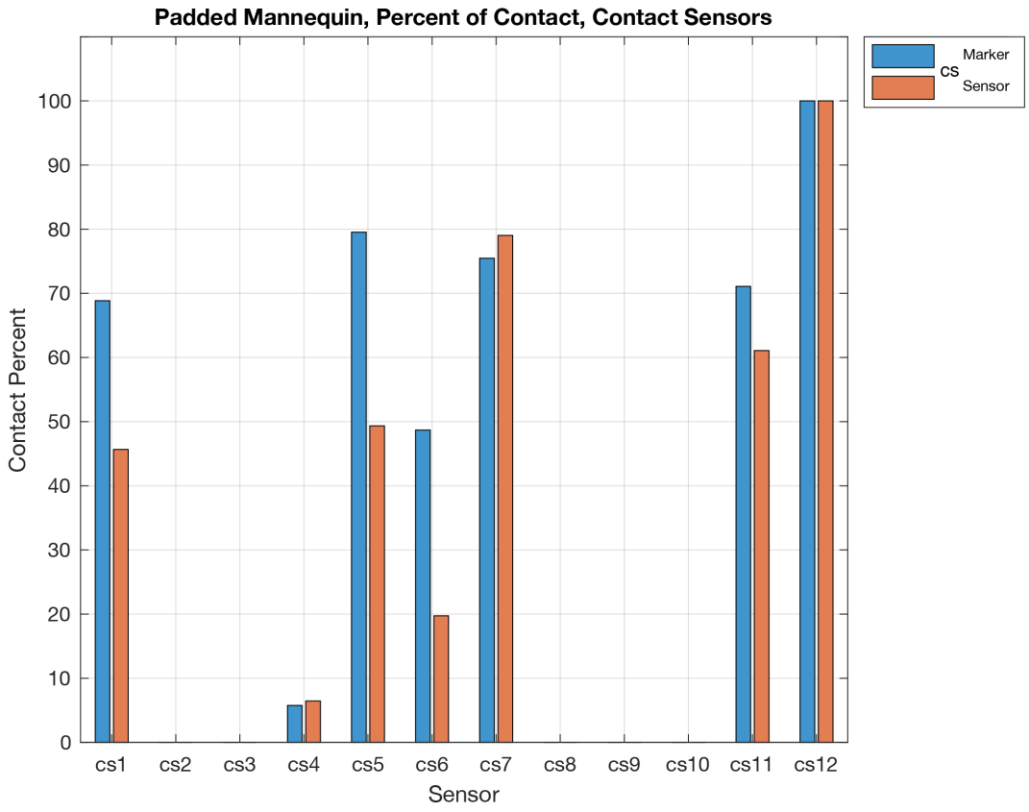

Figure 6.19: Percent of contact for *contact* sensors during the *padded* manikin condition.

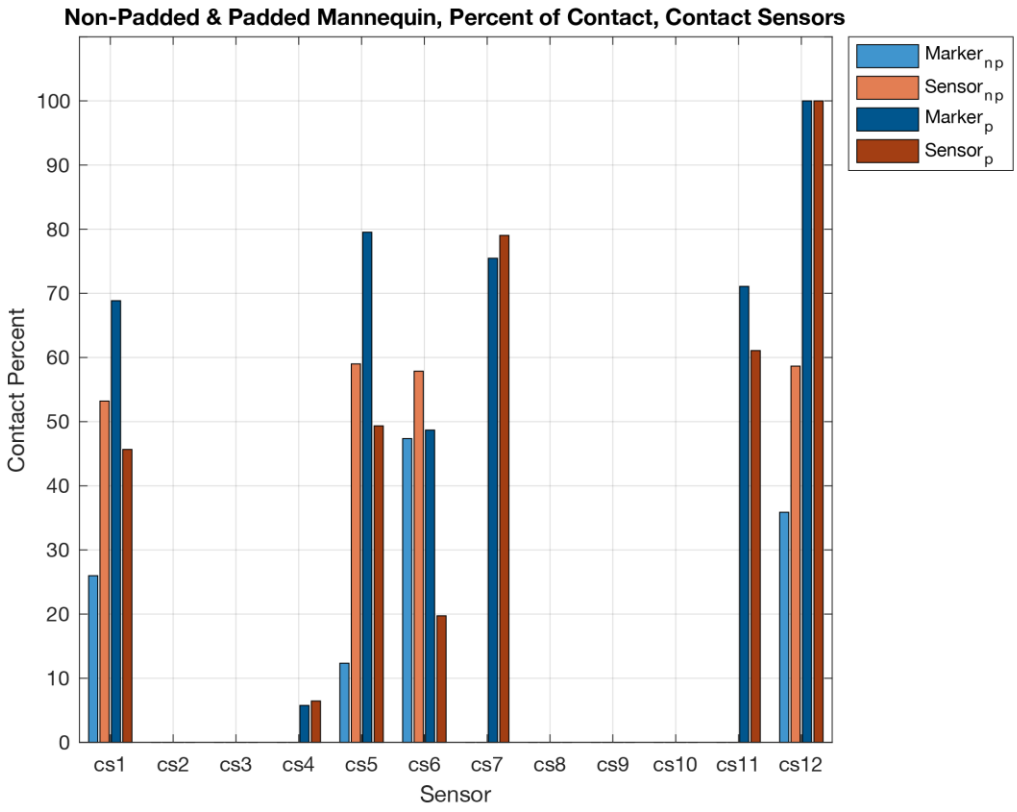

Figure 6.20: Percent of contact for *contact* sensors during the *non-padded* and *padded* manikin conditions.

Selected results showing detailed patterns of contact for marker pairs and contact sensor responses during *padded* manikin testing over the entire test duration are in Figure 6.21-Figure 6.24. These figures illustrate sensors that experience consistent marker and sensor contact (cs7 and cs11) (Figure 6.21 and Figure 6.22) as well as ones that experience inconsistent marker and sensor contact (cs5 and cs6) (Figure 6.23 and Figure 6.24). Individual results for all sensors can be found in the Appendix Section A.2.2.1 Contact Sensors.

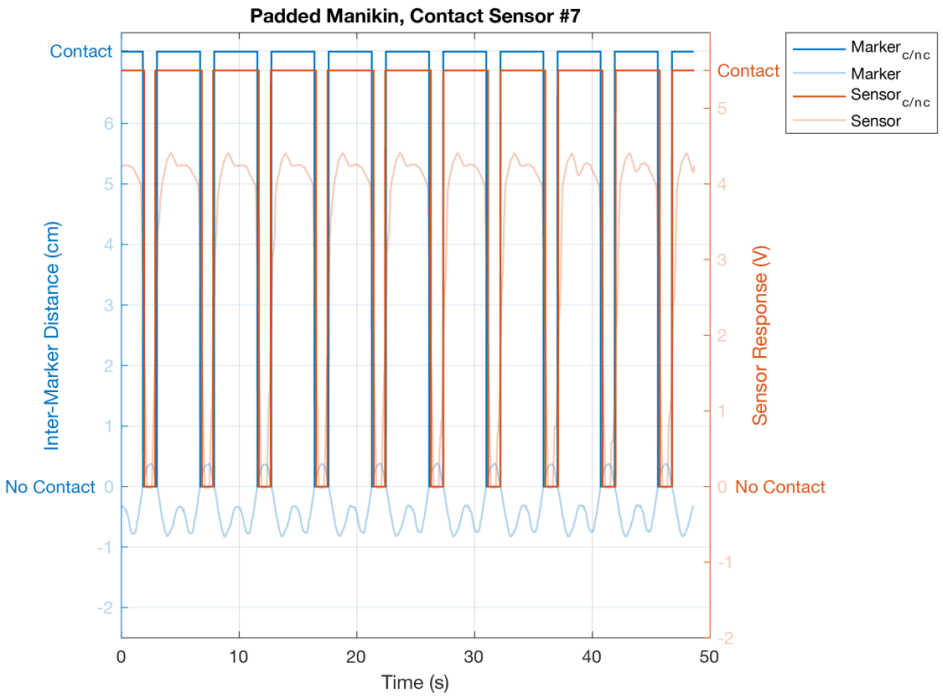

Figure 6.21: Marker pair distance and sensor response for padded manikin, contact sensor #7.

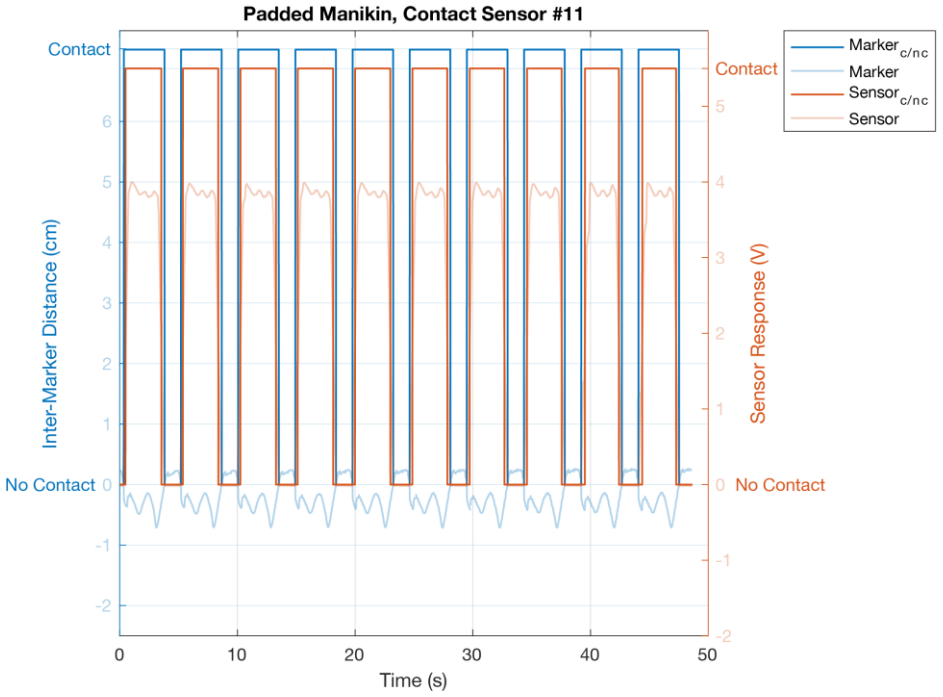

Figure 6.22: Marker pair distance and sensor response for padded manikin, contact sensor #11.

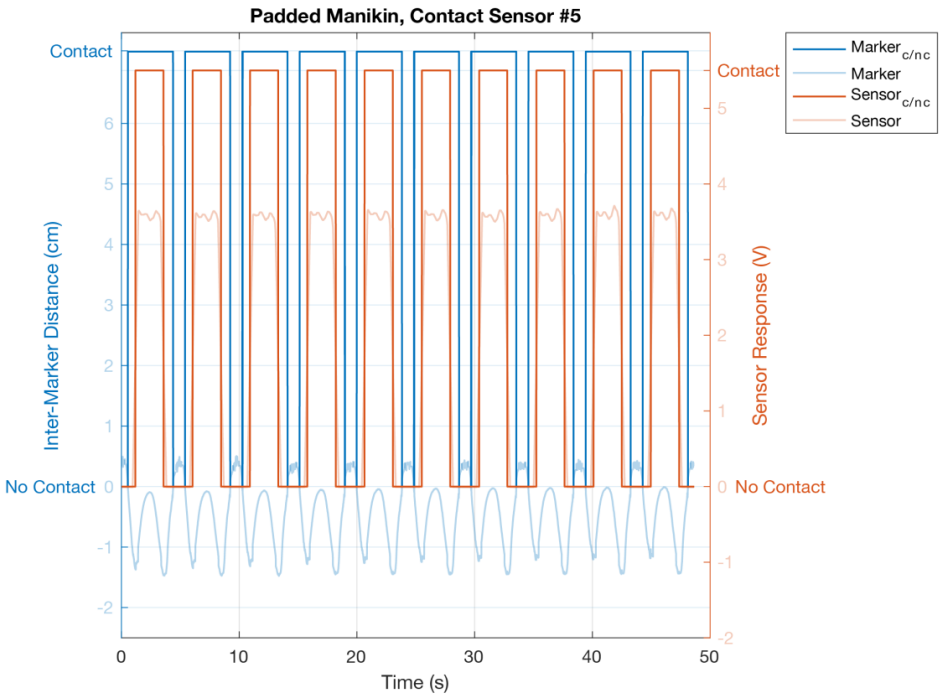

Figure 6.23: Marker pair distance and sensor response for padded manikin, contact sensor #5.

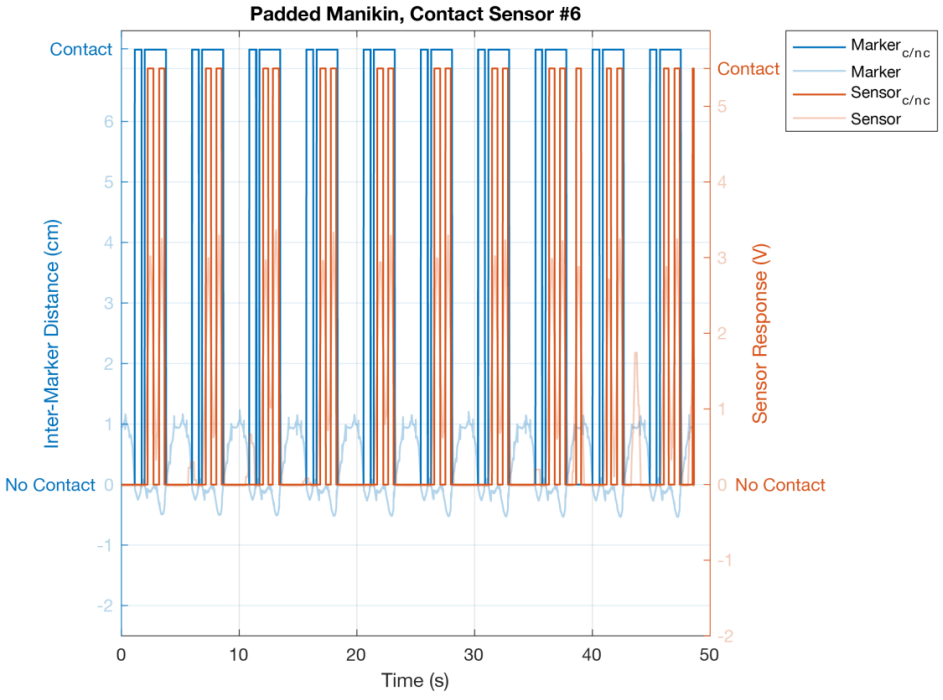

Figure 6.24: Marker pair distance and sensor response for padded manikin, contact sensor #6.

6.2.1.2 Discussion

Overall, there was more alignment with marker and sensor contact for the padded manikin condition compared to the non-padded condition. Adding padding to augment the manikin's body shape/size during the padded condition decreased the distance between the manikin and the brief. This closer fit also resulted in the brief experiencing less shifting on the body during dynamic manikin movement, which was helpful for measuring more accurate sensor location contact using marker pairs during separate trials.

Interestingly there was overall more marker contact than sensor contact, which was opposite for the non-padded manikin condition testing. This may be due to the added manikin padding decreasing the distance between the manikin and the brief and the offset measurement may be slightly off and too much for accurate marker pair contact measurement. During the padded manikin condition the padding expanded the garment across the manikin's surface, which slightly changed the locations of sensors. Some of the sensors were located slightly outside of the brief sensing area due to the expansion from the augmented body shape/size, and a different offset measurement between marker pairs for the padded manikin condition needed to be used. The algorithm that the MoCap system used to detect marker contact may also contribute to the increased marker contact.

There were similar location patterns of contact between the non-padded manikin condition and the padded manikin condition, with some variations. During non-padded manikin testing only four contact sensors (1, 5, 6, 12) detected contact and during padded manikin testing more sensors locations made contact (1, 4, 5, 6, 7, 11, 12).

Figure 6.21 and Figure 6.22 (cs7 and cs11) showed an example of contact sensors that had closely aligned marker and sensor contact. Both sensors were located in higher contact area, where the brief was close to the manikin. These sensors were also located on more stable areas of the manikin that had less influence from varying manikin geometry or folding (e.g., front pelvis area) that occurred during dynamic movement. Cs7 was located

on the side and cs11 was on the back lower side. The back and side area generally had a much smoother manikin geometry and less variation experienced during dynamic movement.

Figure 6.23 and Figure 6.24 (cs5 and cs6) show both markers and sensors making contact but there is some variation between marker contact and sensor contact. There is not a perfect alignment between the two. Cs5 is experiencing more marker contact compared to sensor contact. This is interesting because cs5 is located in a location that experienced a lot of brief shifting for the non-padded condition, which influences detected marker contact. The more marker contact observed here compared to sensor contact could be due to marker positioning. This location is challenging to position markers in the center of sensors. During manikin movement, the manikin's leg would often occlude this area when extended up, and the marker would be folded into the crease of the front pelvis area on the manikin. The marker needed to be slightly offset from the center of the sensor in order for the marker to remain visible. Cs6 is another really challenging area to measure both marker and sensor contact as there are garment variables that influence contact. The padding on the manikin as mentioned expands the garment in some areas but in the crotch area it creates a small amount of excess fabric in the marker location. Both the marker and sensor response show intermittent contact and is likely due to the small amount of excess fabric for the padded manikin condition and the challenging nature of measuring contact in this area.

6.2.2 Force Sensors

6.2.2.1 Results

For the padded manikin condition, the same alternative method to establish a contact-threshold for force sensors on the body using the first instance of marker contact was used.

Similar to the non-padded manikin condition, not all force sensors made contact using the MoCap system. Force sensors 1, 5, 6, and 12 did make marker contact and a contact-threshold was established and used for the results in this section (Table 6.2).

Table 6.2: Padded manikin condition contact-threshold for force sensors (using alternative on-body manikin calibration).

Force Sensor #	Contact-Threshold (V)
1	4.24
2	N/A
3	N/A
4	N/A
5	4.30
6	4.03
7	N/A
8	N/A
9	N/A
10	N/A
11	N/A
12	4.45

Results for the percentage of contact for force sensors during the padded manikin condition are illustrated in Figure 6.25. Results for both the *non-padded* and *padded* manikin conditions are illustrated in Figure 6.26.

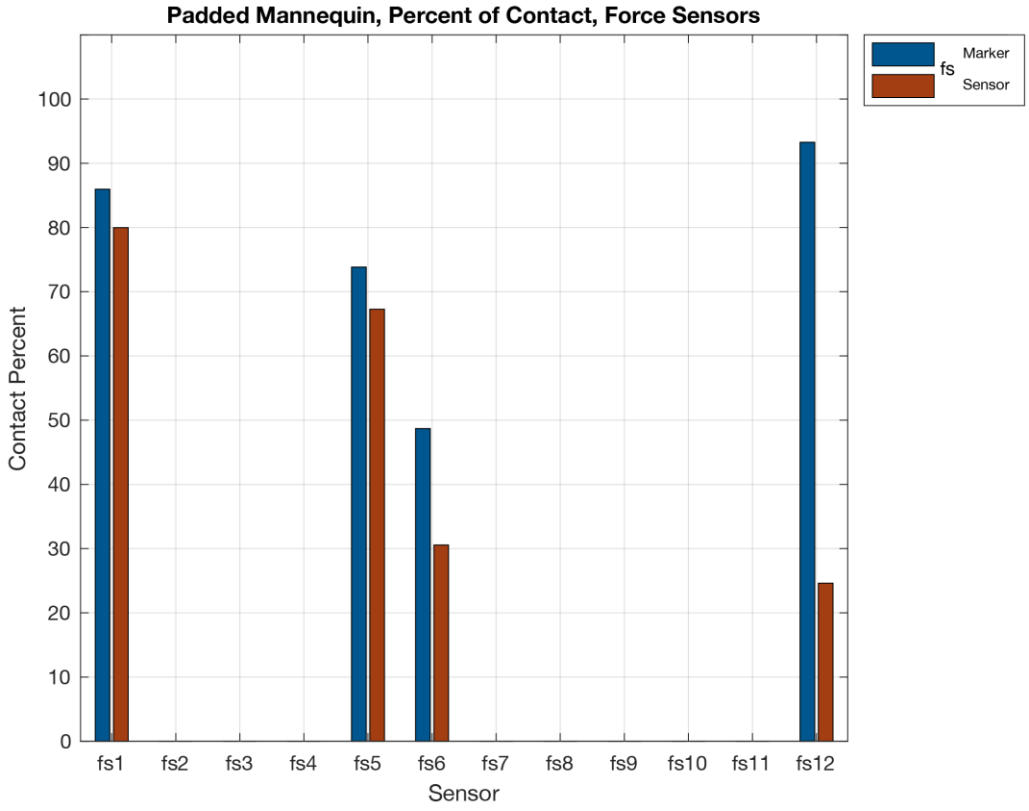

Figure 6.25: Percent of contact for *force* sensors during the *padded* manikin condition.

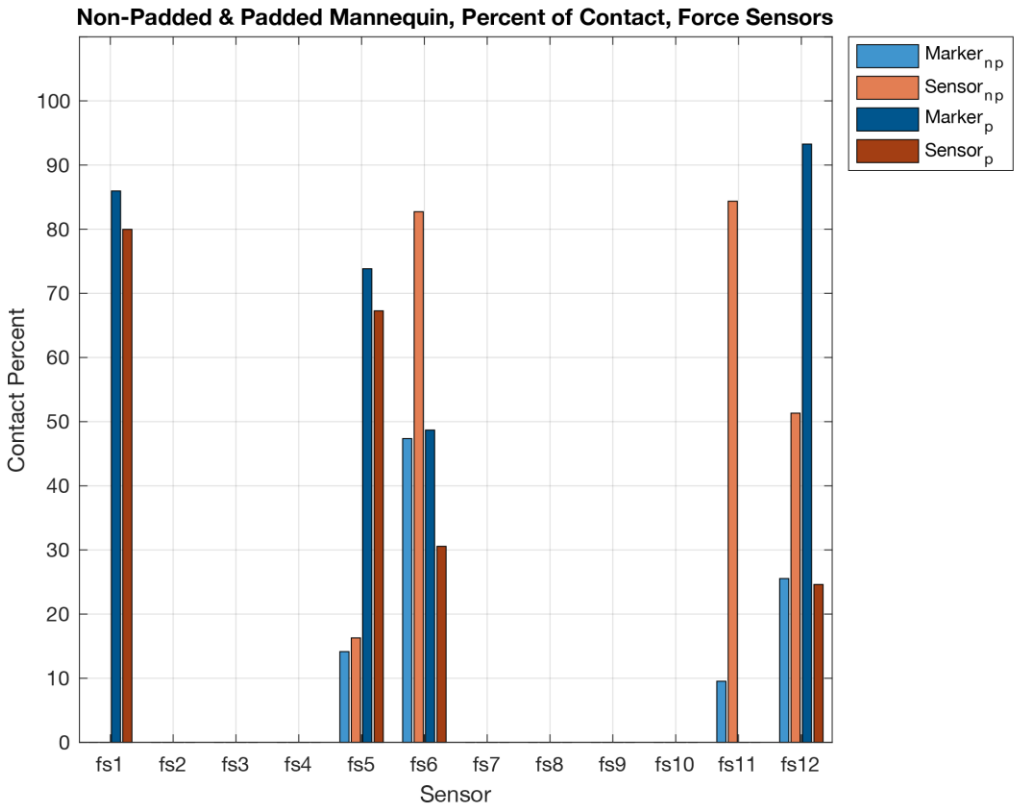

Figure 6.26: Percent of contact for *force* sensors during the *non-padded* and *padded* manikin conditions.

Select results showing detailed patterns of contact for marker pairs and force sensor responses during padded manikin testing over the entire test duration are in Figure 6.27-Figure 6.29. Figure 6.27 shows results from fs10, which did not make marker contact. Figure 6.28 and Figure 6.29 show results for fs5 and fs6, which make marker contact. Individual results for all sensors can be found in the Appendix Section A.2.2.3 Force Sensors.

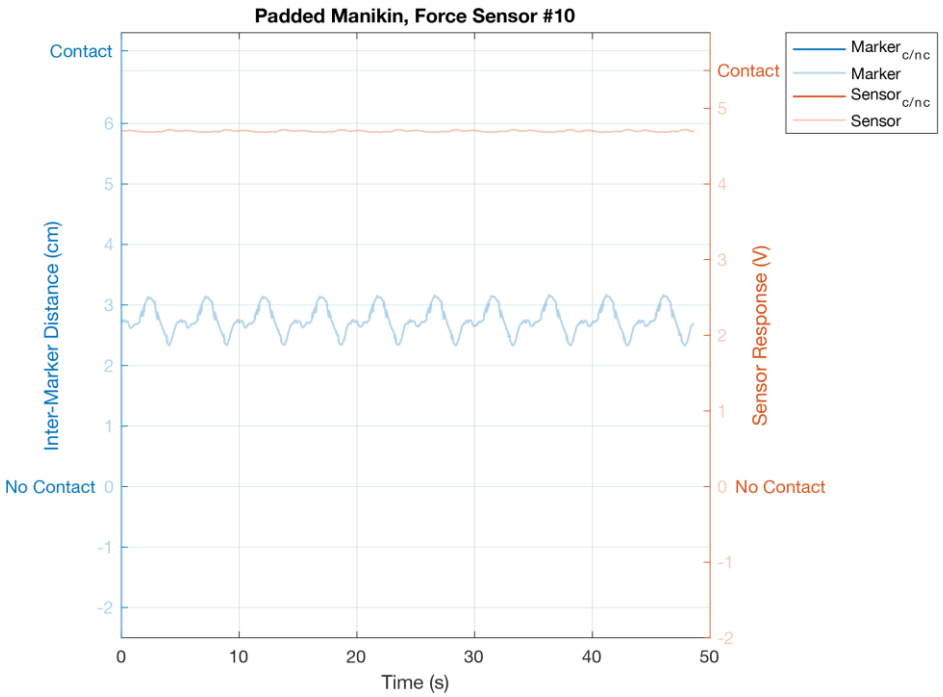

Figure 6.27: Marker pair distance and sensor response for padded manikin, force sensor #10.

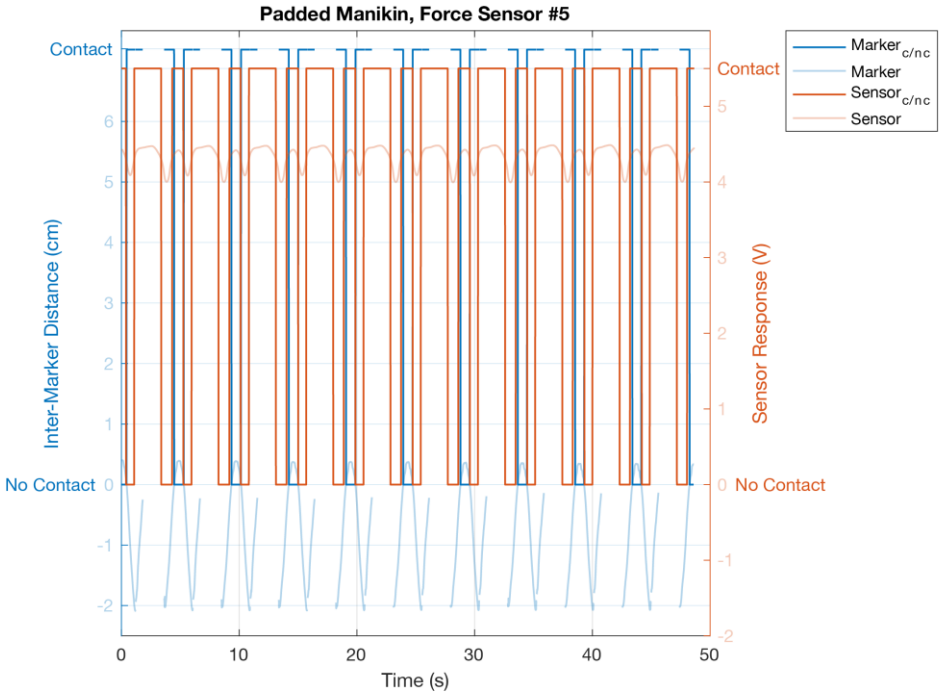

Figure 6.28: Marker pair distance and sensor response for padded manikin, force sensor #5.

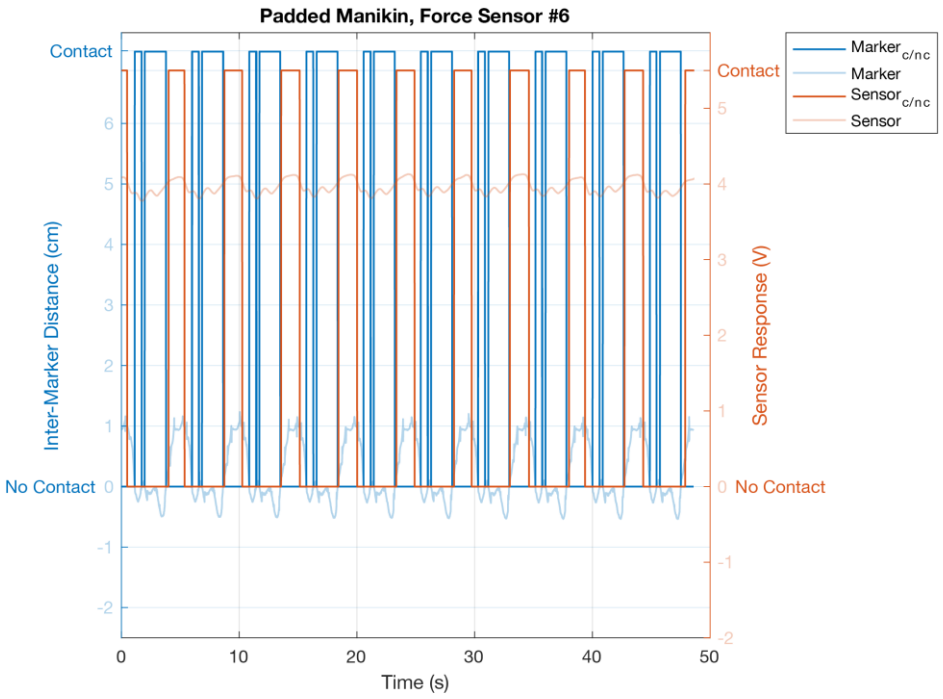

Figure 6.29: Marker pair distance and sensor response for padded manikin, force sensor #6.

6.2.2.2 Discussion

Two sets of contact-threshold results for force sensors were calculated for different manikin conditions, as body size can change the sensor response and alter sensor calibration. For the padded manikin condition contact was made with similar sensors as the non-padded manikin with slight variation. Force sensors that made contact also generally matched contact sensors that made contact. There were still four force sensors (1, 5, 6, 12) that made marker contact during the padded manikin condition and a contact-threshold could be established, but the specific sensors that made marker contact were slightly different. For the non-padded manikin, sensor locations that made marker contact were force sensors 5, 6, 11, and 12, and for the padded-manikin condition it was force sensors 1, 5, 6, and 12. For the padded manikin condition fs1 gained marker contact and fs11 lost marker contact. Fs1 likely gained marker contact in the padded manikin condition due to the augmented body shape decreasing the distance between the manikin and the brief. It would be expected that fs11 also made marker contact during the padded

manikin condition if it made marker contact in the non-padded manikin condition but augmenting the manikin's body shape/size extended the garment over the body surface and brought fs11 outside of the brief area and thus did not make contact. When sensing on bodies of varying shape and size, more or larger sensors may need to be used to be able to capture the same body location on different bodies, if sensor locations are not adjustable. This extending of the garment with through the manikin shape/size augmentation also created less symmetry between contact sensors (left) and force sensors (right) sides on the manikin.

Overall, marker pairs in force sensor locations measured equal or slightly more contact than measured contact from the force sensors. This was a pattern that was also observed with the contact sensor locations for the padded condition. For marker pairs that did experience more contact than corresponding sensors, the offset measurement between marker pairs could be slightly off (too much), resulting in more detected marker contact.

Figure 6.27 (fs10) shows the marker pair distance and sensor response for a sensor location that does not experience contact. This sensor location is on the back side of the manikin around the middle of the brief, away from the edges, and is expected to make less contact. Looking at the marker pair distance it shows that there is more manikin and brief distance compared to most other sensors.

Figure 6.28 and Figure 6.29 (fs5 and fs6) show marker pair distance and sensor response for sensor locations that experience marker contact and a contact-threshold for the sensors is established.

The pattern of marker and sensor contact for fs5 has some alignment but there are gaps in the marker data due to the marker being occluded from the MoCap camera line of sight and there may be periods where the sensor intermittently comes in and out of contact. Fs6 also has some missing marker data, as these two locations are both difficult to capture. The pattern of marker and sensor contact for fs6 is essentially opposite and highlights

the challenges of sensing in the crotch area where excess bunching of fabric is present, fabric and manikin folding is taking place, and markers need to be offset from the sensors.

6.2.3 Comparing Contact and Force Sensing

6.2.3.1 Results

Percentage of contact for both *contact* and *force* sensors for the *padded* manikin condition is shown in Figure 6.30. A comparison of the percentage of contact for both *contact* and *force* sensors for both *non-padded* and *padded* manikin conditions is shown in Figure 6.31.

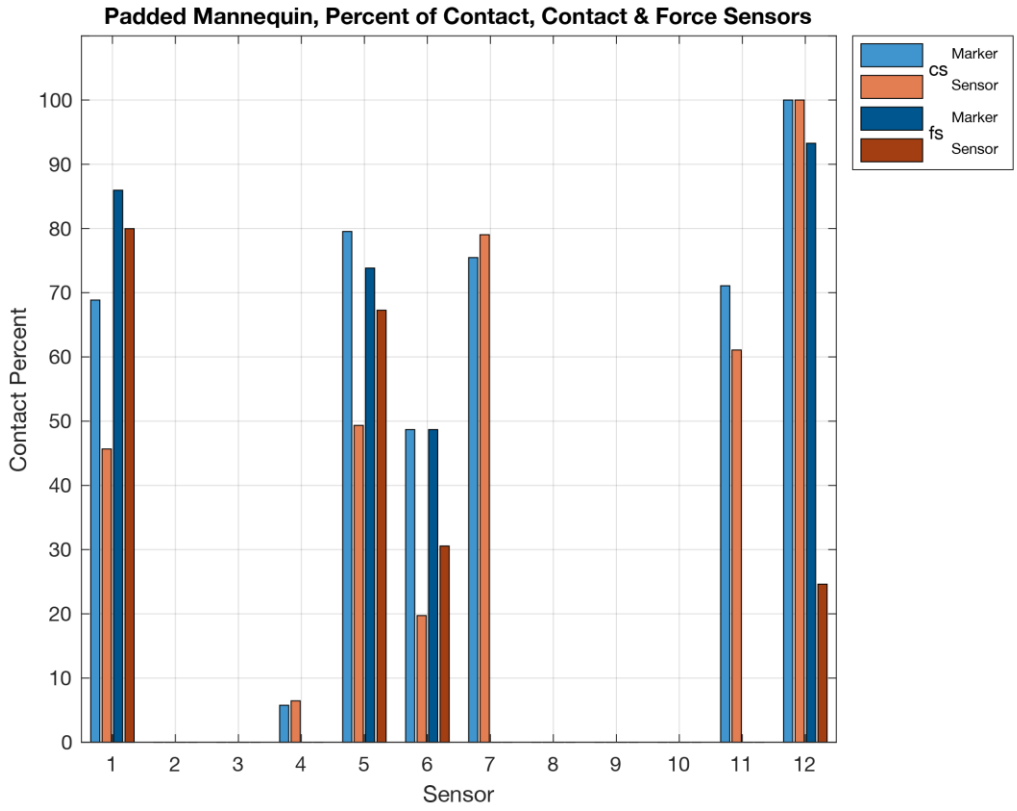

Figure 6.30: Percent of contact for *contact* and *force* sensors during the *padded* manikin condition.

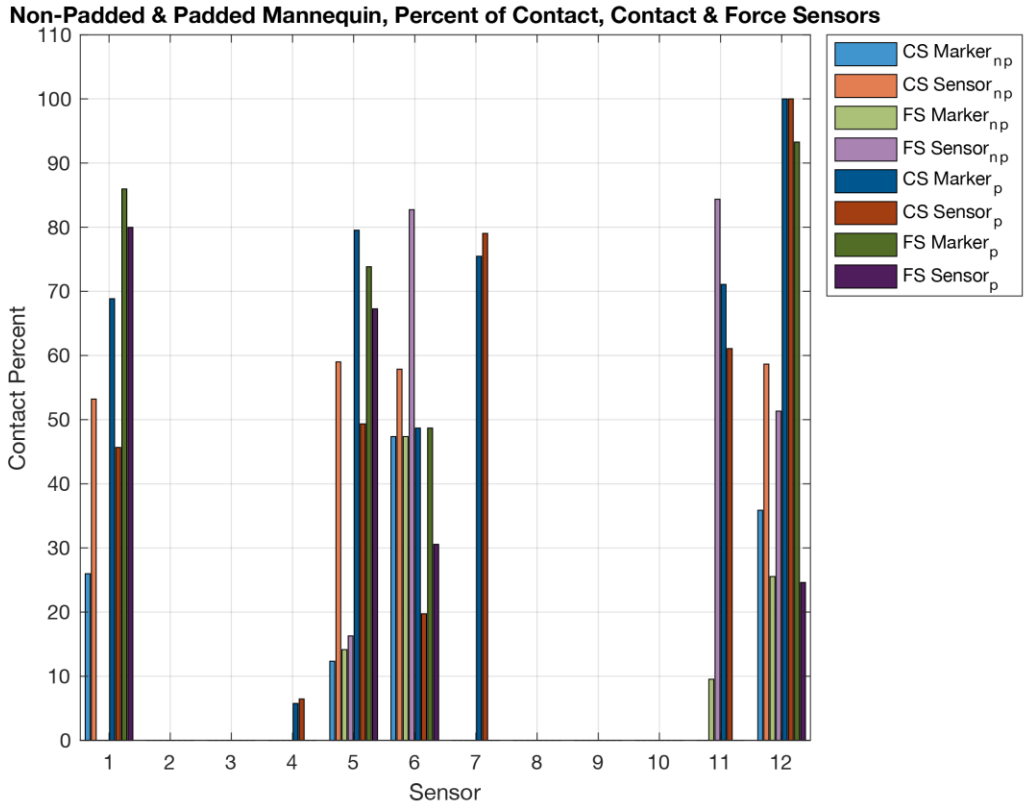

Figure 6.31: Percent of contact for *contact* and *force* sensors during the *non-padded* and *padded* manikin conditions.

6.2.3.2 Discussion

Overall, there was more contact observed in during the padded manikin condition compared to the non-padded manikin condition due to less distance between the manikin's body and brief. The padded manikin condition had more consistency between marker contact and sensor contact but still experienced some variation. There was less brief shifting variation (sliding across manikin surface) for the padded manikin, which likely contributed to this increased marker and sensor contact consistency.

There was generally some agreement with contact measurement between the three methods used here (MoCap marker pairs, force sensing, and contact sensing) but there were no exact similarities. Each method showed variables that can impact the accuracy of measuring contact. Some of these variables are more resolvable than others or may be

method specific and therefore a different method could be used in place of another method's limitation (e.g., use a sensor in an occluded marker area).

Ideally the contact and force sensors should be located symmetrically on the manikin's body; however, the augmentation of the manikin's shape/size expanded the garment in certain areas and created less symmetrical sensing. This is particularly an issue for the backside of the manikin and can be seen with cs11 and fs11. Cs11 makes contact but fs11 does not make contact and is outside of the brief area.

The MoCap system can accurately detect the physical location of a marker in space dynamically. However, in order for the MoCap system to effectively capture a marker, the marker needs to be seen by typically at last 3 cameras. If a marker is in an area where the cameras have no or reduced line-of-sight, the marker may be occluded for part or all of data collection. Measuring both a body and a wearable system that is over the body's surface in a single capture introduces many occlusion challenges. Using a 2-part capture approach (as implemented here) allows the surface of the body and the brief to be captured with less occlusion. However, there are limitations to this approach such as the accuracy of the marker pair position between the two trials. This is a similar challenge for measuring air gaps in clothing using a static 3D scanning approach. The accuracy of the measurement relies on the consistent placement of the initial data points. Using the 2-part capture MoCap approach, if markers are not placed in precisely the same place between the two captures, it could produce results that are less accurate. If an offset measurement needs to be used between marker pairs that cannot be placed in the exact same positioning, the accuracy of the offset measurement can also influence the accuracy of the results. Placing marker pairs in the same location between captures as precisely as possibly as well as reducing the amount of offset needed would benefit future testing.

Since the MoCap marker pair contact only detects contact in the specific location where a marker pair intersects, contact between the brief and the body in those locations can be missed. For example, the brief may be making contact with the body but in a different body location than the original body marker, therefore contact is not measured for the

marker pair. The shifting of the brief over the mannikin's surface plays an important role in the amount of "missed" marker contact. Using marker pairs in locations where the brief is experiencing less shifting or constraining certain axes during data analysis to omit the brief movement (shifting) in specific directions could improve the contact measurement accuracy of the method.

The on-body calibration approach used for force sensors in this study was based on the MoCap marker pair data. This approach allowed a contact-threshold to be established for sensors that made marker contact but it relied heavily on the accuracy of the marker pair contact, which as previously discussed was affected by other variables. Between the non-padded and padded manikin conditions, contact was measured in similar locations by the force sensors, with some differences. Fs1 gained contact for the padded manikin condition, but fs11 lost contact. It was expected that more sensors would gain contact for the padded manikin condition due the decrease in distance between the manikin and the brief, which explains the gained contact with fs1. However, it was expected that fs11 would remain in contact between the non-padded to padded manikin condition, but contact was lost during the padded manikin condition testing. Fs11 lost contact due to the manikin shape augmentation expanding part of the garment outside of the brief sensing area, therefore rendering it unable to make contact with the brief.

The force sensors were able to measure a range of forces and detect contact but had many contaminating variables that impacted the accuracy of the sensor response and ultimately the usefulness of the sensor type. On-body calibration, sensor drift, and sensors responding to body and garment variables were the main sources of contamination that created challenges for accurate sensing. The translation of the e-textile garment from Instron testing in a relaxed, unstretched state to on-body in a stretched state altered the unloaded, static sensor responses. Unloaded, static sensor responses were much higher when placed on the body compared to Instron testing, which makes the translation of Instron characterization not effective. The force sensors also experienced some drift or fluctuation over time, which made using a debiasing approach to calibrate sensors in the on-body condition also ineffective. Finally, during on-body testing it was evident that the

sensors were measuring body and garment movement/deformation and not just externally applied forces. This made the sensor response difficult to parse to extract the information of interest.

The contact sensors use a binary, switch-like approach to measure contact and experienced fewer contaminating variables for on-body sensing. The placement of contact sensors can be affected by garment shifting, and the force at which the sensors close at may be affected by the geometry underneath the sensor. The ability for contact sensors to measure contact using the e-textile garment can be affected by changes in body dimensions, which can alter the placement of sensors on the body. Similar to the force sensors shifting outside of the brief sensing area, contact sensors can also experience shifting. To accommodate this shifting and garment expansion effect on different bodies, more sensors may need to be located near areas of high expansion to ensure a sensor is still within the sensing area. The geometry underneath the sensor may affect the force at which a contact sensor closes/opens. Understanding the sensor performance under more geometry variations could be beneficial for more accurate on-body sensing.

Chapter 7

7 Conclusion

This research evaluated methods to quantify functional fit of a wearable system by measuring contact between the body and a spacesuit component mockup (brief) during controlled robotic manikin testing through a wearable contact and force sensing e-textile garment. This study compared two sensor-based fit quantification methods (contact and force sensors) with a non-wearable reference (optical MoCap). Garment-integrated sensors were characterized in a bench test apparatus (Instron) under controlled loading conditions. The translation of these methods to the wearable environment was investigated using a robotic manikin that performs repeatable dynamic movements for a controlled on-body sensing scenario. Two different manikin conditions were evaluated to simulate effects of anthropometric differences.

The spacesuit brief component was used for initial testing of the methods evaluated here, but other suit components influence how each suit component functions – including interfacing and interacting with the body – as an entire wearable system. The brief by itself (without the other spacesuit components) will interface with the body different and have different interactions with the body. With the entire spacesuit system, the brief component would be coupled with the torso and leg assemblies, which would affect how it moves. Additionally, pressurization of the suit would affect how it moves. The focus for this study was on evaluating methods to measure mechanical interactions (contact)

between the body and the brief spacesuit component. The work can be further implemented in the future to understand more realistic contact patterns with the entire spacesuit system.

Understanding contact or the space between the body and a wearable system is a continuous challenge and is important to understand fit. There are methods that have previously been used such as 3D body scanning but have limitations with accurate alignment and capturing dynamic movement. 4D body scanning can capture dynamic movements but these systems are generally expensive and not as widely available and analysis and interpretation of the data can be challenging. The methods used here (MoCap and sensing) also have limitations and challenges to overcome for more accuracy, such as alignment and shifting for MoCap, sensor deformation and on-body calibration for force sensors, and surface geometry underneath of the sensor for contact sensors, but are a step closer to better understanding the body to wearable system relationship and can be used for dynamic movements.

This study illuminated many challenges for accurate force sensing on the body. For the textile sensors used in this study, the contact sensors showed far fewer contaminating variables for accurate on-body and wearable garment sensing than the force sensors. It was found that the force sensors were responding to other variables besides externally applied forces, such as the garment being donned on the body, body/garment movement, and sensor folding/deformation.

These textile-based sensors can be used for on-body sensing and were successfully integrated into a garment that withstood the rigors of the testing environment. Using textile-based sensors, a soft-to-soft connection was made, which had many advantages including the ability to improve wearability and comfort, as well as the strength/robustness or durability of a mechanical sensor-lead or sensor-garment connection for on-body sensing by minimizing any disparity between the integrated components. The sensors in this study did not experience any complete failures. Textile sensors interfaced with the body more successfully through the ability to conform to and

flex with the body's varying geometry, and contributed to maximizing body mobility and ROM. However, this flexing behavior introduced accuracy challenges for the force sensors. Textile-sensors had the ability to be highly customized (size and shape) for different sensing applications and resolutions.

Sensor leads can be a challenge with on-body sensing. The more sensors used, the more leads are necessary, which can add up quickly and detract from ease of use and wearability. On the garment-side in this study force sensors required two leads per sensor, whereas contact sensors only needed one. Using a multiplexing approach could minimize the number of leads necessary for sensors that require two leads per sensor (such as the force sensor). However, it may limit the surface area that could be sensed (sensors are likely in the form of a matrix/array and not distributed over the body/garment surface) and with multiplexing there also can be issues of electrical crosstalk between sensors in an array. Contact sensing only requires one lead per sensor and drastically reduces the amount of electrical leads/wires in a system with many sensors and is much easier to control and manage wires for on-body and garment-integrated sensing. Having a system with overall less wires also has garment benefits as it can potentially create less pressure points on the body from lead routing and minimize any fabric/garment restriction from lead integration and preserve user mobility. The approach used in this study for garment-lead integration was discrete and did not interfere with the sensing environment. The leads also remained intact and did not break during testing.

Contact sensors used here currently sense contact at a very low force. In the controlled Instron testing environment contact sensors showed some overlap in the forces captured in the below and above contact-threshold. Contact sensors were less accurate in detecting contact in this range of overlapped of forces. Force sensors experienced less of an overlap but were more likely to register false positive contacts and, when placed on a body surface, the force sensors were very susceptible to contaminating on-body sensing variables. The contact sensors were not affected by these on-body variables and were more effective in measuring contact for an on-body sensing environment. The contact

sensors could be further developed to afford sensing different amounts of contact 'forces' by changing the fabrication of the sensor to require higher forces to close the switch (e.g., layer of open structure fabric over one contact electrode). The current study here used multiple contact electrodes on the body surface to provide location information of contact on the body, and a large unified suit side electrode indicating contact was made *at any location* with the suit electrode. Multiple contact sensor electrodes could be placed on both sensing surfaces to sense specific location of contact between the two surfaces.

Force sensors can provide more information due to the analog nature of the sensor and provide a range of forces experienced, but challenges exist for accurate on-body sensing. Contaminating variables are associated with force sensing that can impact the ability to parse and obtain useful information. Force sensors can detect/measure different on-body sensing variables – such as measuring garment and body movement, and external forces applied on the body – which can both be useful depending on the sensing context. But if these things cannot be isolated, it is difficult to distinguish the two and know what and when the sensor is responding to (garment/body movement or external force applied) as there is just a single sensor response that is affected by both. A calibration method for bodies of different anthropometry is needed for accurate force sensing. The sensor response can change given the geometry (body surface) underneath the sensor as well as the level of tension of the fabric around the sensor (how the garment fits on a body). There are tradeoffs with sensor sensitivity/range. If a sensor is not sensitive at lower forces, it may not even be able to collect any on-body information and induce a sensor response. However, if a sensor is sensitive to lower forces, it could come close to saturation when placed on the body. Similar to force sensing, *pressure* sensing can also provide richer information using an analog sensing approach, compared to binary contact sensing. For pressure sensing, the surface area of the applied force needs to be known. With on-body sensing, especially *dynamic* where the location and amount of force could be continuously changing with body movement, it can be difficult to quantify the specific surface area experiencing force – it may not be the entire sensor but rather just a fraction of the sensor's surface area. Given the same amount of force, a smaller surface area will be a higher pressure and could be a point of discomfort or concern for

on-body evaluation compared to a larger surface area where force is more distributed and not as concentrated, thus resulting in a lower overall pressure amount. Pressure can better inform things like areas of potential discomfort or risk of injury since the surface area of the force can have an impact on how the body experiences it. An approach that could be implemented to attempt to sense pressures on the body is if sensors are small enough, the assumption could be made that the entire surface area of the sensor is experiencing force because of how small the sensor is – that it would be unlikely for only part of the sensor to be experiencing force due to how small it is. With a larger sensor surface area, it is more challenging to make this assumption as there is just more variation and possibility on the amount of contact that can be made. To sense pressures on the body, ideally multiple small sensors all close to each other would be concentrated to an area of interest on the body.

7.1 Future Work

Contact sensors were found to be able to sense interactions with the body with fewer confounding variables than the force sensors, but as implemented here, they could only reliably measure contact at or above a certain force. This force was also relatively low as it was measuring unimpeded contact between two surfaces. The sensing approach could be further expanded to reflect a variety of contact forces by modifying the sensor fabrication. An additional layer could be added on top of one side of the contact electrode, such as a semi-open structure textile or spacer material, to increase the contact force.

As illuminated through this study, there are many areas for future work for accurate on-body force sensing. An on-body sensor calibration method to be used for different bodies is needed, as the force sensor responses can change with a change in body dimension. It would be beneficial to understand in more depth the variables that influence on-body and textile-integrated force sensing, such as how the sensor is responding to stretch. The force sensors present challenges when being placed on the body with the form-fit garment style from the garment and textile forming around the body, which is not present when in a relaxed/unstretched state not on the body. It is likely that when the

garment and textile wrap around the body to achieve a low-profile and form-fit for sensor accuracy, the garment or textile is stretching and generating normal forces between the sensor and the body.

It is possible that the addition of a non-stretch/woven material integrated around and under the sensor may help minimize stretch and mitigate some of these issues. This may however have an impact on wearability, since non-stretch materials could potentially restrict user movement/mobility. There may still be issues present with the body pressing up against and applying force to the underside of the sensor and inducing a response. An attempt to mitigate this issue might involve introducing a more stable material underneath the sensor, but that may decrease the ability of the sensor to flex and conform to the body's geometry underneath. Finding the right balance between these aspects may be important for successful development of a sensing system.

There were challenges with the method of MoCap testing and measuring marker pair distance that could be investigated for future work. The two main variables that likely affected measured marker contact were the need to offset some marker pairs for the marker-contact threshold and the shifting of the brief over the manikin's surface during dynamic movement. Minimizing the amount of offset required for analysis and the amount of shifting or sliding over the manikin's surface would likely improve the accuracy of the MoCap method for measuring contact. The ideal scenario would be if markers could line up identically/perfectly between trials and the brief marker pair would extend outward and move back in towards the manikin (without shifting over the surface). In this study, some sensors were outside of the brief area, especially for the padded manikin condition as the padding brought the sensors farther out on the manikin's body. This presented challenges for perfectly lining up marker pairs between the no brief and brief trials as the brief was not even over some sensor locations. Testing the method on a body area where more precise marker pair placement can occur and reducing the amount of shifting or sliding over the manikin's surface would likely contribute to improved accuracy for marker contact results. For situations where shifting cannot be preventing, constraining or fixing certain axis/axes could improve marker

contact analysis by minimizing marker contact only being detected in the very specific marker pair location.

Although variables for sensor manufacture were evaluated for durability, they were not tested with a standard protocol. Performing controlled durability tests would provide more rigorous insights into the optimal materials and fabrication processes for maximum product lifecycle and understand if the sensor would be appropriate for different sensing environments.

References

[1] Kenneth S. Thomas and Harold J. McMann. *U.S. Spacesuits*. Space Exploration. Springer-Verlag, New York, 2nd edition, 2012. doi: 10.1007/978-1-4419-9566-7.

[2] Elizabeth Benson and Sudhakar Rajulu. Complexity of Sizing for Space Suit Applications. In *Digital Human Modeling*, Vincent G. Duffy, editor, Lecture Notes in Computer Science, pages 599–607, Berlin, Heidelberg, 2009. Springer. doi: 10.1007/978-3-642-02809-0_63.

[3] K. Han Kim, Karen S. Young, Yaritza Bernal, Abhishektha Boppana, Linh Q. Vu, Elizabeth A. Benson, Sarah Jarvis, and Sudhakar L. Rajulu. A Parametric Model of Shoulder Articulation for Virtual Assessment of Space Suit Fit. In *Proceedings of the 7th International Conference on 3D Body Scanning Technologies*, pages 201–207, Lugano, Switzerland, November 2016. Hometrica Consulting - Dr. Nicola D'Apuzzo. doi: 10.15221/16.201.

[4] Christopher R. Reid, Lauren R. Harvill, Jason R. Norcross, Elizabeth A. Benson, Scott A. England, Karen Young, and Sudhakar L. Rajulu. An Ergonomic Evaluation of the Extravehicular Mobility Unit (EMU) Spacesuit Hard Upper Torso (HUT) Size Effect on Mobility, Strength, and Metabolic Performance. *Proceedings of the Human Factors and Ergonomics Society Annual Meeting*, 58(1):1595–1599, September 2014. doi: 10.1177/1541931214581332.

[5] Andrew Abercromby, Scott Cupples, Sudhakar Rajulu, Jesse Buffington, Jason Norcross, and Steven Chappell. Integrated Extravehicular Activity (EVA) Human

Research Plan: 2016. In *46th International Conference on Environmental Systems*, Vienna, Austria, July 2016. Available: https://ttuir.tdl.org/handle/2346/67694.

[6] Karen L. LaBat and Karen S. Ryan. *Human Body: A Wearable Product Designer's Guide*. CRC Press, February 2019. doi: 10.1201/9780429055690.

[7] Yijing Zong and Young-A Lee. An exploratory study of integrative approach between 3D body scanning technology and motion capture systems in the apparel industry. *International Journal of Fashion Design, Technology and Education*, 4(2):91–101, July 2011. doi: 10.1080/17543266.2010.537281.

[8] David G. Parry, Leroy R. Curry Jr, Donald B. Hanson, and George B. Towle. A study of techniques and equipment for the evaluation of extravehicular protective garments. Technical report, UNITED TECHNOLOGIES CORP WINDSOR LOCKS CT HAMILTON STANDARD DIV, February 1966. Section: Technical Reports. Available: https://apps.dtic.mil/sti/citations/AD0635206.

[9] Samuel Strauss. Extravehicular Mobility Unit Training Suit Symptom Study Report. Technical report, Johnson Space Center, Houston, TX, June 2004. https://ntrs.nasa.gov/search.jsp?R=20060017061.

[10] A. Anderson, A. Hilbert, P. Bertrand, S. McFarland, and D. J. Newman. In-Suit Sensor Systems for Characterizing Human-Space Suit Interaction. In *44th International Conference on Environmental Systems*, July 2014. Available: https://ttu-ir.tdl.org/handle/2346/59683

[11] Matthew A. Gast and Sandra K. Moore. A glimpse from the inside of a space suit: What is it really like to train for an EVA? *Acta Astronautica*, 68(1):316–325, January 2011. doi: 10.1016/j.actaastro.2010.08.015.

[12] Karen Louise Lilevjen LaBat. *Consumer satisfaction/dissatisfaction with the fit of ready-to-wear clothing*. Ph.D., University of Minnesota, United States – Minnesota, 1987. Available: http://www.proquest.com/docview/303656665/abstract/E10698895BEB468DPQ/1

[13] Mabel Deane Erwin, Lila A. Kinchen, and Kathleen A. Peters. *Clothing for Moderns*. Macmillan, New York, 6th edition, 1979.

[14] Susan P. Ashdown and Elizabeth K. O'Connell. Comparison of Test Protocols for Judging the Fit of Mature Women's Apparel. *Clothing and Textiles Research Journal*, 24(2):137–146, March 2006. Publisher: SAGE Publications Inc. doi: 10.1177/0887302X0602400207.

[15] Chin-Man Chen. *Female body characteristics related to bra fit*. Ph.D., University of Minnesota, United States – Minnesota, 2007. ISBN: 9780549279297. Available: http://search.proquest.com/docview/304841164/abstract/B17253DFBC0741CAPQ/1

[16] H. A. M. Daanen and P. A. Reffeltrath. Function, fit and sizing. In *Sizing in clothing: Developing effective sizing systems for ready-to-wear clothing*, S. P. Ashdown, editor, Woodhead Publishing Series in Textiles, pages 202–219. Woodhead Publishing, January 2007.

[17] Elizabeth Bye, Karen LaBat, Ellen McKinney, and Dong-Eun Kim. Optimized pattern grading. *International Journal of Clothing Science and Technology*, 20(2):79– 92, January 2008. Publisher: Emerald Group Publishing Limited. doi: 10.1108/09556220810850469.

[18] Susan P Ashdown, Suzanne Loker, Katherine Schoenfelder, and Lindsay Lyman-Clarke. Using 3D Scans for Fit Analysis. *Journal of Textile and Apparel, Technology and Management*, 4(1):1–12, 2004.

[19] Susan P. Ashdown. An investigation of the structure of sizing systems: A comparison of three multidimensional optimized sizing systems generated from anthropometric data with the ASTM standard D5585-94. *International Journal of Clothing Science and Technology*, 10(5):324–341, January 1998. Publisher: MCB UP Ltd. doi: 10.1108/09556229810239324.

[20] A. Petrova. Creating sizing systems. In *Sizing in Clothing*, pages 57–87. Published by Woodhead Publishing Limited in association with The Textile Institute, April 2007.

[21] Brett Allen, Brian Curless, and Zoran Popovi´c. The space of human body shapes: reconstruction and parameterization from range scans. *ACM Transactions on Graphics*, 22(3):587–594, July 2003. doi: 10.1145/882262.882311.

[22] Z Ben Azouz, Zouhour Benazouz, M Rioux, Marc Rioux, C Shu, Chang Shu, R Lepage, and Richard Lepage. Analysis of Human Shape Variation Using Volumetric Techniques. In *17th Annual Conference on Computer Animation and Social Agents (CASA 2004)*, page 11, July 2004.

[23] Zouhour Ben Azouz, Marc Rioux, Chang Shu, and Richard Lepage. Characterizing human shape variation using 3D anthropometric data. *The Visual Computer*, 22(5):302–314, May 2006. doi: 10.1007/s00371-006-0006-6.

[24] A. C. K. Chan. The development of apparel sizing systems from anthropometric data. In *Anthropometry, Apparel Sizing and Design*, Deepti Gupta and Norsaadah Zakaria, editors, pages 167–196. Woodhead Publishing, January 2014. doi: 10.1533/9780857096890.2.167.

[25] Susan M. Watkins and Lucy E. Dunne. *Functional Clothing Design: From Sportswear to Spacesuits*. Bloomsbury Publishing USA, January 2015.

[26] Deepti Gupta. Design and engineering of functional clothing. *Indian Journal of Fibre & Textile Research*, 36(4):327–335, December 2011.

[27] Lynn M Boorady. Functional clothing—Principles of fit. *Indian Journal of Fibre & Textile Research*, 36:344–347, 2011.

[28] Nancy J. Currie and David Graziosi. Space Suit Design Enhancements to Improve Size Accommodation and Mobility. *Proceedings of the Human Factors and Ergonomics Society Annual Meeting*, 47(1):1–5, October 2003. Publisher: SAGE Publications Inc. doi: 10.1177/154193120304700101.

[29] Karla P. Simmons and Cynthia L. Istook. Body measurement techniques: Comparing 3D body-scanning and anthropometric methods for apparel applications. *Journal of Fashion Marketing and Management: An International Journal*, 7(3):306– 332, January 2003. doi: 10.1108/13612020310484852.

[30] Adriana Petrova and Susan P. Ashdown. Three-Dimensional Body Scan Data Analysis: Body Size and Shape Dependence of Ease Values for Pants' Fit. *Clothing and Textiles Research Journal*, 26(3):227–252, July 2008. doi: 10.1177/0887302X07309479.

[31] Karla Simmons, Cynthia L Istook, and Priya Devarajan. Female Figure Identification Technique (FFIT) for Apparel Part I: Describing Female Shapes. *Journal of Textile and Apparel Technology and Management*, 4(1):16, 2004.

[32] Karla Simmons, Cynthia L Istook, and Priya Devarajan. Female Figure Identification Technique (FFIT) for Apparel Part II: Development of Shape Sorting Software. 4(1):15, 2004.

[33] L. Griffin, S. Sokolowski, and E. Seifert, "Process Considerations in 3D Hand Anthropometric Data Collection," in *Proceedings of 3DBODY.TECH 2018 - 9th International Conference and Exhibition on 3D Body Scanning and Processing Technologies*, Lugano, Switzerland, Oct. 2018, pp. 123–123. doi: 10.15221/18.123.

[34] Linsey Griffin, Emily Seifert, Chris Curry, and Susan Sokolowski. 3D Hand Scanning to Digital Draping for Glove Design. In *Advances in Interdisciplinary Practice in Industrial Design*, Cliff Sungsoo Shin, editor, Advances in Intelligent Systems and Computing, pages 112–123, Cham, 2020. Springer International Publishing. doi: 10.1007/978-3-030-20470-9_14.

[35] "3dMD | The world leader in anatomically-precise 3D and 'temporal-3D' (4D) surface imaging systems and software." http://www.3dmd.com/

[36] K. Han Kim, Karen Young, Elizabeth Benson, Sarah Jarvis, Linh Vu, Yaritza Hernandez, and Sudhakar Rajulu. Human modeling tools for spacesuit and hardware design and assessment. In *DHM and Posturography*, Sofia Scataglini and Gunther Paul, editors, pages 613–625. Academic Press, January 2019. doi: 10.1016/B978-0-12-816713-7.00046-5.

[37] Sarah Jarvis, Linh Vu, Elizabeth Benson, and Sudhakar Rajulu. Development of Human-Spacesuit Interaction Models. In *49th International Conference on Environmental Systems*, July 2019. Available: https://ttu-ir.tdl.org/handle/2346/84605

[38] Sarah E. Margerum, Mike A. Ferrer, Karen S. Young, and Sudhakar Rajulu. Relating Linear and Volumetric Variables Through Body Scanning to Improve Human Interfaces in Space. Lugano, Switzerland, January 2010. NTRS Author Affiliations: Lockheed Martin Corp., MEI Technologies, Inc., NASA Johnson Space Center NTRS Report/Patent Number: JSC-CN-20723 NTRS Document ID: 20100020965 NTRS Research Center: Johnson Space Center (JSC). Available: https://ntrs.nasa.gov/citations/20100020965

[39] Kristine Davis, Richard Rhodes, Han Kim, Elizabeth Benson, Yaritza Hernandez, Linh Vu, and Sudhakar Rajulu. xEMU Lower Torso Assembly (LTA) Brief Fleet Sizing Study. In *2020 International Conference on Environmental Systems*, July 2020. Available: https://ttu-ir.tdl.org/handle/2346/86422

[40] Al Reinhardt and James S. Walton. The Recovery and Utilization of Space Suit Range-of-Motion Data. SAE Technical Paper 881091, SAE International, Warrendale, PA, July 1988. ISSN: 0148-7191, 2688-3627. doi: 10.4271/881091.

[41] Al Reinhardt. Results and Applications of a Space Suit Range-of-Motion Study. *SAE Transactions*, 98:1184–1196, 1989. Publisher: SAE International.

[42] Rosana Martins Ferreira de Carvalho, Nilton Mazzer, and Claudio Henrique Barbieri. Analysis of the reliability and reproducibility of goniometry compared to hand photogrammetry. *Acta Ortopedica Brasileira*, 20(3):139–149, 2012. doi: 10.1590/S1413-78522012000300003.

[43] Amy Ross. Advanced Space Suit Isolated Joint Mobility Test for the Space Suit Comparative Technology Evaluation Test. *JSC-39522 (CTSDADV-387)*, 2000.

[44] Peter K. Larsen, Erik B. Simonsen, and Niels Lynnerup. Use of photogrammetry and biomechanical gait analysis to identify individuals. In *2010 18th European Signal Processing Conference*, pages 1660–1664. IEEE, August 2010. ISSN: 2219- 5491.

[45] Edith Gazzuolo, Marilyn DeLong, Sharon Lohr, Karen LaBat, and Elizabeth Bye. Predicting garment pattern dimensions from photographic and anthropometric data. *Applied Ergonomics*, 23(3):161–171, June 1992. doi: 10.1016/0003-6870(92)90219-L.

[46] David R Williams, Saint Hubert, and Brian J Johnson. EMU Shoulder Injury Tiger Team Report. Technical report, National Aeronautics and Space Administration, Lyndon B. Johnson Space Center, Houston, TX, 2003.

[47] Samuel Strauss, Ralph L. Krog, and Alan H. Feiveson. Extravehicular Mobility Unit Training and Astronaut Injuries. *Aviation, Space, and Environmental Medicine*, 76(5):469–474, May 2005.

[48] Allison Paige Anderson. *Understanding human-space suit interaction to prevent injury during extravehicular activity*. Ph.D. dissertation, Massachusetts Institute of Technology, June 2014. Available: https://dspace.mit.edu/handle/1721.1/90597

[49] Alexandra Marie Hilbert. *Human-Spacesuit Interaction: Understanding Astronaut Shoulder Injury*. Thesis, Massachusetts Institute of Technology, 2015. Available: https://dspace.mit.edu/handle/1721.1/98558

[50] VICON, "Motion Capture Systems," *VICON*. http://www.vicon.com

[51] Xsens, "Xsens," *Xsens 3D motion tracking*.

[52] Andrew F. J. Abercromby, Sherry S. Thaxton, Elizabeth A. Onady, and Sudhakar L. Rajulu. Reach Envelope and Field of Vision Quantification in Mark III Space Suit Using Delaunay Triangulation. Technical Report NASA/TP-2006-213729, National Aeronautics and Space Administration Lyndon B. Johnson Space Center, Houston, TX, November 2006. NTRS Author Affiliations: MEI Technologies, Inc., Lockheed Martin Corp., LZ Tech, NASA Johnson Space Center NTRS Report/Patent Number: S-987 NTRS Document ID: 20070001117 NTRS Research Center: Johnson Space Center (JSC). Available: https://ntrs.nasa.gov/citations/20070001117

[53] Lindsay Aitchison. A Comparison of Methods for Assessing Space Suit Joint Ranges of Motion. In *42nd International Conference on Environmental Systems*, San Diego,

California, 2012. American Institute of Aeronautics and Astronautics. doi: 10.2514/6.2012-3534.

[54] Massimiliano Di Capua and David Akin. Body Pose Measurement System (BPMS): An Inertial Motion Capture System for Biomechanics Analysis and Robot Control from Within a Pressure Suit. In *42nd International Conference on Environmental Systems*. American Institute of Aeronautics and Astronautics, July 2012. doi: 10.2514/6.2012-3643.

[55] Massimiliano Di Capua and David L. Akin. Body Pose Measurement System: System Validation and Range of Motion/Kinematic Analysis of Three Pressure Suits. In *43rd International Conference on Environmental Systems*. American Institute of Aeronautics and Astronautics, July 2013. doi: 10.2514/6.2013-3424.

[56] Yaritza Bernal, K. Han Kim, Elizabeth Benson, Sarah Jarvis, Lauren Harvill, Ian Meginnis, and Sudhakar Rajulu. Development of Underwater Motion Capture System for Space Suit Mobility Assessment. *Proceedings of the Human Factors and Ergonomics Society Annual Meeting*, 61(1):945–949, September 2017. doi: 10.1177/1541931213601718.

[57] Ryan Kobrick, Nicholas Lopac, Chase Covello, Michael Fornito II, Benjamin Banner, Theodore Southern, and Nikolay Moiseev. Range of Motion Evaluation of a Final Frontier Design IVA Spacesuit using Motion Capture. In *49th International Conference on Environmental Systems*, Boston, Massachusetts, July 2019. Available: https://ttu-ir.tdl.org/handle/2346/84504

[58] Pierre J. Bertrand, Allison Anderson, Alexandra Hilbert, and Dava J. Newman. Feasibility of Spacesuit Kinematics and Human-Suit Interactions. In *44th International Conference on Environmental Systems*, July 2014. Available: https://ttu-ir.tdl.org/handle/2346/59680

[59] Richard A. Fineman, Timothy M. McGrath, Damian G. Kelty-Stephen, Andrew F. J. Abercromby, and Leia A. Stirling. Objective Metrics Quantifying Fit and

Performance in Spacesuit Assemblies. *Aerospace Medicine and Human Performance*, 89(11):985–995, November 2018. doi: 10.3357/AMHP.5123.2018.

[60] StretchSense Limited, "StretchSense," *StretchSense*. https://stretchsense.com/

[61] Linh Q. Vu. *Modeling Torso Shape and Assessing Lumbar Kinematics with Flexible Strain Sensors*. Thesis, May 2018. Available: https://uh-ir.tdl.org/handle/10657/3407

[62] Linh Q. Vu, Ryan Z. Amick, K. Han Kim, and Sudhakar L. Rajulu. Evaluation of lumbar motion with fabric strain sensors: A pilot study. *International Journal of Industrial Ergonomics*, 69:194–199, January 2019. doi: 10.1016/j.ergon.2018.11.007.

[63] Linh Q. Vu, K. Han Kim, Lawrence J. H. Schulze, and Sudhakar L. Rajulu. Lumbar posture assessment with fabric strain sensors. *Computers in Biology and Medicine*, 118:103624, March 2020. doi: 10.1016/j.compbiomed.2020.103624.

[64] Ryan Z. Amick, Christopher R. Reid, Linh Q. Vu, Dan Nguyen, Robert Sweet, Shane McFarland, and Sudhakar Rajulu. Preliminary Assessment of Ergonomic Injury Risk Factors in the Extravehicular Mobility Unit Spacesuit Glove. *Proceedings of the Human Factors and Ergonomics Society Annual Meeting*, 60(1):982–986, September 2016. doi: 10.1177/1541931213601227.

[65] Shane McFarland and Dan Nguyen. Analysis of Potential Glove-Induced Hand Injury Metrics during Typical Neutral Buoyancy Training Operations. In *47th International Conference on Environmental Systems*, July 2017. Available: https://ttu-ir.tdl.org/handle/2346/72922

[66] Md. Tahmidul Islam Molla, Steven Goodman, Nicholas Schleif, Mary Ellen Berglund, Cade Zacharias, Crystal Compton, and Lucy E. Dunne. Surface-mount manufacturing for e-textile circuits. In *Proceedings of the 2017 ACM International Symposium on Wearable Computers*, ISWC '17, pages 18–25, New York, NY, USA, September 2017. Association for Computing Machinery. doi: 10.1145/3123021.3123058.

[67] Md. Tahmidul Islam Molla. A scalable manufacturing method for garment-integrated technologies. In *Proceedings of the 2017 ACM International Joint*

Conference on Pervasive and Ubiquitous Computing and Proceedings of the 2017 ACM International Symposium on Wearable Computers, UbiComp '17, pages 344–349, New York, NY, USA, September 2017. Association for Computing Machinery. doi: 10.1145/3123024.3123194.

[68] Crystal Compton and Lucy Dunne. Pilot Investigation of a Novel Technique for Measuring Dynamic Body-Garment Contact. In *46th International Conference on Environmental Systems*, Vienna, Austria, July 2016. Available: https://ttu-ir.tdl.org/handle/2346/67546

[69] Crystal Marie Compton. Fit for space: Leveraging a novel skin contact measurement technique toward a more efficient liquid cooled garment. Master's thesis, University of Minnesota, United States – Minnesota, 2016. ISBN: 9781369354959. Available: http://www.proquest.com/docview/1853480755/abstract/EE133F51F588447BPQ/1

[70] Crystal Compton, Mary Ellen Berglund, Jin Chen, Derek Brubaker, Clayton Bunyard, and Lucy Dunne. Development and Characterization of a Mannequin-Based Method for Fit Measurement of Wearable Systems. In *48th International Conference on Environmental Systems*, Albuquerque, New Mexico, July 2018. Available: https://ttu-ir.tdl.org/handle/2346/74172

[71] Crystal Compton, Alireza Golgouneh, Brad Holschuh, and Lucy Dunne. Towards Large-area On-body Force Sensing Using Soft, Flexible Materials: Challenges of Textile-Based Array Sensing. In *2020 International Conference on Environmental Systems*, July 2020. Available: https://ttu-ir.tdl.org/handle/2346/86441

[72] SparkFun Electronics ®, "EeonTex Conductive Fabric - COM-14110 - SparkFun Electronics," *SparkFun*. https://www.sparkfun.com/products/14110

[73] Less EMF, "Electromagnetic Field Shielding Fabrics with a Natural Look and Feel," *Shielding & Conductive Fabrics*. https://www.lessemf.com/fabric1.html#321

[74] JOANN Fabric and Craft, "Pellon 911FF Fusible Featherweight 20" Interfacing White | JOANN." https://www.joann.com/pellon-911ff-fusible-featherweight-20in-interfacing-white/16698102.html

[75] Julie Christine Cole. *Patternmaking with Stretch Knit Fabrics*. Bloomsbury, 2016.

[76] Guido Gioberto, Crystal Compton, and Lucy E. Dunne. Machine-Stitched E-textile Stretch Sensors. *Sensors & Transducers Journal*, 202(7):25–37, 2016.

[77] "Conductive Fabric - 12"x13" Ripstop - DEV-10056 - SparkFun Electronics," *SparkFun Electronics*. https://www.sparkfun.com/products/retired/10056

[78] Adafruit Industries, "Woven Conductive Fabric - 20cm square." https://www.adafruit.com/product/1168

[79] JOANN Fabric and Craft, "Dritz Iron-On Mending Tape, 3" x 8", 3 pc, Dark Colors | JOANN." https://www.joann.com/dritz-iron-on-mending-fabric-3-1-4inx8in-1-pkg-white/1020742.html

[80] Seattle Fabrics, "Melco Iron on Seam Tape | 12 Inch Melco Seam Tape," *Seattle Fabrics*. https://www.seattlefabrics.com/12-Melco-Iron-On-Seam-Tape-Sold-by-the-Inch_p_511.html

[81] Shieldex, "Yarns/Threads," *Shieldex Trading*. https://www.shieldextrading.net/products/yarns-threads/

[82] Syscom Advanced Materials, "Liberator Conductive Fiber," *Syscom Advanced Materials*. http://www.metalcladfibers.com/liberator/

[83] W. L. Gore & Associates, Inc., "Gore | Improving lives through advanced materials." https://www.gore.com/

[84] CBAZY, "CBAZY Hook up Wire Kit (Stranded Wire Kit) 18 Gauge Flexible Silicone Rubber Electric Wire 6 Colors 16.4 feet Each 18 AWG." https://www.amazon.com/CBAZY-Stranded-Flexible-Silicone-Electric/dp/B073RDGTPB?th=1

[85] JOANN Fabric and Craft, "Wonder Under 2 Yds x 15" | JOANN." https://www.joann.com/wonder-under-2-yds-x-15in/5943147.html

[86] "2-Layer Seam Tapes," *Bemis Associates Inc. | Bemis.* https://www.bemisworldwide.com/products/2-layer-seam-tapes/

[87] 3M™, "3M™ Super 77™ Multipurpose Spray Adhesive." https://www.3m.com/3M/en_US/p/d/b40071862/

[88] Instron, "Instron - 3360 Series Universal Testing Systems up to 50 kN (11,250 lbf) Force Capacity," *Instron.* https://www.instron.us/en-US/Products/Testing Systems/Universal Testing Systems/Electromechanical/3300/3360 Dual Column

[89] Instron, "Compression Platens," *Instron.* http://www.instron.com/en-us/products/testing-accessories/compression-platens-anvils-spherical-seating

[90] "Form 2: Affordable Desktop SLA 3D Printer," *Formlabs.* https://formlabs.com/3d-printers/form-2/

[91] Lucy E Dunne, Guido Gioberto, Varun Ramesh, and Helen Koo. Measuring movement of denim trousers for garment-integrated sensing applications. In *Engineering in Medicine and Biology Society, EMBC, 2011 Annual International Conference of the IEEE*, pages 3990–3993. IEEE, 2011. doi: 10.1109/IEMBS.2011.6090991.

Appendix A

Plots

A.1 Instron Testing

A.1.1 Contact Sensors

A.1.1.1 Cyclic Testing

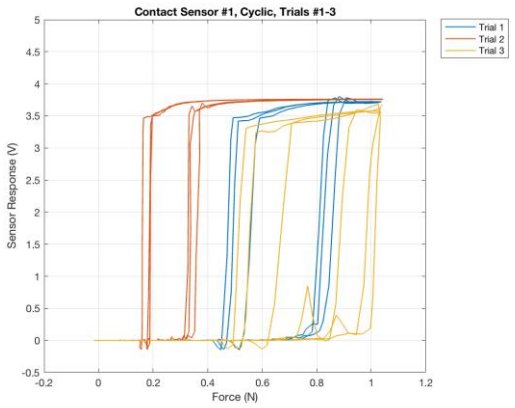

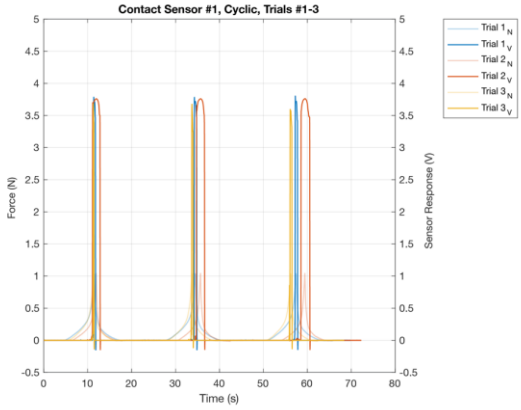

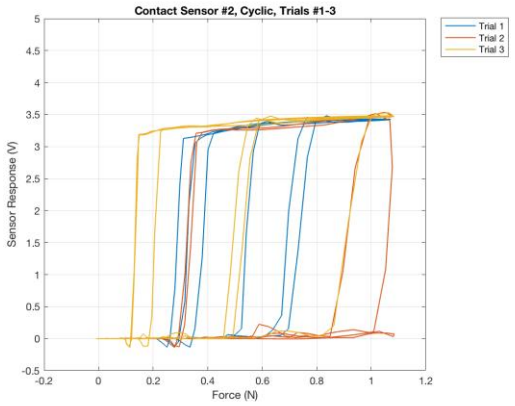
Contact Sensor #2, Cyclic, Trials #1-3
Sensor Response (V)
Force (N)
Trial 1
Trial 2
Trial 3

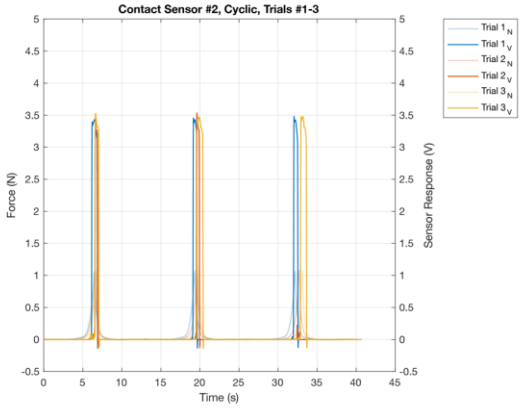
Contact Sensor #2, Cyclic, Trials #1-3
Force (N)
Sensor Response (V)
Time (s)
Trial 1 N
Trial 1 V
Trial 2 N
Trial 2 V
Trial 3 N
Trial 3 V

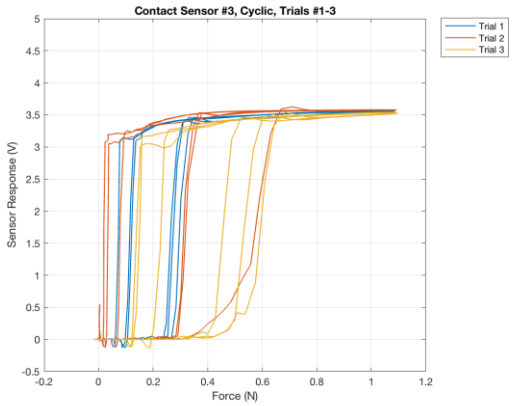
Contact Sensor #3, Cyclic, Trials #1-3
Sensor Response (V)
Force (N)
Trial 1
Trial 2
Trial 3

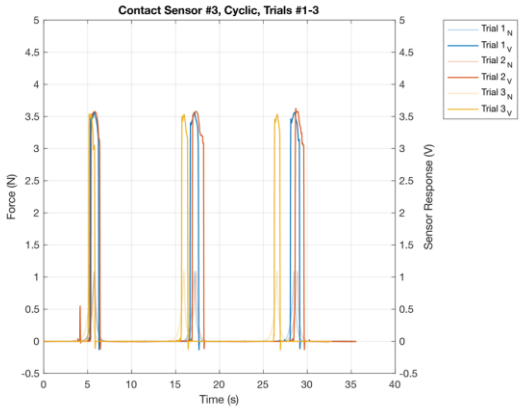
Contact Sensor #3, Cyclic, Trials #1-3
Force (N)
Sensor Response (V)
Time (s)
Trial 1 N
Trial 1 V
Trial 2 N
Trial 2 V
Trial 3 N
Trial 3 V

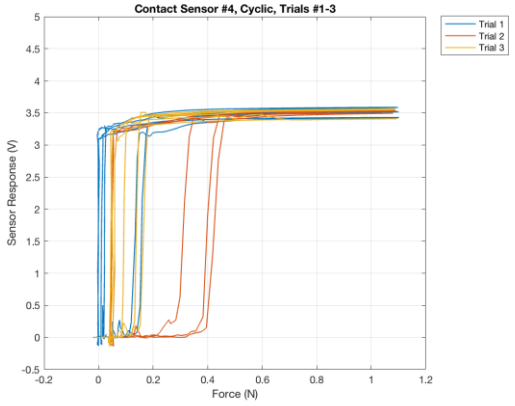
Contact Sensor #4, Cyclic, Trials #1-3
Sensor Response (V)
Force (N)
Trial 1
Trial 2
Trial 3

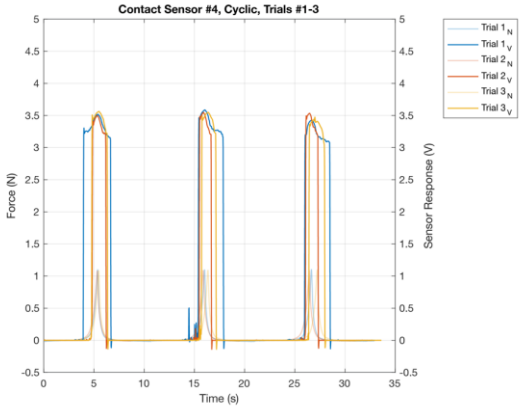
Contact Sensor #4, Cyclic, Trials #1-3
Force (N)
Sensor Response (V)
Time (s)
Trial 1 N
Trial 1 V
Trial 2 N
Trial 2 V
Trial 3 N
Trial 3 V

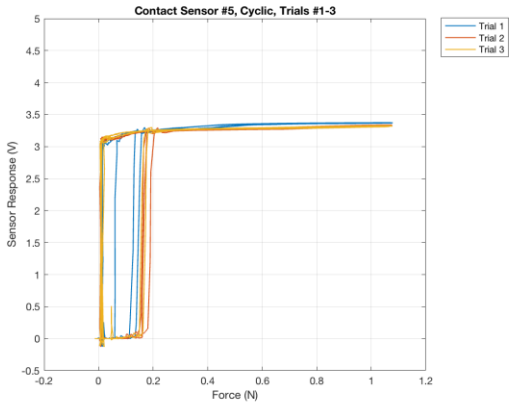
Contact Sensor #5, Cyclic, Trials #1-3
Sensor Response (V)
Force (N)
Trial 1
Trial 2
Trial 3

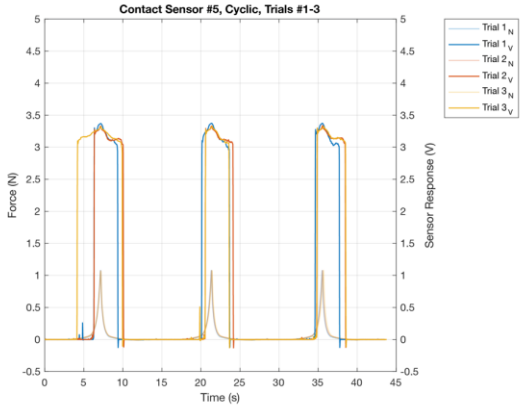
Contact Sensor #5, Cyclic, Trials #1-3
Force (N)
Sensor Response (V)
Time (s)
Trial 1 N
Trial 1 V
Trial 2 N
Trial 2 V
Trial 3 N
Trial 3 V

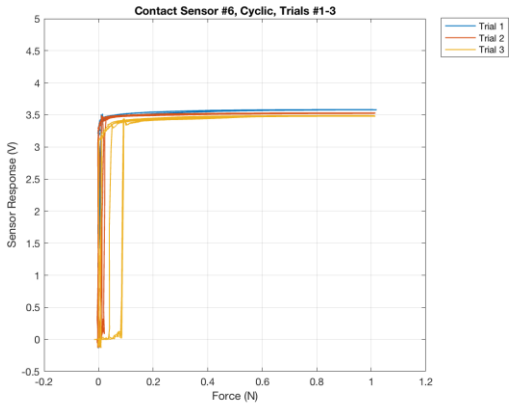
Contact Sensor #6, Cyclic, Trials #1-3
Sensor Response (V)
Force (N)
Trial 1
Trial 2
Trial 3

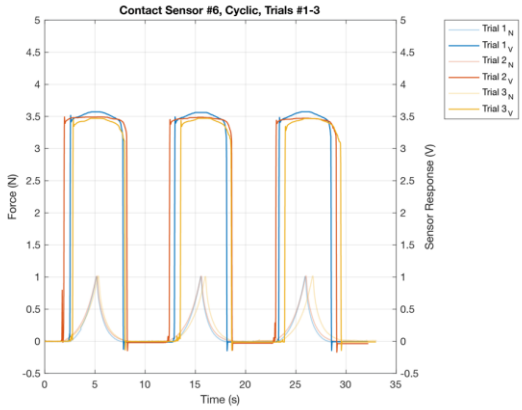
Contact Sensor #6, Cyclic, Trials #1-3
Force (N)
Sensor Response (V)
Time (s)
Trial 1 N
Trial 1 V
Trial 2 N
Trial 2 V
Trial 3 N
Trial 3 V

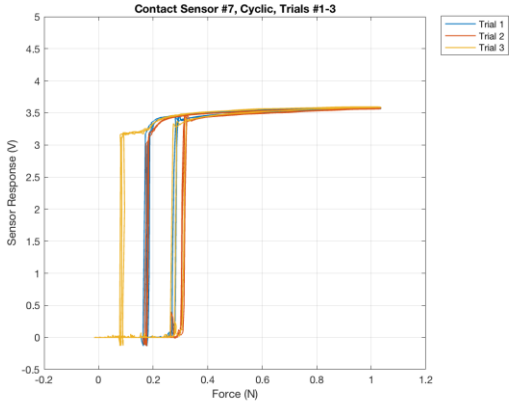
Contact Sensor #7, Cyclic, Trials #1-3
Sensor Response (V)
Force (N)
Trial 1
Trial 2
Trial 3

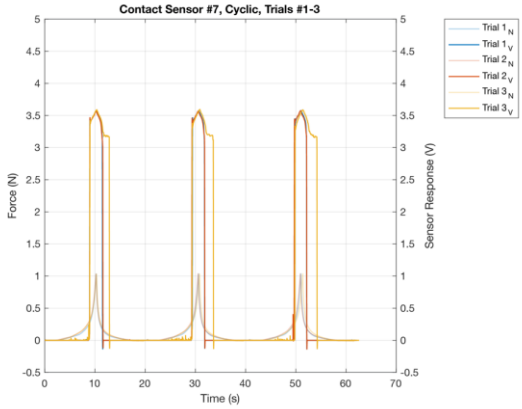
Contact Sensor #7, Cyclic, Trials #1-3
Force (N)
Sensor Response (V)
Time (s)
Trial 1 N
Trial 1 V
Trial 2 N
Trial 2 V
Trial 3 N
Trial 3 V

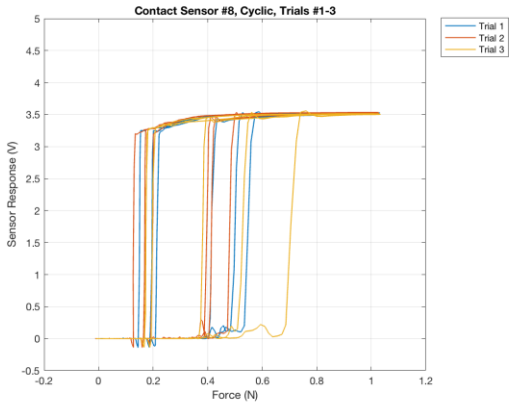
Contact Sensor #8, Cyclic, Trials #1-3
Trial 1
Trial 2
Trial 3
Sensor Response (V)
Force (N)

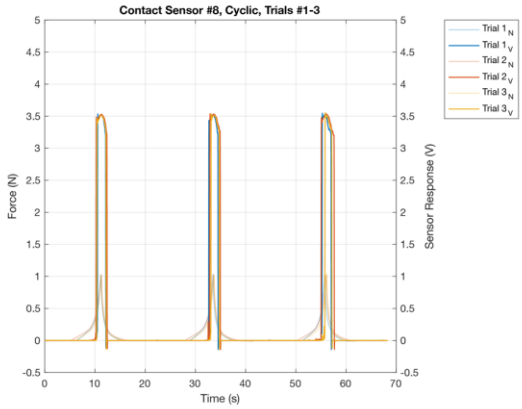
Contact Sensor #8, Cyclic, Trials #1-3
Trial 1 N
Trial 1 V
Trial 2 N
Trial 2 V
Trial 3 N
Trial 3 V
Force (N)
Sensor Response (V)
Time (s)

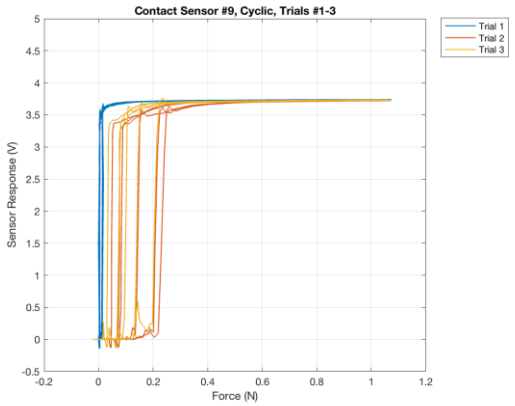
Contact Sensor #9, Cyclic, Trials #1-3
Trial 1
Trial 2
Trial 3
Sensor Response (V)
Force (N)

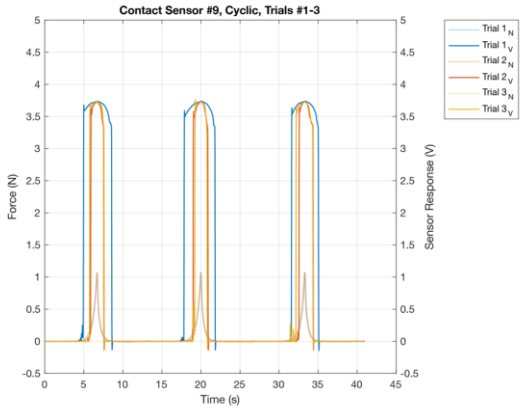
Contact Sensor #9, Cyclic, Trials #1-3
Trial 1 N
Trial 1 V
Trial 2 N
Trial 2 V
Trial 3 N
Trial 3 V
Force (N)
Sensor Response (V)
Time (s)

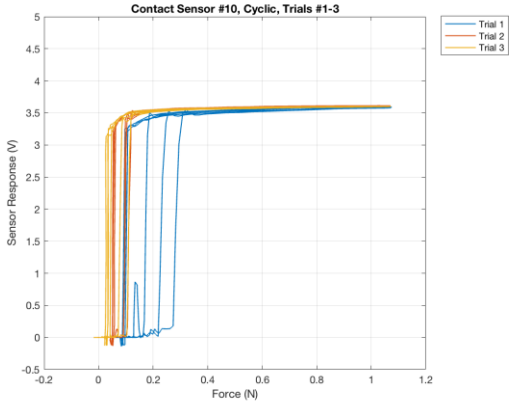
Contact Sensor #10, Cyclic, Trials #1-3
Trial 1
Trial 2
Trial 3
Sensor Response (V)
Force (N)

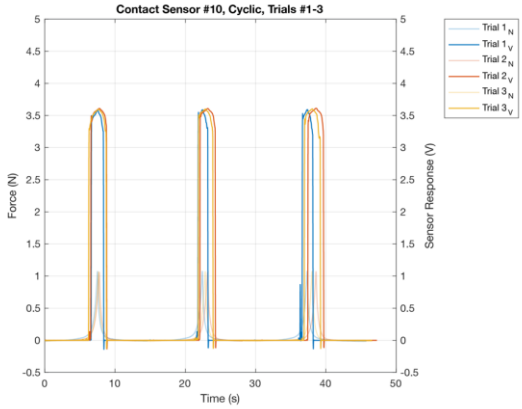
Contact Sensor #10, Cyclic, Trials #1-3
Trial 1 N
Trial 1 V
Trial 2 N
Trial 2 V
Trial 3 N
Trial 3 V
Force (N)
Sensor Response (V)
Time (s)

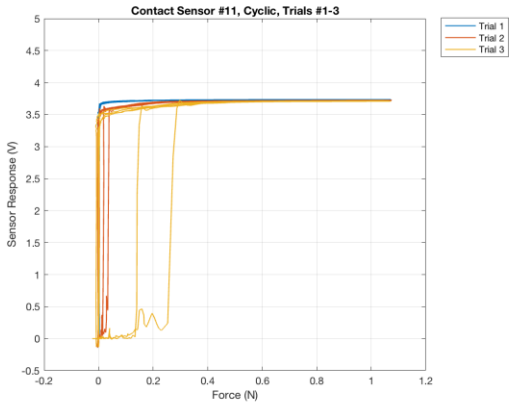
Contact Sensor #11, Cyclic, Trials #1-3
Sensor Response (V)
Force (N)
Trial 1
Trial 2
Trial 3

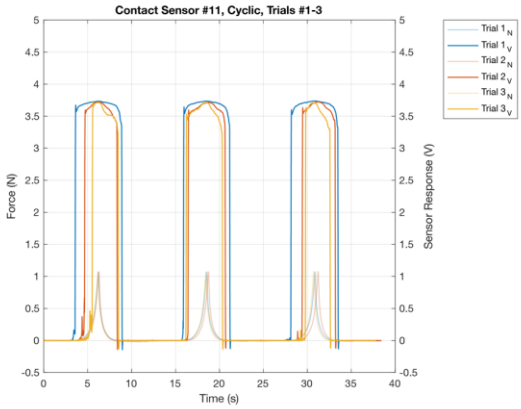
Contact Sensor #11, Cyclic, Trials #1-3
Force (N)
Sensor Response (V)
Time (s)
Trial 1 N
Trial 1 V
Trial 2 N
Trial 2 V
Trial 3 N
Trial 3 V

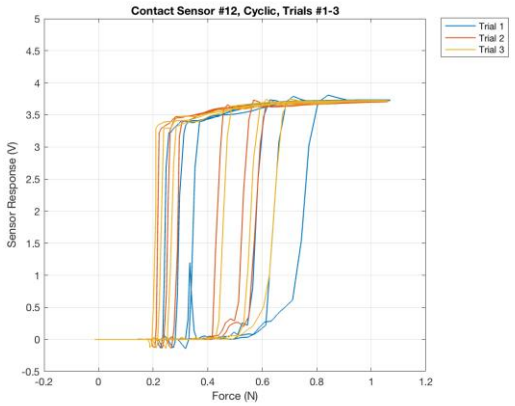
Contact Sensor #12, Cyclic, Trials #1-3
Sensor Response (V)
Force (N)
Trial 1
Trial 2
Trial 3

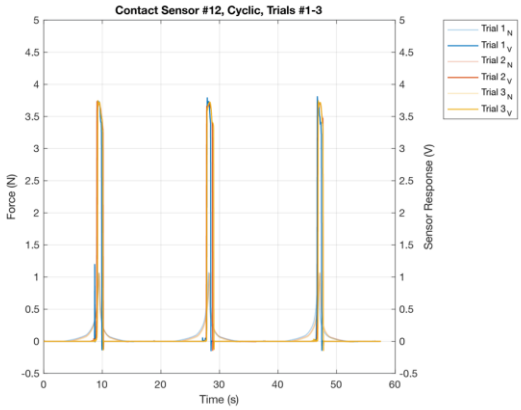
Contact Sensor #12, Cyclic, Trials #1-3
Force (N)
Sensor Response (V)
Time (s)
Trial 1 N
Trial 1 V
Trial 2 N
Trial 2 V
Trial 3 N
Trial 3 V

A.1.1.2 Static Testing

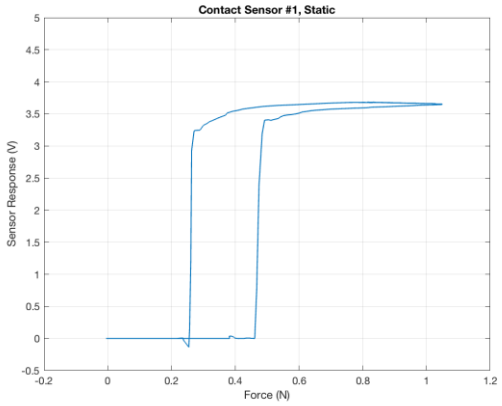

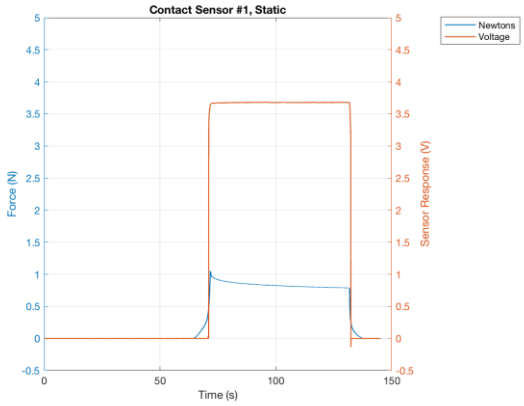

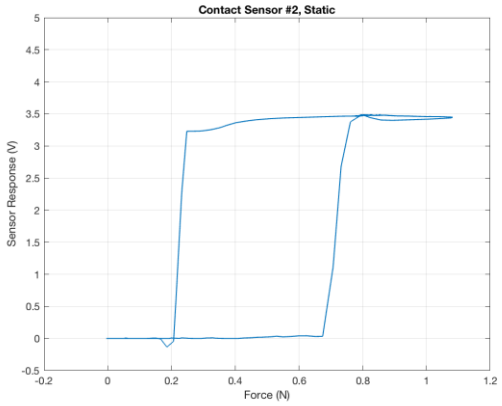

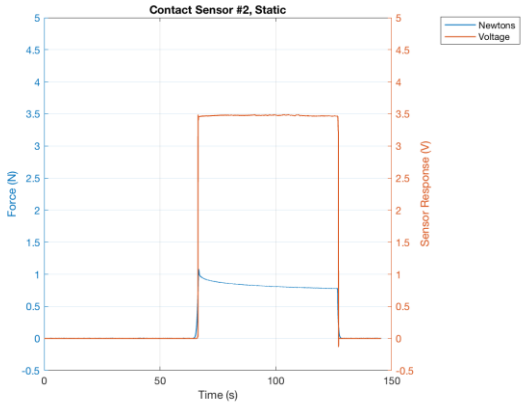

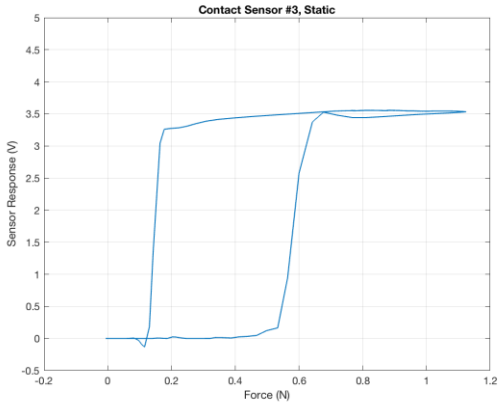

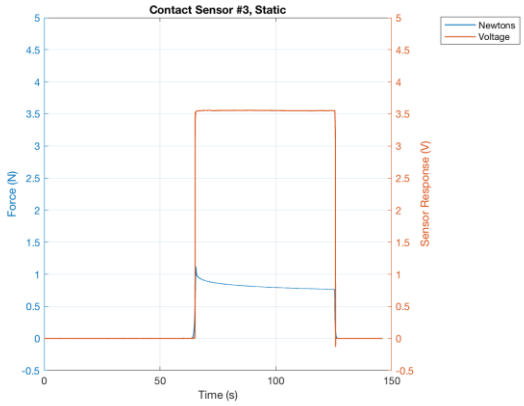

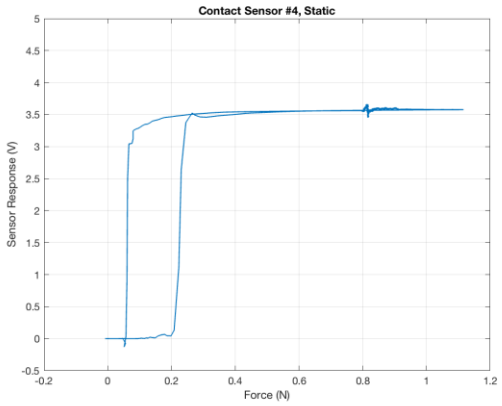
Contact Sensor #4, Static
Sensor Response (V)
Force (N)

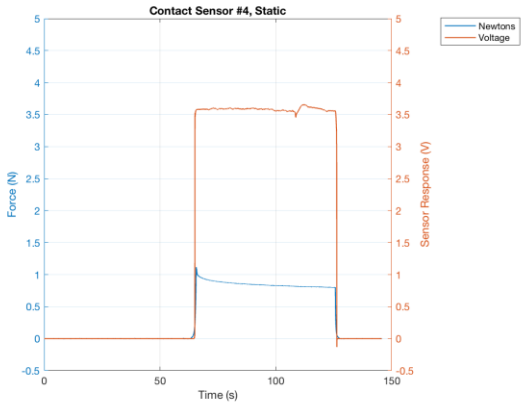
Contact Sensor #4, Static
Newtons
Voltage
Force (N)
Sensor Response (V)
Time (s)

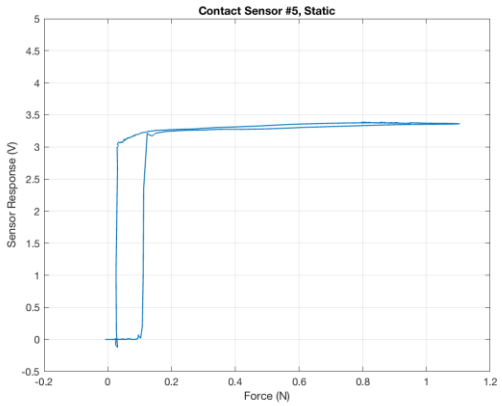
Contact Sensor #5, Static
Sensor Response (V)
Force (N)

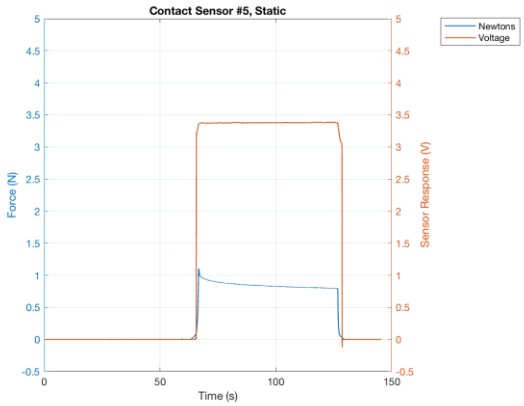
Contact Sensor #5, Static
Newtons
Voltage
Force (N)
Sensor Response (V)
Time (s)

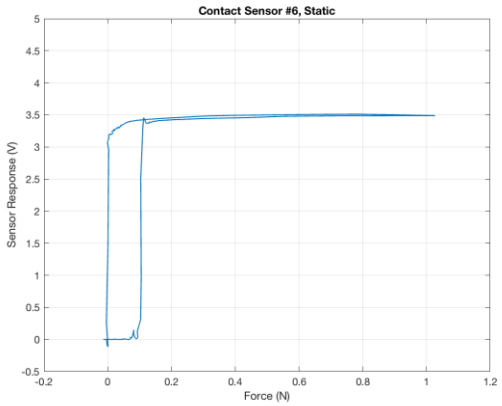
Contact Sensor #6, Static
Sensor Response (V)
Force (N)

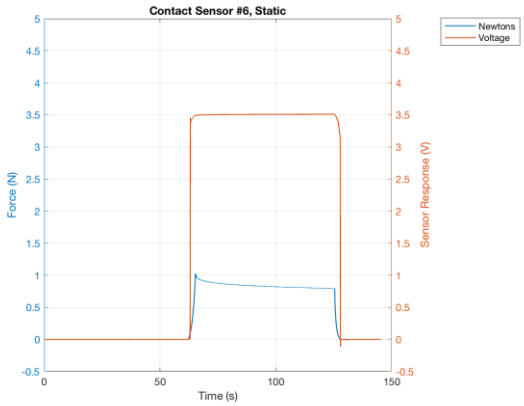
Contact Sensor #6, Static
Newtons
Voltage
Force (N)
Sensor Response (V)
Time (s)

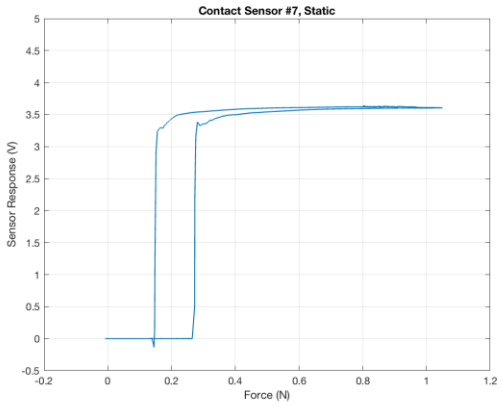
Contact Sensor #7, Static
Sensor Response (V)
Force (N)

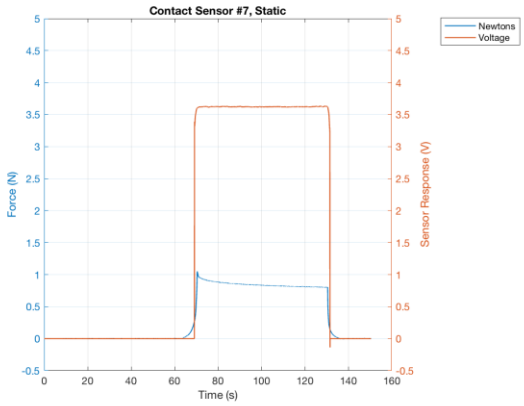
Contact Sensor #7, Static
Newtons
Voltage
Force (N)
Sensor Response (V)
Time (s)

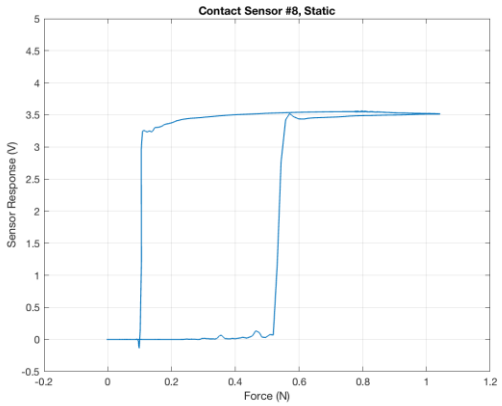
Contact Sensor #8, Static
Sensor Response (V)
Force (N)

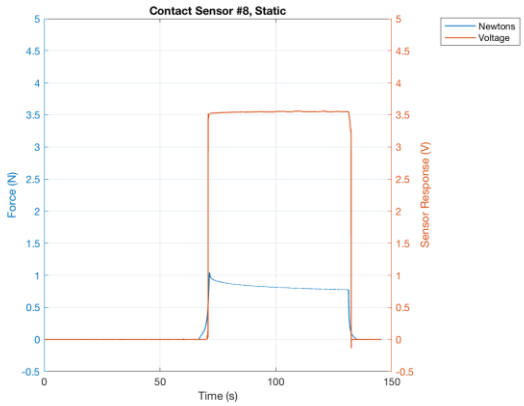
Contact Sensor #8, Static
Newtons
Voltage
Force (N)
Sensor Response (V)
Time (s)

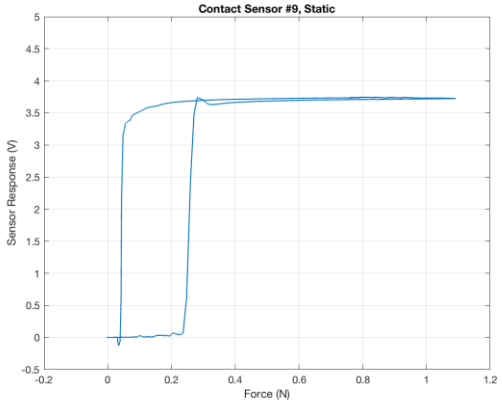
Contact Sensor #9, Static
Sensor Response (V)
Force (N)

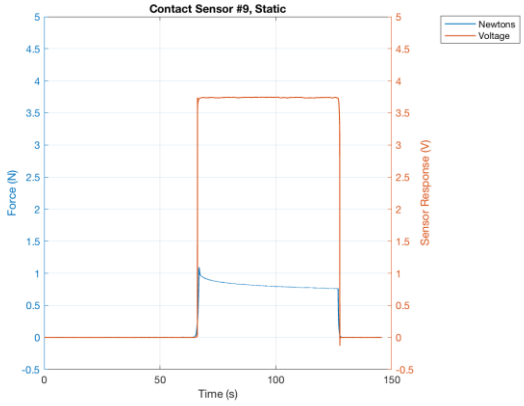
Contact Sensor #9, Static
Newtons
Voltage
Force (N)
Sensor Response (V)
Time (s)

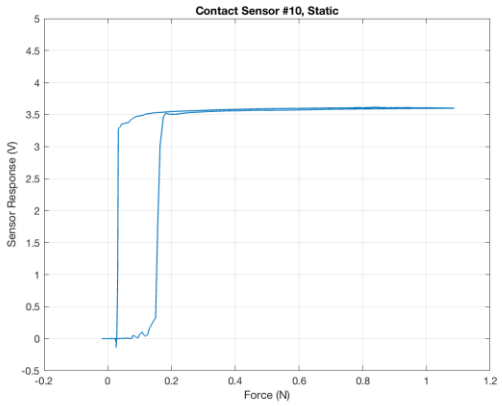
Contact Sensor #10, Static
Sensor Response (V)
Force (N)

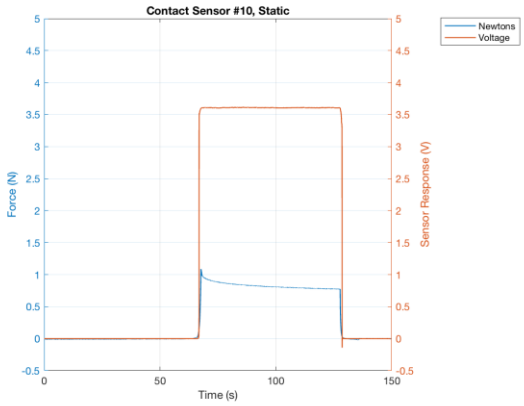
Contact Sensor #10, Static
Newtons
Voltage
Force (N)
Sensor Response (V)
Time (s)

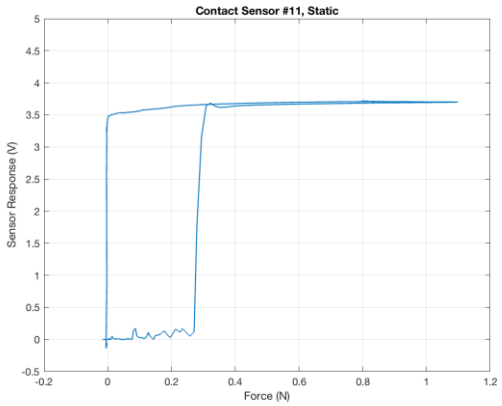
Contact Sensor #11, Static
Sensor Response (V)
Force (N)

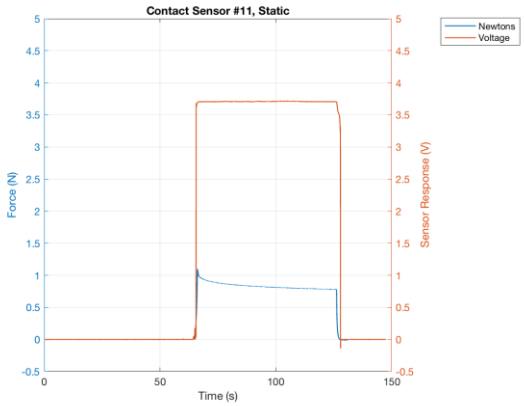
Contact Sensor #11, Static
Newtons
Voltage
Force (N)
Sensor Response (V)
Time (s)

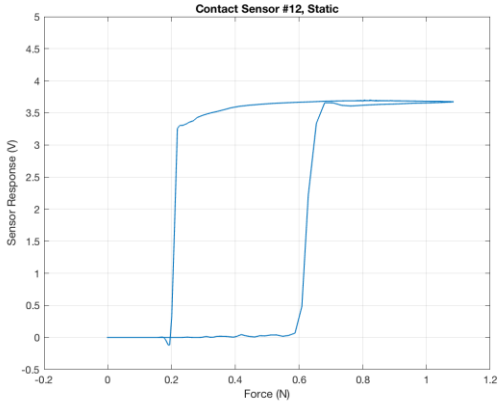
Contact Sensor #12, Static
Sensor Response (V)
Force (N)

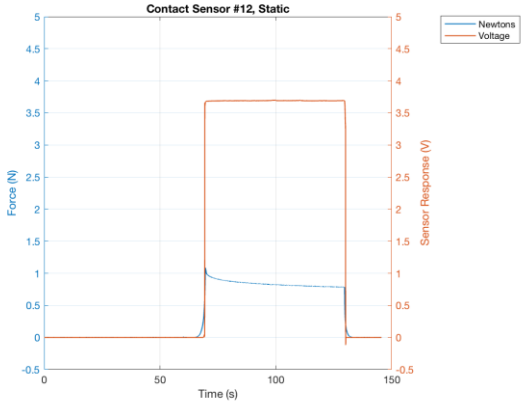
Contact Sensor #12, Static
Newtons
Voltage
Force (N)
Sensor Response (V)
Time (s)

A.1.1.3 Forces Below and Above the Contact-Threshold

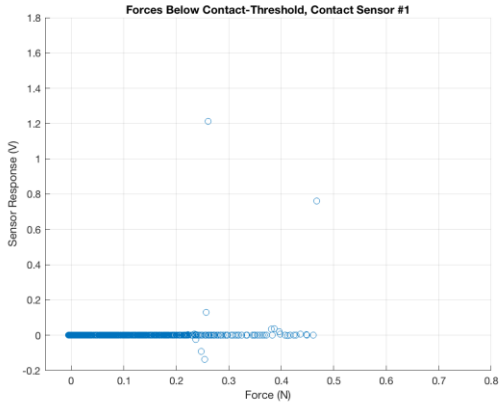

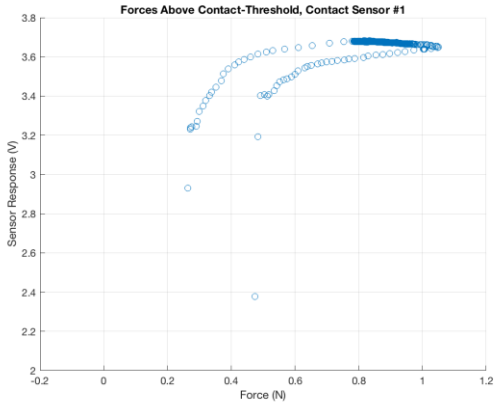

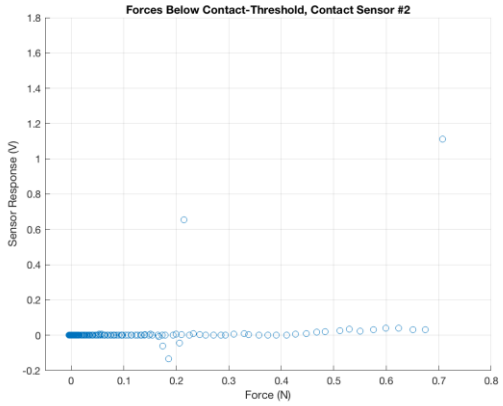

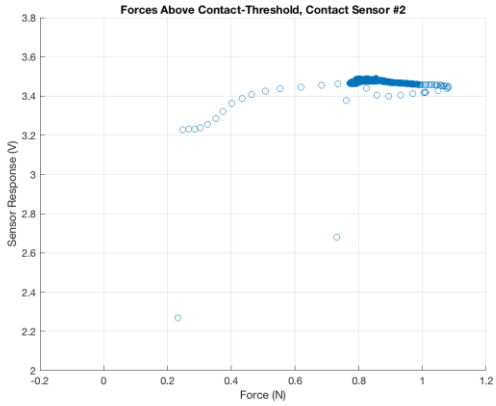

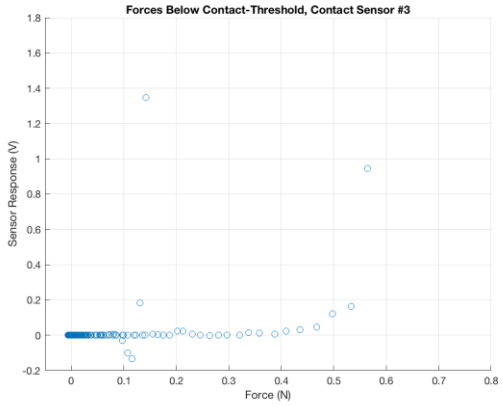

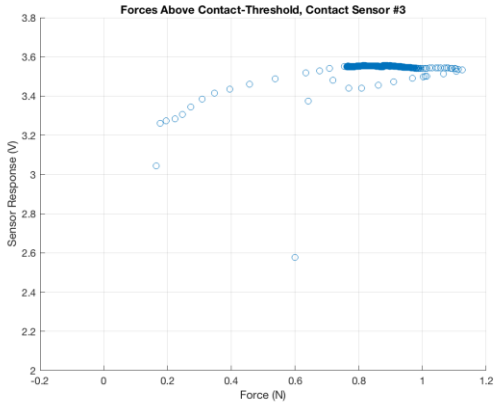

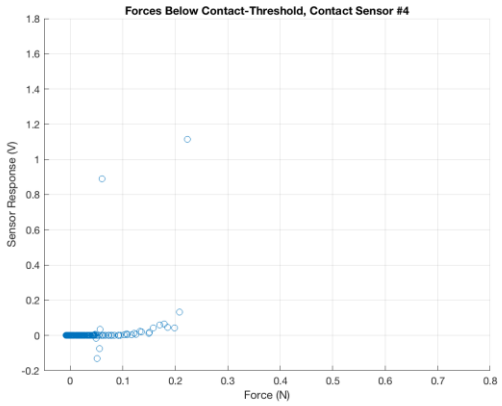
Forces Below Contact-Threshold, Contact Sensor #4
Sensor Response (V)
Force (N)

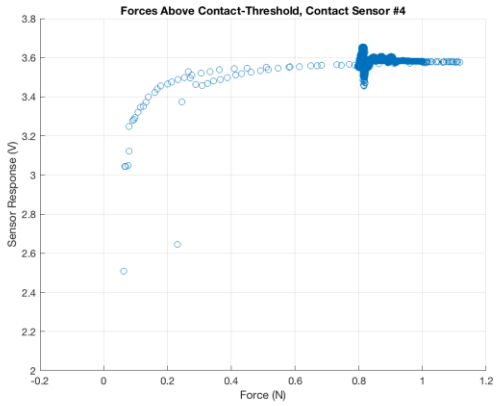
Forces Above Contact-Threshold, Contact Sensor #4
Sensor Response (V)
Force (N)

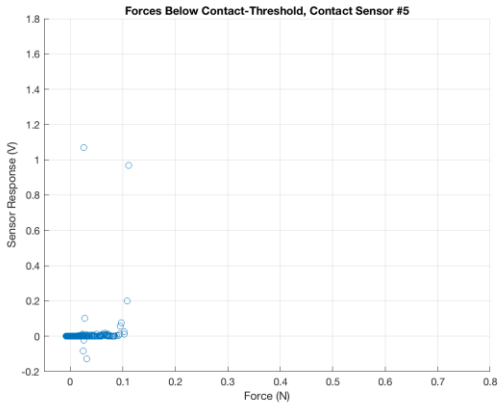
Forces Below Contact-Threshold, Contact Sensor #5
Sensor Response (V)
Force (N)

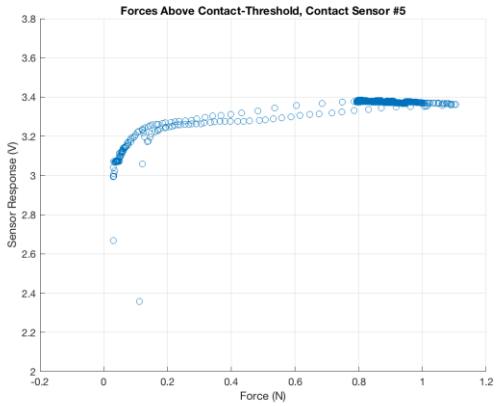
Forces Above Contact-Threshold, Contact Sensor #5
Sensor Response (V)
Force (N)

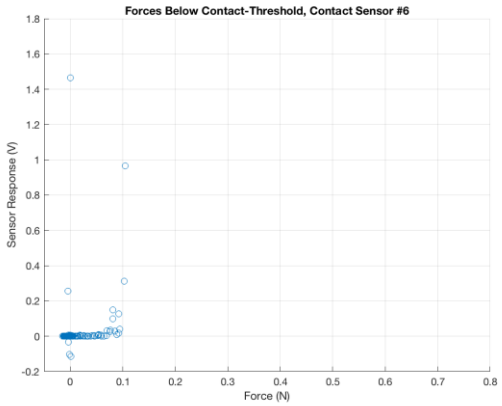
Forces Below Contact-Threshold, Contact Sensor #6
Sensor Response (V)
Force (N)

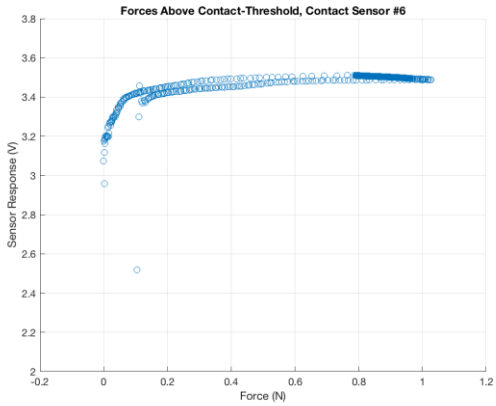
Forces Above Contact-Threshold, Contact Sensor #6
Sensor Response (V)
Force (N)

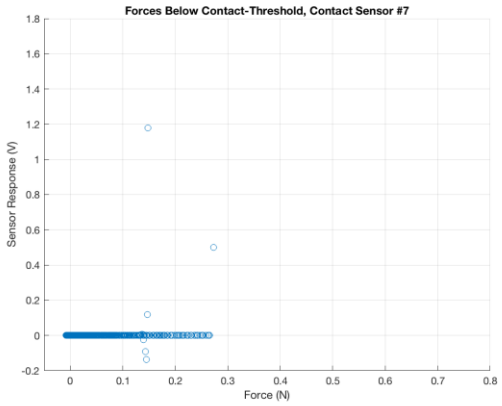
Forces Below Contact-Threshold, Contact Sensor #7
Sensor Response (V)
Force (N)

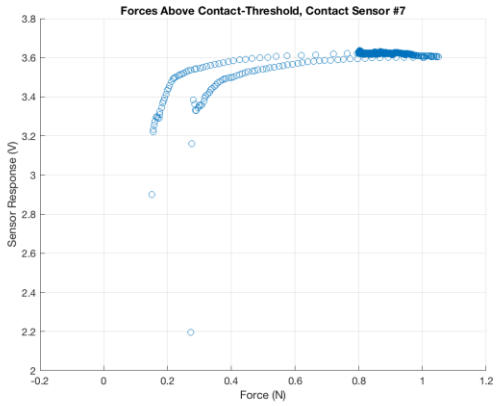
Forces Above Contact-Threshold, Contact Sensor #7
Sensor Response (V)
Force (N)

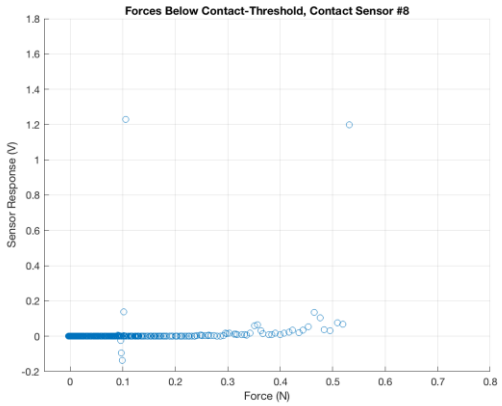
Forces Below Contact-Threshold, Contact Sensor #8
Sensor Response (V)
Force (N)

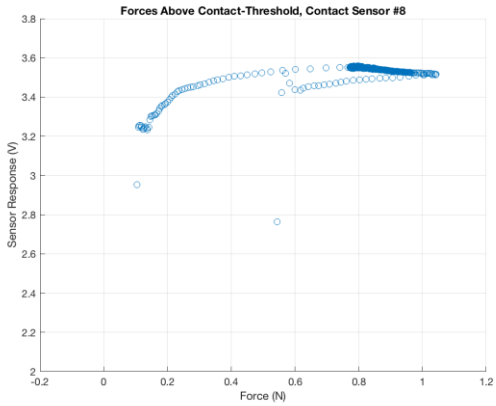
Forces Above Contact-Threshold, Contact Sensor #8
Sensor Response (V)
Force (N)

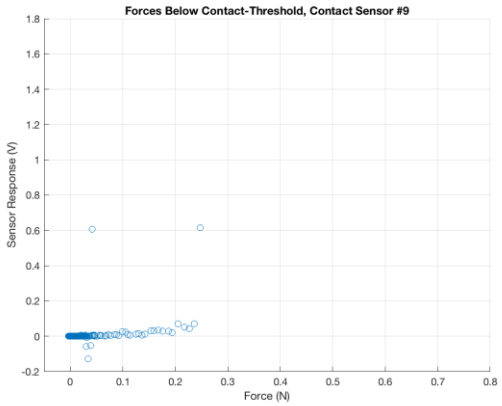
Forces Below Contact-Threshold, Contact Sensor #9
Sensor Response (V)
Force (N)

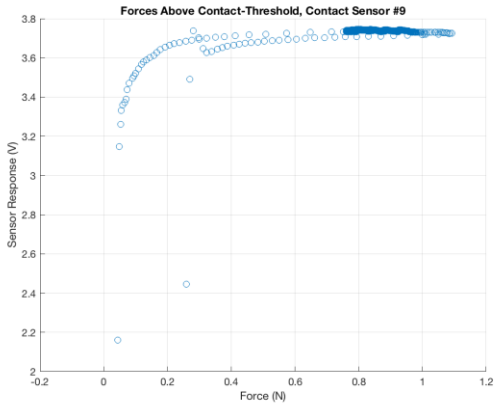
Forces Above Contact-Threshold, Contact Sensor #9
Sensor Response (V)
Force (N)

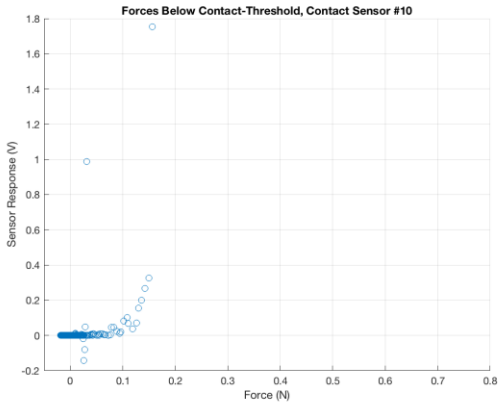
Forces Below Contact-Threshold, Contact Sensor #10
Sensor Response (V)
Force (N)

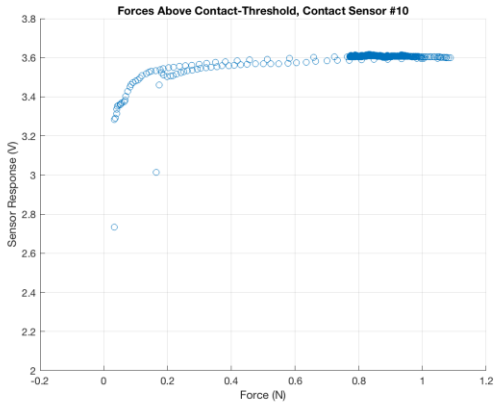
Forces Above Contact-Threshold, Contact Sensor #10
Sensor Response (V)
Force (N)

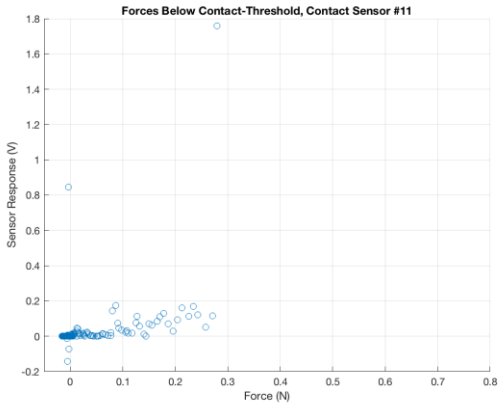
Forces Below Contact-Threshold, Contact Sensor #11
Sensor Response (V)
Force (N)

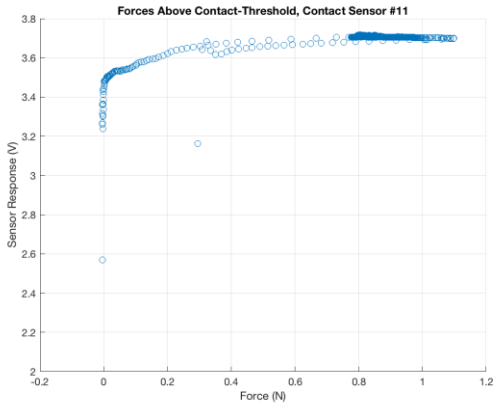
Forces Above Contact-Threshold, Contact Sensor #11
Sensor Response (V)
Force (N)

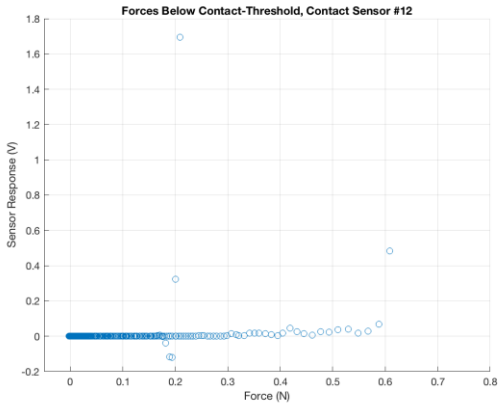
Forces Below Contact-Threshold, Contact Sensor #12
Sensor Response (V)
Force (N)

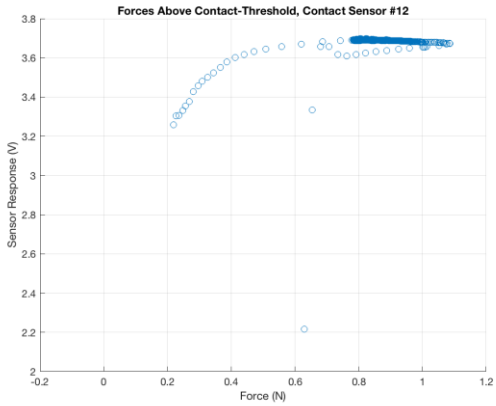
Forces Above Contact-Threshold, Contact Sensor #12
Sensor Response (V)
Force (N)

A.1.2 Force Sensors

A.1.2.1 Cyclic Testing

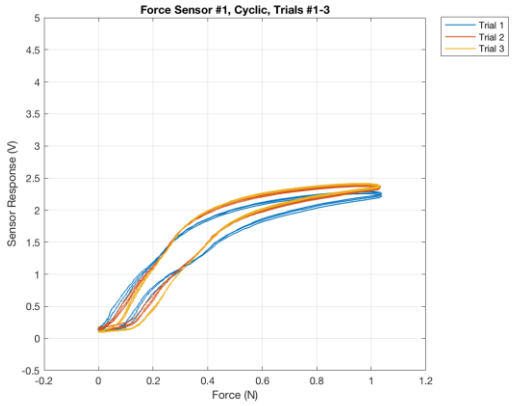

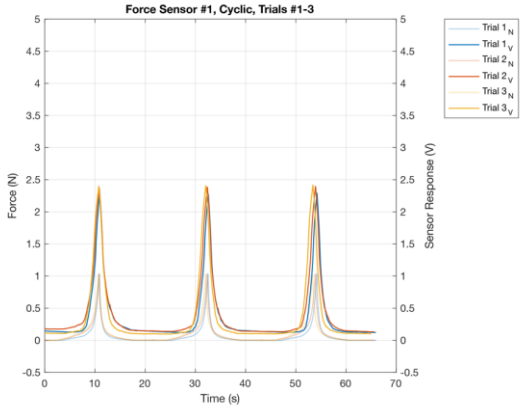

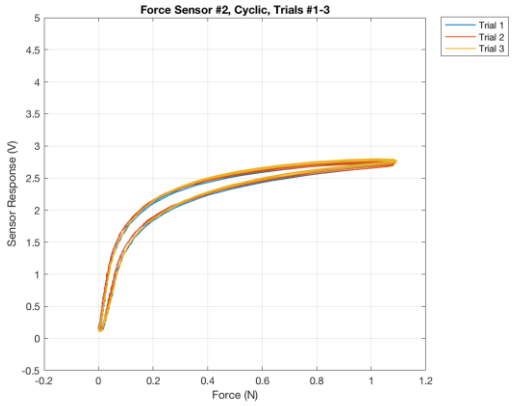

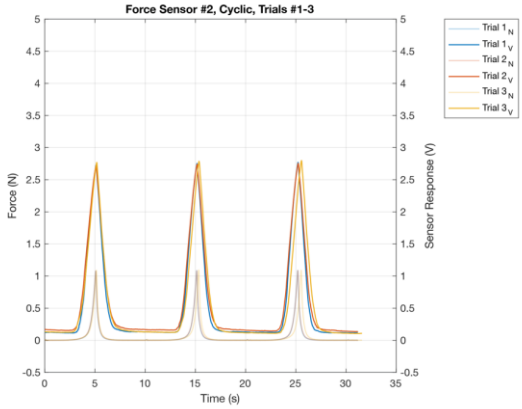

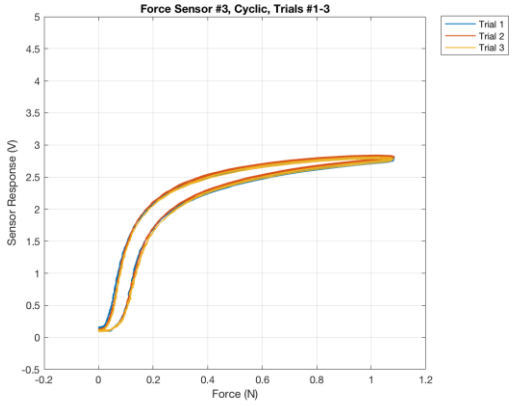

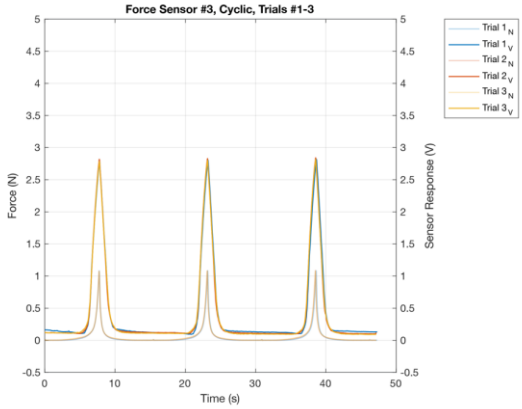

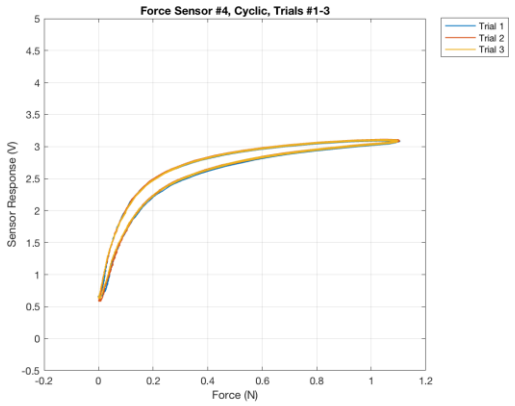
Force Sensor #4, Cyclic, Trials #1-3
Trial 1
Trial 2
Trial 3
Sensor Response (V)
Force (N)

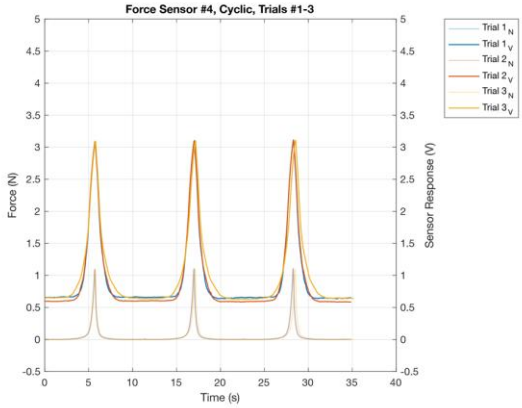
Force Sensor #4, Cyclic, Trials #1-3
Trial 1 N
Trial 1 V
Trial 2 N
Trial 2 V
Trial 3 N
Trial 3 V
Force (N)
Sensor Response (V)
Time (s)

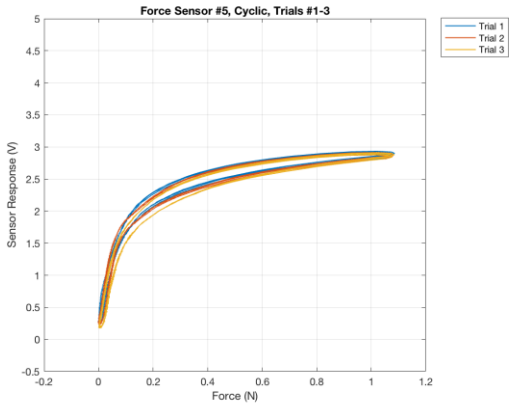
Force Sensor #5, Cyclic, Trials #1-3
Trial 1
Trial 2
Trial 3
Sensor Response (V)
Force (N)

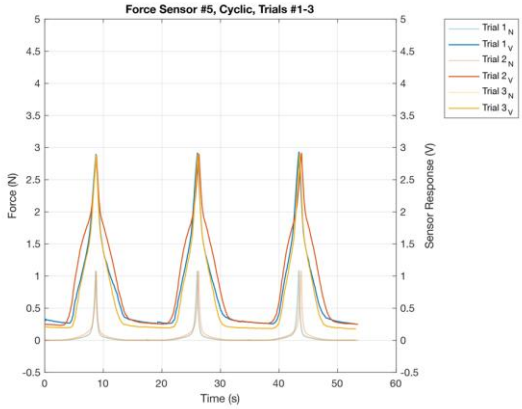
Force Sensor #5, Cyclic, Trials #1-3
Trial 1 N
Trial 1 V
Trial 2 N
Trial 2 V
Trial 3 N
Trial 3 V
Force (N)
Sensor Response (V)
Time (s)

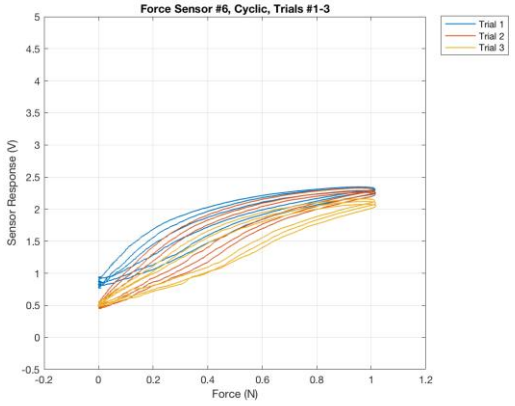
Force Sensor #6, Cyclic, Trials #1-3
Trial 1
Trial 2
Trial 3
Sensor Response (V)
Force (N)

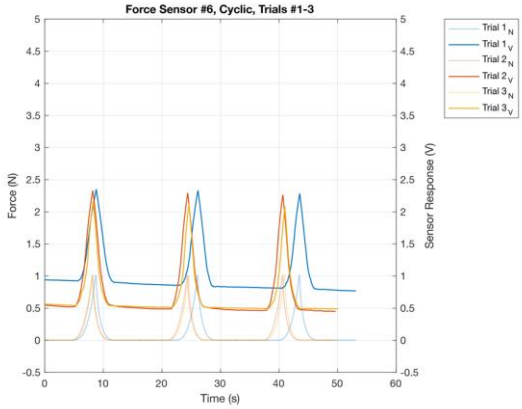
Force Sensor #6, Cyclic, Trials #1-3
Trial 1 N
Trial 1 V
Trial 2 N
Trial 2 V
Trial 3 N
Trial 3 V
Force (N)
Sensor Response (V)
Time (s)

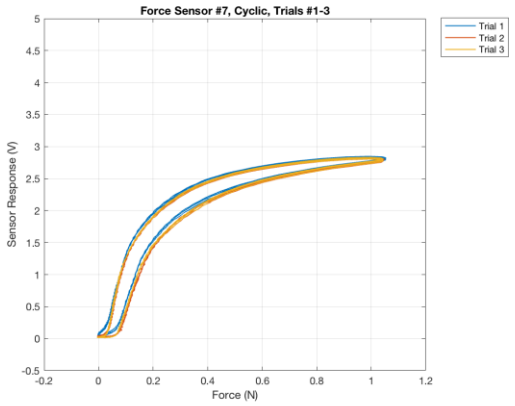
Force Sensor #7, Cyclic, Trials #1-3
Trial 1
Trial 2
Trial 3
Sensor Response (V)
Force (N)

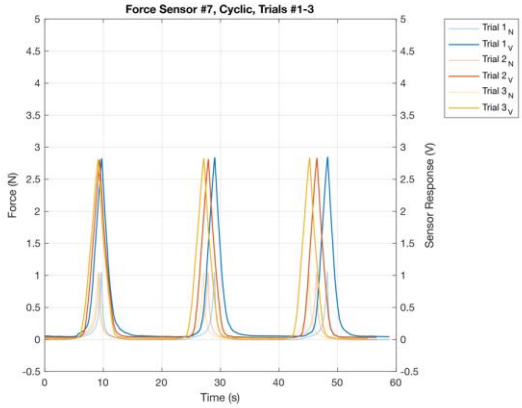
Force Sensor #7, Cyclic, Trials #1-3
Trial 1 N
Trial 1 V
Trial 2 N
Trial 2 V
Trial 3 N
Trial 3 V
Force (N)
Sensor Response (V)
Time (s)

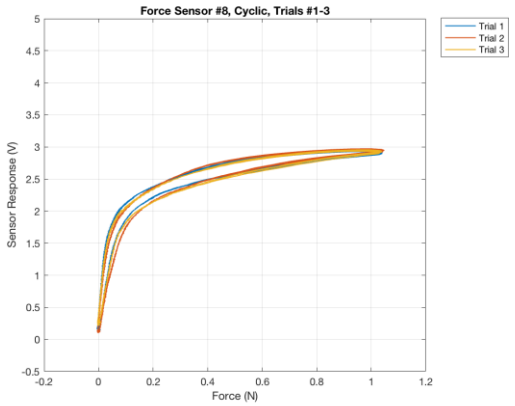
Force Sensor #8, Cyclic, Trials #1-3
Trial 1
Trial 2
Trial 3
Sensor Response (V)
Force (N)

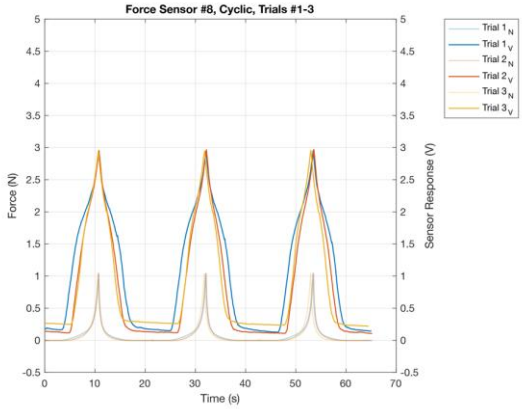
Force Sensor #8, Cyclic, Trials #1-3
Trial 1 N
Trial 1 V
Trial 2 N
Trial 2 V
Trial 3 N
Trial 3 V
Force (N)
Sensor Response (V)
Time (s)

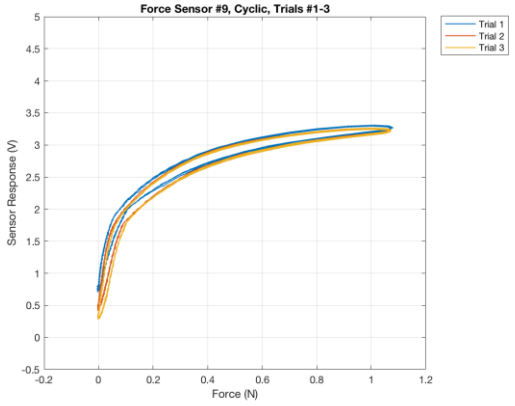
Force Sensor #9, Cyclic, Trials #1-3
Trial 1
Trial 2
Trial 3
Sensor Response (V)
Force (N)

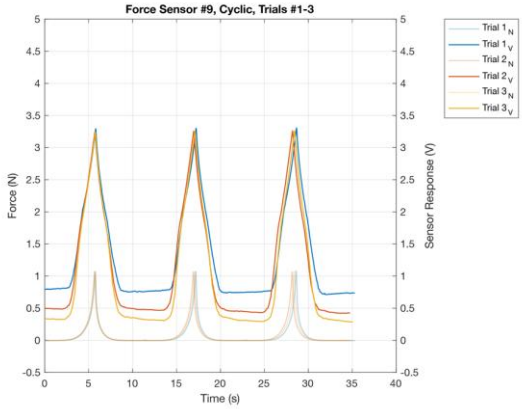
Force Sensor #9, Cyclic, Trials #1-3
Trial 1 N
Trial 1 V
Trial 2 N
Trial 2 V
Trial 3 N
Trial 3 V
Force (N)
Sensor Response (V)
Time (s)

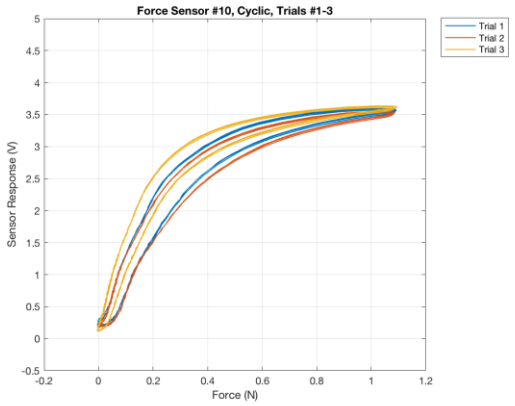
Force Sensor #10, Cyclic, Trials #1-3
Trial 1
Trial 2
Trial 3
Sensor Response (V)
Force (N)

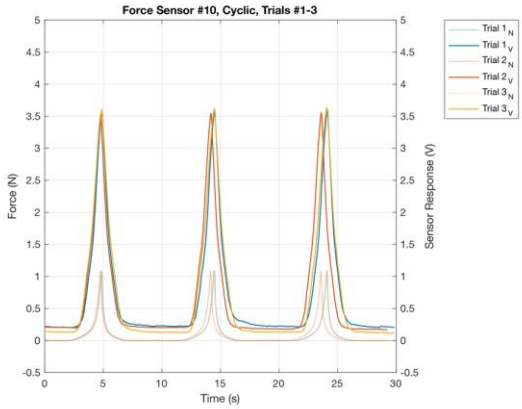
Force Sensor #10, Cyclic, Trials #1-3
Trial 1 N
Trial 1 V
Trial 2 N
Trial 2 V
Trial 3 N
Trial 3 V
Force (N)
Sensor Response (V)
Time (s)

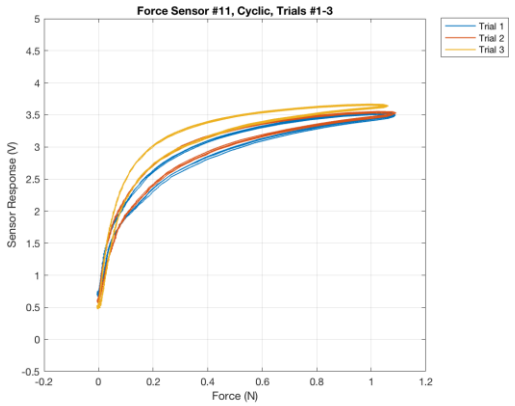
Force Sensor #11, Cyclic, Trials #1-3
Trial 1
Trial 2
Trial 3
Sensor Response (V)
Force (N)

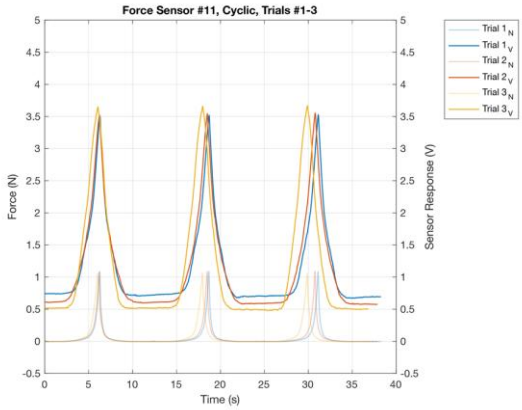
Force Sensor #11, Cyclic, Trials #1-3
Trial 1 N
Trial 1 V
Trial 2 N
Trial 2 V
Trial 3 N
Trial 3 V
Force (N)
Sensor Response (V)
Time (s)

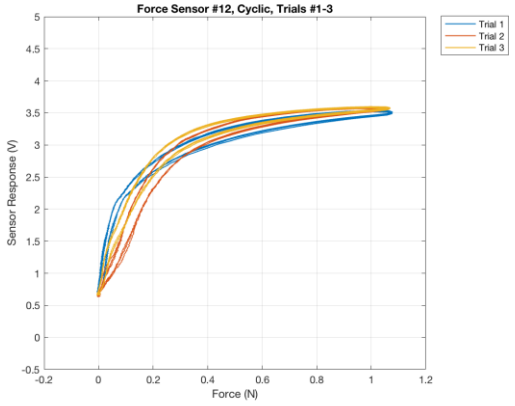
Force Sensor #12, Cyclic, Trials #1-3
Trial 1
Trial 2
Trial 3
Sensor Response (V)
Force (N)

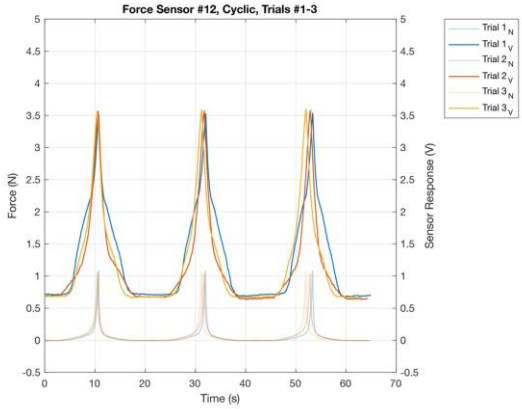
Force Sensor #12, Cyclic, Trials #1-3
Trial 1 N
Trial 1 V
Trial 2 N
Trial 2 V
Trial 3 N
Trial 3 V
Force (N)
Sensor Response (V)
Time (s)

A.1.2.2 Static Testing

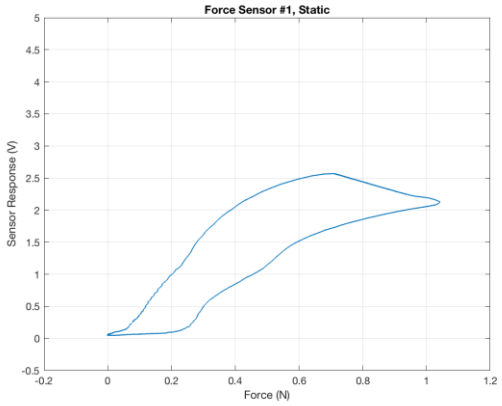

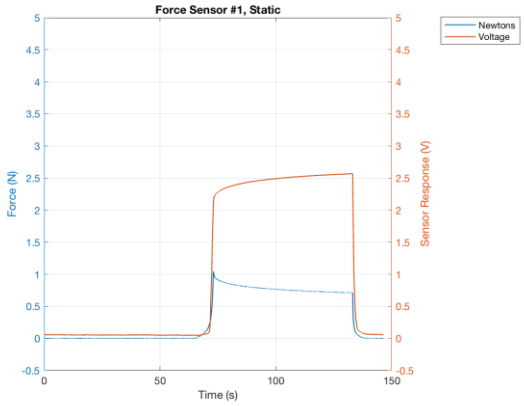

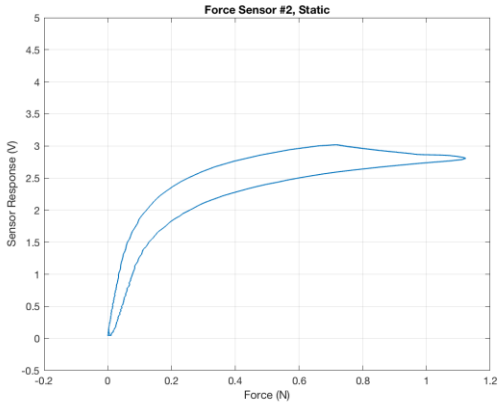

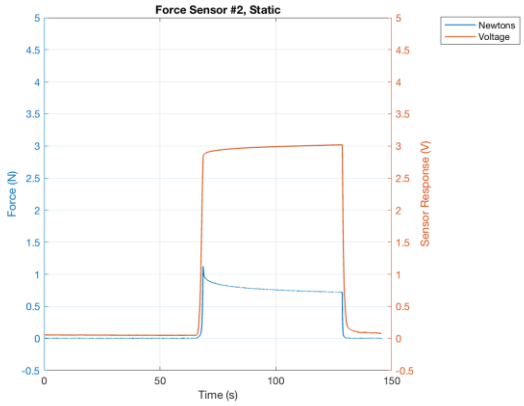

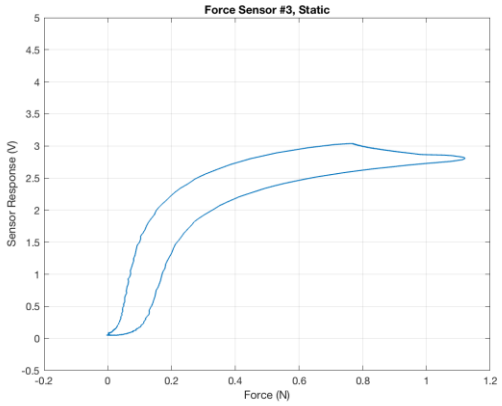

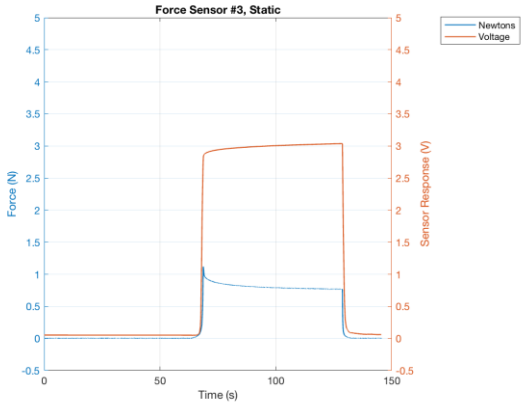

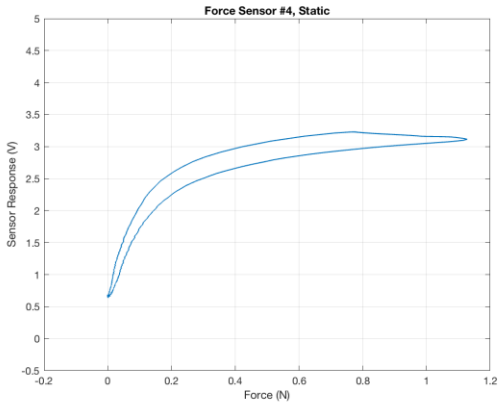
Force Sensor #4, Static
Sensor Response (V)
Force (N)

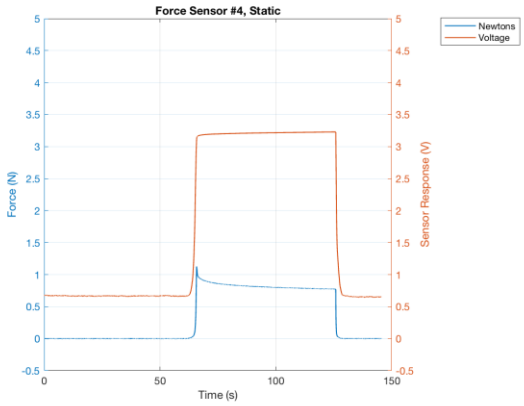
Force Sensor #4, Static
Newtons
Voltage
Force (N)
Sensor Response (V)
Time (s)

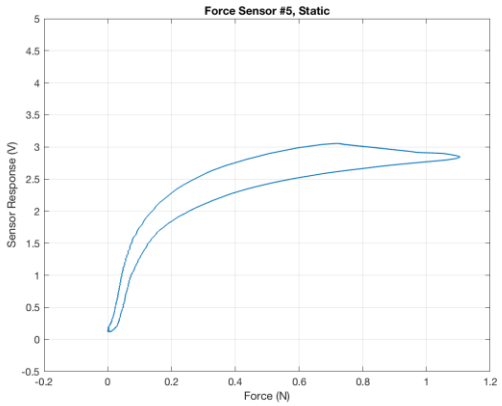
Force Sensor #5, Static
Sensor Response (V)
Force (N)

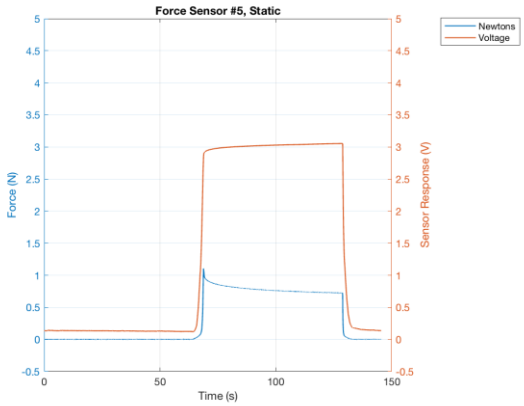
Force Sensor #5, Static
Newtons
Voltage
Force (N)
Sensor Response (V)
Time (s)

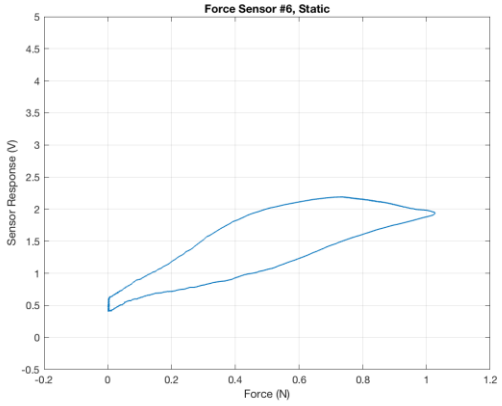
Force Sensor #6, Static
Sensor Response (V)
Force (N)

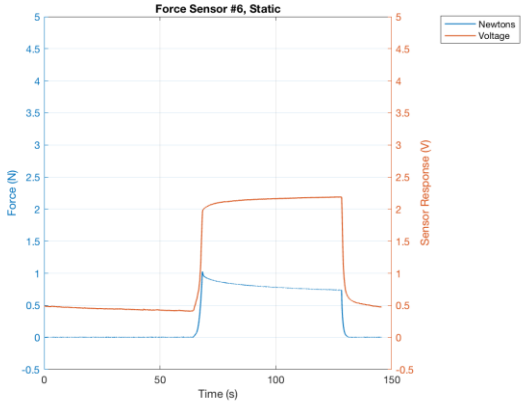
Force Sensor #6, Static
Newtons
Voltage
Force (N)
Sensor Response (V)
Time (s)

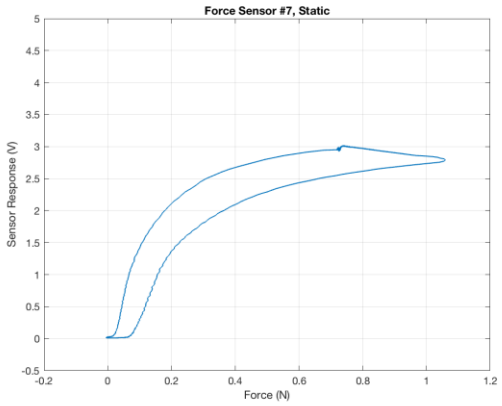
Force Sensor #7, Static
Sensor Response (V)
Force (N)

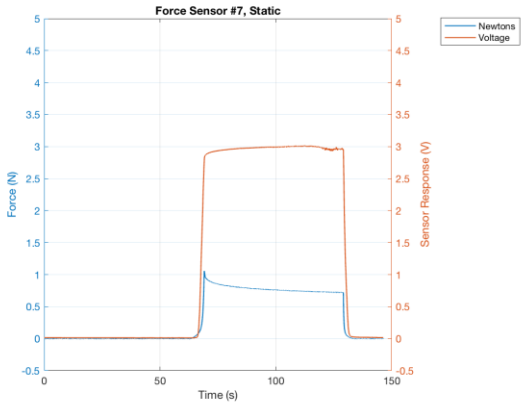
Force Sensor #7, Static
Newtons
Voltage
Force (N)
Sensor Response (V)
Time (s)

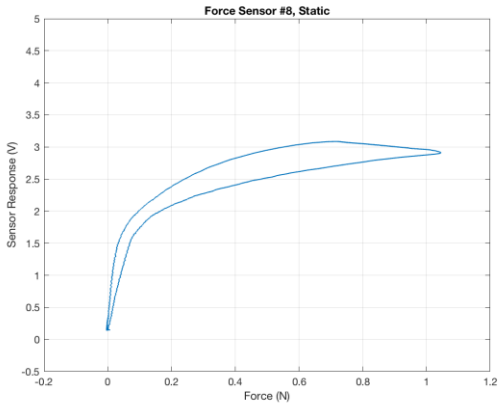
Force Sensor #8, Static
Sensor Response (V)
Force (N)

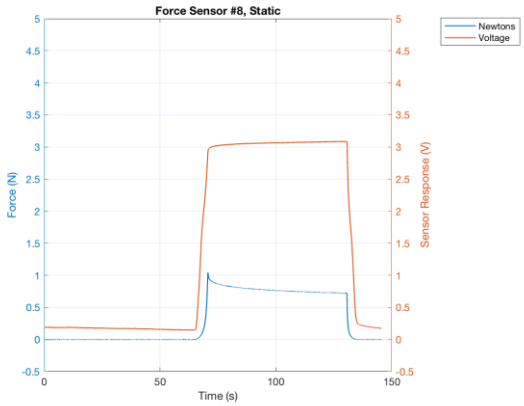
Force Sensor #8, Static
Newtons
Voltage
Force (N)
Sensor Response (V)
Time (s)

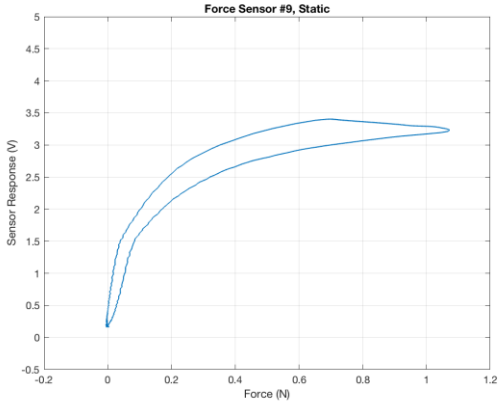
Force Sensor #9, Static
Sensor Response (V)
Force (N)

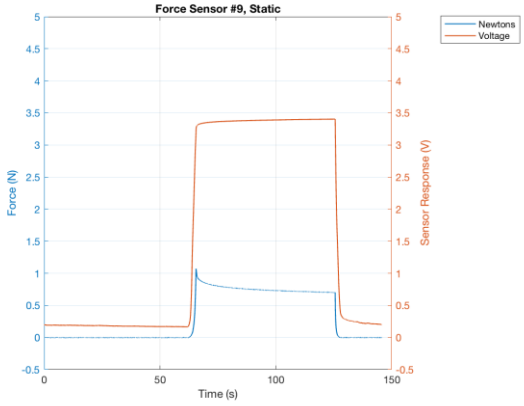
Force Sensor #9, Static
Newtons
Voltage
Force (N)
Sensor Response (V)
Time (s)

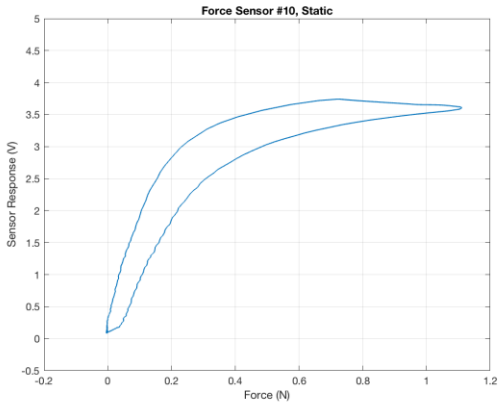
Force Sensor #10, Static
Sensor Response (V)
Force (N)

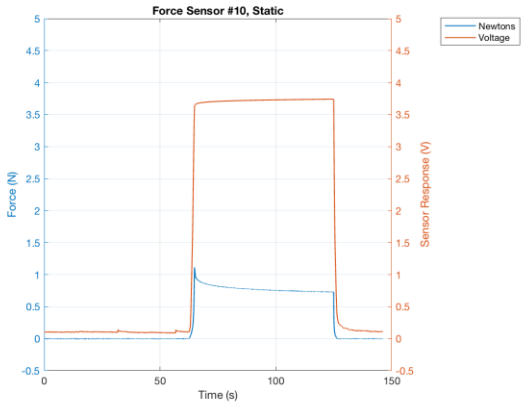
Force Sensor #10, Static
Newtons
Voltage
Force (N)
Sensor Response (V)
Time (s)

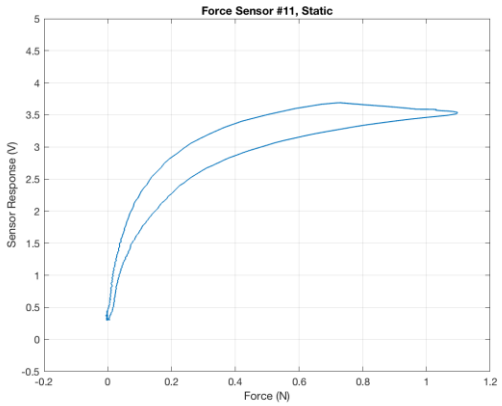
Force Sensor #11, Static
Sensor Response (V)
Force (N)

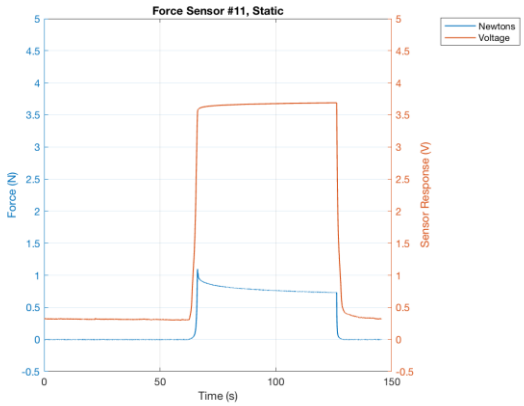
Force Sensor #11, Static
Newtons
Voltage
Force (N)
Sensor Response (V)
Time (s)

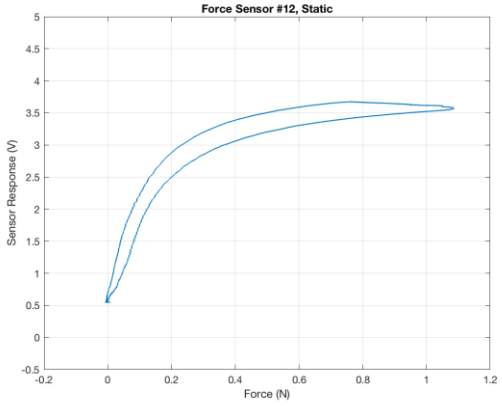
Force Sensor #12, Static
Sensor Response (V)
Force (N)

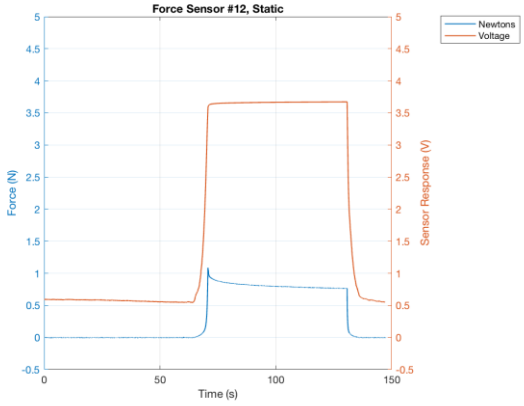
Force Sensor #12, Static
Newtons
Voltage
Force (N)
Sensor Response (V)
Time (s)

A.1.2.3 Forces Below and Above the Contact-Threshold

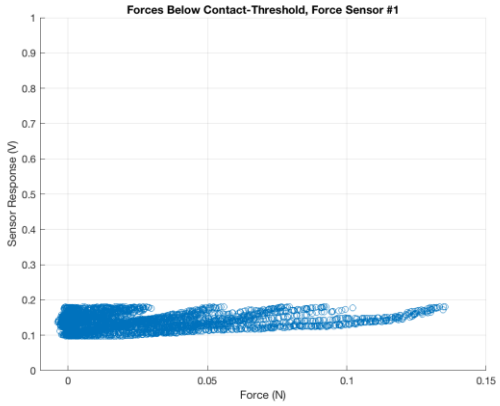

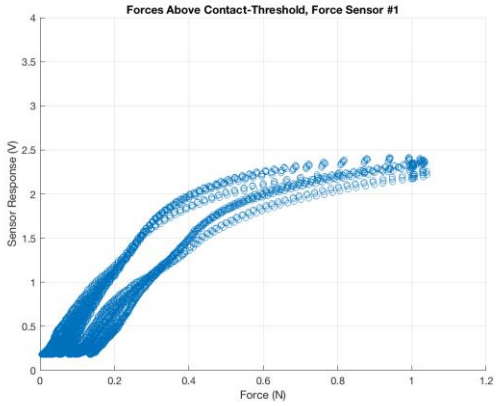

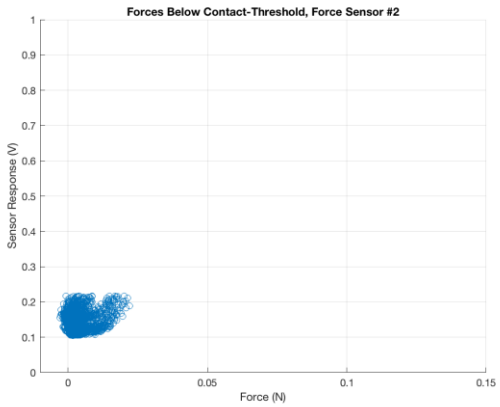

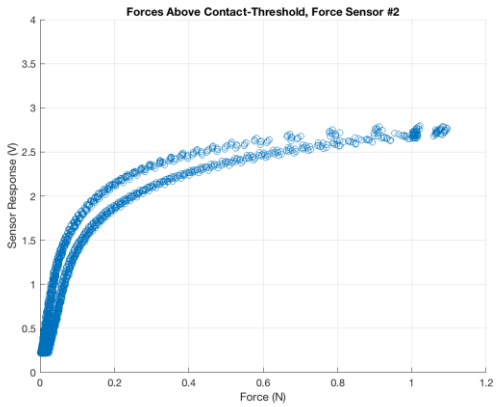

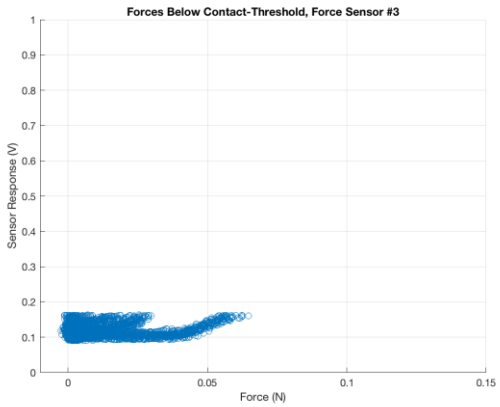

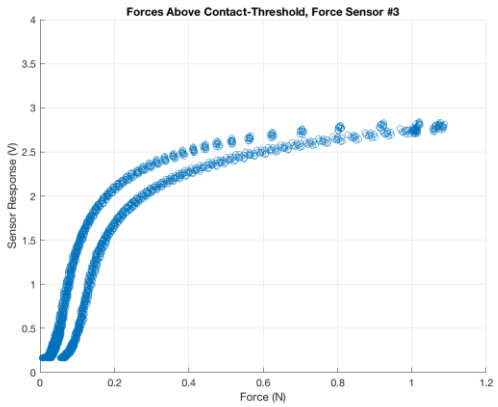

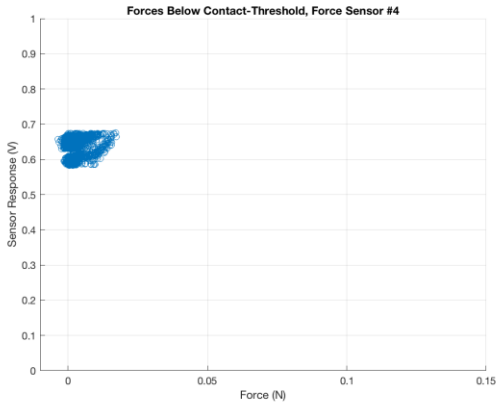
Forces Below Contact-Threshold, Force Sensor #4
Sensor Response (V)
Force (N)

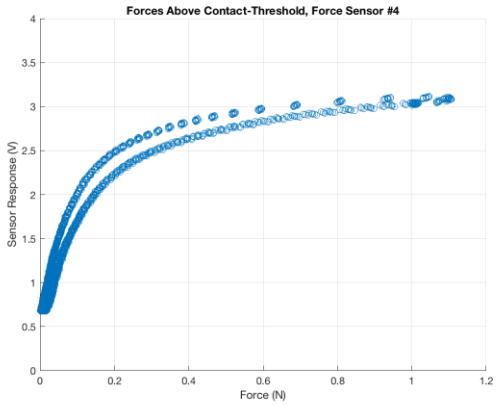
Forces Above Contact-Threshold, Force Sensor #4
Sensor Response (V)
Force (N)

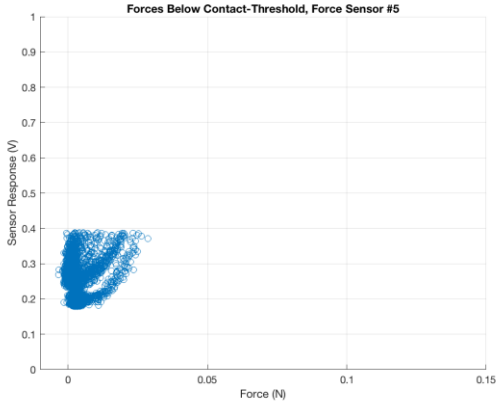
Forces Below Contact-Threshold, Force Sensor #5
Sensor Response (V)
Force (N)

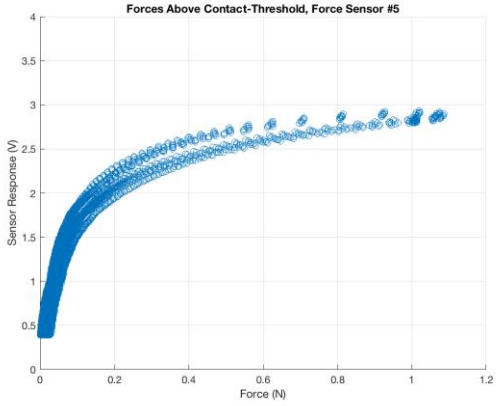
Forces Above Contact-Threshold, Force Sensor #5
Sensor Response (V)
Force (N)

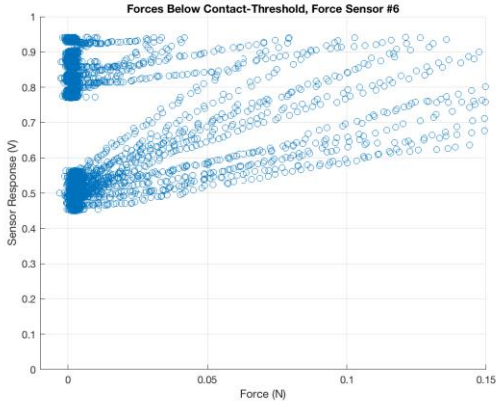
Forces Below Contact-Threshold, Force Sensor #6
Sensor Response (V)
Force (N)

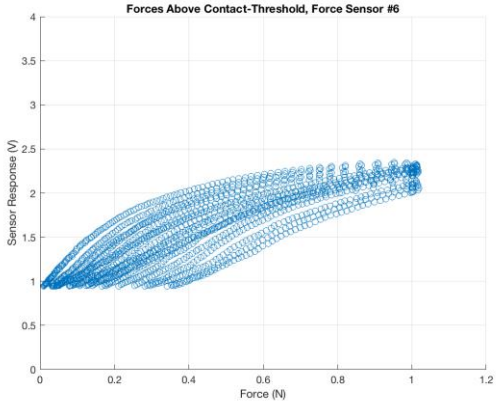
Forces Above Contact-Threshold, Force Sensor #6
Sensor Response (V)
Force (N)

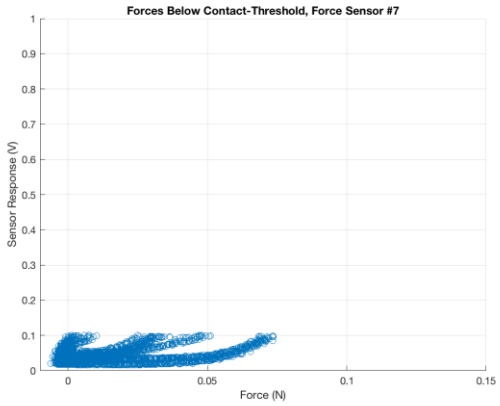
Forces Below Contact-Threshold, Force Sensor #7
Sensor Response (V)
Force (N)

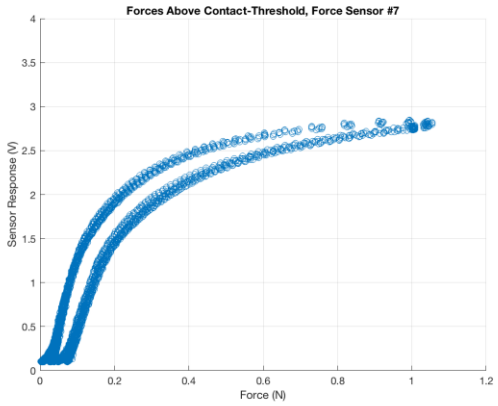
Forces Above Contact-Threshold, Force Sensor #7
Sensor Response (V)
Force (N)

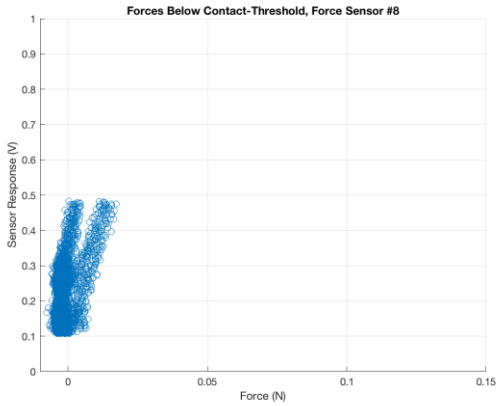
Forces Below Contact-Threshold, Force Sensor #8
Sensor Response (V)
Force (N)

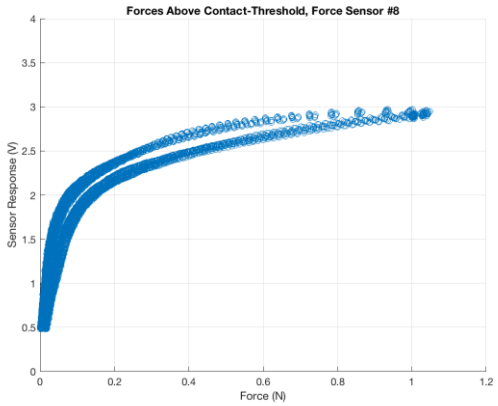
Forces Above Contact-Threshold, Force Sensor #8
Sensor Response (V)
Force (N)

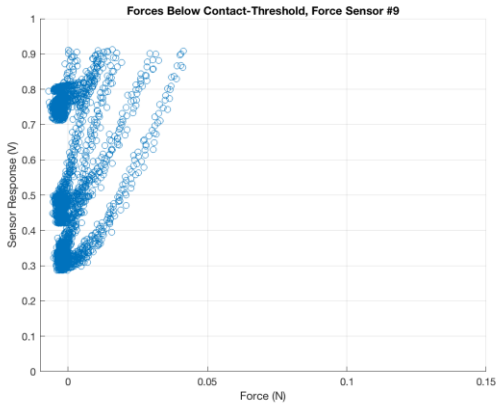
Forces Below Contact-Threshold, Force Sensor #9
Sensor Response (V)
Force (N)

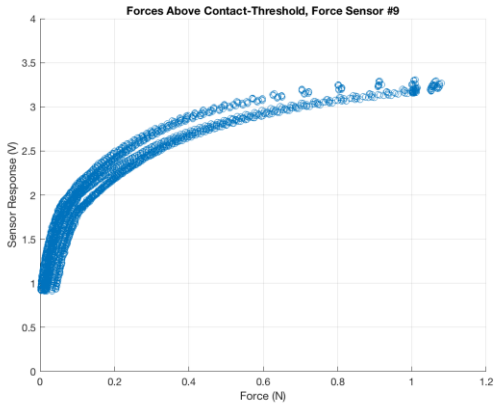
Forces Above Contact-Threshold, Force Sensor #9
Sensor Response (V)
Force (N)

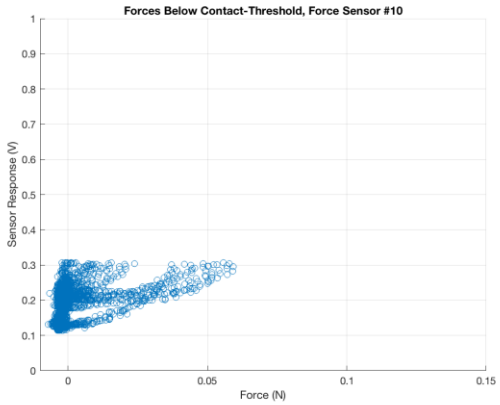
Forces Below Contact-Threshold, Force Sensor #10
Sensor Response (V)
Force (N)

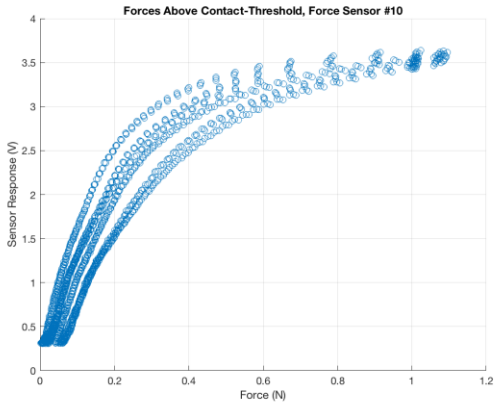
Forces Above Contact-Threshold, Force Sensor #10
Sensor Response (V)
Force (N)

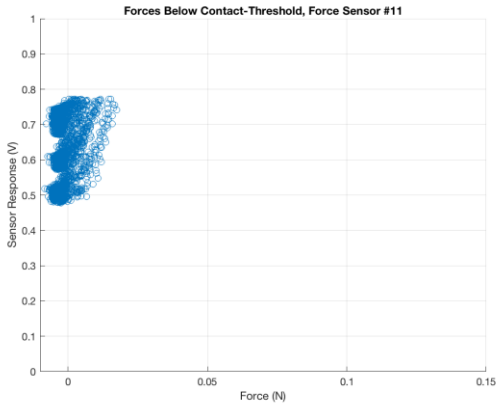
Forces Below Contact-Threshold, Force Sensor #11
Sensor Response (V)
Force (N)

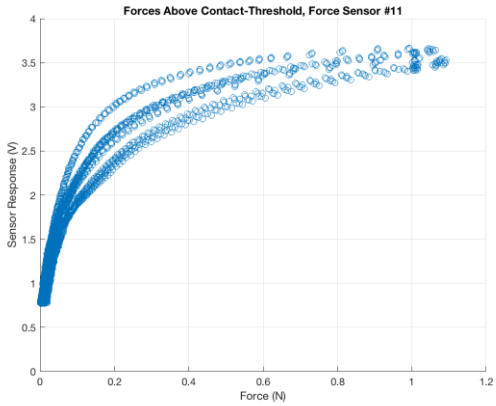
Forces Above Contact-Threshold, Force Sensor #11
Sensor Response (V)
Force (N)

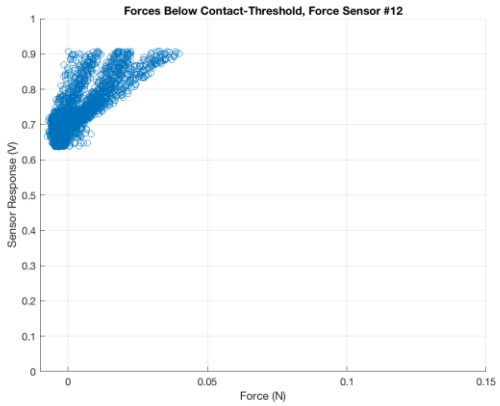
Forces Below Contact-Threshold, Force Sensor #12
Sensor Response (V)
Force (N)

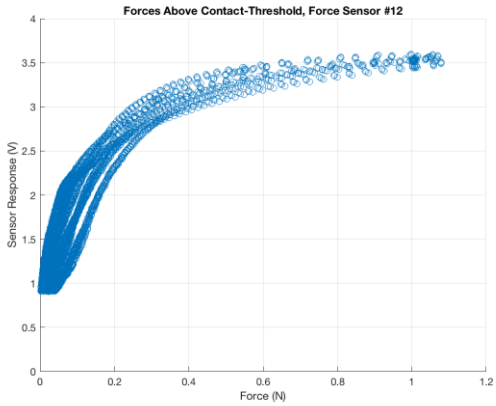
Forces Above Contact-Threshold, Force Sensor #12
Sensor Response (V)
Force (N)

A.2 Manikin Testing

A.2.1 Non-Padded Manikin

A.2.1.1 Contact Sensors

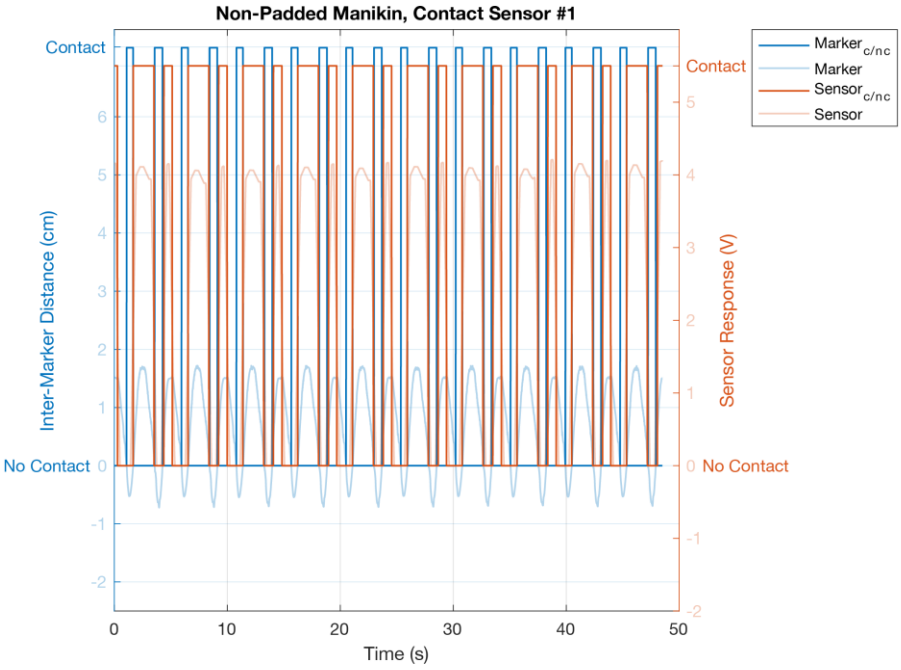

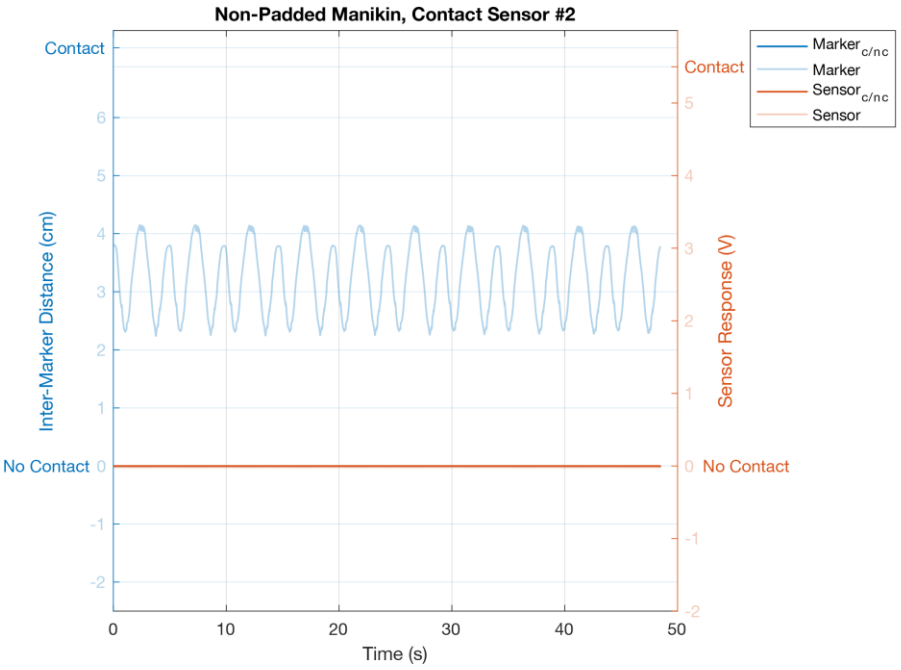

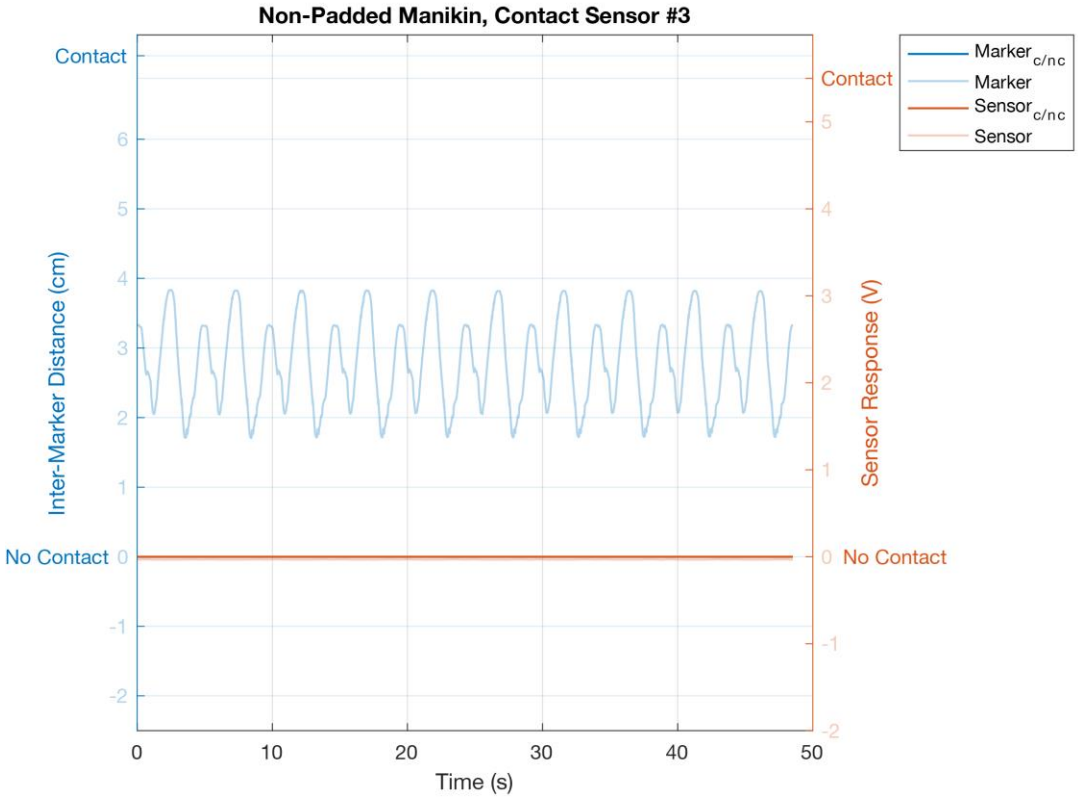
Non-Padded Manikin, Contact Sensor #3
Contact
No Contact
Inter-Marker Distance (cm)
Sensor Response (V)
Time (s)
Marker c/nc
Marker
Sensor c/nc
Sensor

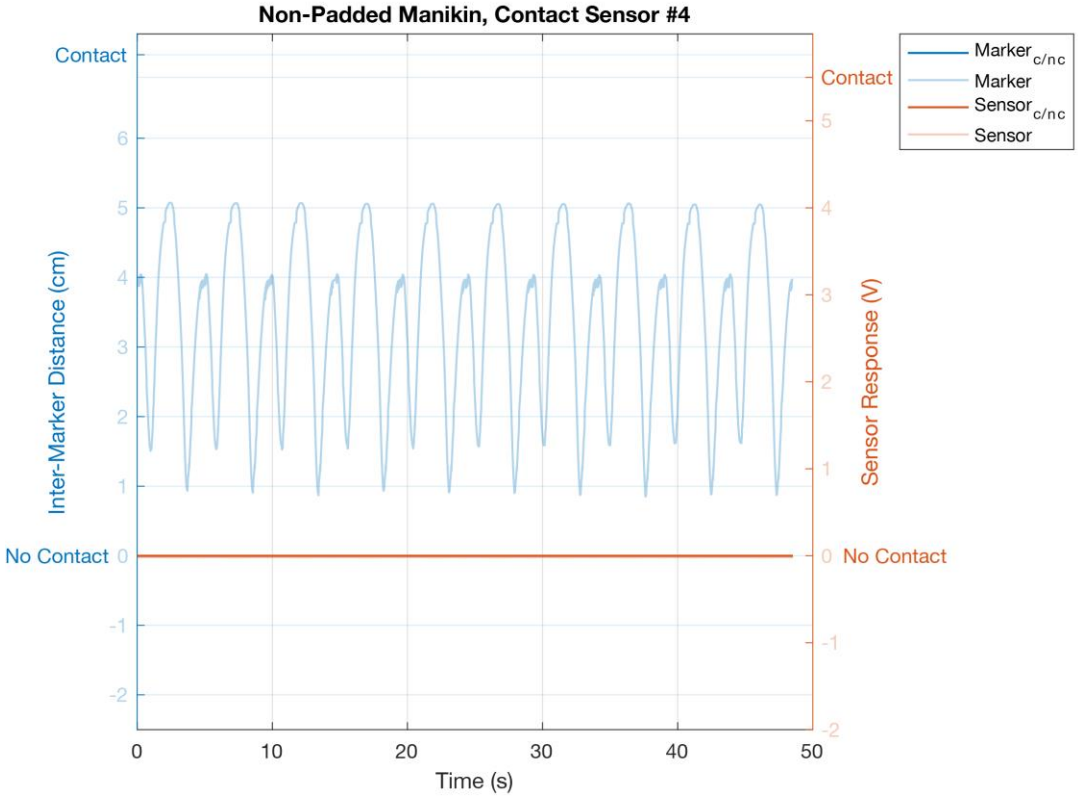
Non-Padded Manikin, Contact Sensor #4
Contact
No Contact
Inter-Marker Distance (cm)
Sensor Response (V)
Time (s)
Marker c/nc
Marker
Sensor c/nc
Sensor

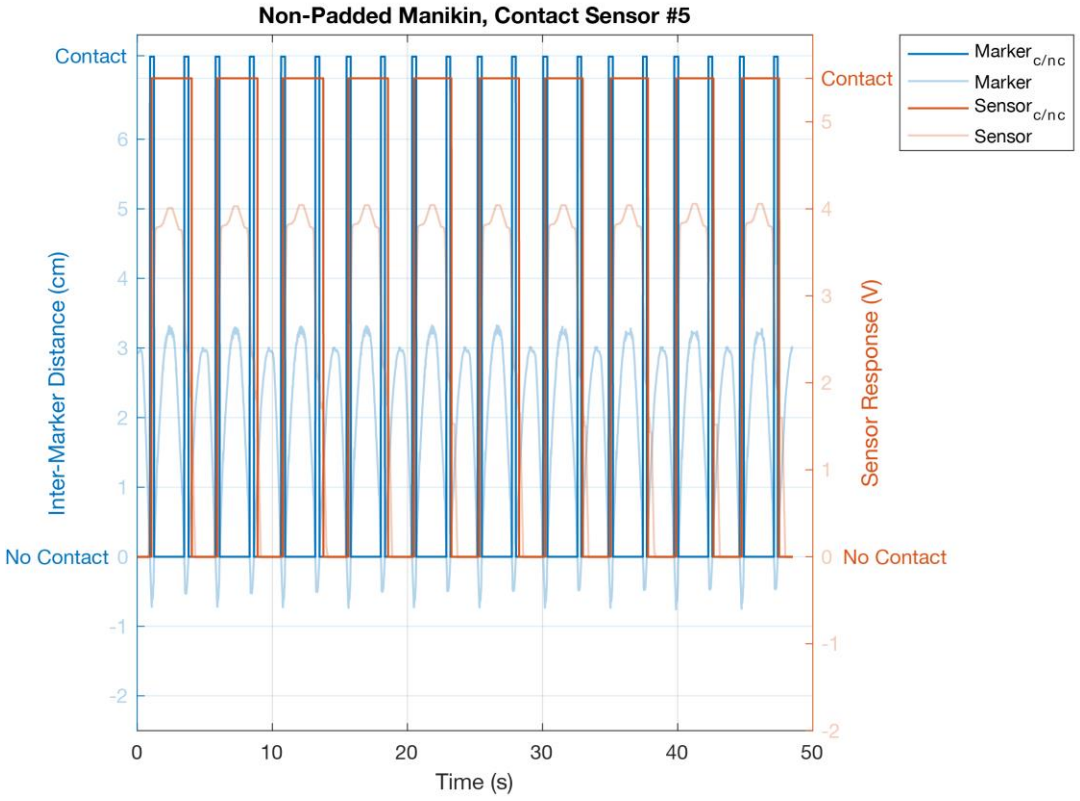
Non-Padded Manikin, Contact Sensor #5
Contact
No Contact
Inter-Marker Distance (cm)
Sensor Response (V)
Contact
No Contact
Marker c/nc
Marker
Sensor c/nc
Sensor
Time (s)
0
10
20
30
40
50

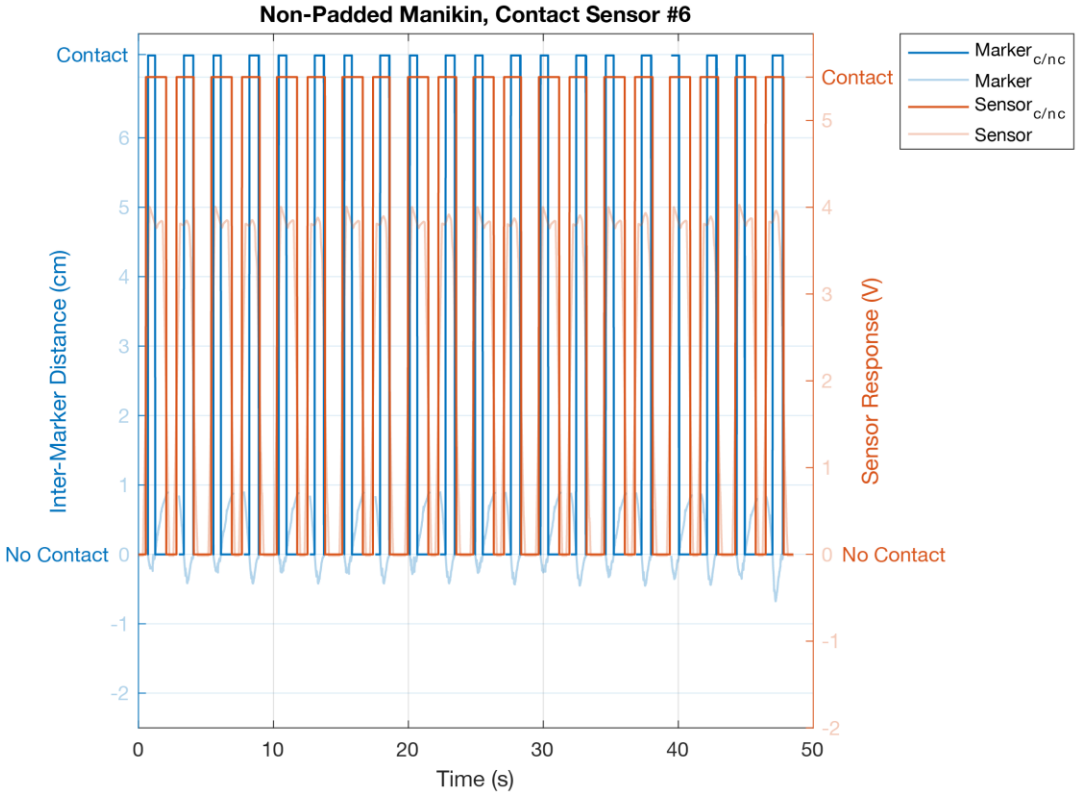
Non-Padded Manikin, Contact Sensor #6
Contact
No Contact
Inter-Marker Distance (cm)
Sensor Response (V)
Contact
No Contact
Marker c/nc
Marker
Sensor c/nc
Sensor
Time (s)
0
10
20
30
40
50

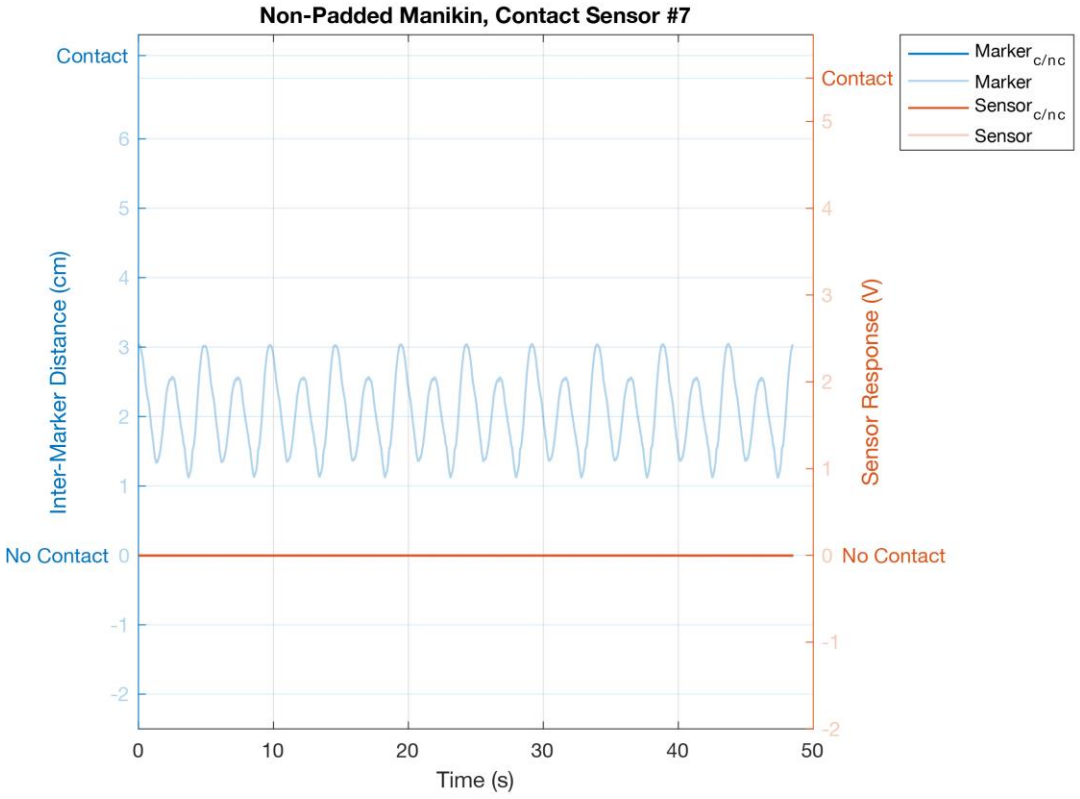
Non-Padded Manikin, Contact Sensor #7
Contact
No Contact
Inter-Marker Distance (cm)
Sensor Response (V)
Time (s)
Marker c/nc
Marker
Sensor c/nc
Sensor

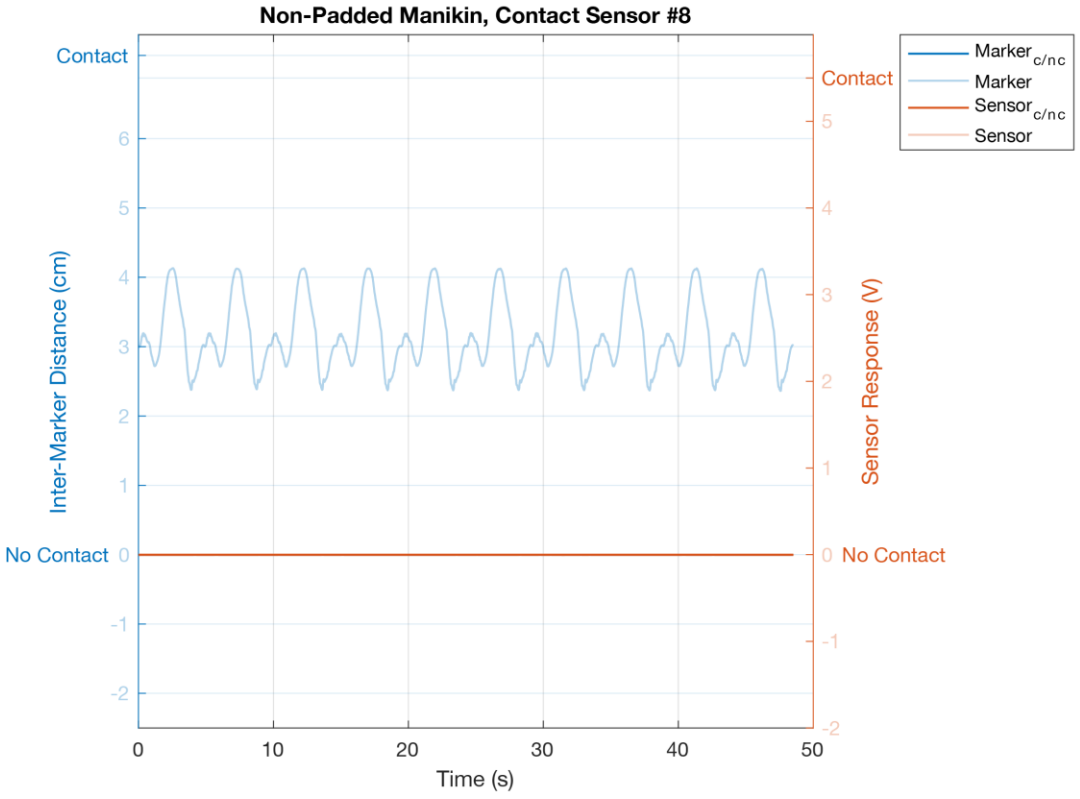
Non-Padded Manikin, Contact Sensor #8
Contact
No Contact
Inter-Marker Distance (cm)
Sensor Response (V)
Time (s)
Marker c/nc
Marker
Sensor c/nc
Sensor

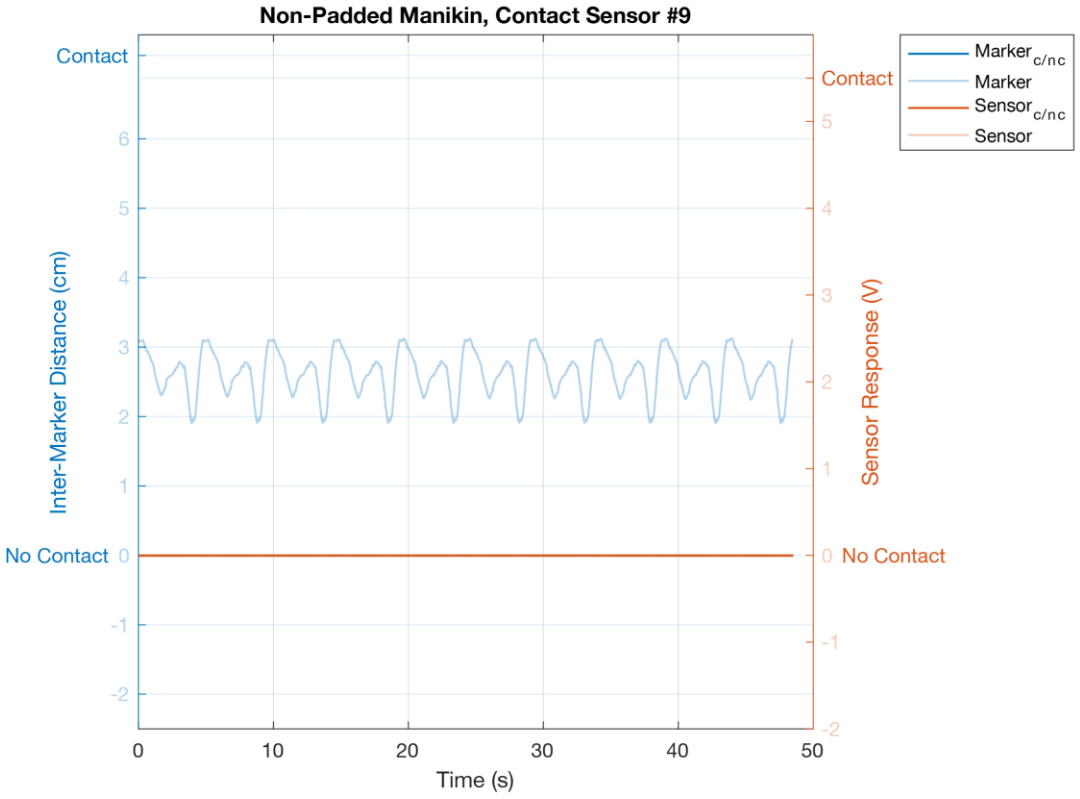
Non-Padded Manikin, Contact Sensor #9
Contact
No Contact
Inter-Marker Distance (cm)
Sensor Response (V)
Time (s)
Marker c/nc
Marker
Sensor c/nc
Sensor

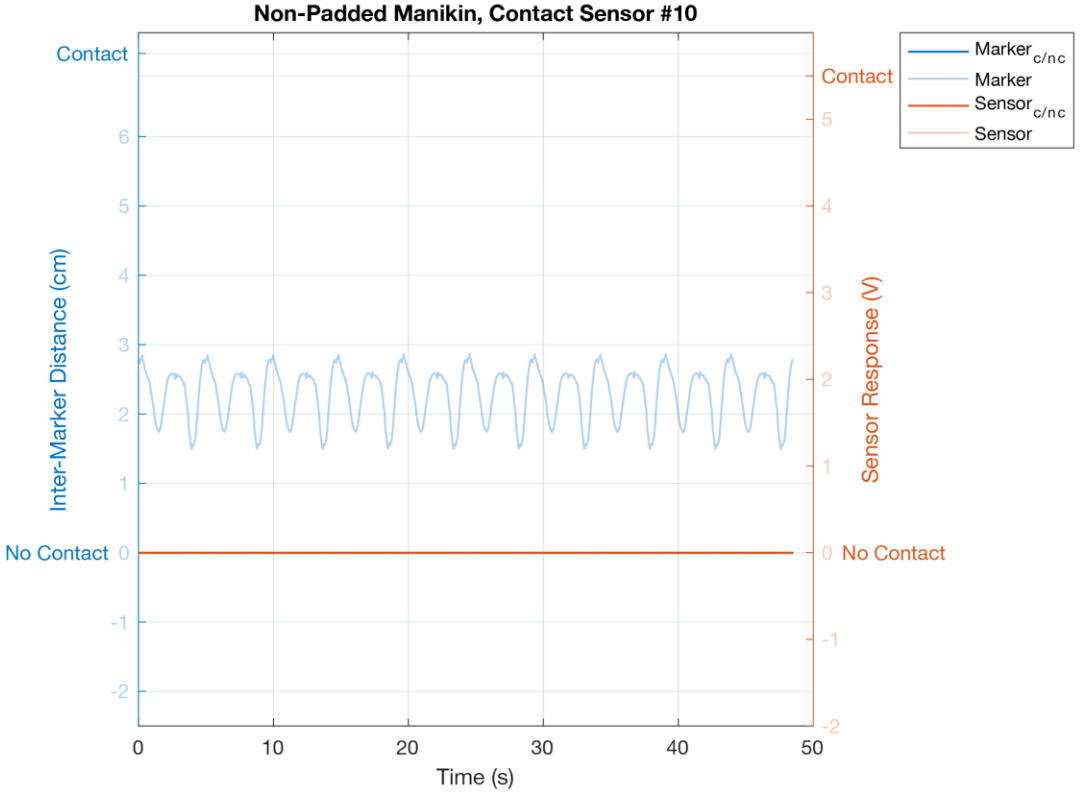
Non-Padded Manikin, Contact Sensor #10
Contact
No Contact
Inter-Marker Distance (cm)
Sensor Response (V)
Time (s)
Marker c/nc
Marker
Sensor c/nc
Sensor

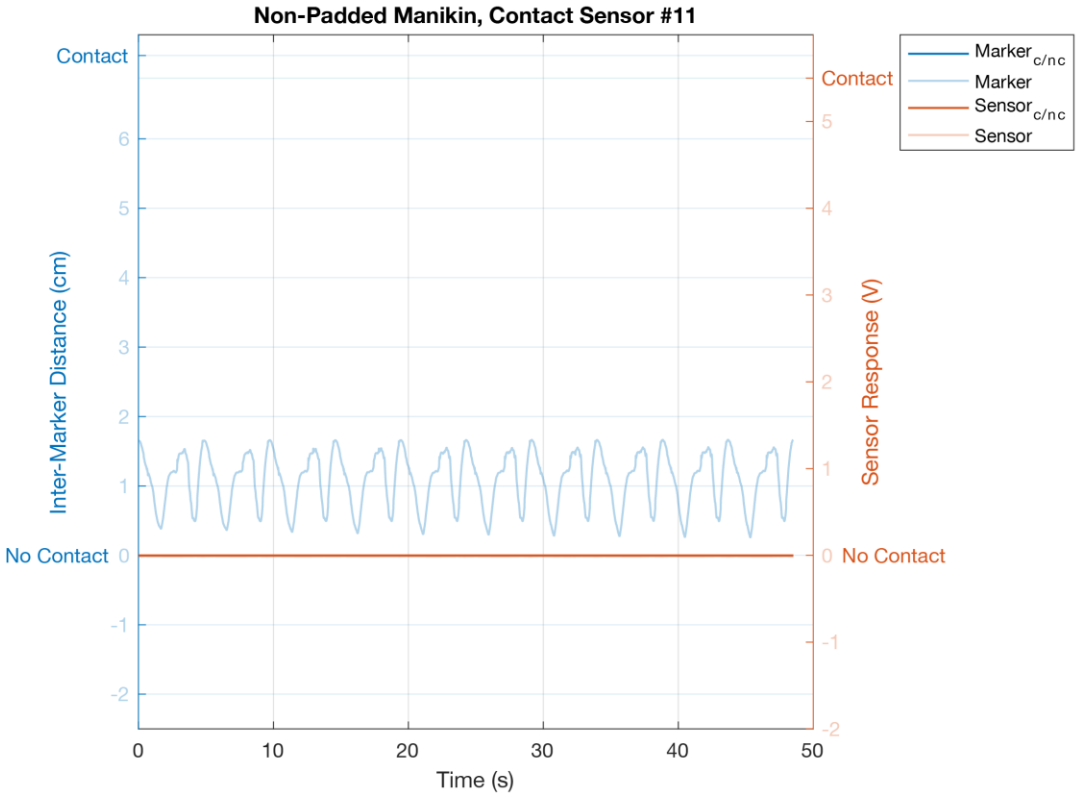
Non-Padded Manikin, Contact Sensor #11
Contact
No Contact
Inter-Marker Distance (cm)
Sensor Response (V)
Contact
No Contact
Marker c/nc
Marker
Sensor c/nc
Sensor
Time (s)

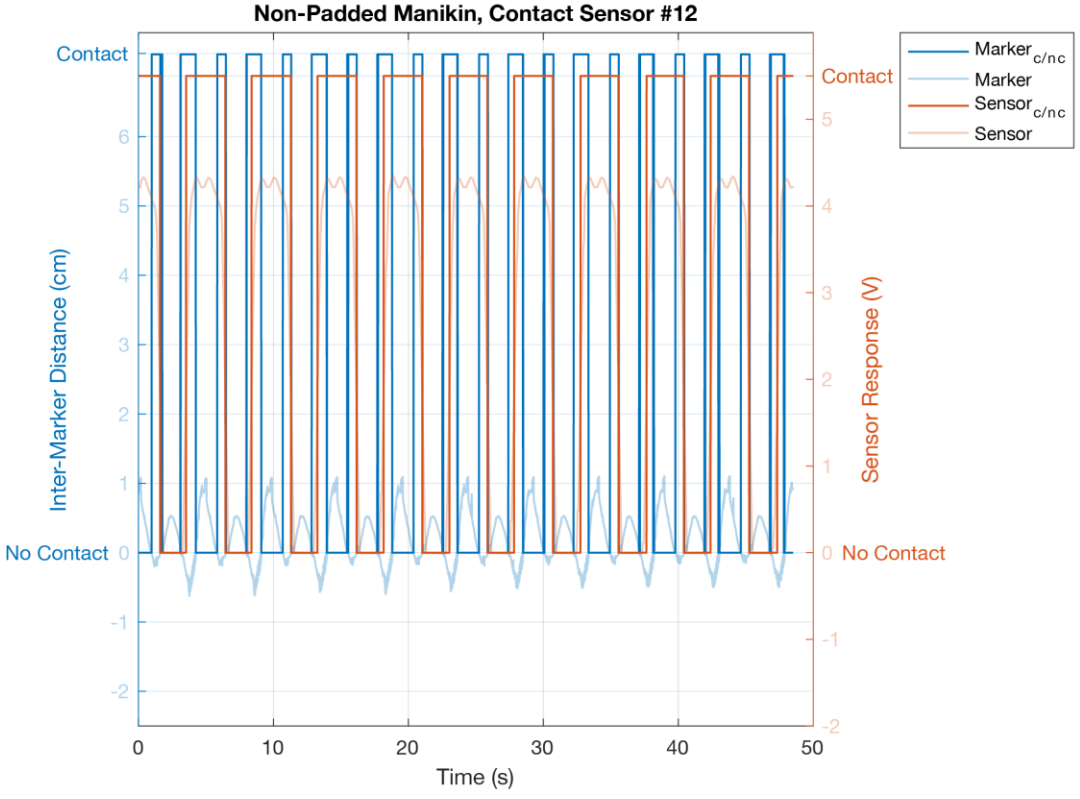
Non-Padded Manikin, Contact Sensor #12
Contact
No Contact
Inter-Marker Distance (cm)
Sensor Response (V)
Contact
No Contact
Marker c/nc
Marker
Sensor c/nc
Sensor
Time (s)

A.2.1.2 Force Sensors (Drift)

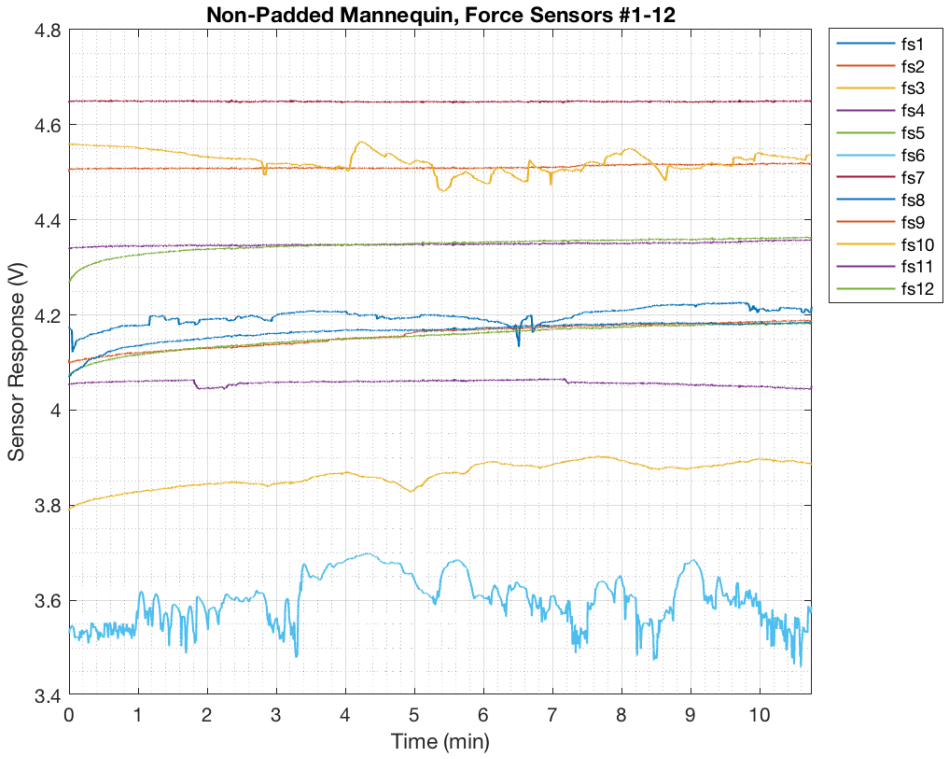

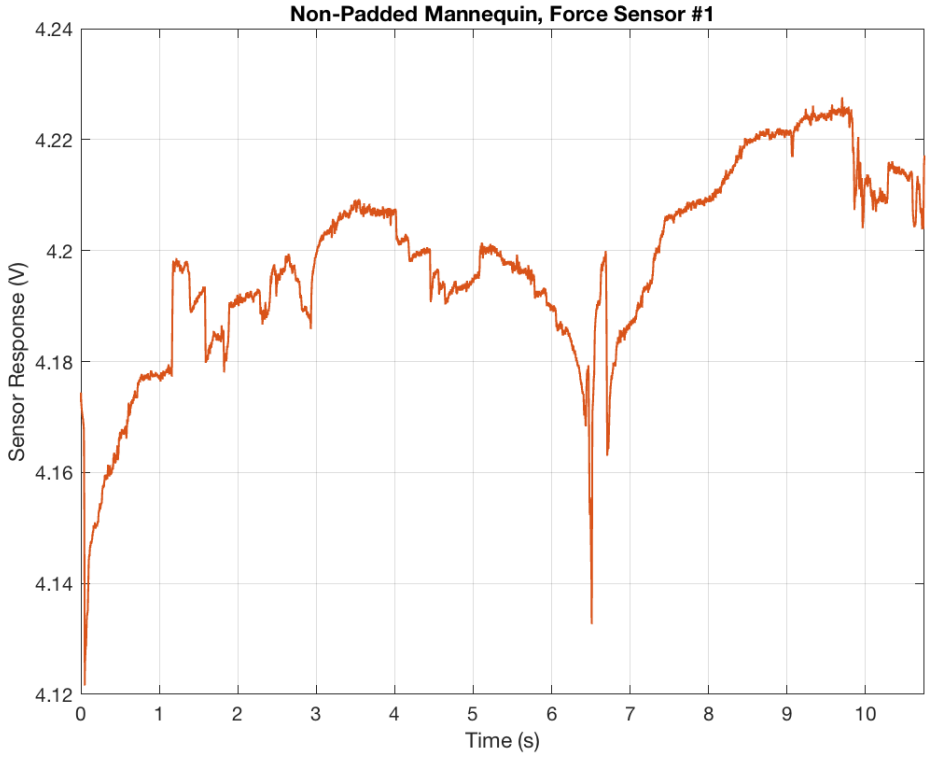

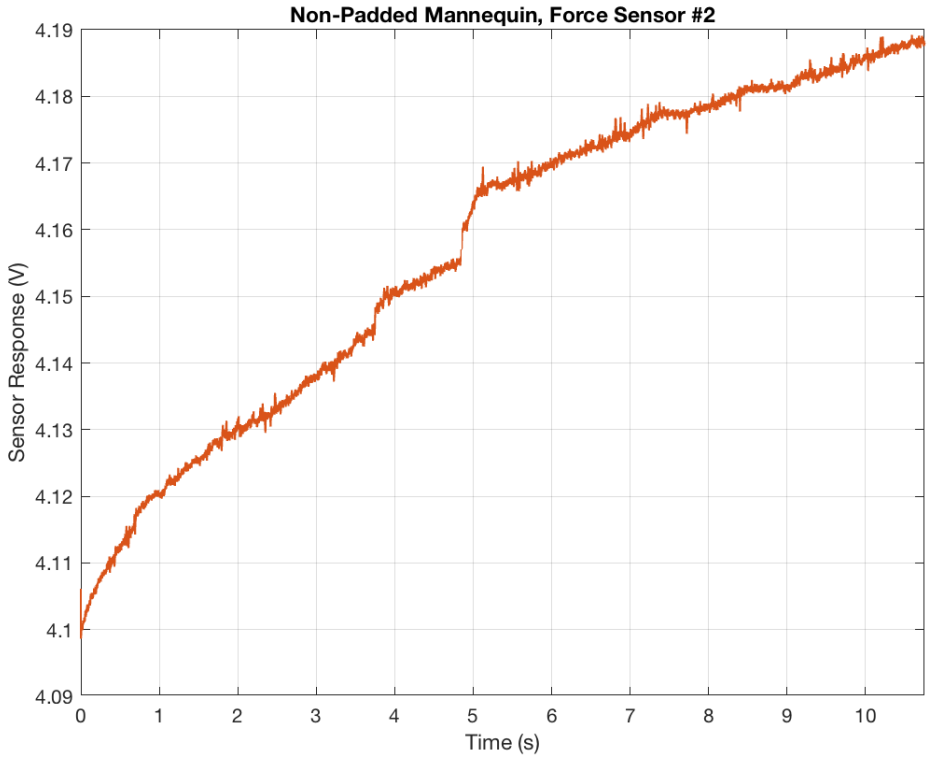
Non-Padded Mannequin, Force Sensor #2
Sensor Response (V)
Time (s)
4.19
4.18
4.17
4.16
4.15
4.14
4.13
4.12
4.11
4.1
4.09
0
1
2
3
4
5
6
7
8
9
10

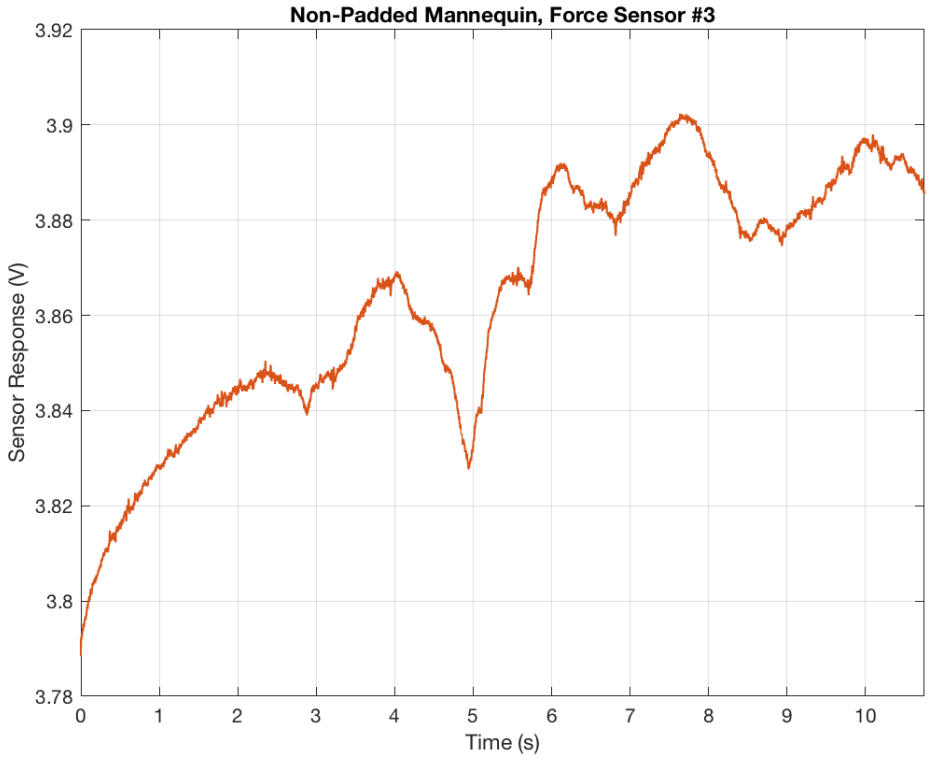
Non-Padded Mannequin, Force Sensor #3
Sensor Response (V)
Time (s)
3.92
3.9
3.88
3.86
3.84
3.82
3.8
3.78
0
1
2
3
4
5
6
7
8
9
10


Non-Padded Mannequin, Force Sensor #4
Sensor Response (V)
Time (s)
4.07
4.065
4.06
4.055
4.05
4.045
4.04
0
1
2
3
4
5
6
7
8
9
10

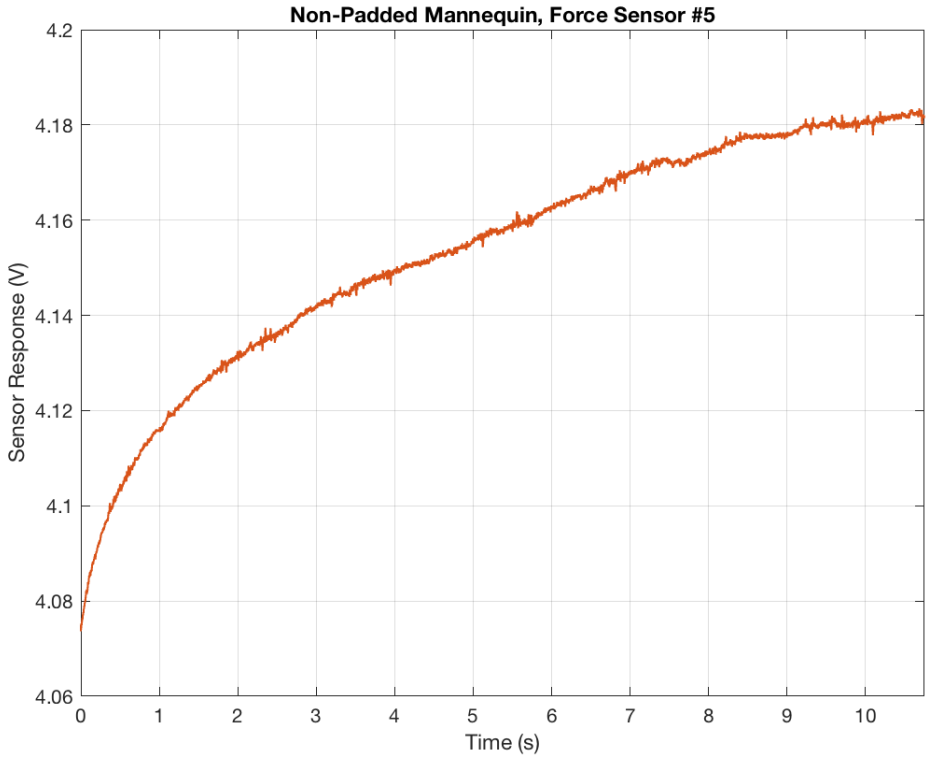
Non-Padded Mannequin, Force Sensor #5
Sensor Response (V)
Time (s)
4.2
4.18
4.16
4.14
4.12
4.1
4.08
4.06
0
1
2
3
4
5
6
7
8
9
10

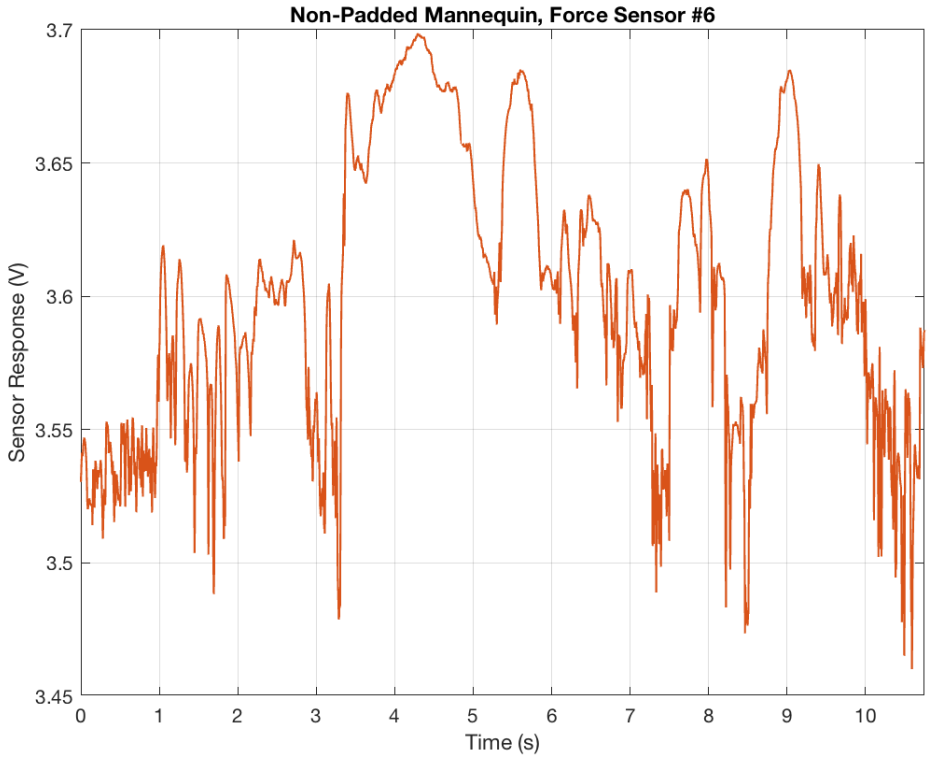
Non-Padded Mannequin, Force Sensor #6
Sensor Response (V)
Time (s)
3.7
3.65
3.6
3.55
3.5
3.45
0
1
2
3
4
5
6
7
8
9
10

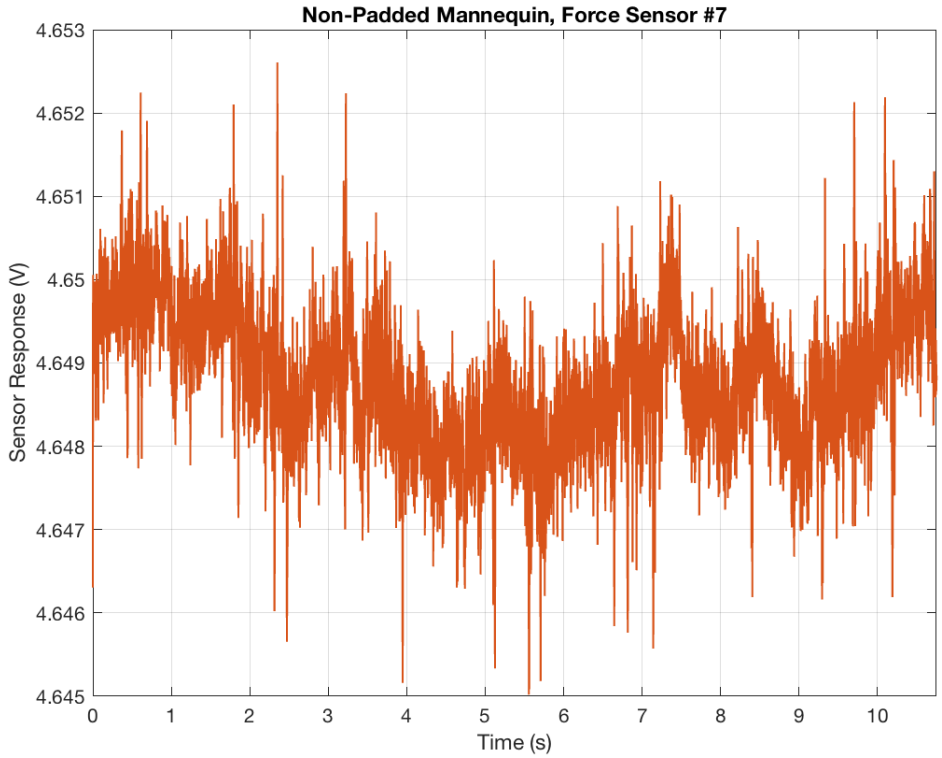
Non-Padded Mannequin, Force Sensor #7
Sensor Response (V)
Time (s)
4.653
4.652
4.651
4.65
4.649
4.648
4.647
4.646
4.645
0
1
2
3
4
5
6
7
8
9
10

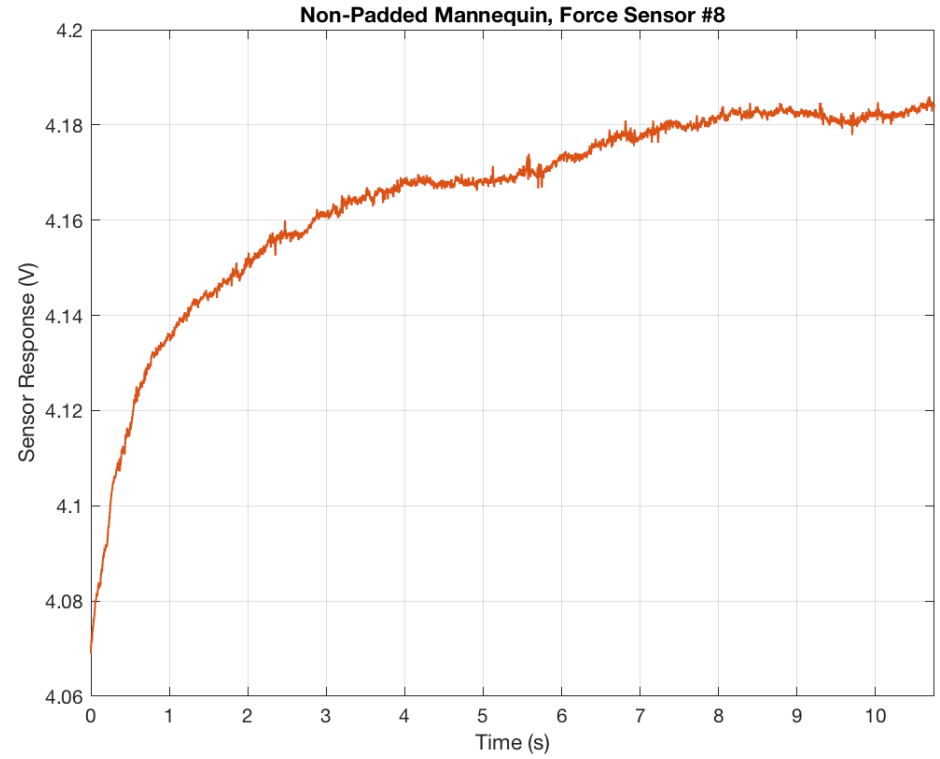
Non-Padded Mannequin, Force Sensor #8
Sensor Response (V)
Time (s)
4.2
4.18
4.16
4.14
4.12
4.1
4.08
4.06
0
1
2
3
4
5
6
7
8
9
10

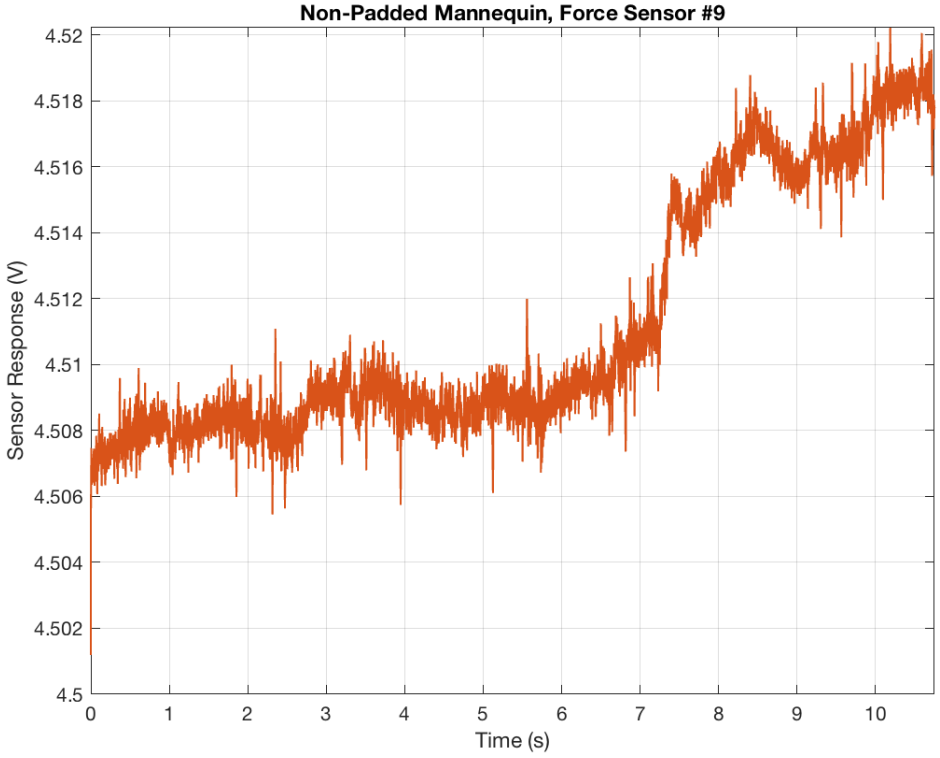
Non-Padded Mannequin, Force Sensor #9
Sensor Response (V)
Time (s)
4.52
4.518
4.516
4.514
4.512
4.51
4.508
4.506
4.504
4.502
4.5
0
1
2
3
4
5
6
7
8
9
10

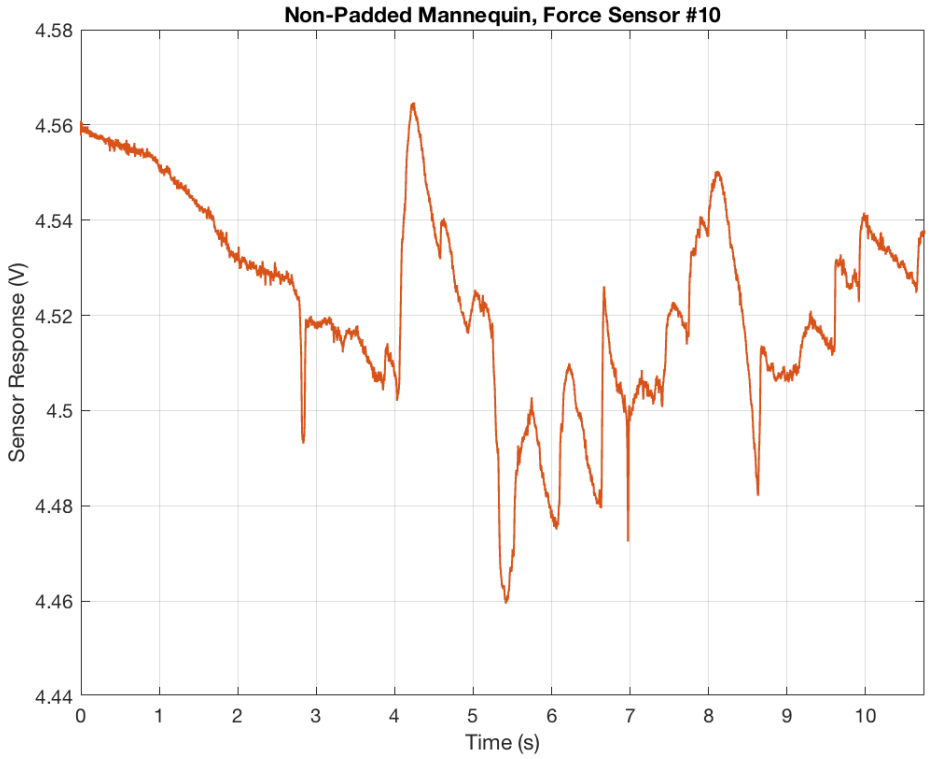
Non-Padded Mannequin, Force Sensor #10
Sensor Response (V)
Time (s)
4.58
4.56
4.54
4.52
4.5
4.48
4.46
4.44
0
1
2
3
4
5
6
7
8
9
10

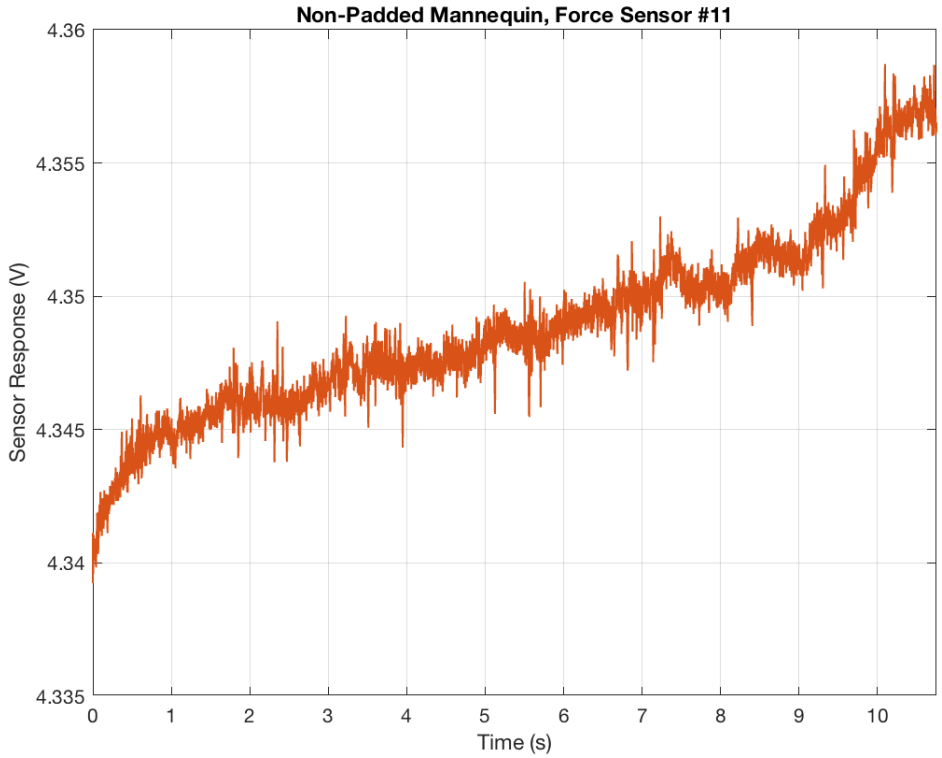
Non-Padded Mannequin, Force Sensor #11
Sensor Response (V)
Time (s)
4.36
4.355
4.35
4.345
4.34
4.335
0
1
2
3
4
5
6
7
8
9
10

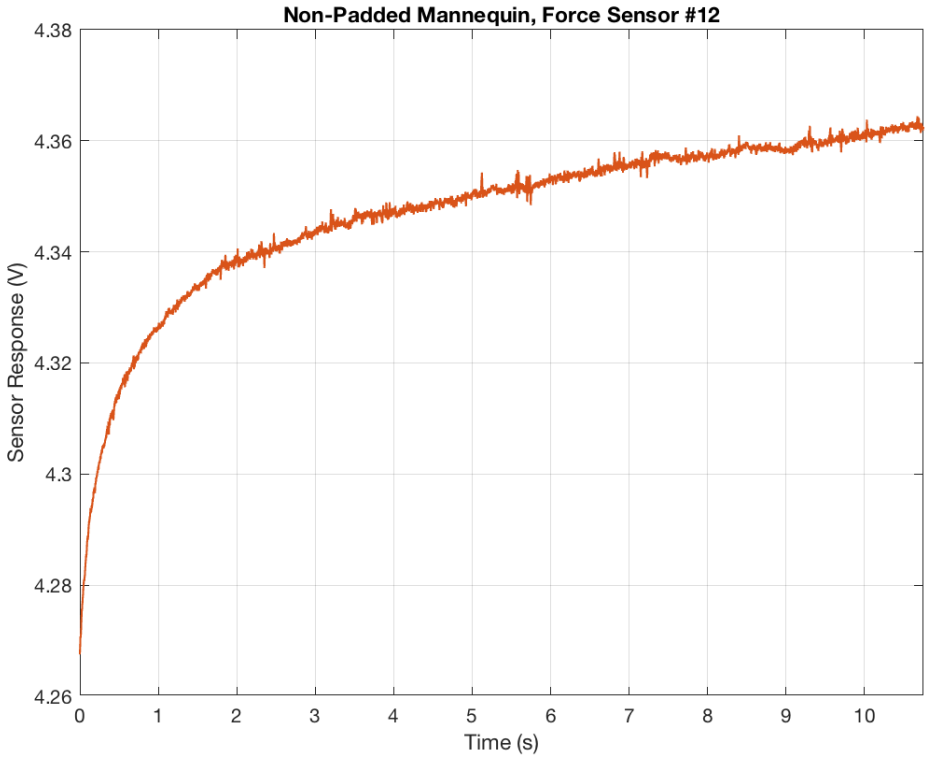
Non-Padded Mannequin, Force Sensor #12
Sensor Response (V)
Time (s)
4.38
4.36
4.34
4.32
4.3
4.28
4.26
0
1
2
3
4
5
6
7
8
9
10

A.2.1.3 Force Sensors

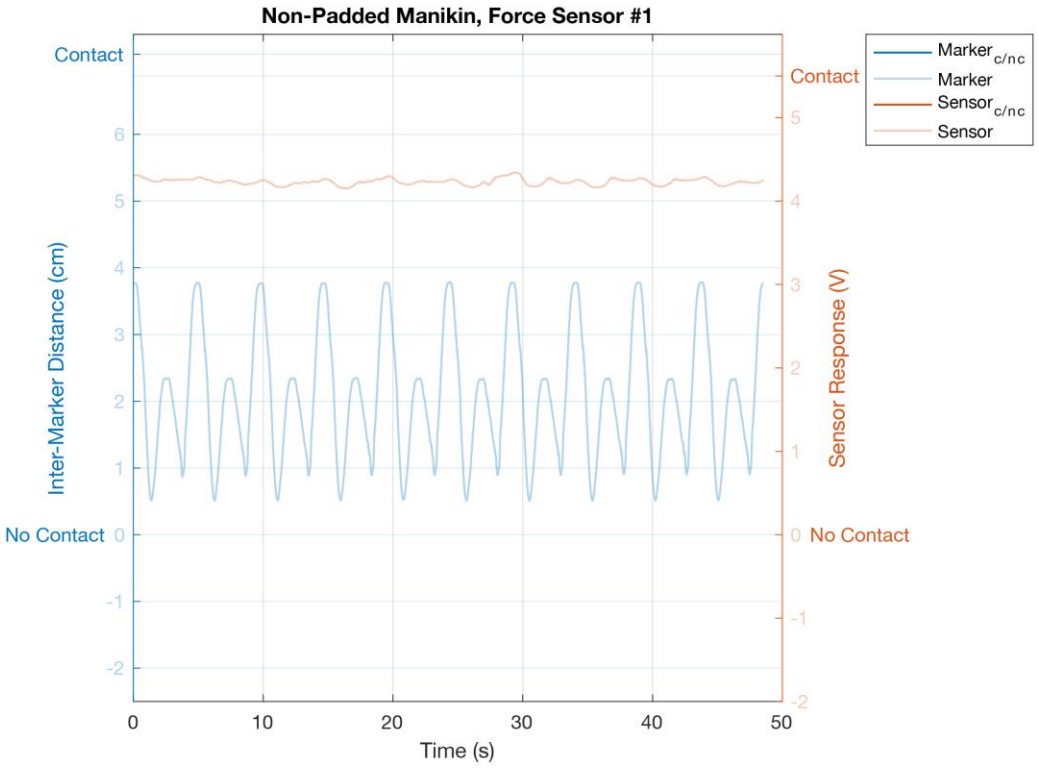

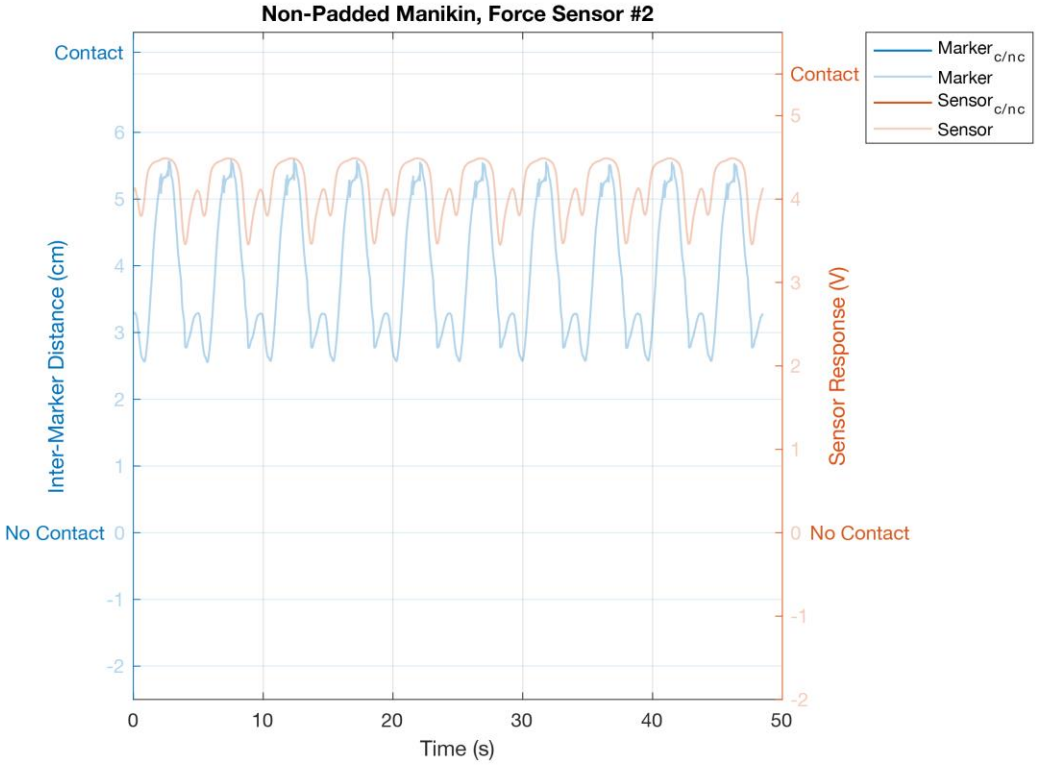

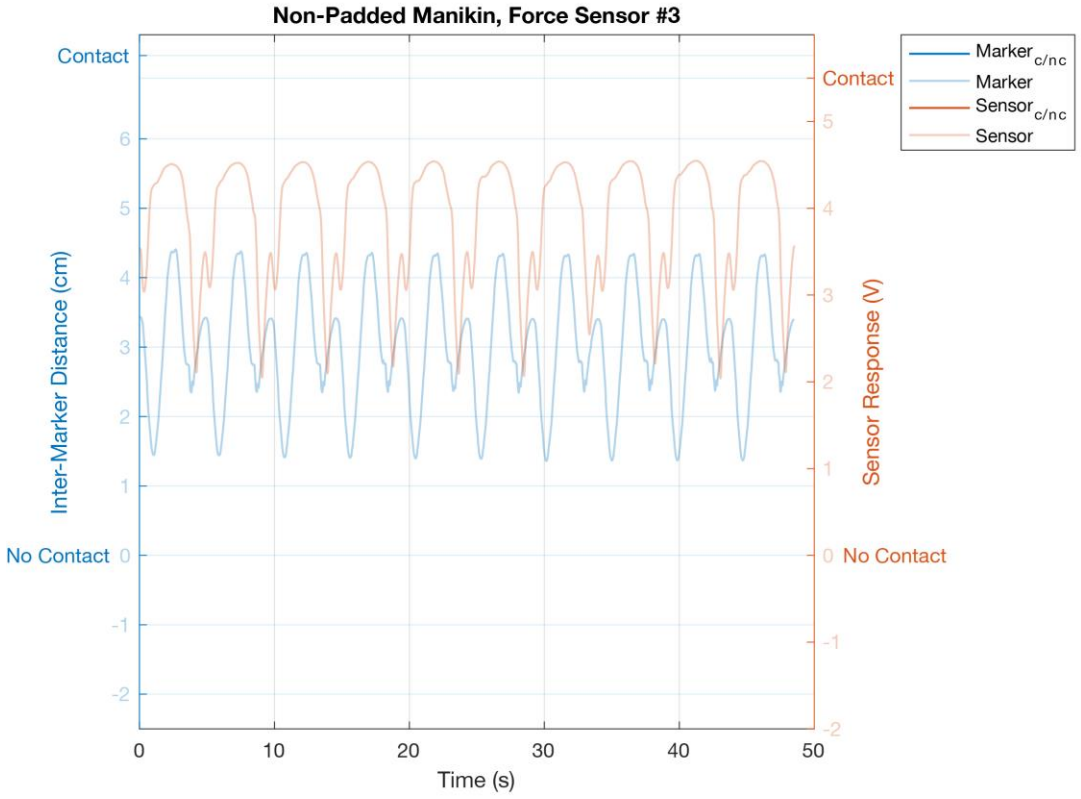
Non-Padded Manikin, Force Sensor #3
Contact
No Contact
Inter-Marker Distance (cm)
Sensor Response (V)
Time (s)
Marker c/nc
Marker
Sensor c/nc
Sensor

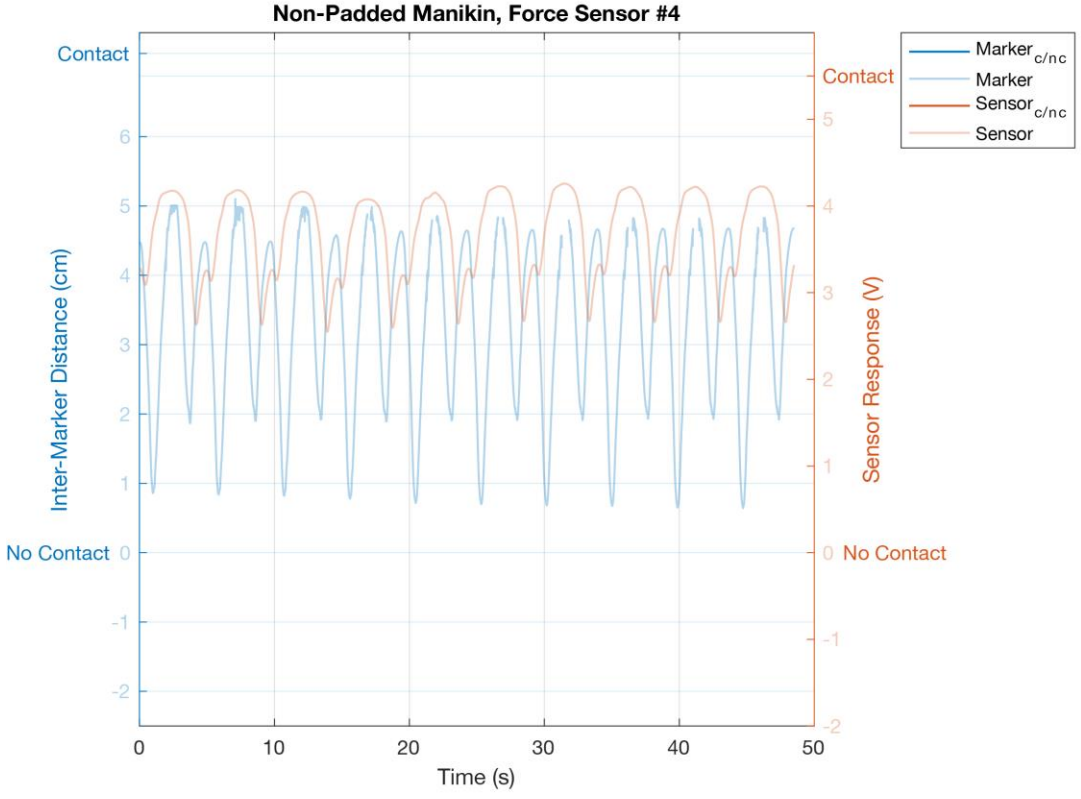
Non-Padded Manikin, Force Sensor #4
Contact
No Contact
Inter-Marker Distance (cm)
Sensor Response (V)
Time (s)
Marker c/nc
Marker
Sensor c/nc
Sensor

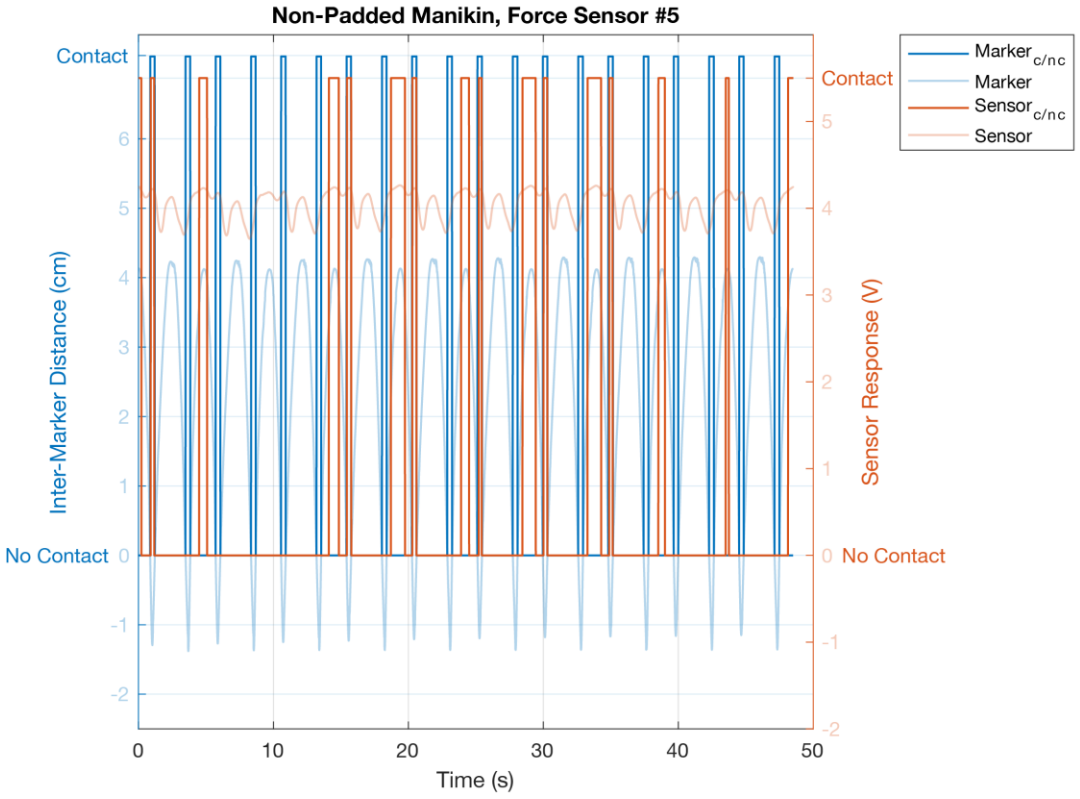
Non-Padded Manikin, Force Sensor #5
Contact
No Contact
Inter-Marker Distance (cm)
Sensor Response (V)
Time (s)
Marker c/nc
Marker
Sensor c/nc
Sensor

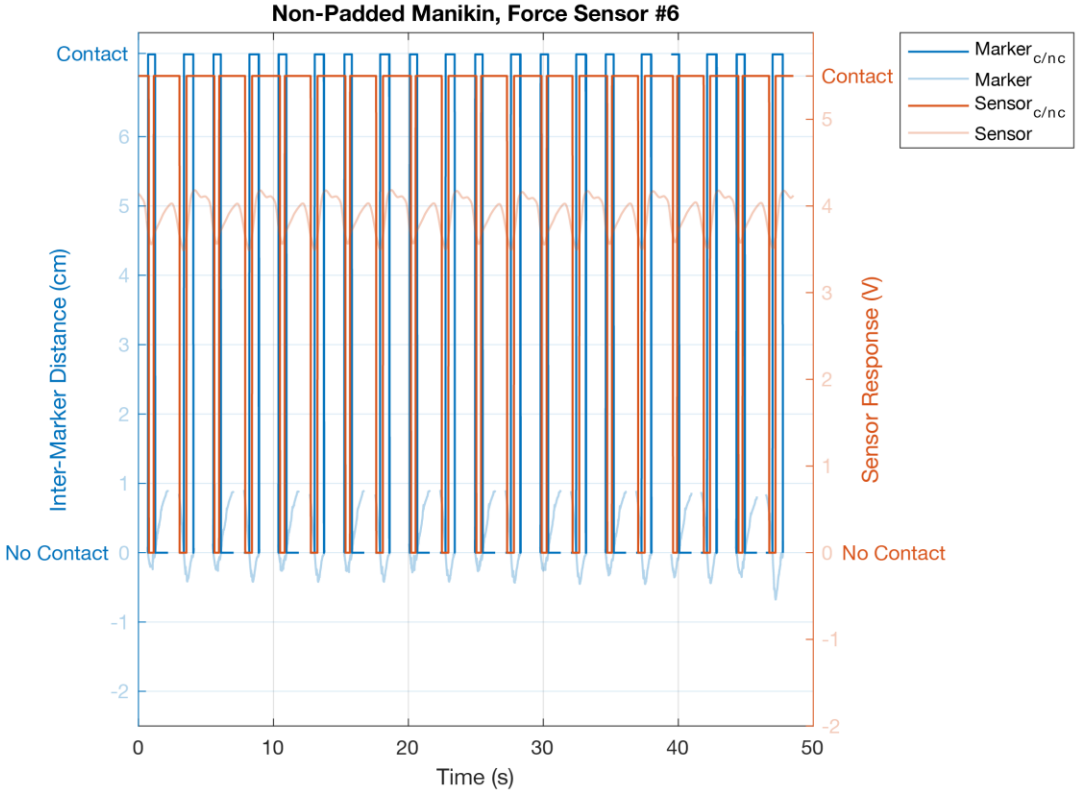
Non-Padded Manikin, Force Sensor #6
Contact
No Contact
Inter-Marker Distance (cm)
Sensor Response (V)
Time (s)
Marker c/nc
Marker
Sensor c/nc
Sensor

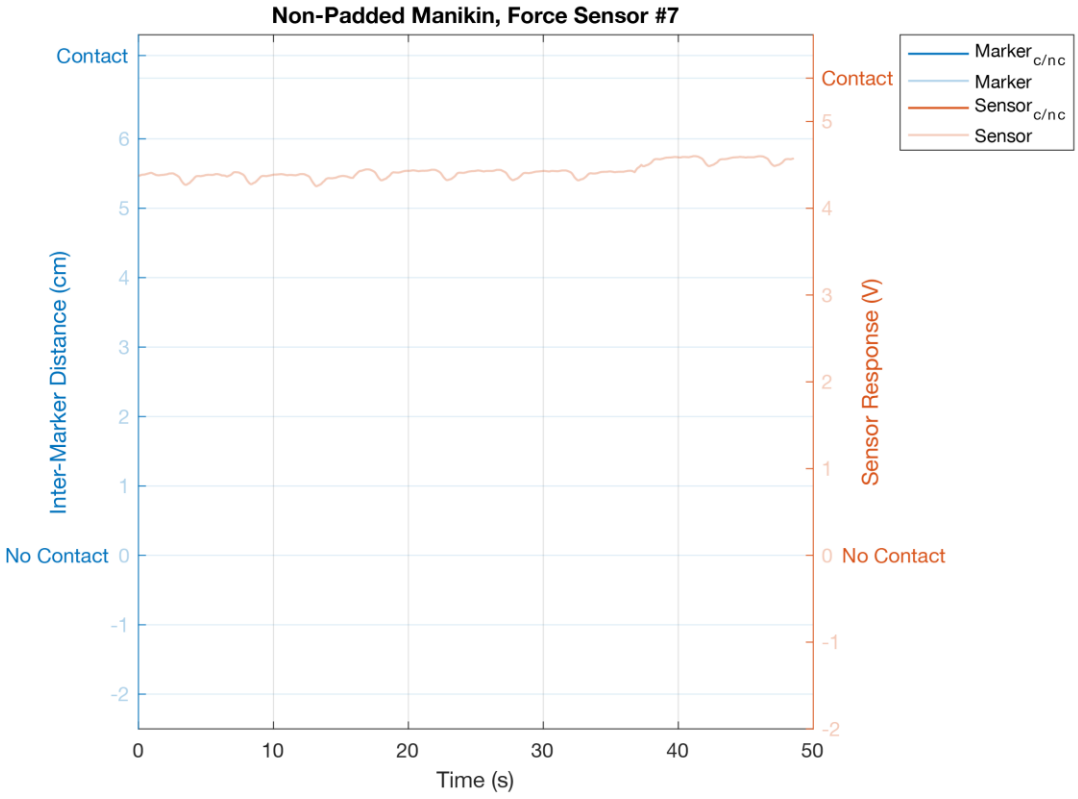
Non-Padded Manikin, Force Sensor #7
Contact
No Contact
Inter-Marker Distance (cm)
Sensor Response (V)
Time (s)
Marker c/nc
Marker
Sensor c/nc
Sensor

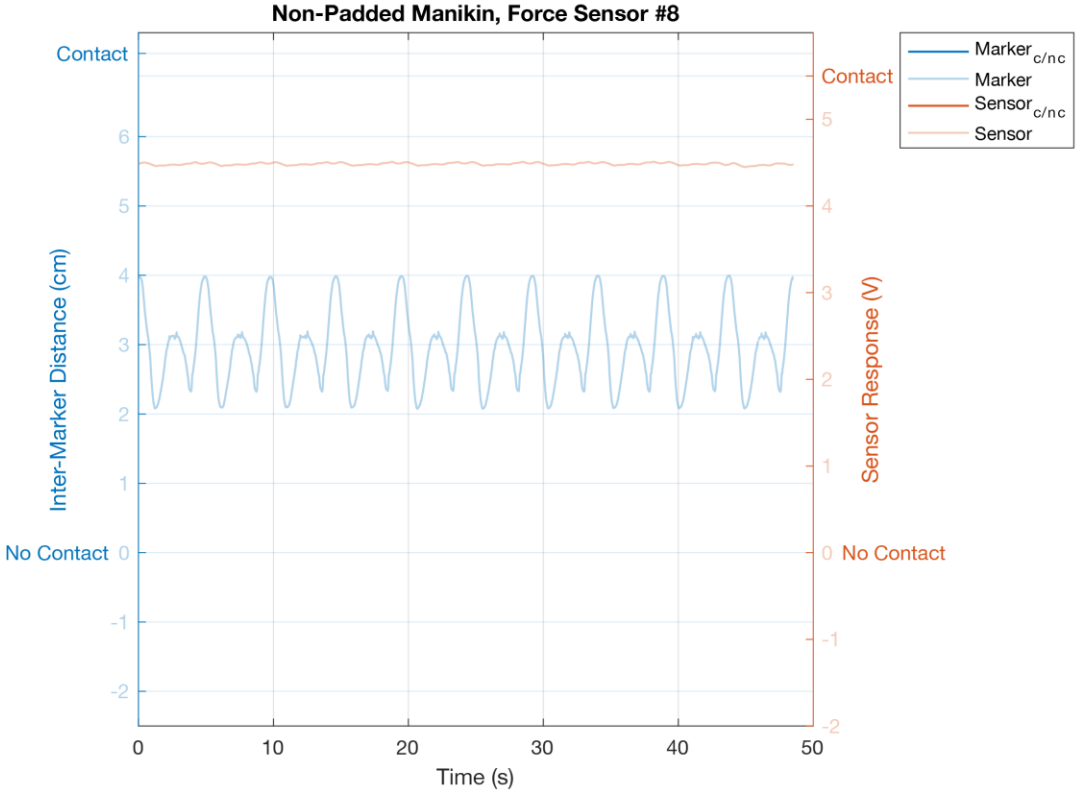
Non-Padded Manikin, Force Sensor #8
Contact
No Contact
Inter-Marker Distance (cm)
Sensor Response (V)
Time (s)
Marker c/nc
Marker
Sensor c/nc
Sensor

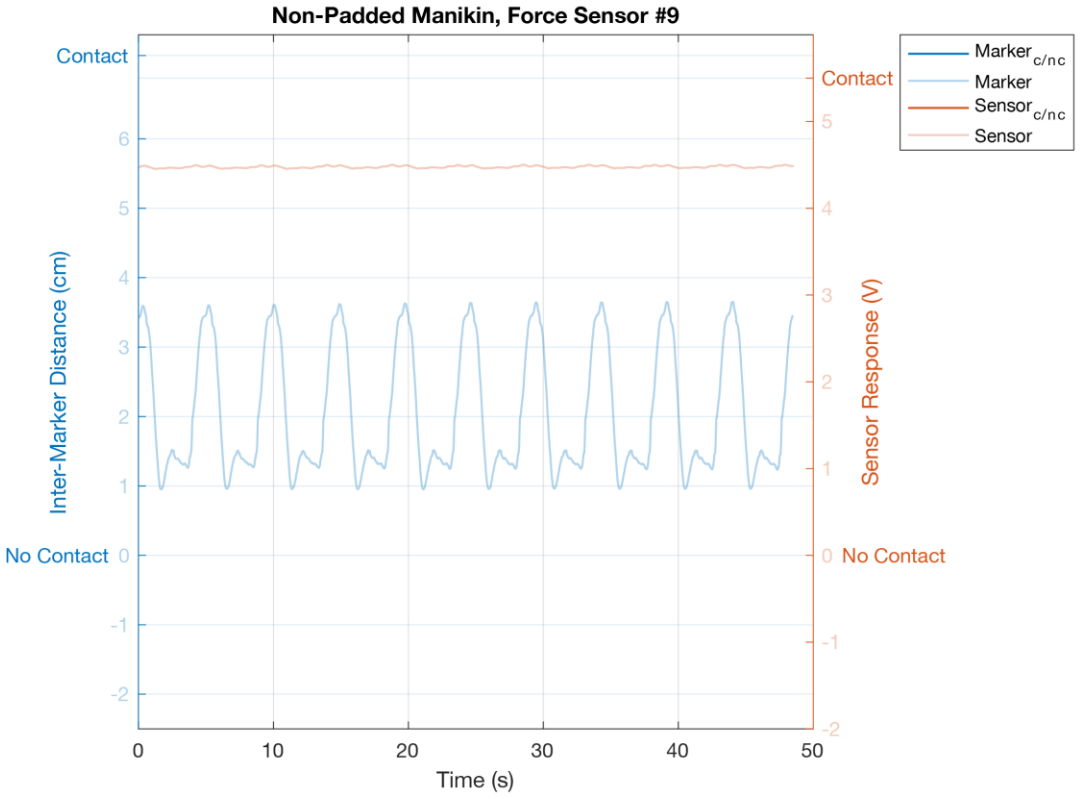
Non-Padded Manikin, Force Sensor #9
Contact
No Contact
Inter-Marker Distance (cm)
Sensor Response (V)
Time (s)
Marker c/nc
Marker
Sensor c/nc
Sensor

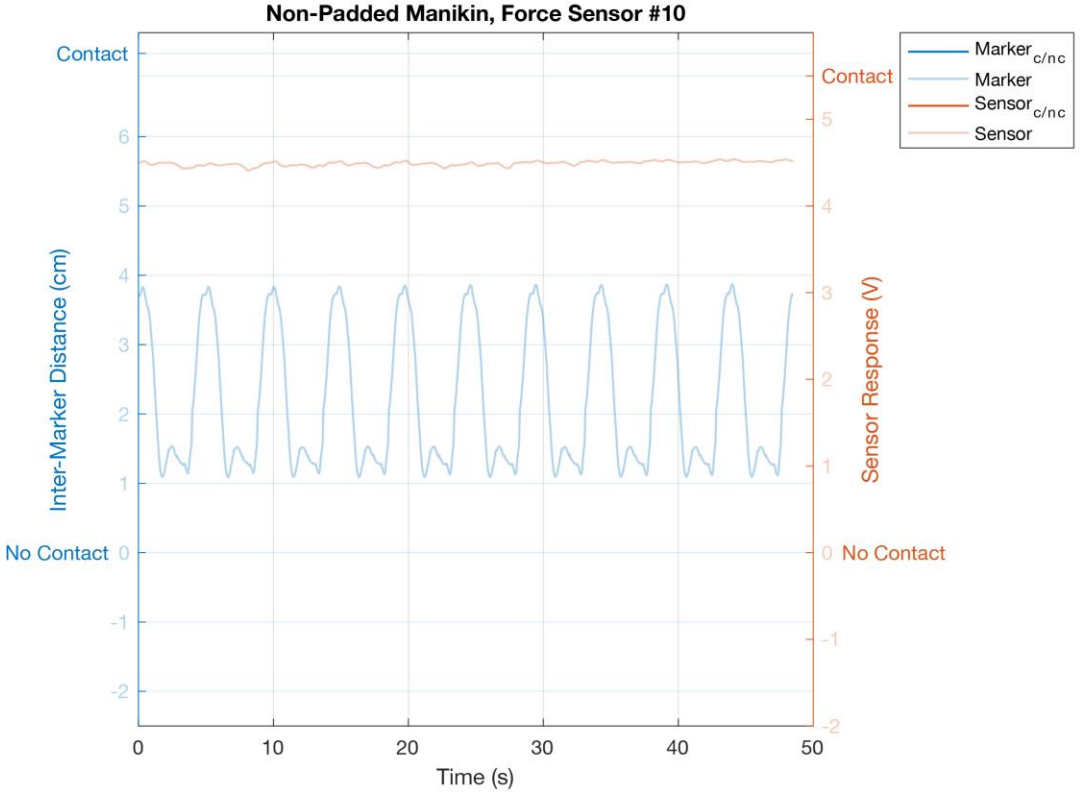
Non-Padded Manikin, Force Sensor #10
Contact
No Contact
Inter-Marker Distance (cm)
Sensor Response (V)
Time (s)
Marker c/nc
Marker
Sensor c/nc
Sensor

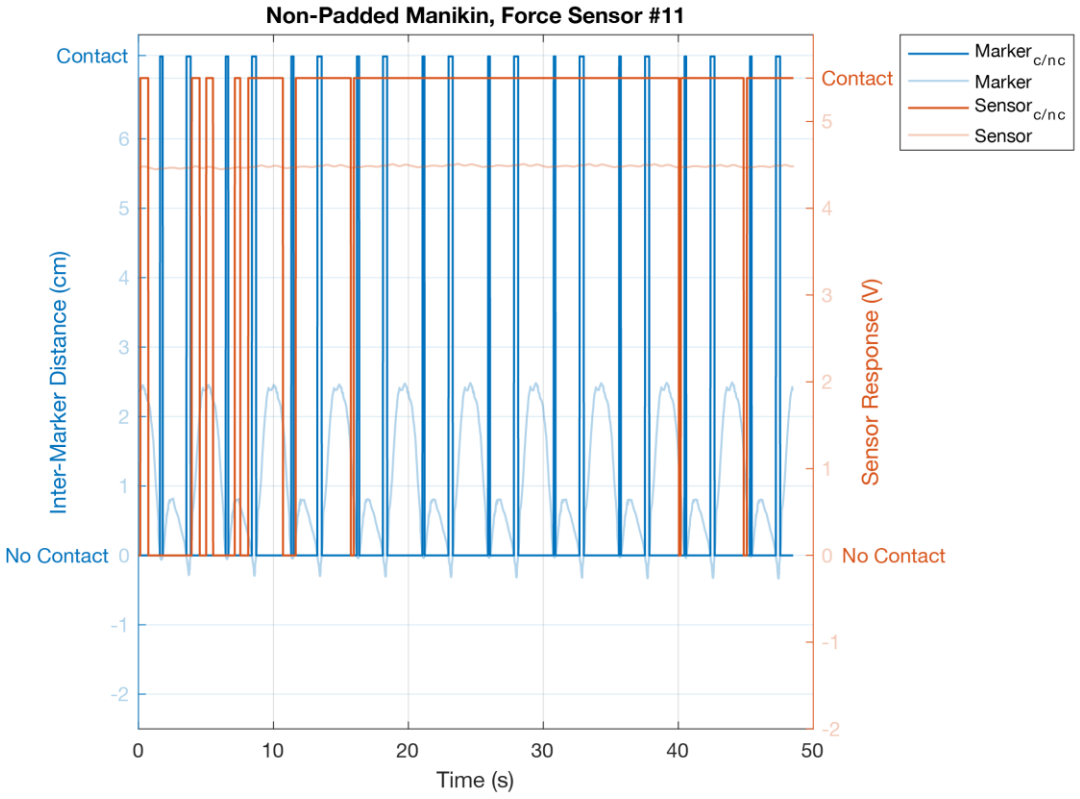
Non-Padded Manikin, Force Sensor #11
Contact
No Contact
Inter-Marker Distance (cm)
Sensor Response (V)
Time (s)
Marker c/nc
Marker
Sensor c/nc
Sensor

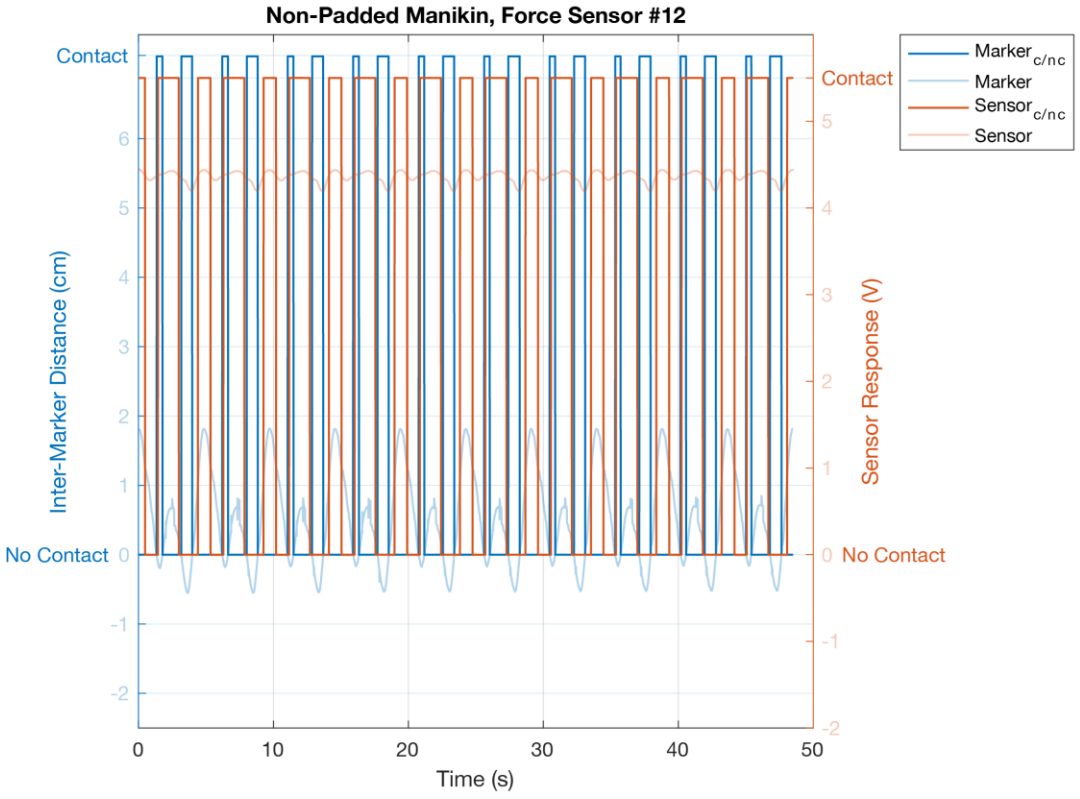
Non-Padded Manikin, Force Sensor #12
Contact
No Contact
Inter-Marker Distance (cm)
Sensor Response (V)
Time (s)
Marker c/nc
Marker
Sensor c/nc
Sensor

A.2.2 Padded Manikin

A.2.2.1 Contact Sensors

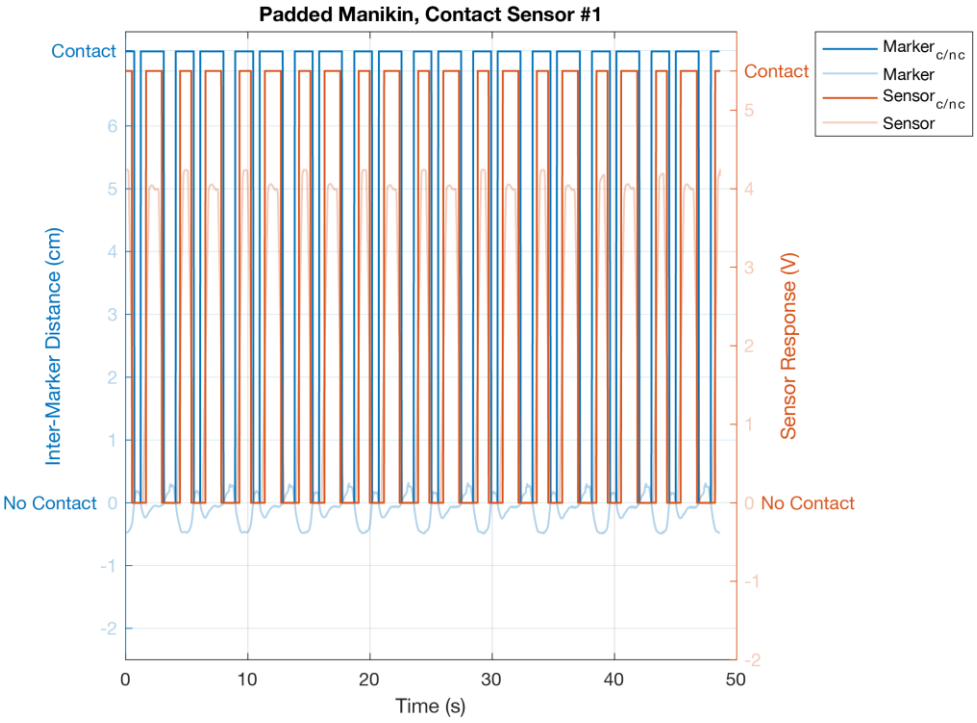

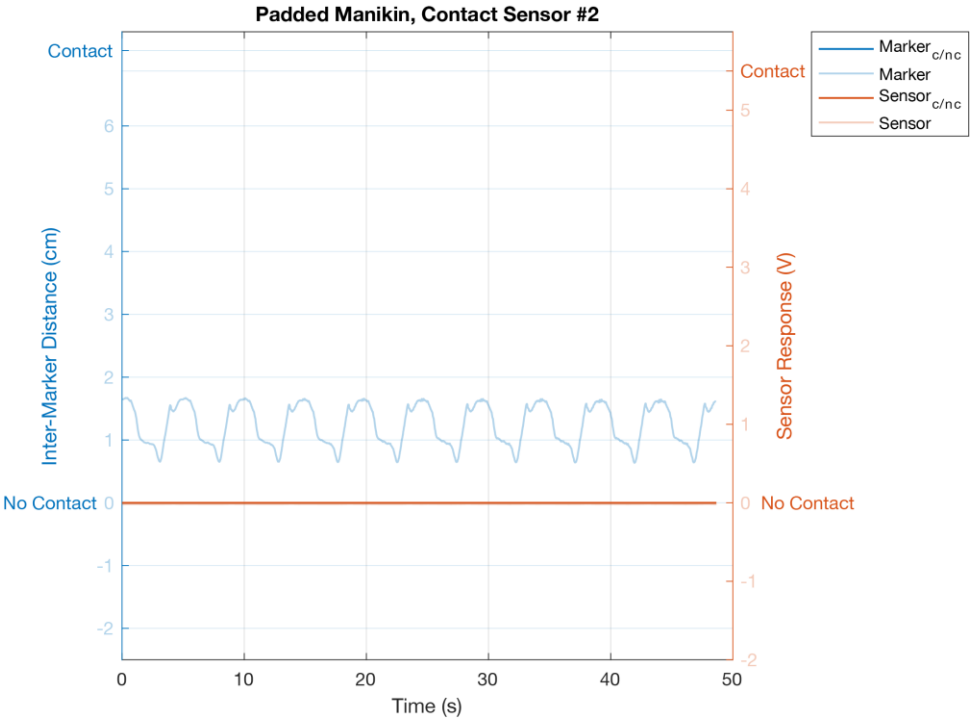

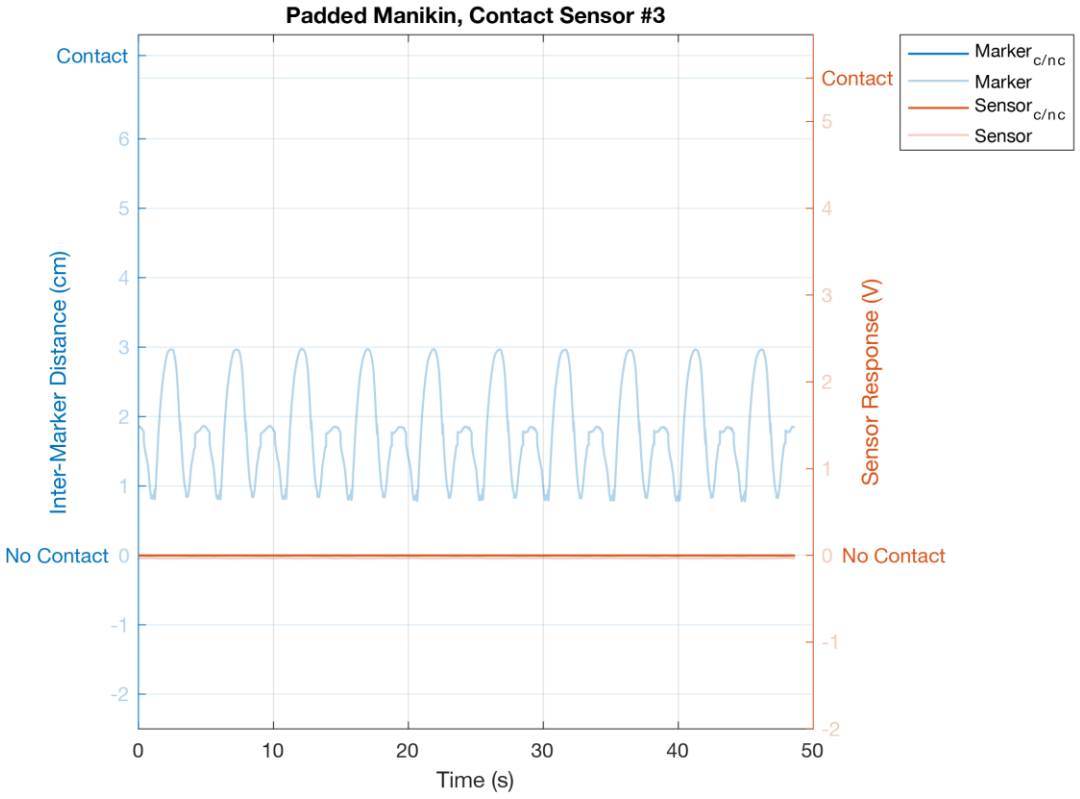
Padded Manikin, Contact Sensor #3
Contact
No Contact
Inter-Marker Distance (cm)
Sensor Response (V)
Time (s)
Marker c/nc
Marker
Sensor c/nc
Sensor

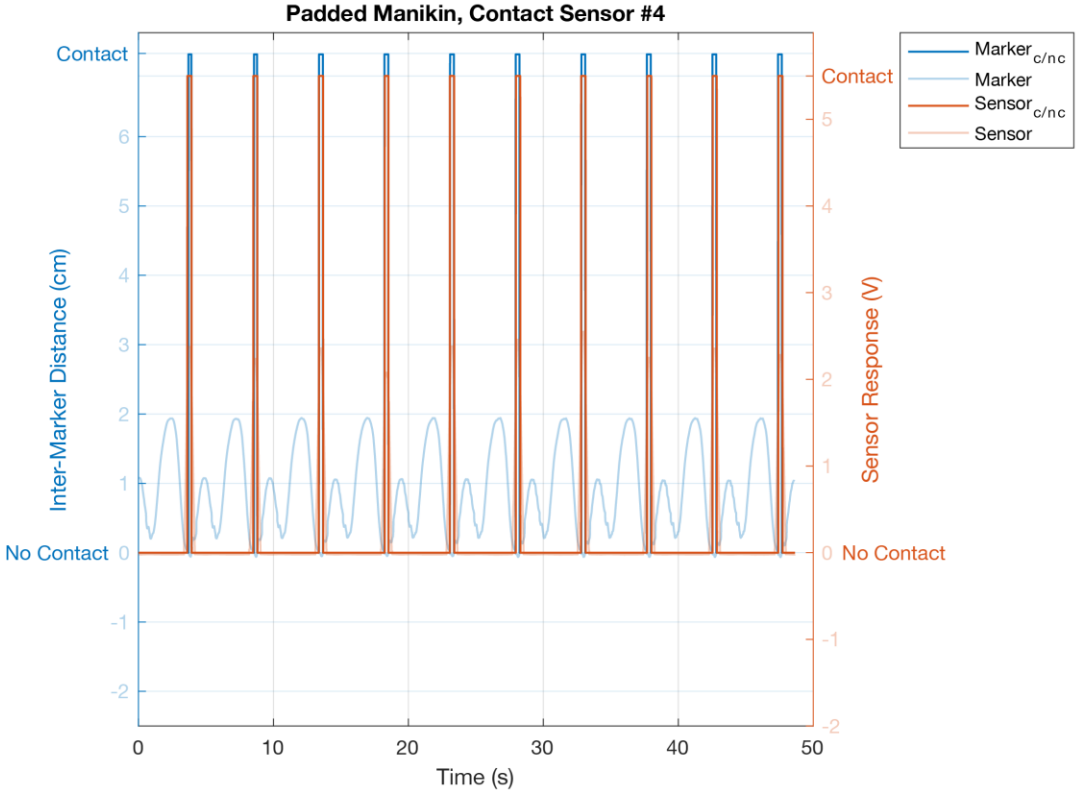
Padded Manikin, Contact Sensor #4
Contact
No Contact
Inter-Marker Distance (cm)
Sensor Response (V)
Time (s)
Marker c/nc
Marker
Sensor c/nc
Sensor

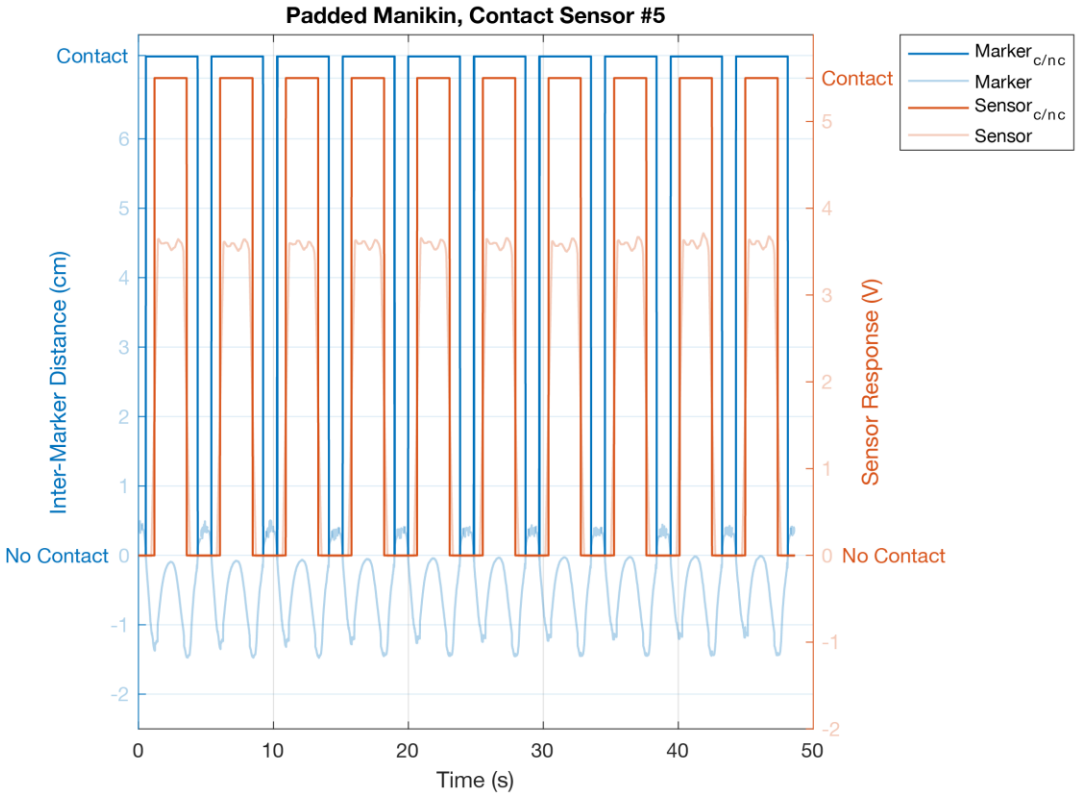
Padded Manikin, Contact Sensor #5
Contact
No Contact
Inter-Marker Distance (cm)
Sensor Response (V)
Time (s)
Marker c/nc
Marker
Sensor c/nc
Sensor

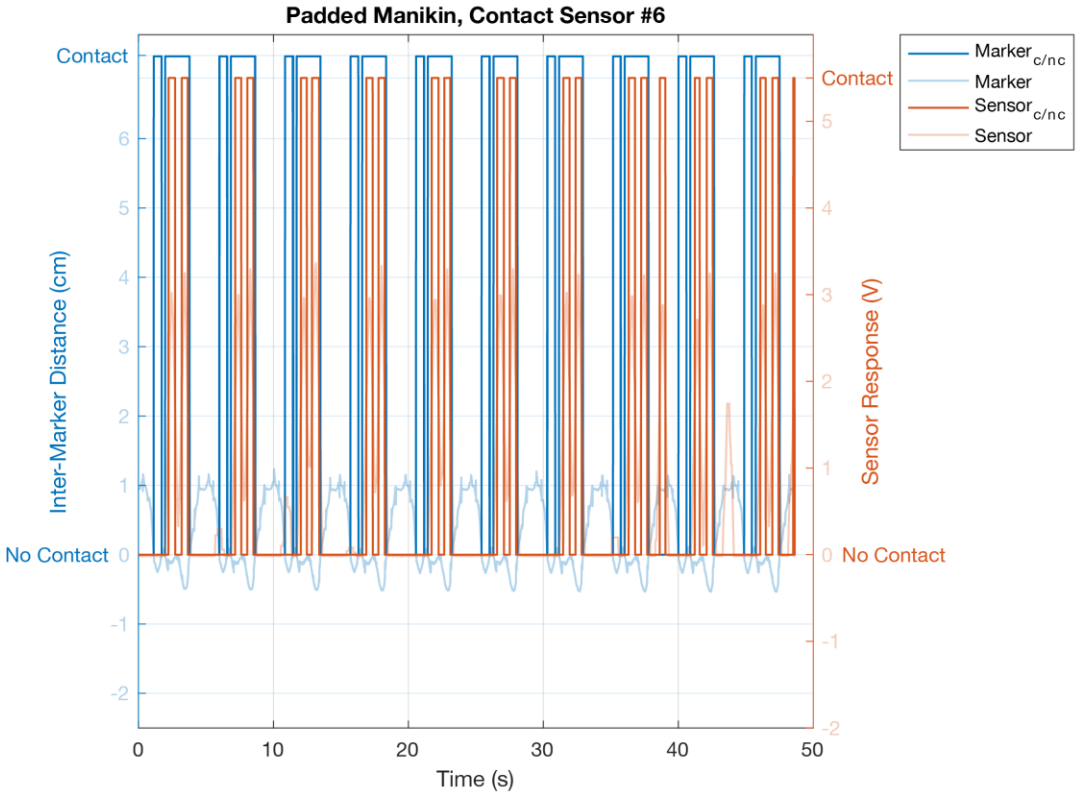
Padded Manikin, Contact Sensor #6
Contact
No Contact
Inter-Marker Distance (cm)
Sensor Response (V)
Time (s)
Marker c/nc
Marker
Sensor c/nc
Sensor

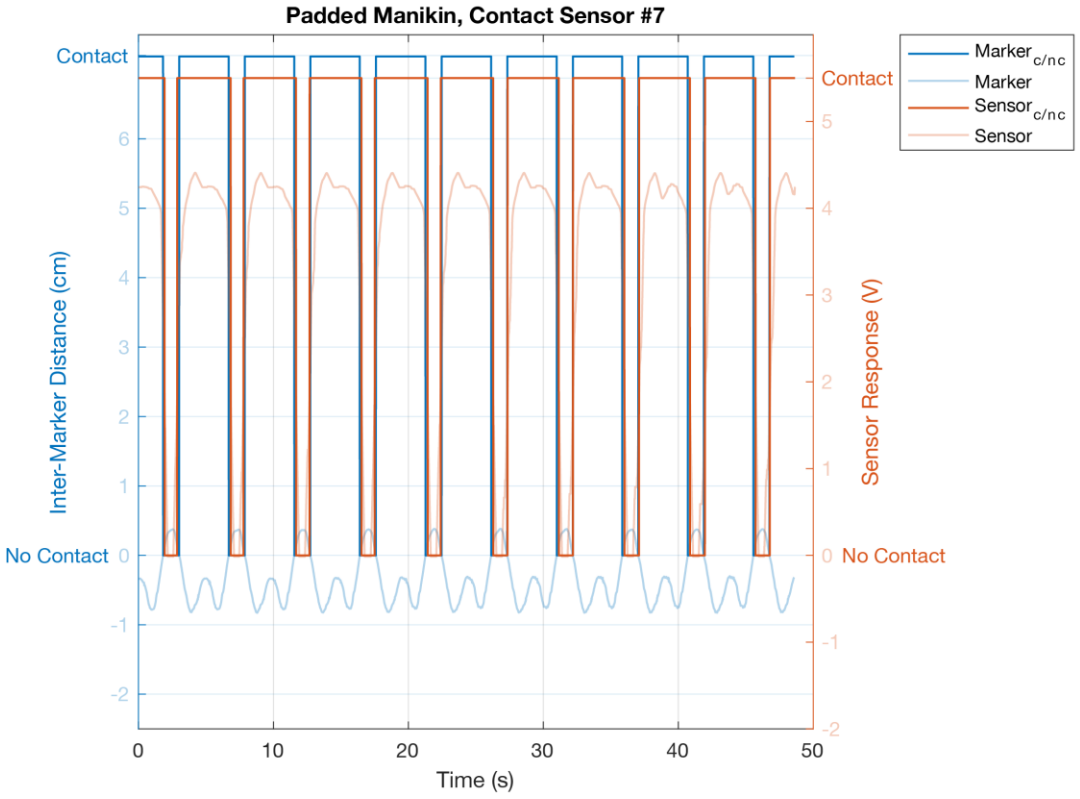
Padded Manikin, Contact Sensor #7
Contact
No Contact
Inter-Marker Distance (cm)
Sensor Response (V)
Time (s)
Marker c/nc
Marker
Sensor c/nc
Sensor

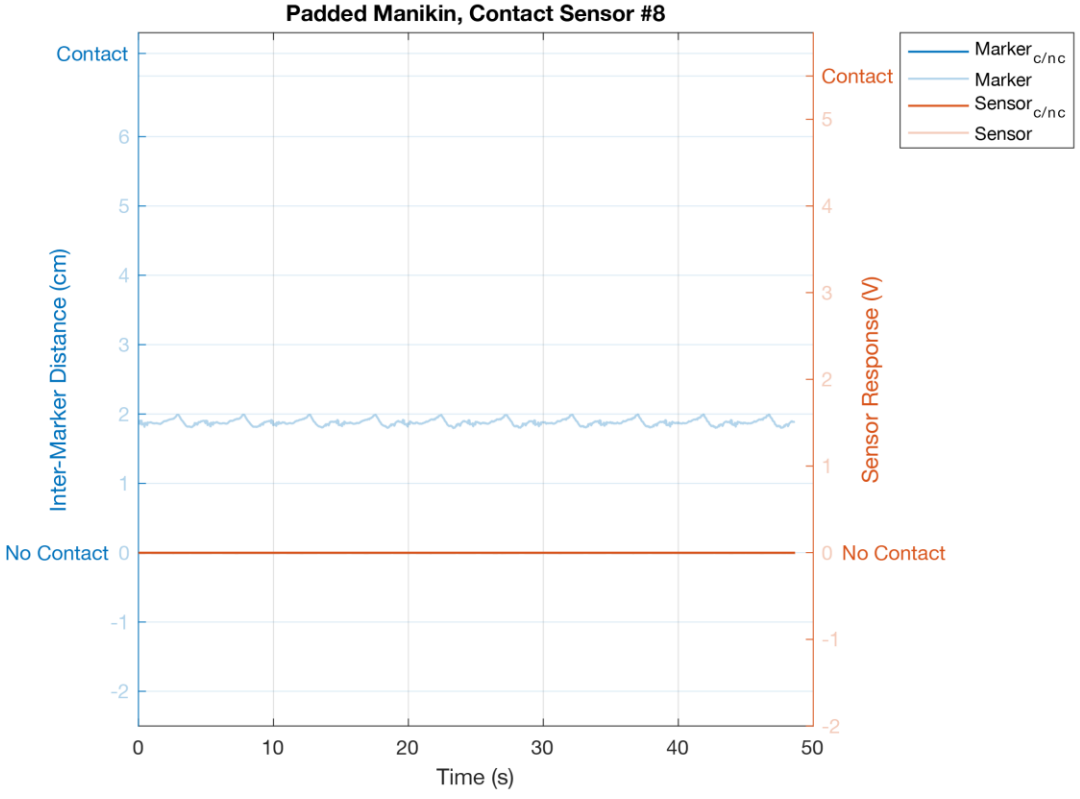
Padded Manikin, Contact Sensor #8
Contact
No Contact
Inter-Marker Distance (cm)
Sensor Response (V)
Time (s)
Marker c/nc
Marker
Sensor c/nc
Sensor

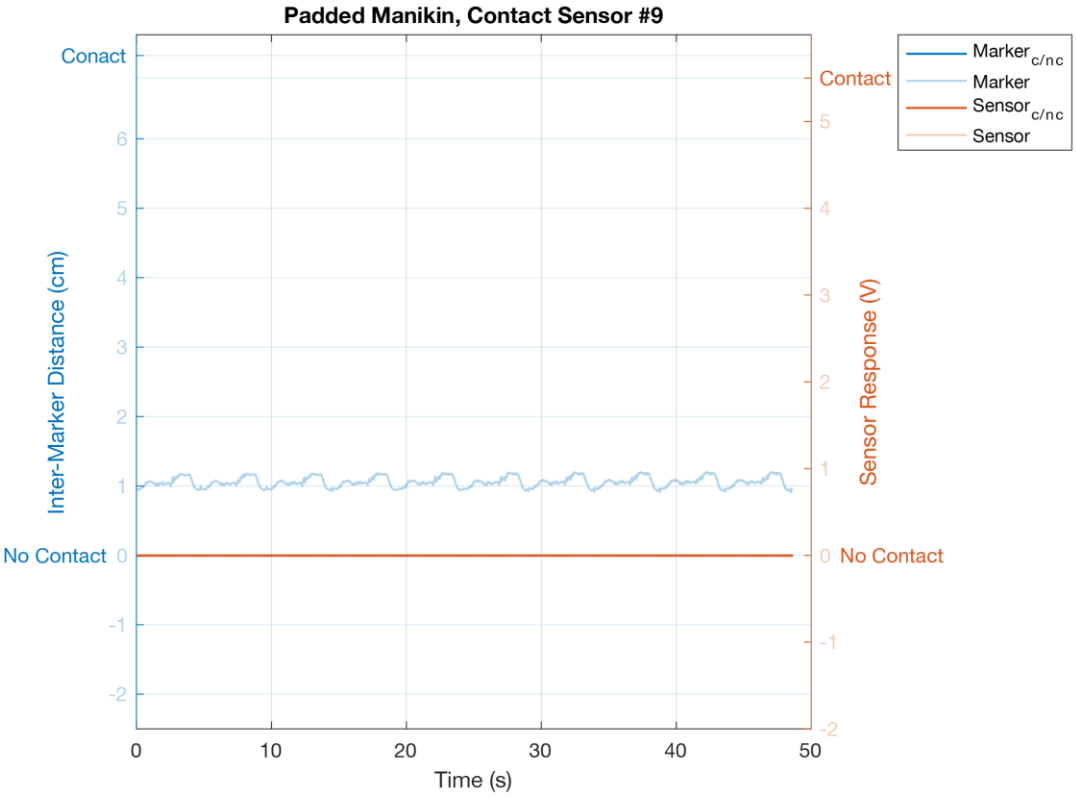
Padded Manikin, Contact Sensor #9
Conact
No Contact
Inter-Marker Distance (cm)
Contact
No Contact
Sensor Response (V)
Marker c/nc
Marker
Sensor c/nc
Sensor
Time (s)

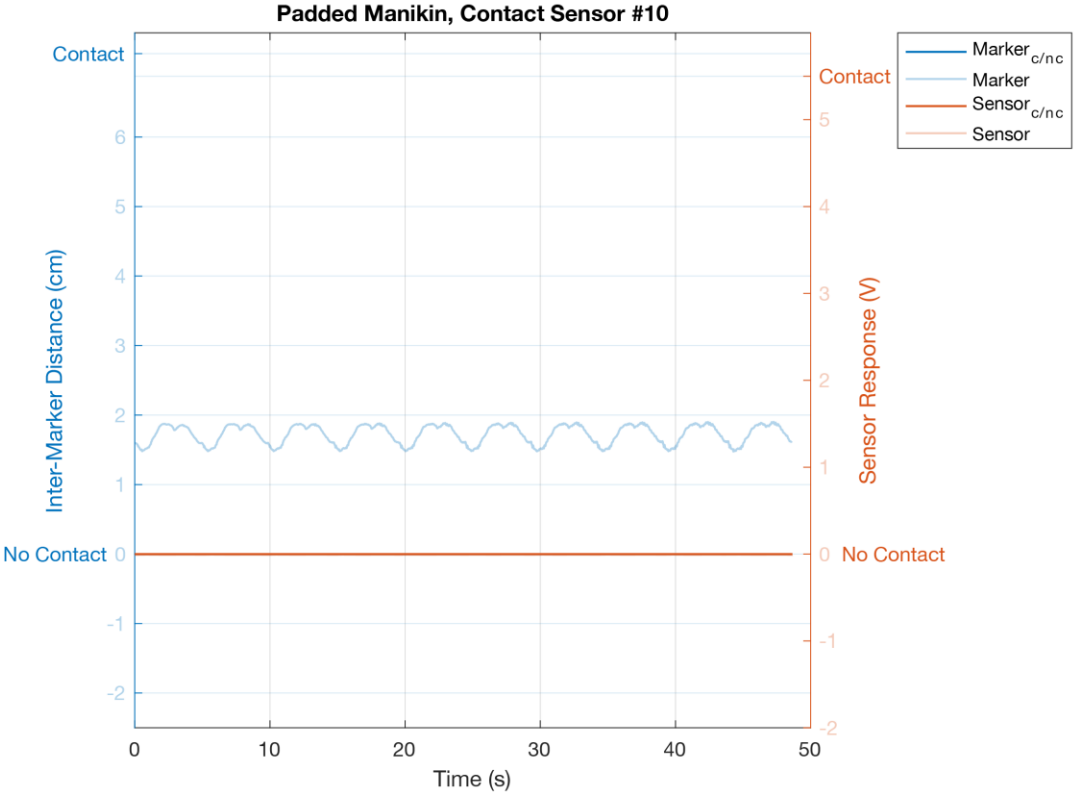
Padded Manikin, Contact Sensor #10
Contact
No Contact
Inter-Marker Distance (cm)
Contact
No Contact
Sensor Response (V)
Marker c/nc
Marker
Sensor c/nc
Sensor
Time (s)

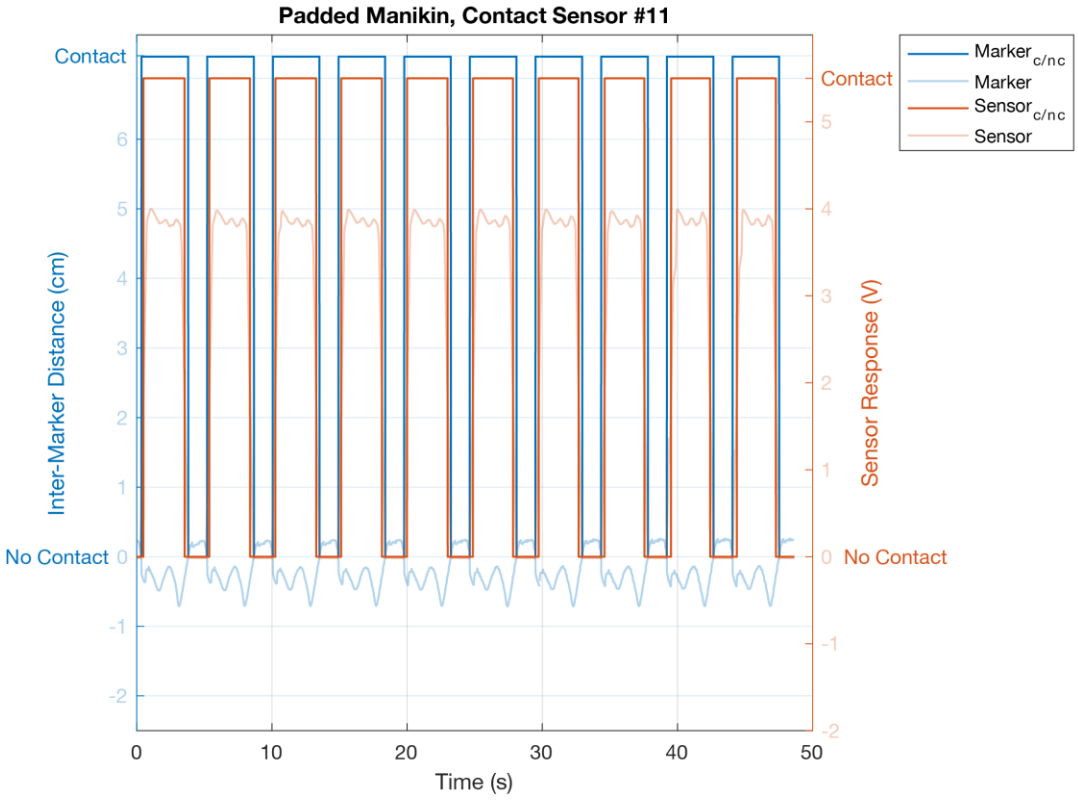
Padded Manikin, Contact Sensor #11
Contact
No Contact
Inter-Marker Distance (cm)
Sensor Response (V)
Time (s)
Marker c/nc
Marker
Sensor c/nc
Sensor

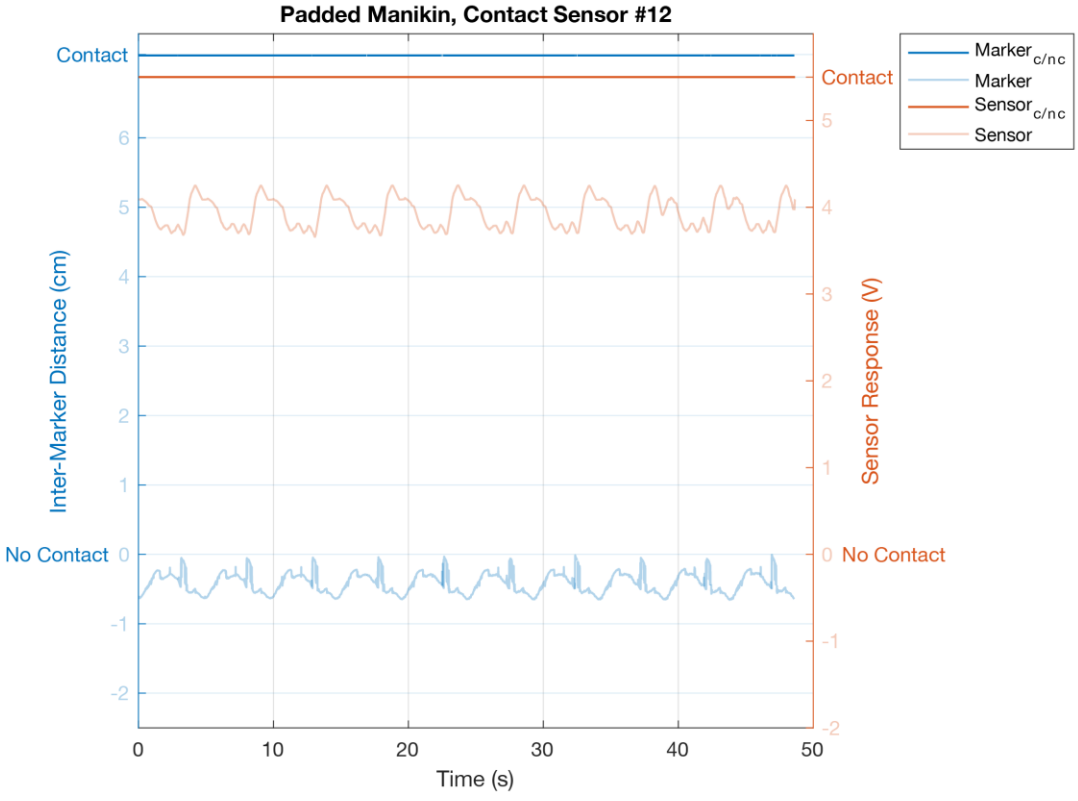
Padded Manikin, Contact Sensor #12
Contact
No Contact
Inter-Marker Distance (cm)
Sensor Response (V)
Time (s)
Marker c/nc
Marker
Sensor c/nc
Sensor

A.2.2.2 Force Sensors (Drift)

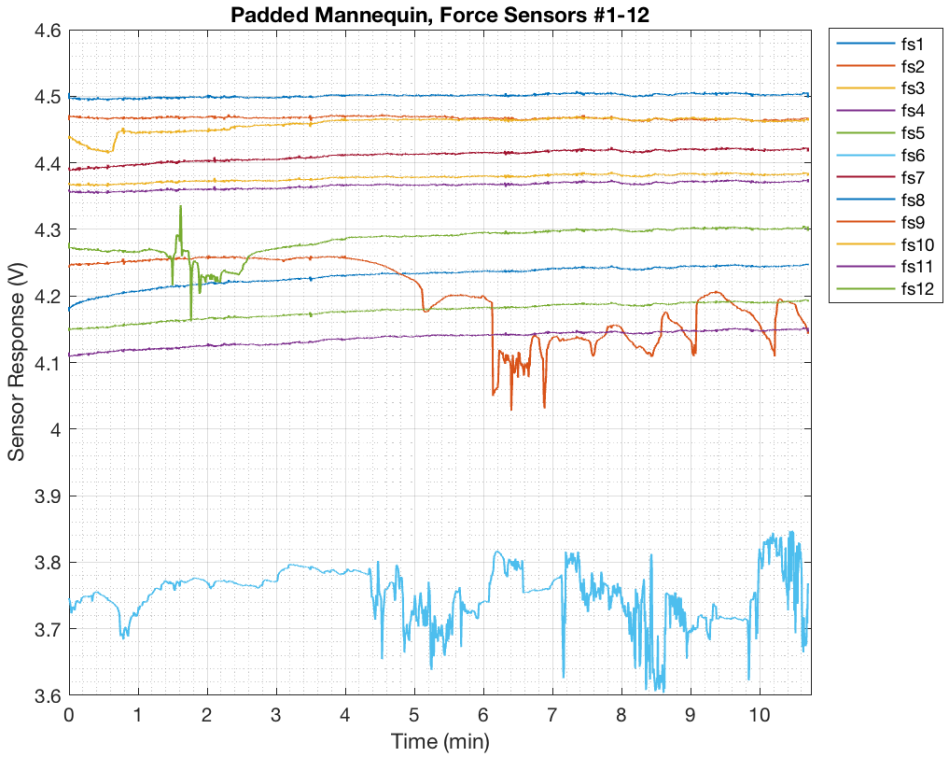

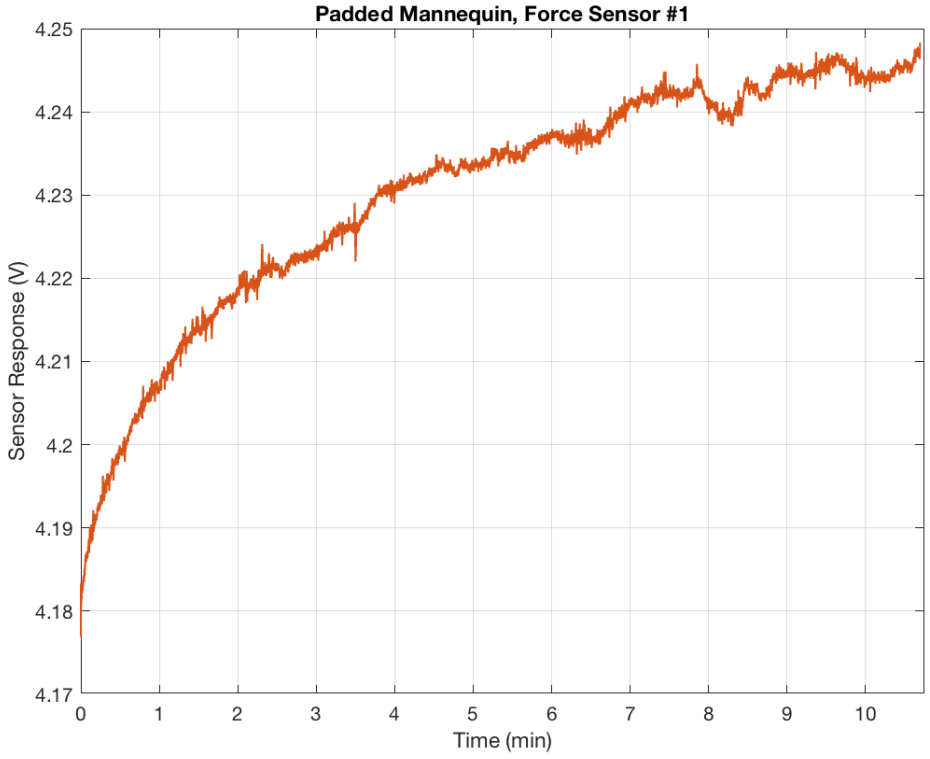

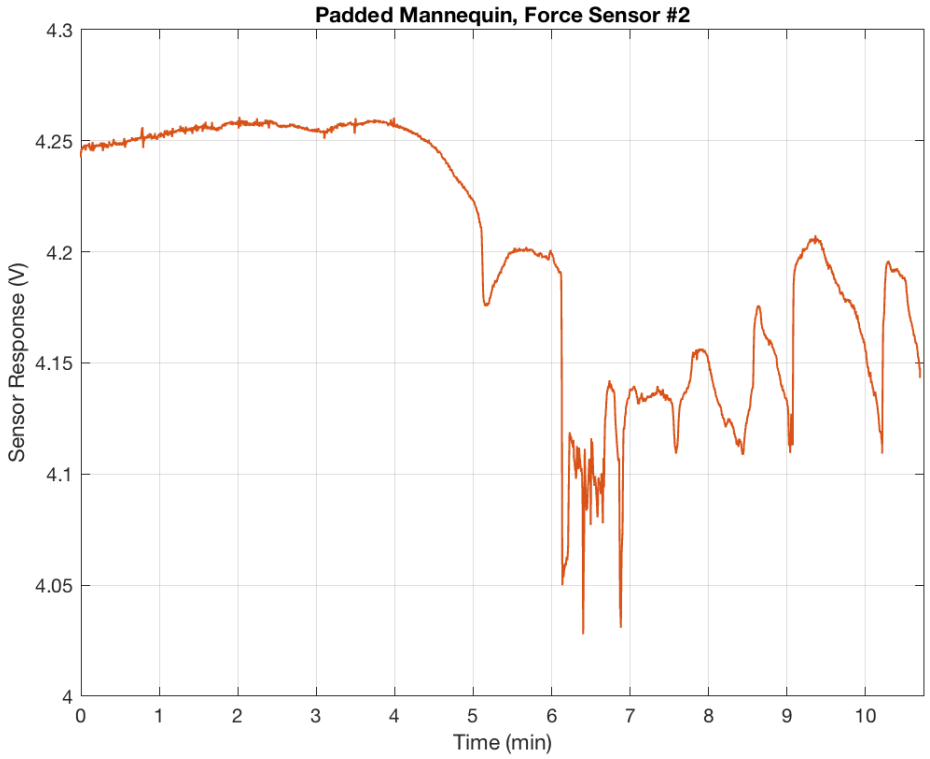
Padded Mannequin, Force Sensor #2
Sensor Response (V)
Time (min)
4.3
4.25
4.2
4.15
4.1
4.05
4
0
1
2
3
4
5
6
7
8
9
10

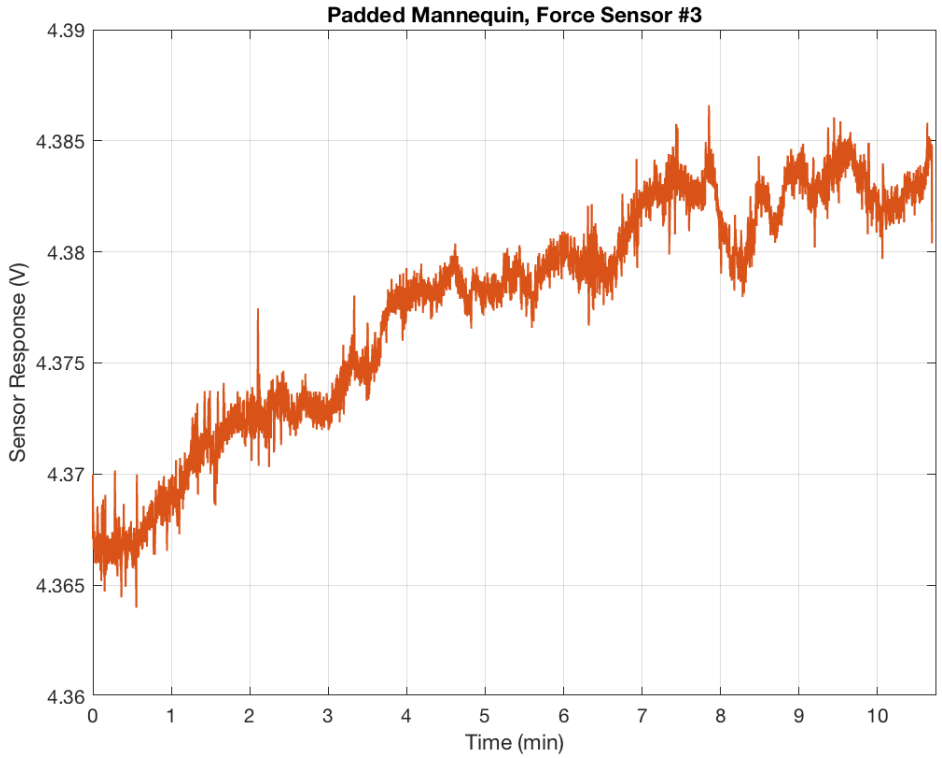
Padded Mannequin, Force Sensor #3
Sensor Response (V)
Time (min)
4.39
4.385
4.38
4.375
4.37
4.365
4.36
0
1
2
3
4
5
6
7
8
9
10

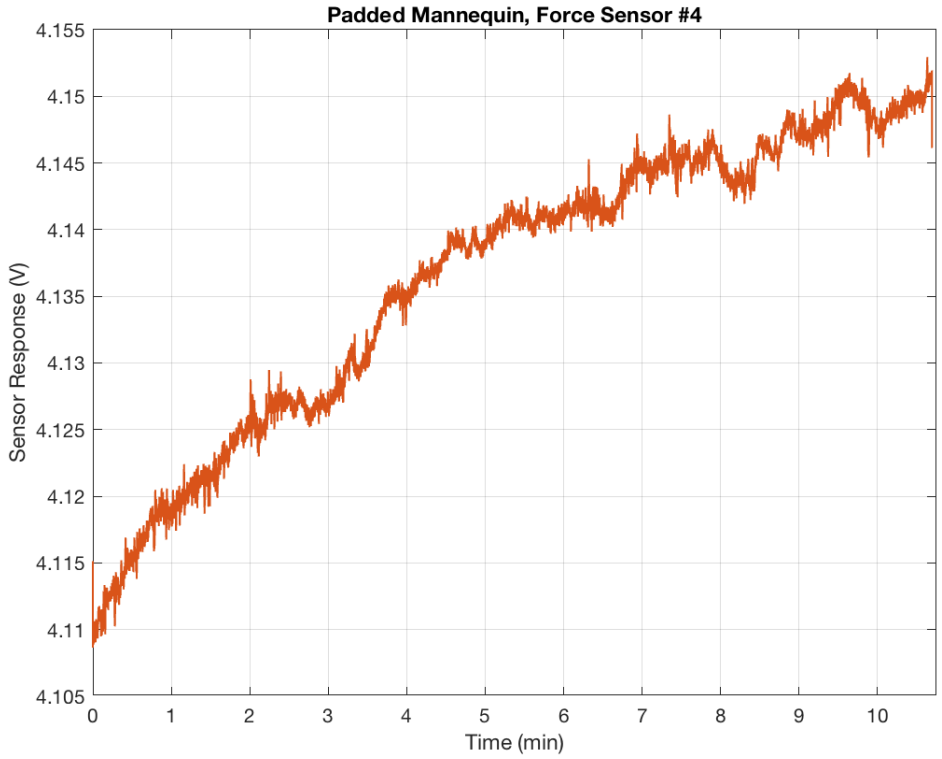
Padded Mannequin, Force Sensor #4
Sensor Response (V)
Time (min)
4.155
4.15
4.145
4.14
4.135
4.13
4.125
4.12
4.115
4.11
4.105
0
1
2
3
4
5
6
7
8
9
10

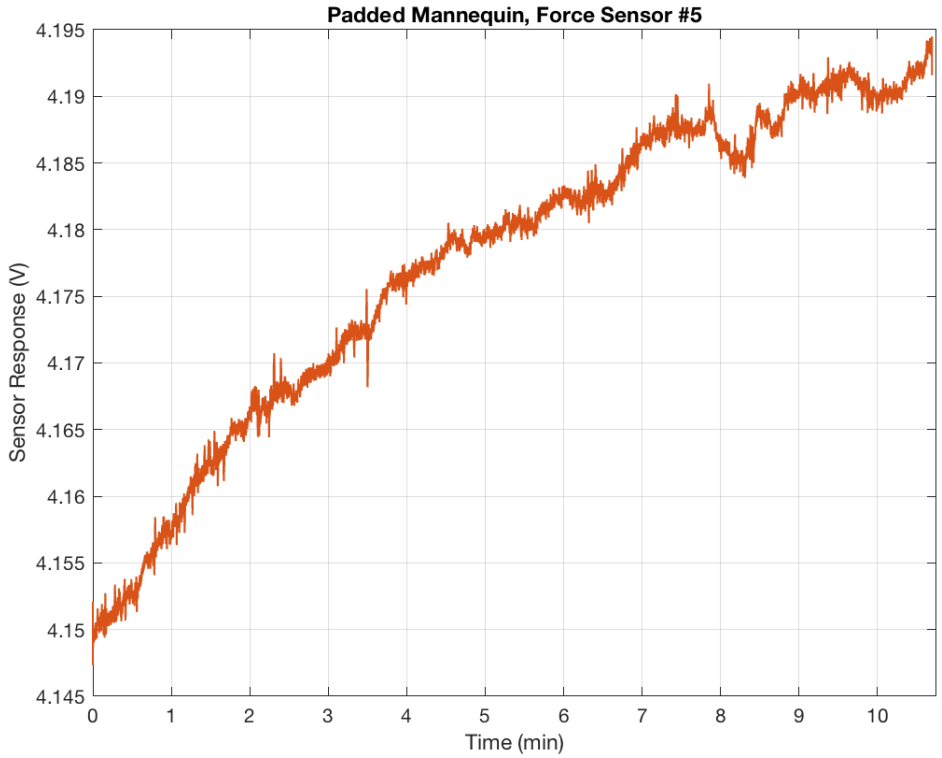
Padded Mannequin, Force Sensor #5
Sensor Response (V)
Time (min)
4.195
4.19
4.185
4.18
4.175
4.17
4.165
4.16
4.155
4.15
4.145
0
1
2
3
4
5
6
7
8
9
10

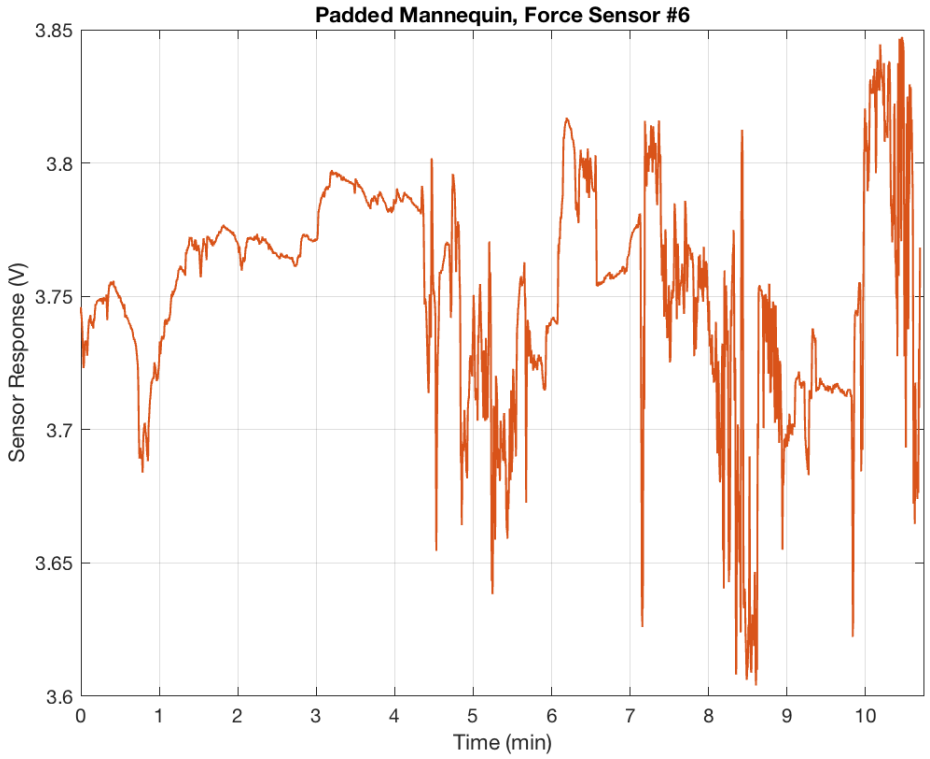
Padded Mannequin, Force Sensor #6
Sensor Response (V)
Time (min)
3.85
3.8
3.75
3.7
3.65
3.6
0
1
2
3
4
5
6
7
8
9
10

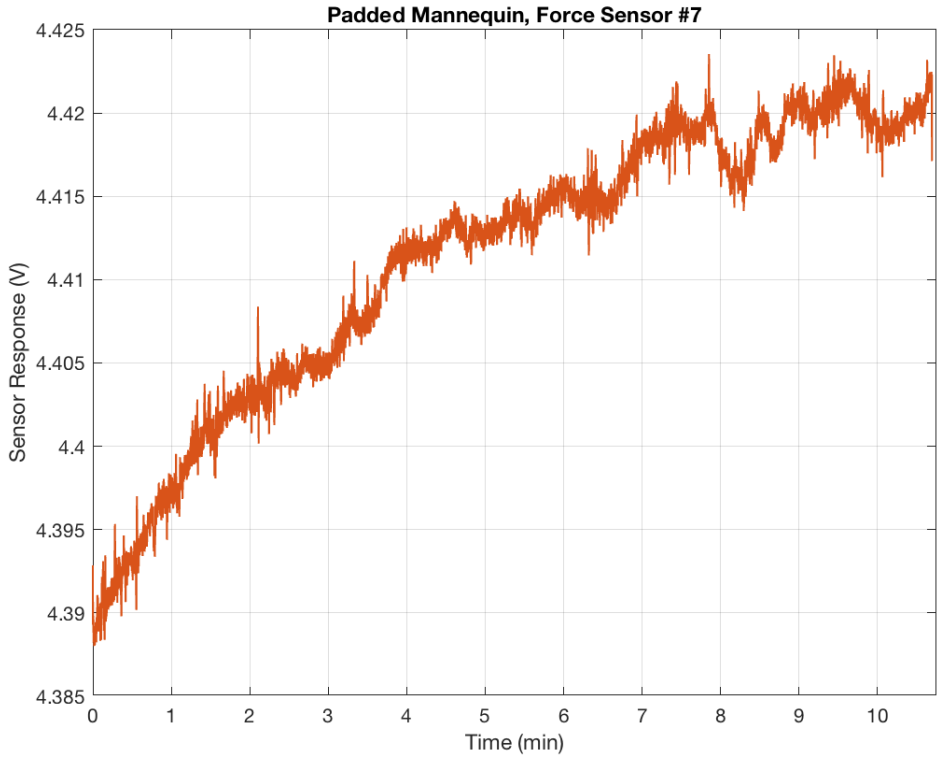
Padded Mannequin, Force Sensor #7
Sensor Response (V)
Time (min)
4.425
4.42
4.415
4.41
4.405
4.4
4.395
4.39
4.385
0
1
2
3
4
5
6
7
8
9
10

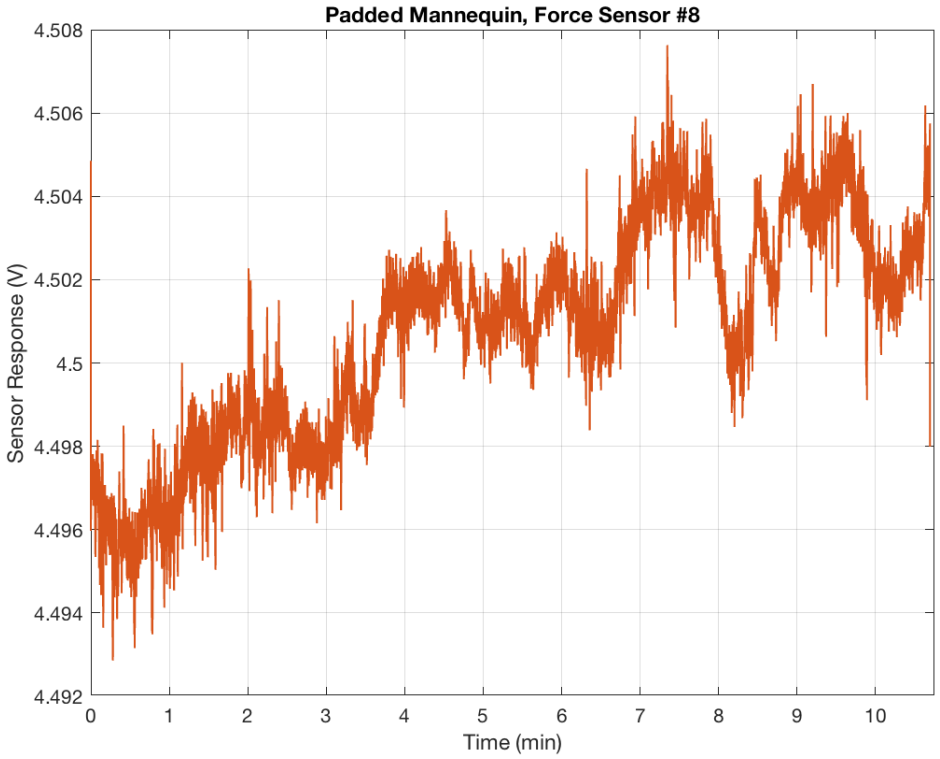
Padded Mannequin, Force Sensor #8
Sensor Response (V)
Time (min)
4.508
4.506
4.504
4.502
4.5
4.498
4.496
4.494
4.492
0
1
2
3
4
5
6
7
8
9
10

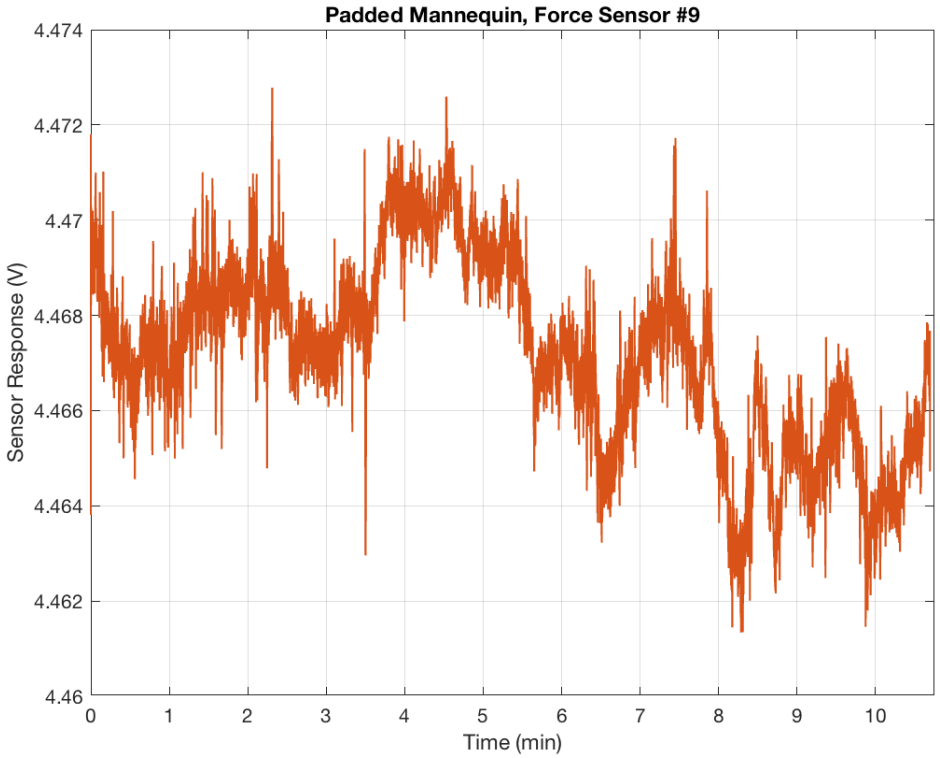
Padded Mannequin, Force Sensor #9
Sensor Response (V)
Time (min)
4.474
4.472
4.47
4.468
4.466
4.464
4.462
4.46
0
1
2
3
4
5
6
7
8
9
10

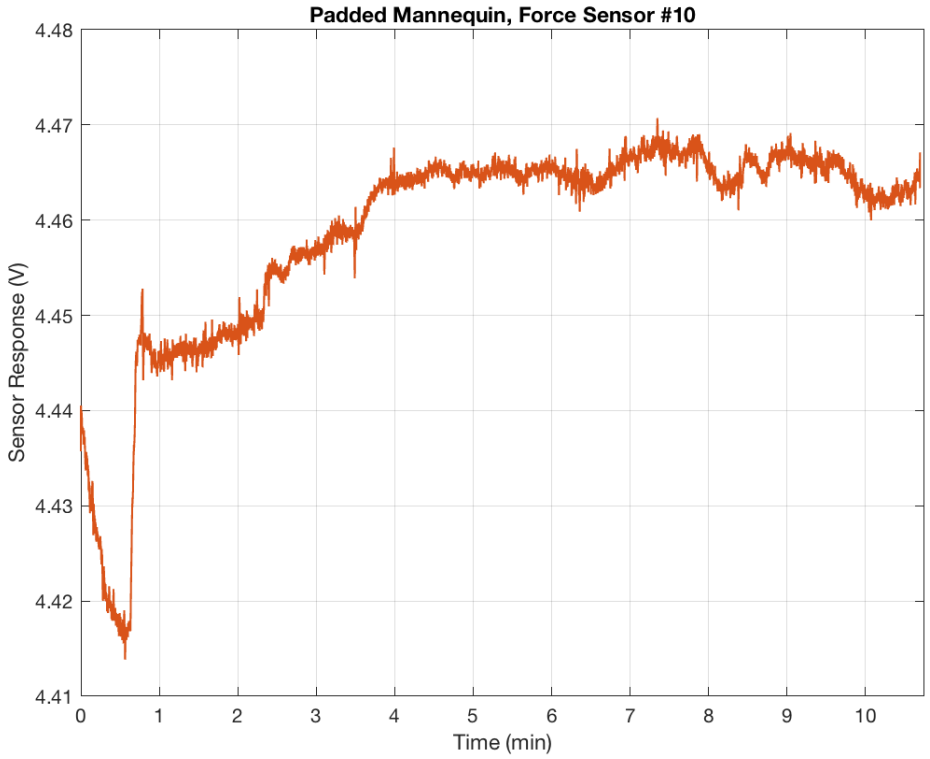
Padded Mannequin, Force Sensor #10
Sensor Response (V)
Time (min)
4.48
4.47
4.46
4.45
4.44
4.43
4.42
4.41
0
1
2
3
4
5
6
7
8
9
10

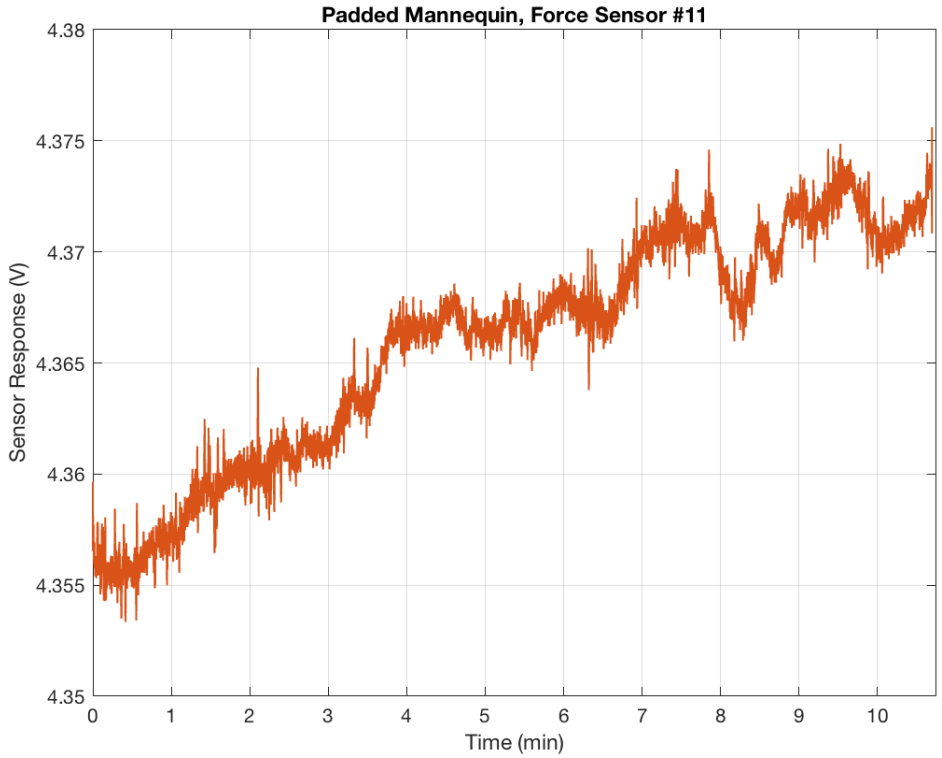
Padded Mannequin, Force Sensor #11
Sensor Response (V)
Time (min)
4.38
4.375
4.37
4.365
4.36
4.355
4.35
0
1
2
3
4
5
6
7
8
9
10

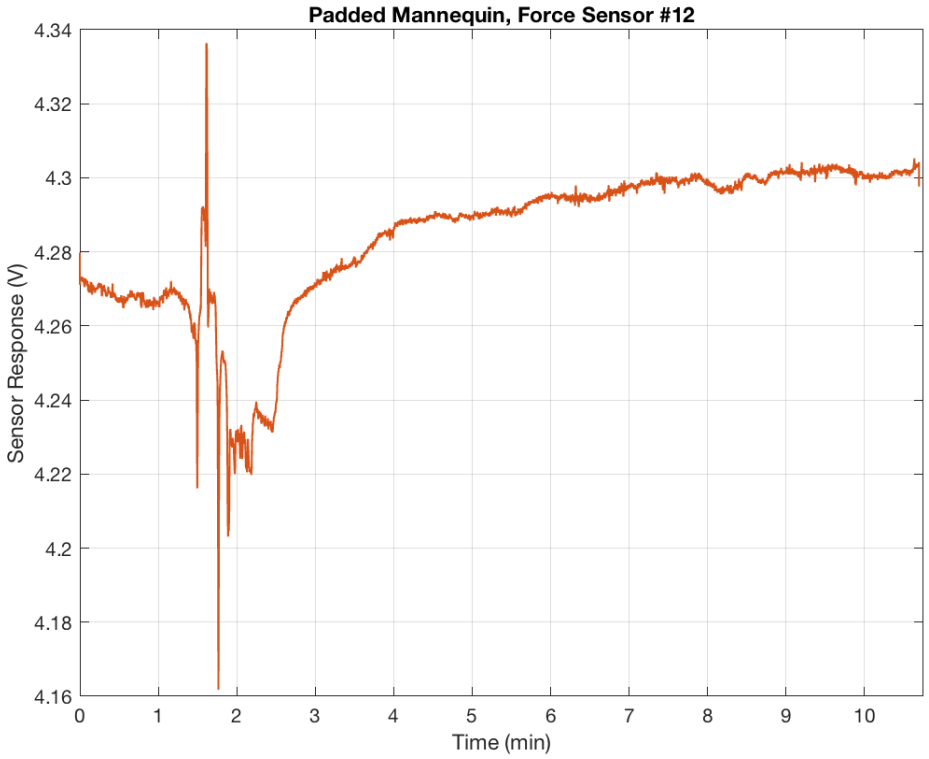
Padded Mannequin, Force Sensor #12
Sensor Response (V)
Time (min)
4.34
4.32
4.3
4.28
4.26
4.24
4.22
4.2
4.18
4.16
0
1
2
3
4
5
6
7
8
9
10

A.2.2.3 Force Sensors

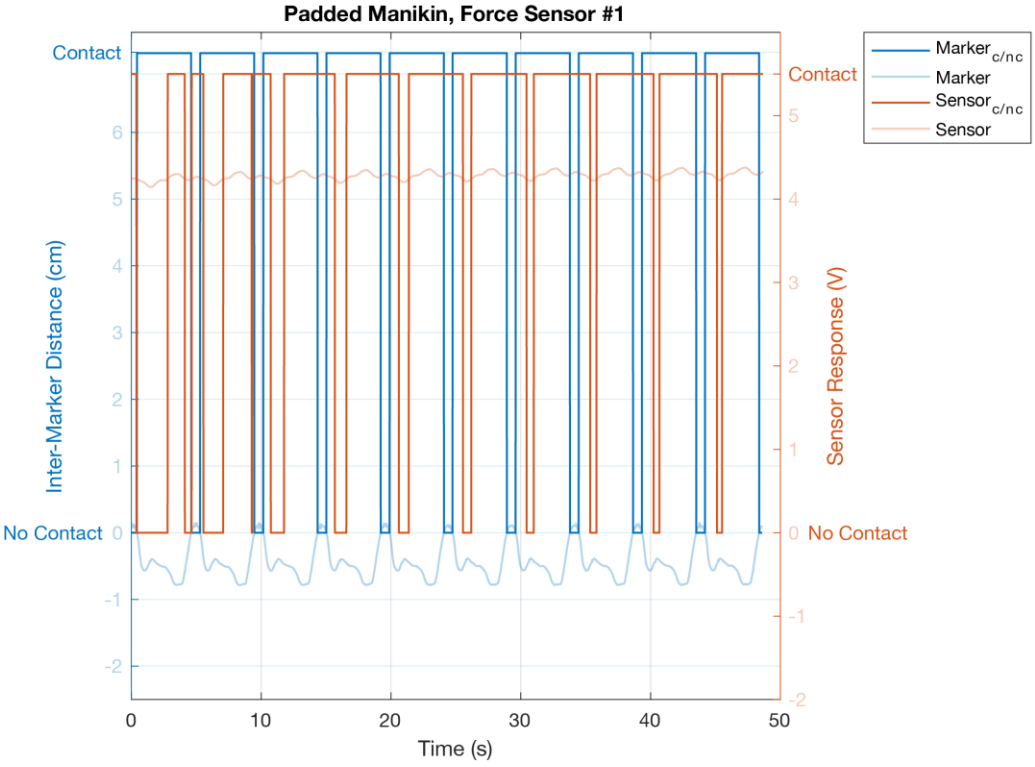

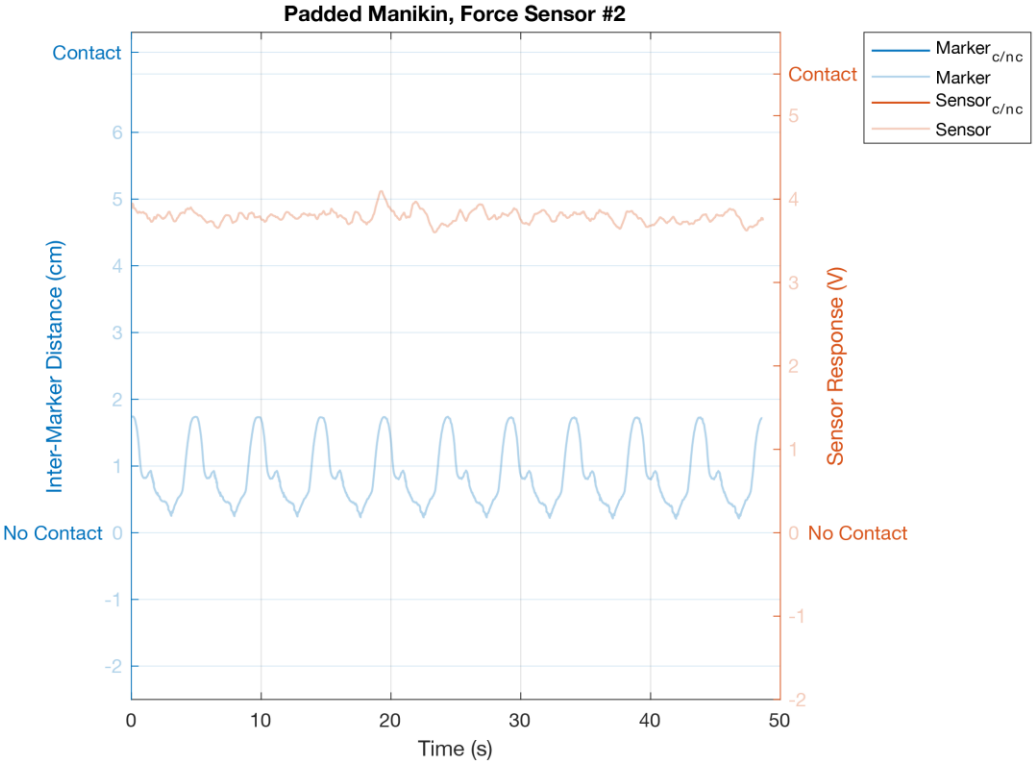

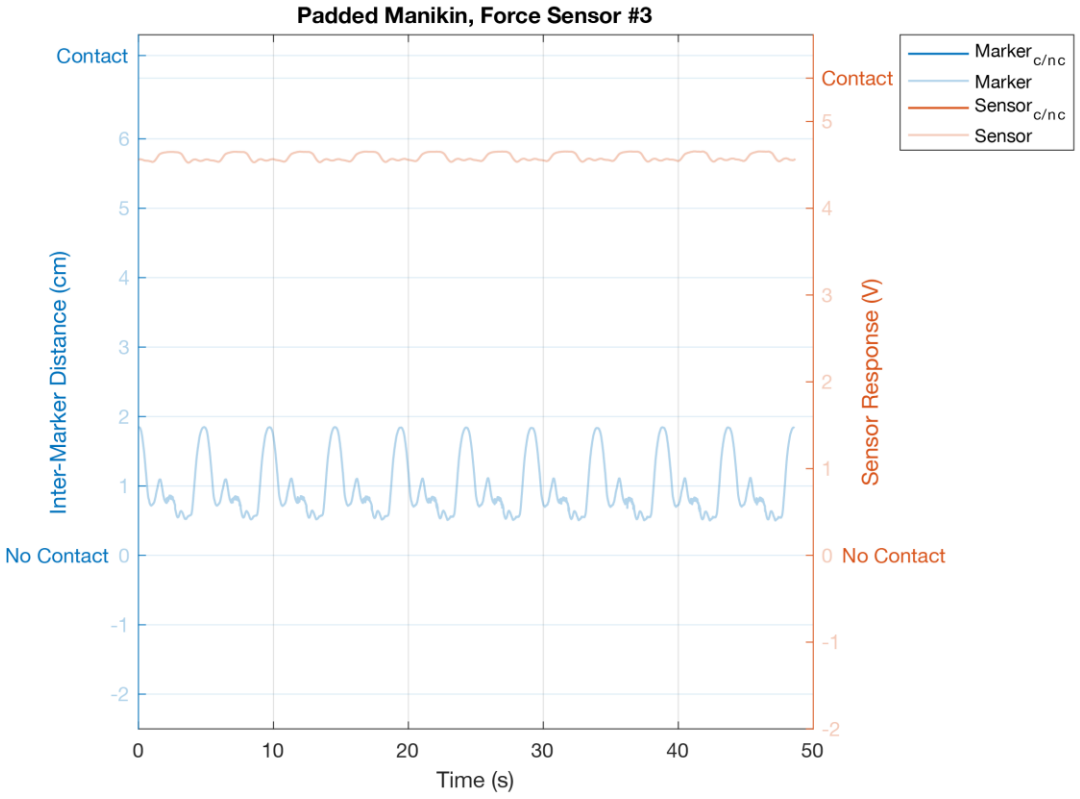
Padded Manikin, Force Sensor #3
Contact
No Contact
Inter-Marker Distance (cm)
Sensor Response (V)
Time (s)
Marker c/nc
Marker
Sensor c/nc
Sensor

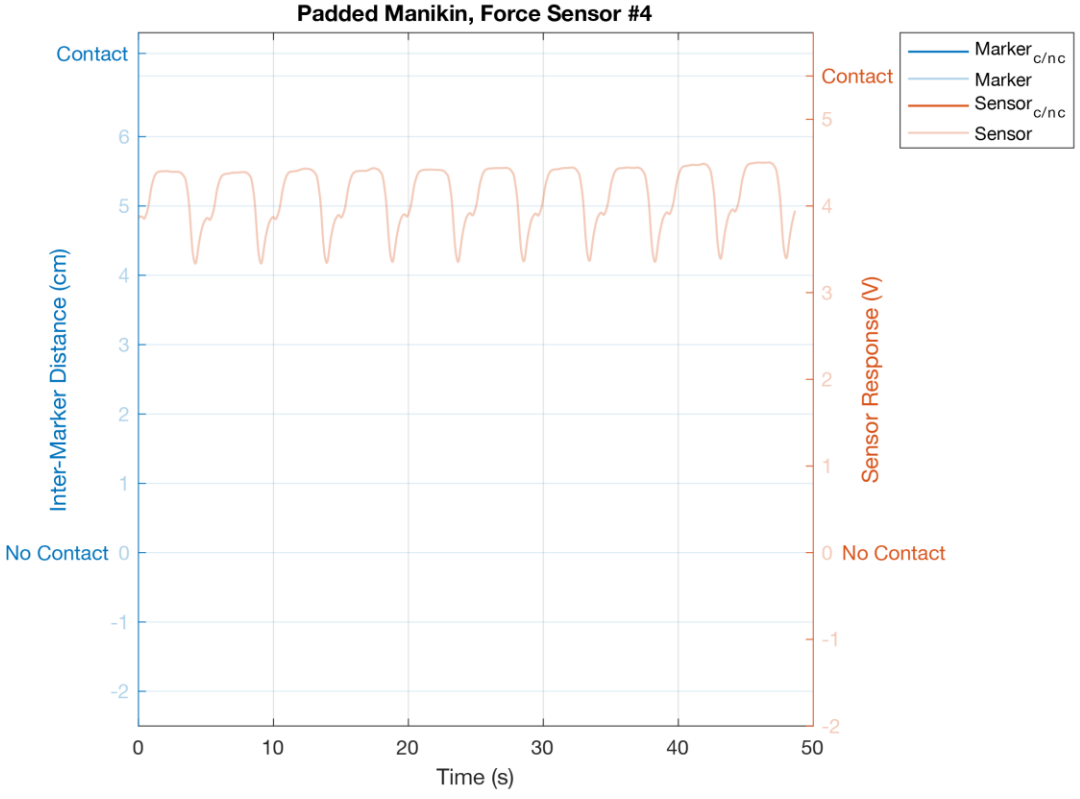
Padded Manikin, Force Sensor #4
Contact
No Contact
Inter-Marker Distance (cm)
Sensor Response (V)
Time (s)
Marker c/nc
Marker
Sensor c/nc
Sensor

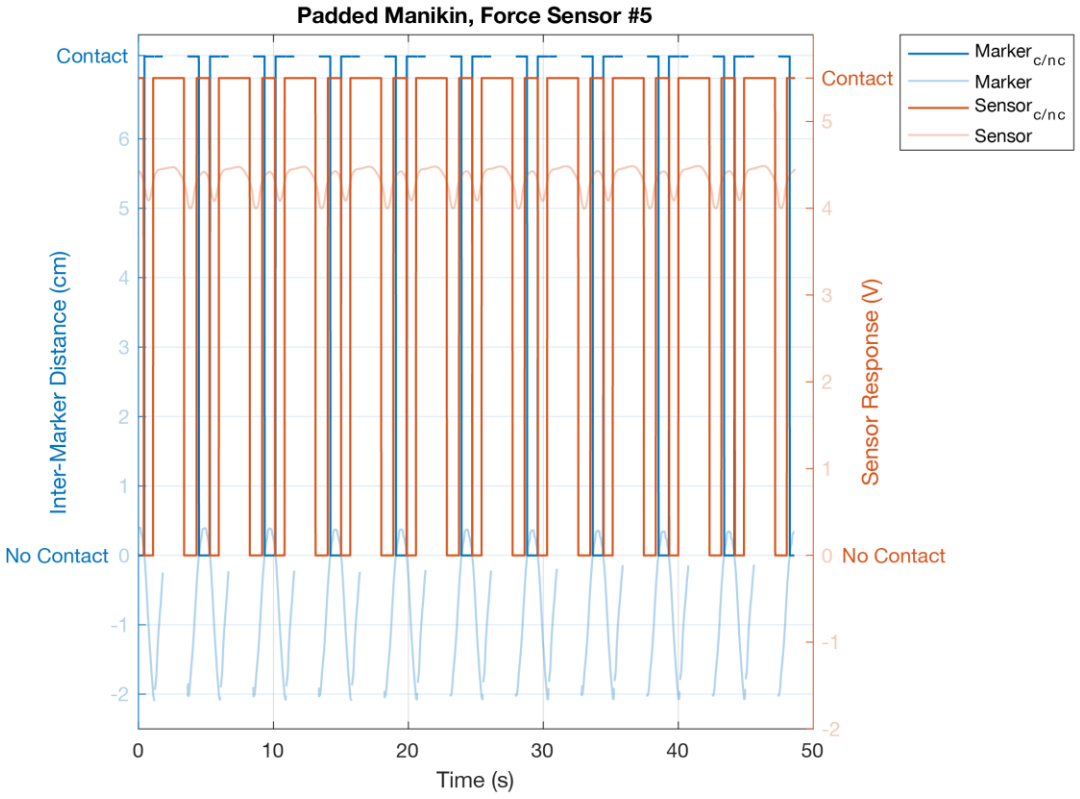
Padded Manikin, Force Sensor #5
Contact
No Contact
Inter-Marker Distance (cm)
Sensor Response (V)
Time (s)
Marker c/nc
Marker
Sensor c/nc
Sensor

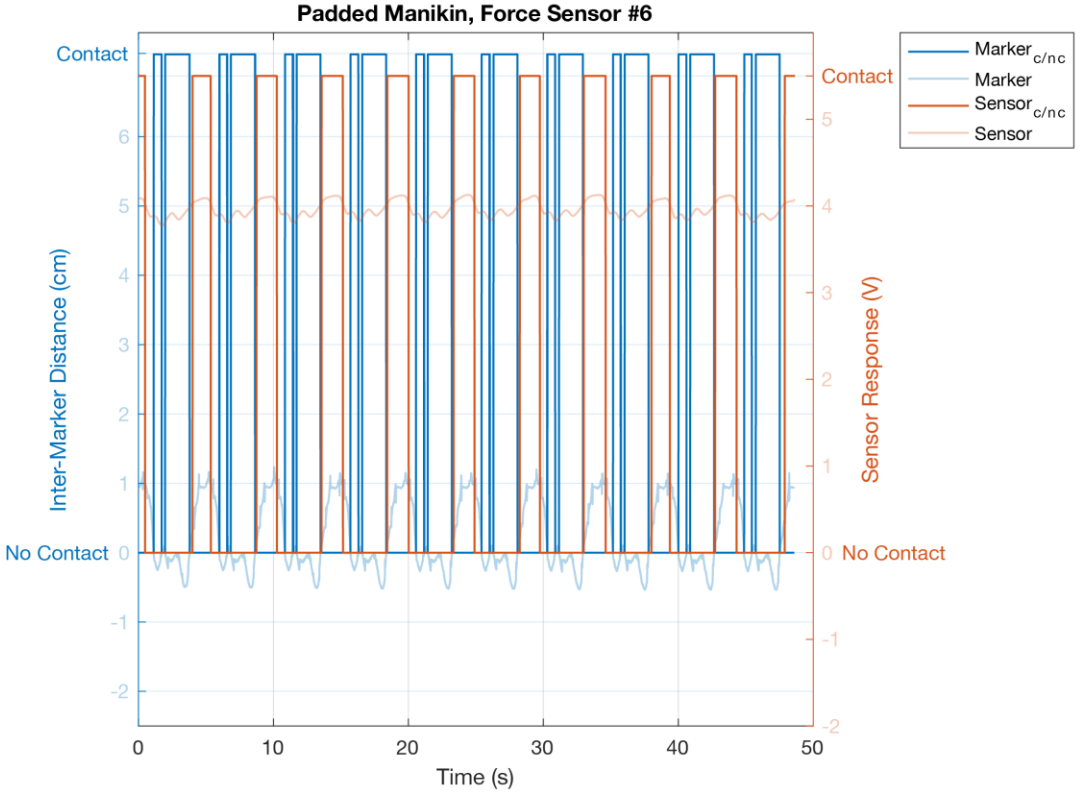
Padded Manikin, Force Sensor #6
Contact
No Contact
Inter-Marker Distance (cm)
Sensor Response (V)
Time (s)
Marker c/nc
Marker
Sensor c/nc
Sensor

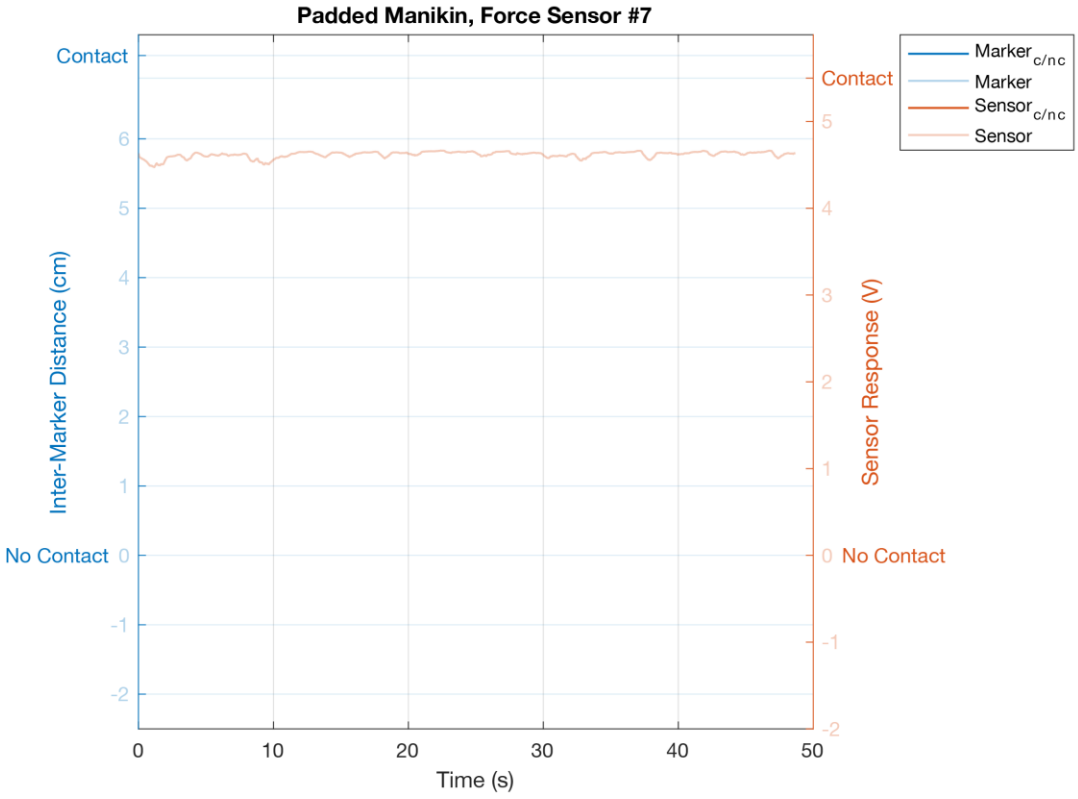
Padded Manikin, Force Sensor #7
Contact
No Contact
Inter-Marker Distance (cm)
Sensor Response (V)
Time (s)
Marker c/nc
Marker
Sensor c/nc
Sensor

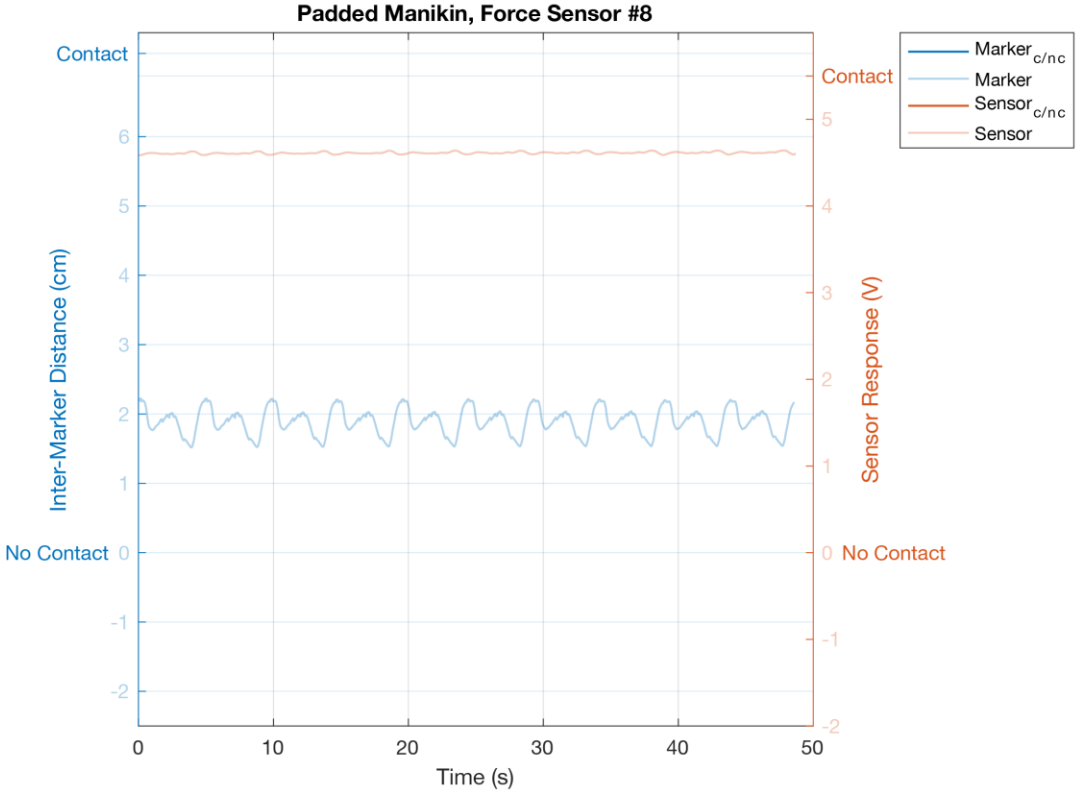
Padded Manikin, Force Sensor #8
Contact
No Contact
Inter-Marker Distance (cm)
Sensor Response (V)
Time (s)
Marker c/nc
Marker
Sensor c/nc
Sensor

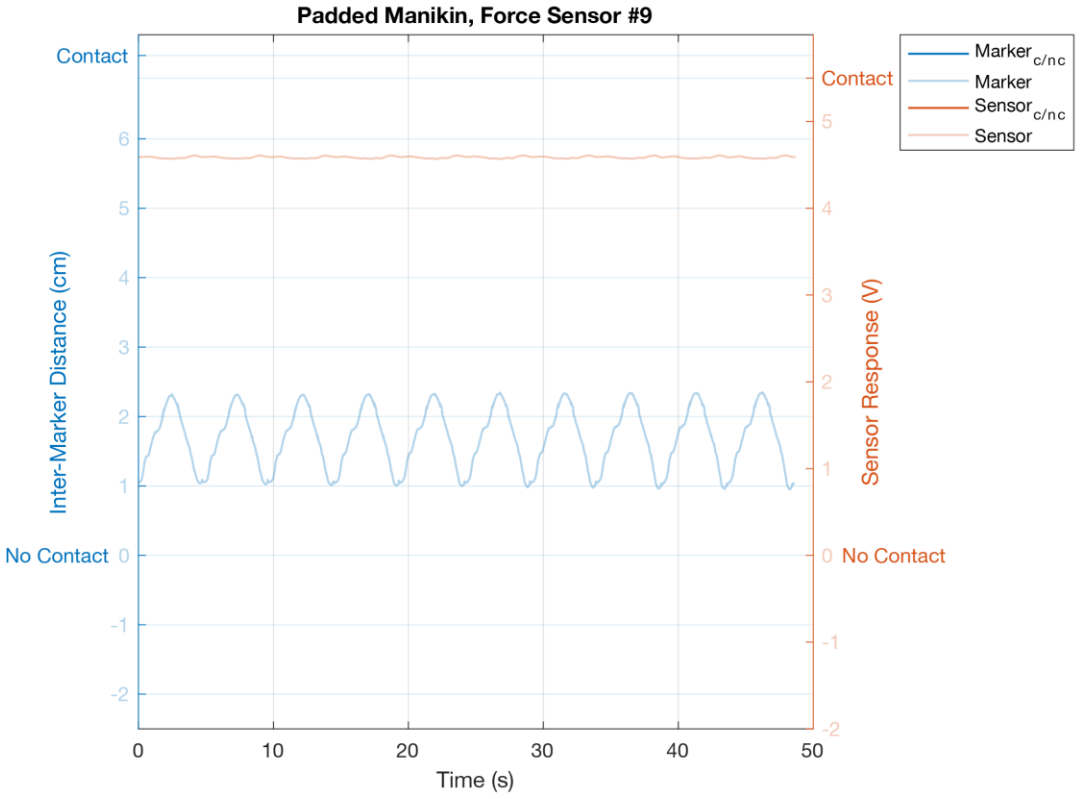
Padded Manikin, Force Sensor #9
Contact
No Contact
Inter-Marker Distance (cm)
Sensor Response (V)
Time (s)
Marker c/nc
Marker
Sensor c/nc
Sensor

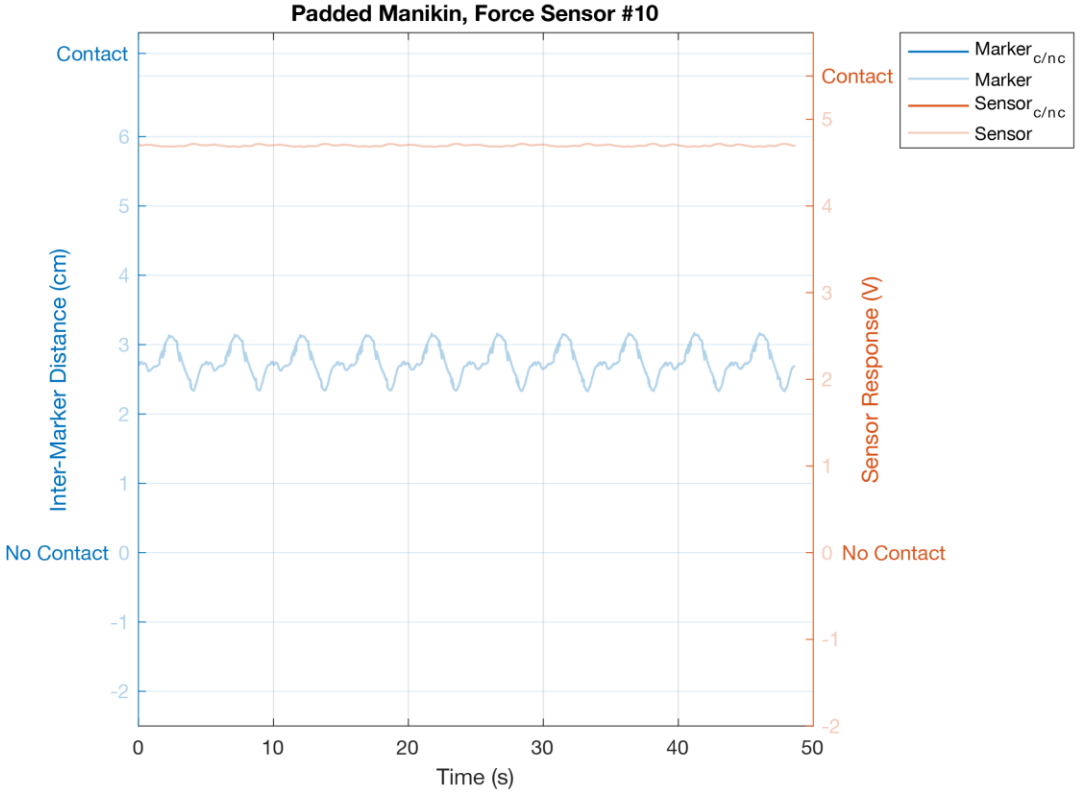
Padded Manikin, Force Sensor #10
Contact
No Contact
Inter-Marker Distance (cm)
Sensor Response (V)
Time (s)
Marker c/nc
Marker
Sensor c/nc
Sensor

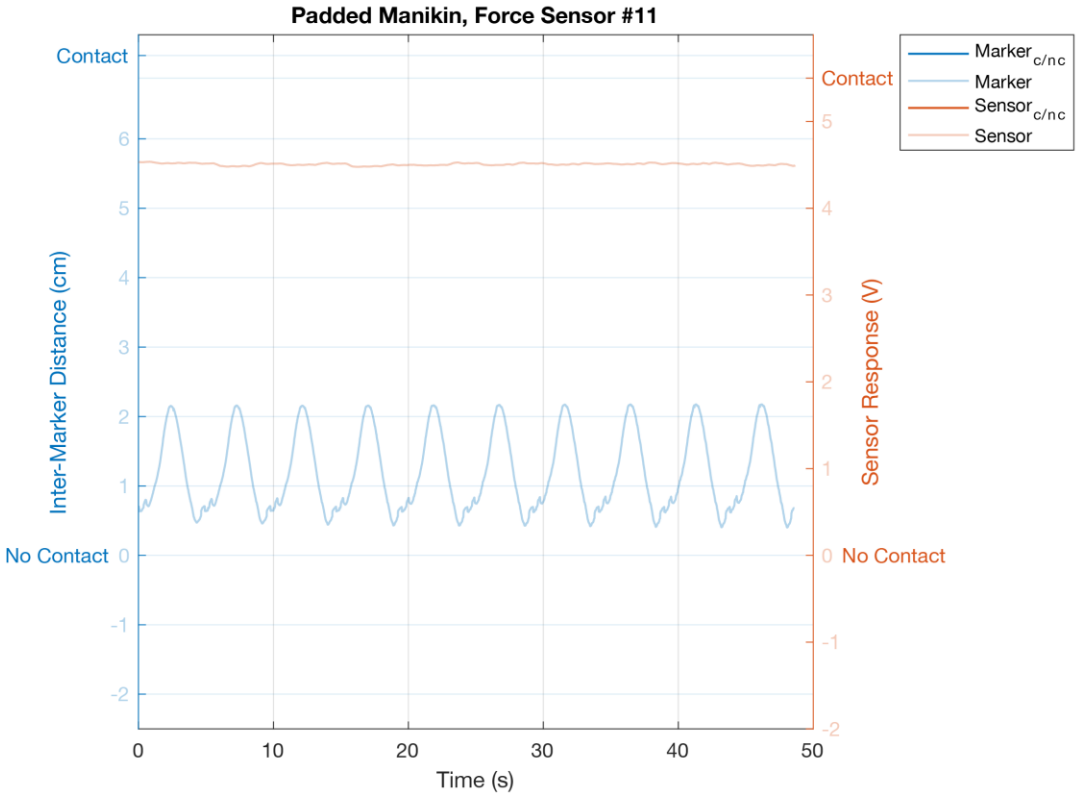
Padded Manikin, Force Sensor #11
Contact
No Contact
Inter-Marker Distance (cm)
Sensor Response (V)
Time (s)
Marker c/nc
Marker
Sensor c/nc
Sensor

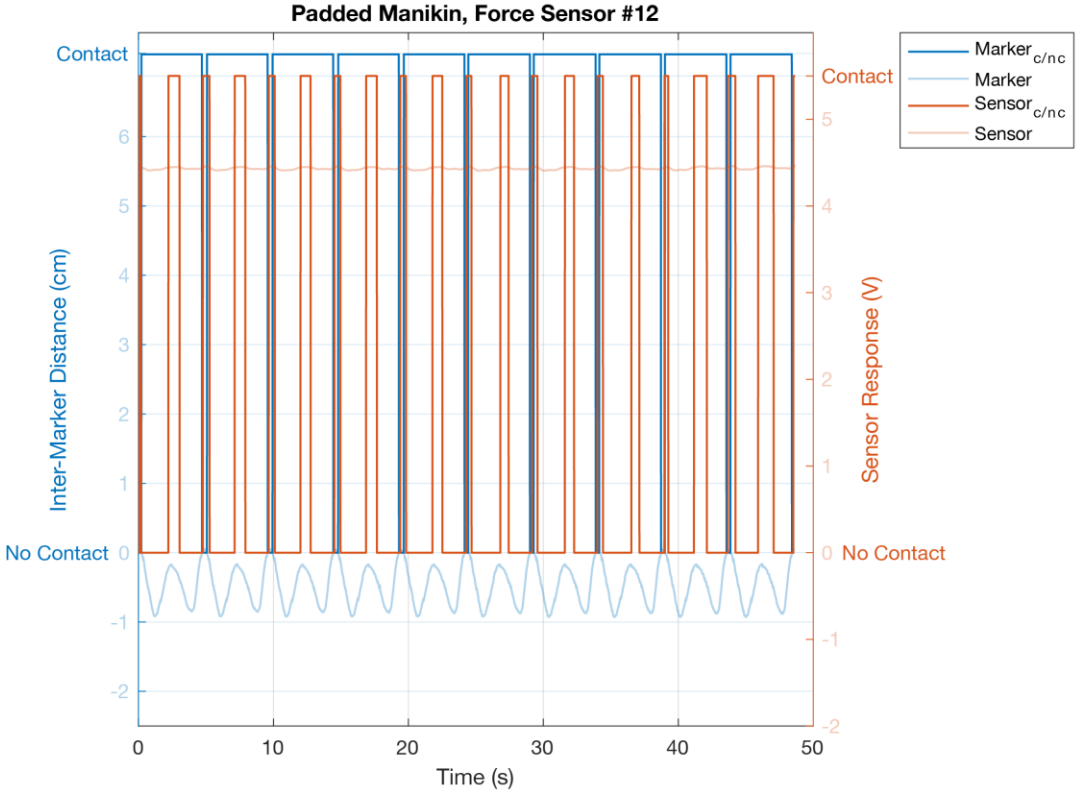
Padded Manikin, Force Sensor #12
Contact
No Contact
Inter-Marker Distance (cm)
Sensor Response (V)
Time (s)
Marker c/nc
Marker
Sensor c/nc
Sensor